The effect of uniaxial orientation upon the structural properties of polvaniline films

Laughlin, Paul Jonathan

The Effect of Uniaxial Orientation upon the Structural Properties of Polyaniline Films

by

Paul Jonathan Laughlin

A thesis submitted to the faculty of science,

Durham University for the degree of Ph.D.

Department of Physics

University of Durham

September 1996

Abstract

The effects of elongation upon the structural and electronic properties of the conducting polymer polyaniline have been investigated. In particular, the properties of high molecular weight (ca. 150 000 Daltons) polyaniline have been examined, and the effects of increased molecular weight assessed. A method has been found to elongate the emeraldine base (EB) form up to 700% (l/l_0=8). This induces partial molecular alignment in the polymer which, upon doping, exhibits electrical conductivity of up to 700 Scm^{-1} and electrical anisotropy of almost 4.

The mechanical properties of high molecular weight emeraldine base have been investigated as a function of elongation. The breaking stress has been observed to increase by almost one order of magnitude for a 500% elongated film compared with its unoriented counterpart. The breaking strain is found to decrease initially with increasing elongation, though no noticeable change is evident for samples elongated to more than 300%. Similarly, Young's modulus increases by a factor of 2 with increased elongation, but above 300% remains approximately constant. The behaviour has been interpreted in terms of the crystalline fraction of the samples.

X-ray diffraction experiments have enabled the crystalline fraction of emeraldine base and emeraldine salt (ES) to be assessed. 300% elongated EB samples exhibit increased crystallinity compared with as-cast samples. However, no further increase in crystallinity is evident for 600% elongated samples. Unoriented ES samples have a crystalline fraction of approximately 0.3. The crystallinity of 300% and 600% elongated ES samples is slightly less than for unoriented ES.

The polarised reflectance spectra of EB and ES have been measured in the region 0.5-5.6 eV. The results show increased optical anisotropy with increasing elongation for EB samples, but no change in anisotropy for ES samples above 300% elongation. A Kramers-Kronig analysis of the reflectance data reveals near metallic behaviour parallel to the direction of elongation, and a high degree of localisation perpendicular to this direction.

Declaration

The material in this thesis has not been submitted for examination for any other degree, or part thereof at the University of Durham or any other institution. The material in this thesis is the work of the author except where formally acknowledged by reference.

Acknowledgements

I would like to thank a number of people for their support, advice, help and friendship during my time here at Durham.

Firstly, thanks to my supervisor, Dr. A. P. Monkman for all the help, advice and encouragement he has given me over the years. He's not a bad footballer either.

Thanks to Phil Adams for his help in getting me started and for continually providing me with different versions of his polyaniline to 'try out'. Much thanks to Lee Abell for sharing his computer expertise and helping me with seemingly never-ending problems.

To my friends in the Department: Steve Pomfret, Paul 'Smaaaalusss' Barker, Pete Devasagayam, Eggie, Mackam, Eymard, Stu, Mounir, Marek, Tony, Anna, Debbie and the rest.

To Norman Thompson and Davey Pattinson, and those technical staff who helped design and build the various bits and bobs.

To John Vinson, my industrial supervisor, for his help and hospitality, and to B.I.C.C. Cables Ltd. for their C.A.S.E. sponsorship award and for financing John Vinson's hospitality (great hotels!).

Finally, thanks to my parents for putting up with me during my time of 'writing up' and not minding too much when I use their house "like a hotel".

Dedication

To Eileen Dunne

Contents

Preface

Polymer science is an immense subject, and despite polymeric materials in general being fundamental to many of our everyday commodities, it has not been until recent years that a novel and potentially technologically important aspect of the science has come to light. The discovery of electrically conducting polymers has provoked intense research, which is still in an early stage. Among the forerunners as a research material is polyaniline (PANi) which, because of its air stability, good mechanical properties and processibility, is perfectly suited to experimental investigation.

The work contained in this thesis is based on the changes in structural properties of polyaniline when stretch-oriented under uniaxial tension to achieve elongations between 0 and 700%. This is a subject of concentrated research due to the increases in conductivity upon orientation and subsequently the vast outlet for possible applications.

The first chapter gives a brief historical review and introduces the main theoretical concepts relating to electronic and geometric structure of conducting polymers.

Chapter two describes methods of achieving increases in the molecular weight of polyaniline. It is shown that variation of a number of parameters affects the molecular weight of the polymer; in particular low temperature synthesis is shown to increase the molecular weight by a factor of almost seven. The chapter goes on to describe the preparation of thin films of polyaniline using NMP as a plasticiser/solvent. A procedure to elongate the films by up to 700 per cent is described and the subsequent conductivity measurement techniques and results are reported.

In chapter three the effect of elongation upon the mechanical properties of the emeraldine base form of polyaniline is analysed. A number of samples of each elongation have been tested to assess the consistency of mechanical behaviour. The results from these experiments have been linked to the crystalline fraction of the polymer as well as orientation of polymer chains.

Chapter four is concerned with X-ray diffraction measurements of both the insulating emeraldine base and conducting emeraldine salt forms of polyaniline. This work has allowed for the variations in crystallinity, d-spacings, lattice parameters and crystallite size with elongation ratio to be assessed.

Chapter five reports the results of polarised reflectance analysis of oriented polyaniline samples. The reflectance spectra can be related to the electronic band structure, and the differences observed both parallel and perpendicular to the stretch direction as a function of elongation. A Kramers-Kronig analysis of the reflectance data has allowed for a number of optical constants of the base and salt forms of polyaniline to be calculated.

Finally, chapter six summarises the results and conclusions from the experimental work and concludes with suggestions for further work.

CHAPTER 1: INTRODUCTION TO CONDUCTING POLYMERS

1.1 History of Conducting Polymers

The ability of polymers to conduct electricity has been recognised for many years, but the last two decades have seen more of an explosion of interest in such materials than at any other time. The existence of polyaniline, for example, was documented in 1834 by Runge, but very little was understood about the polymer for the next 100 years. One reason for the recent interest is the large commercial potential of conducting polymers and hence the input of substantial funds for research into the materials. Possible applications of conducting polymers exist, for example, within the cable shielding[1], gas sensing[2] and anti-corrosion[3] industries.

The major breakthrough, which popularised conducting polymers as a research subject, was the successful synthesis[4] of polyacetylene thin films by Shirakawa in the mid-1970s. It was found that the conductivity could be increased by up to 11 orders of magnitude upon doping[5], posing a host of questions concerning the possible mechanisms of conductivity. In an effort to answer these questions numerous theoretical and experimental techniques have been used. Possible ways of increasing the conductivity of polymers such as polyaniline, polypyrrole and polyacetylene have been the subject of intense research. The main results and conclusions from these efforts shall be summarised in this chapter, and the associated concepts introduced.

1.2 Conductivity Phenomenon in Polymers

To describe the nature of conducting polymers, polyacetylene shall first be considered. This polymer has received more attention than any other for a number of reasons. Firstly, it has the simplest structure of all the conducting polymers, as shown in figure 1.1. Also, it is easily synthesised[5] into a form suitable for experimental investigation -

although many conjugated polymers have been synthesised, most are insoluble and can only be prepared as powders.

a) trans-transoidal

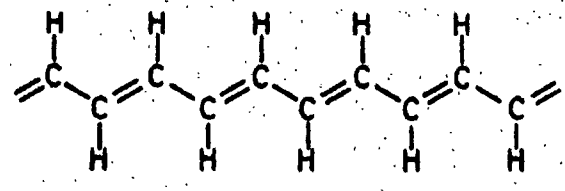

b) cis-transoidal

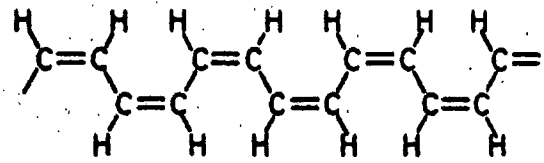

c) trans-cisoidal

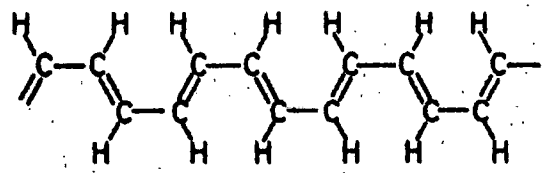

Figure 1.1: Isomers of Polyacetylene

Acetylene was first polymerised by Natta[30] and co-workers in 1958 using a $Ti(OBu)_4$ - $AlEt_3$ catalyst. The polymer obtained was a grey infusible powdery material, which is not soluble in any common solvents. Later, Shirakawa[4] and co-workers succeeded in preparing free-standing polyacetylene films of metallic lustre. They used the same catalyst as Natta but worked under different experimental conditions. The films were grown at low temperature (ca. -78°C) and were red in colour and of the cis structure, figure 1(b). It was found that high temperature polymerisation led to blue-coloured trans polymer films. Using the same catalyst, but varying experimental conditions, Hatano et al[6] were able to prepare polyacetylene with varying degrees of crystallinity. They reported a Bragg reflection of 23-25°, corresponding to a d-spacing of 3.5-3.8Å.[7] A further breakthrough occurred in 1974 when Ito et al[8] succeeded in preparing high-quality, free-standing films. The workers employed a very high concentration of $Ti(OBu)_4$ - $AlEt_3$, again at -78°C, which resulted in 88% cis-polyacetylene. It was

found that the polymer had increasingly higher trans content as the polymerisation temperature was raised, with trans structure predominant at 150°C. The films obtained were shown to have a density of 0.4 gcm^{-3}. Electron microscopy showed them to consist of fibrils of ~20nm in diameter, figure 1.2, and X-ray diffraction showed them to be highly crystalline.

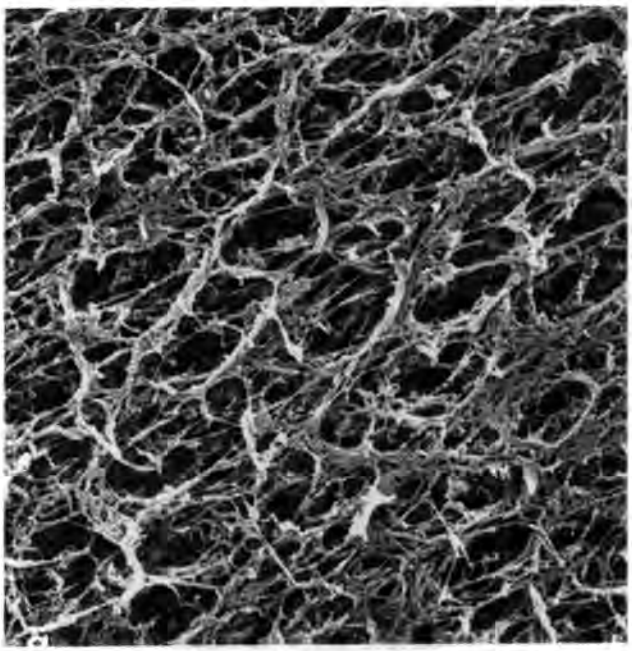

Figure 1.2: SEM of free-standing PA film, showing fibrillar morphology[9].

Trans-polyacetylene consists of a sequence of carbon atoms along the backbone, with each carbon bonded to a hydrogen. The carbons are bonded by alternating single and double bonds along the chain, deeming the polymer conjugated. Consideration of the chemical bonding of polyacetylene allows a simple explanation of the electronic structure of the polymer. Four valence electrons exist for each carbon in the chain. These electrons are contained in bonding orbitals. Three of the four electrons are in sp^2 hybridised orbitals, which form the strong covalent or σ bonds along the polymer chain and with the C-H. The fourth valence electron is in a p_z orbital perpendicular to the chain. When many molecules with this configuration bond together the π-bonding becomes extended along the chain and this produces a π-conjugated system. The electrons are not localised as in the case of the σ-bonding electrons, but extend throughout the π-orbital system. This delocalisation of the π-electrons provides the

means for conjugated polymers to be potentially conducting. For high molecular weight $[CH]_x$, where x is large, and a polymer backbone which has uniform bond order (alternate single and double bonds along the backbone, with equal separation between the carbon atoms) the polymer should be an intrinsic metal. This can be seen by considering the evolution of π molecular orbitals and the decrease in their energy difference as the length of the chain increases, figure 1.3.

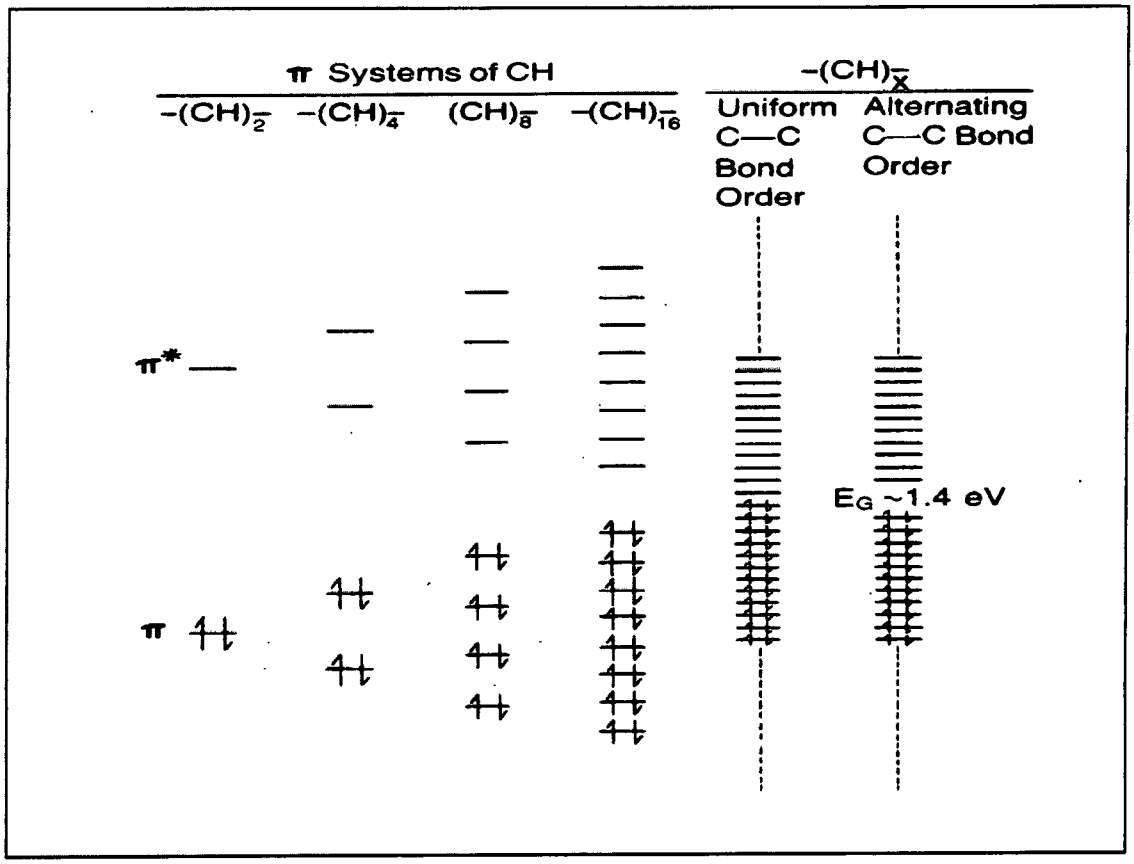

Figure 1.3: Diagrammatic representation of the energy levels of π molecular orbitals with increasing size of the molecule for $[CH]_x$[9]

Each carbon site donates one π-electron to the system. From Pauli's exclusion principle each site can be doubly occupied with electrons of opposite spin, constituting a half-filled system which would exhibit metallic behaviour. However, polyacetylene is found to be semiconducting with a band gap of ca. 1.4eV. This band gap originates from a Peierls distortion due to alternation in bond lengths, as described below by the Su-Schrieffer-Heeger Model.

1.3 The Su-Schrieffer-Heeger Model

The Su-Schrieffer-Heeger[10,11] model (SSH) provides a simple model for the electronic nature of trans-polyacetylene. A Hamiltonian consisting of two parts associated with the σ- and π-electrons is used to describe the polymer. The first part is the lattice elastic energy describing the σ bonds:

$$H_o = (K_o/2) \Sigma (u_{n+1} - u_n)^2$$

where K_o is the lattice force constant, and u_n is the displacement of the n^{th} atom from its equilibrium position. The lattice force constant describes the elastic potential energy of the chain as a function of the relative displacement of the carbon atoms.

The second part is the tight-binding term describing the π-electrons and their hopping between carbon atoms:

$$H_\pi = - \Sigma t_{n,n+1} (c^+_{n,s} c_{n+1,s} + c^+_{n+1,s} c_{n,s})$$

where the $c^+_{n,s}$ and $c_{n,s}$ are creation and annihilation operators for π-electrons at position n with spin s (s=± 1). The term $t_{n,n+1}$ is known as the transfer integral and is a measure of the amount of overlap of neighbouring electron wavefunctions. For small displacements this term can be expanded linearly about the equilibrium spacing to give:

$$t_{n,n+1} = t_o - \alpha (u_{n+1} - u_n)$$

where α is the electron-phonon coupling constant.

If the assumption is made that all C-C bond lengths are equal on the chain, i.e. u_n=0 for all n, the solution to the π-electron part of the Hamiltonian is a one-dimensional tight-binding band, with band energies:

$$\varepsilon_k = - 2t_o \cos ka$$

Figure 1.4 shows the conduction and valence bands for undimerised trans-polyacetylene:

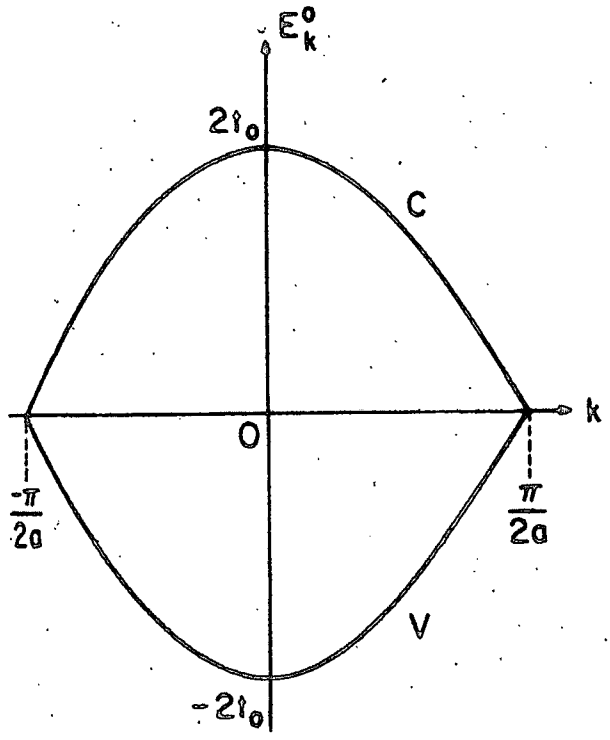

Figure 1.4 π-bands for undimerised trans-polyacetylene

It can be seen from the diagram that the bandwidth is $4t_o$, with each carbon atom contributing one electron, thus making the highest energy band half-filled. This regime constitutes metallic behaviour. This condition, however, is known to be untrue experimentally because of bond alternation. In other words, the system is dimerised.

Dimerisation of the system is essentially equivalent to the Peierls instability of a one-dimensional metal[12]. Peierls showed that distortion of the lattice, as depicted in figure 1.5, can result in lower energy of the system. This lattice distortion causes a gap to open up at the Fermi level, figure 1.6.

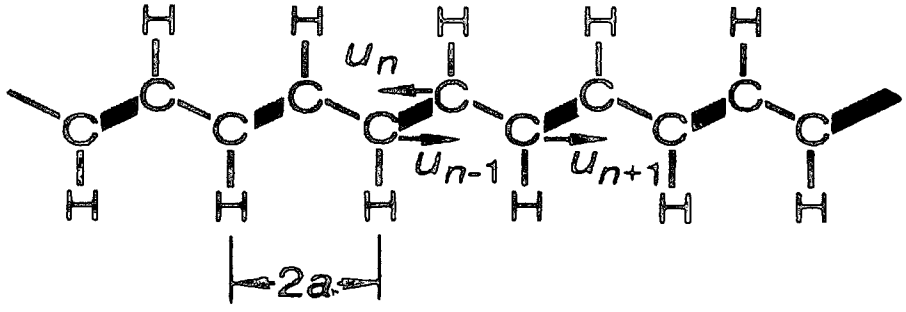

Figure 1.5: Dimerisation of polyacetylene

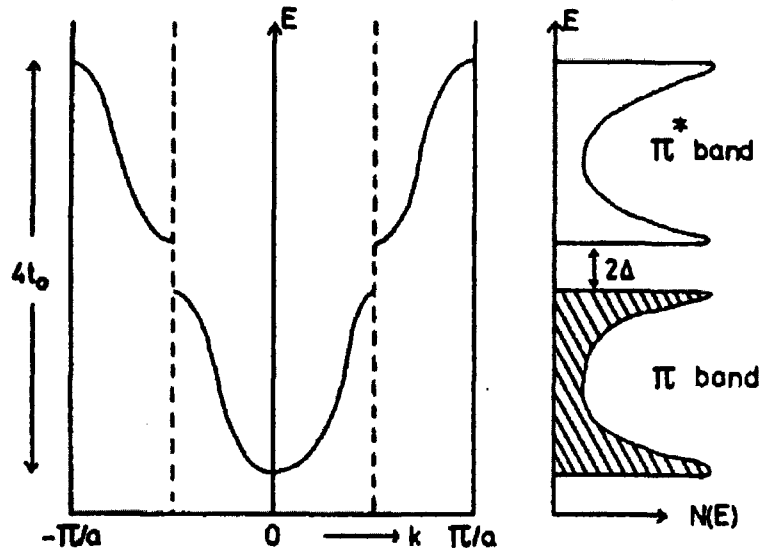

Figure 1.6 Peierls distortion in a half-filled band

The displacement of the carbon sites is expressed as:

$$u_n = (-1)^n u_o$$

which gives the band structure equation:

$$E_k = (4t_o^2 \cos^2 ka + 4\alpha^2 u_o^2 \sin^2 ka)^{\frac{1}{2}}$$

This reveals a discontinuity in the structure at $k=\pi/2a$, which results in an energy gap between unoccupied and occupied states having the value $8\alpha u_o$.

Experimentally and theoretically it is evident that trans-polyacetylene is intrinsically semiconducting, with filled π-bands (valence band) and empty π^* bands (conduction band). To increase the conductivity to significant values the polymer must be chemically doped, i.e. the number of electrons on the backbone must be either increased or decreased. Experimental work such as Raman scattering[13] has verified the proposed bond alternation for polyacetylene, revealing a band gap approximately equal to that predicted by the SSH model.

The SSH model provides a very successful description for the electronic behaviour of trans-PA. Its simplicity is partly due to some initial assumptions made, the most important of which is the neglection of electron-electron interactions. In the case where e^--e^- Coulomb interactions are very strong, the approach is invalid[28]. Despite this approximation, however, the model still allows for some useful predictions to be made concerning the electronic nature of the polymer.

1.4 Bond Alternation Defects

In order to visualise the existence of charge-carriers within conducting polymers, it is advantageous to continue to deal with polyacetylene. Study of this polymer will allow the simplest introduction to the concepts involved which will later be modified when the polymer relevant to this research, polyaniline, is considered.

If we consider again the dimerised form of polyacetylene, it is clear that this form can occur in two degenerate states, as shown in figure 1.7.

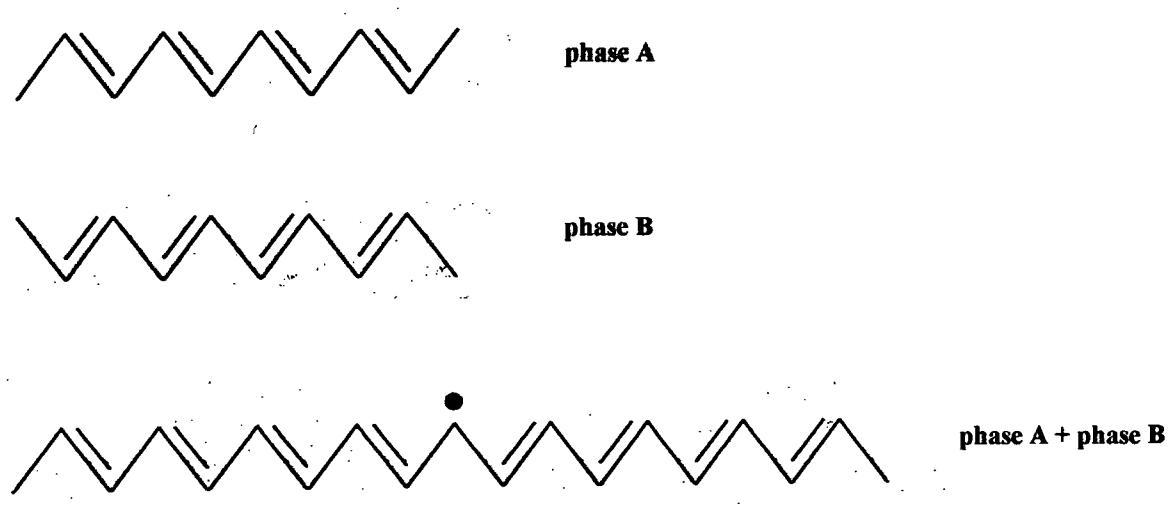

Figure 1.7. Bond alternation defect on trans-PA chain

If a chain containing either an odd number of carbon atoms or both A and B phases is formed, then a bond mismatch occurs as shown, leaving one carbon atom unable to form a π-bond with either of its neighbours. The dot in the diagram represents an unpaired electron, indicating a defect with an associated spin of $\frac{1}{2}$. However, no net charge is associated with this defect. This type of defect has been termed a soliton.

Figure 1.7 is, however, oversimplified, as it does not take into account Heisenberg's uncertainty principle which states that the position of a particle can only be known within certain limits depending on the measured momentum of the particle. In other words, the soliton defect is considered to extend along the chain. The length scale over which this defect extends has been calculated by Rice[14] and Su, Schrieffer and Heeger[15]. A wave function for solitons has been suggested which is of the form:

$$\varphi_n = u_o \tanh (na / \xi)$$

where a is the repeat unit length of the dimerised chain and ξ is a variational parameter which represents the length scale over which the soliton extends. Numerical minimisation of the energy of the defect with respect to ξ gives a value of $\xi \approx 7a$, indicating that a soliton is actually a gradual switch between the two degenerate phases of trans-PA extending across approximately 14 carbon sites.

The concept of the existence of solitons will affect the electronic band structure from that depicted in figure 1.6 to one with a band halfway between the top of the valence band and the bottom of the conduction band. The lone electron occupies this new level which is localised to the soliton defect.

The soliton discussed above is termed neutral (S^o) as there is no net charge on the chain. The defect level can, however, also exist in the form of a positive, spinless soliton (S^+), if the electron is removed, or a negative spinless soliton (S^-), in the case of an extra electron being added. These three states are shown in figure 1.8.

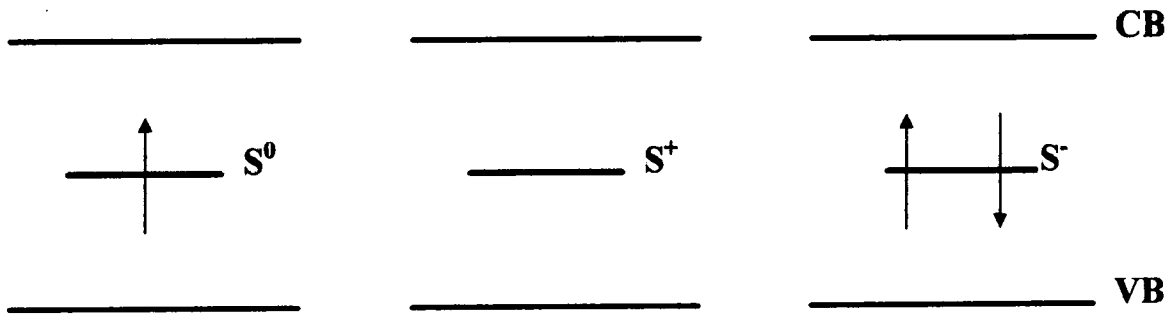

Figure 1.8. Neutral and charged soliton levels.

The importance of soliton defects is most apparent when considering chemically doped trans-PA. This is because it costs less energy to create charged soliton defects upon doping compared with adding or removing electrons from the valence or conduction bands[16]. The transfer of an electron to the conduction band is found to cost energy of $E_g=2\Delta$, where $\Delta=4\alpha u_0$, whereas the energy needed to create a negatively charged soliton is $2\Delta/\pi$. Creation of the soliton state is therefore energetically favoured.

As doping is increased, the discrete soliton defects are transformed to a soliton band due to soliton wavefunction overlap, figure 1.9. This is known to occur when approximately 6% of the carbon sites are doped.

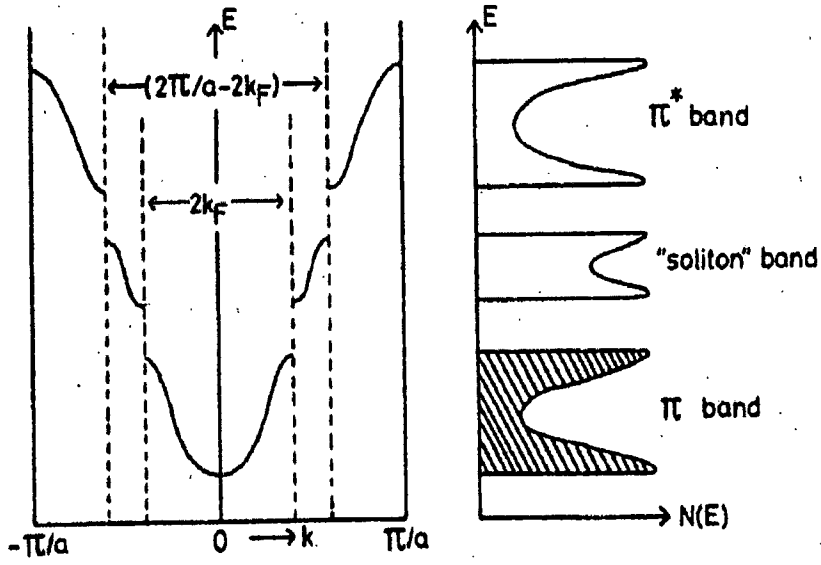

Figure 1.9. Creation of soliton band[16]

At this point the mean distance between the soliton defects is comparable with the length scale over which a single soliton is estimated to exist, i.e. ≈7a, thus producing a continuum of defect states.

1.5 Polarons and Bipolarons

The soliton defect described for trans-polyacetylene is the result of the combining of two degenerate forms, as described earlier. For most other conjugated polymers, however, the two regions that are separated by this bond alternation are no longer degenerate. An example of this is polyparaphenylene (PPP), shown in figure 1.10.

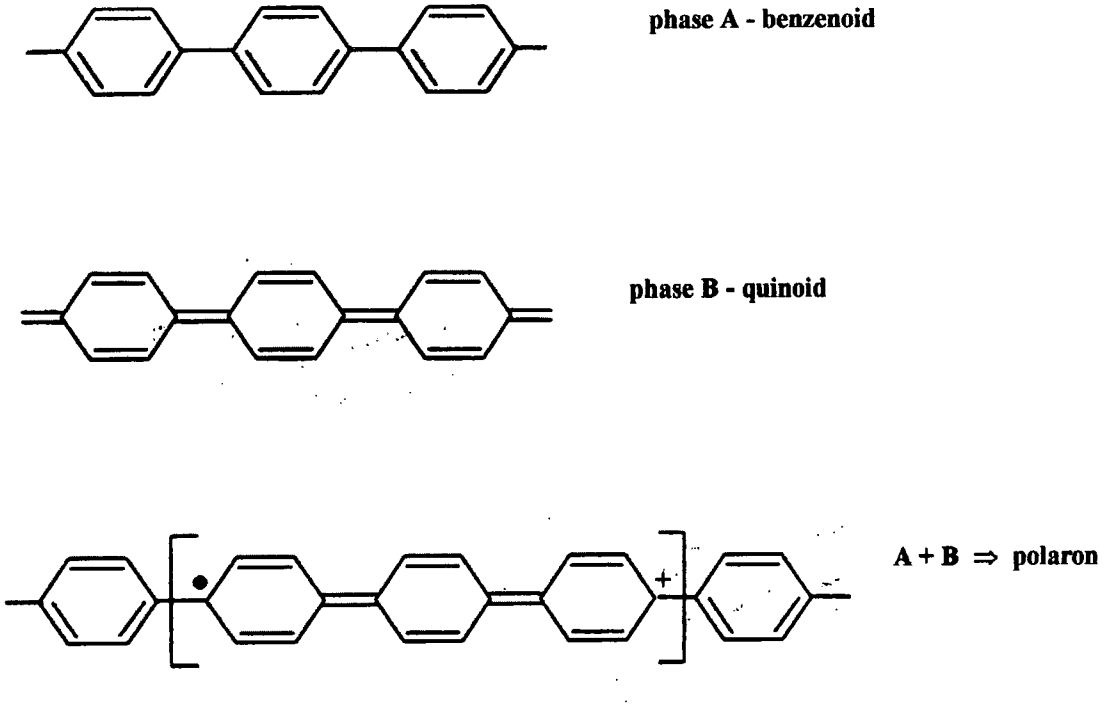

Figure 1.10. Formation of a polaron due to non-degenerate phases of PPP

In the situation depicted above it is not possible for a single defect (soliton) to exist because the A and B phases have different energies. Bond alternation defects would have to occur in pairs, otherwise total relaxation of the chain would take place to the lowest energy configuration, i.e. the benzenoid structure.

If the solitons were to exist in pairs, however, they would not be able to separate because they would be bound by regions of higher energy. If both the defects were neutral they would decay rapidly, but if the defects are charged then a stable configuration can be formed, as shown in figure 1.10. Such a defect is termed a polaron[27], and is essentially the binding of two solitons - one charged and one neutral.

The existence of polarons again causes changes to the electronic band structure of the system. The combination of two mid-gap soliton defects to form the polaron results in two energy levels existing symmetrically about the mid-gap[31], figure 1.11.

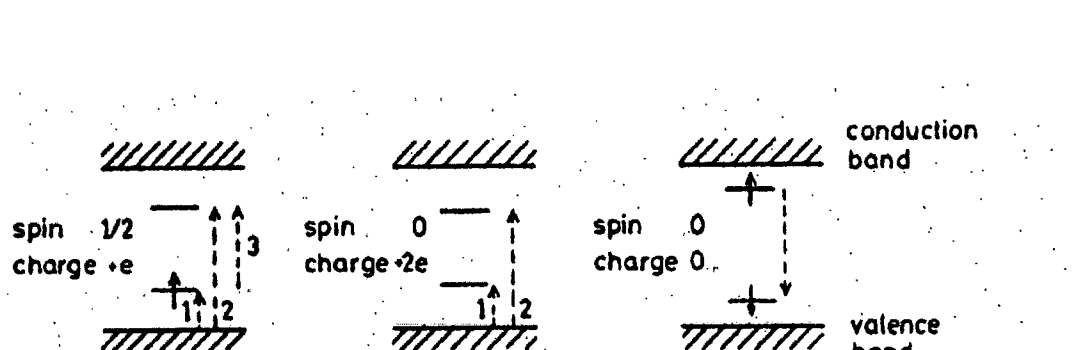

Figure 1.11. Energy level diagram for polaron and bipolaron defects.

It can be seen from figure 1.11 that the polaron has an associated spin of $\frac{1}{2}$ due to the presence of an unpaired electron. This electron can be removed to produce a doubly ionised defect with no spin, termed a bipolaron (b). Furthermore, if there is one electron on each of the intra-gap energy levels, one coming from the conduction band and one from the valence band, then the defect remains uncharged and spinless, figure c.

1.6 Polyaniline

The term polyaniline applies in general to three possible structures depending on degree of oxidation, as shown in figure 1.12.

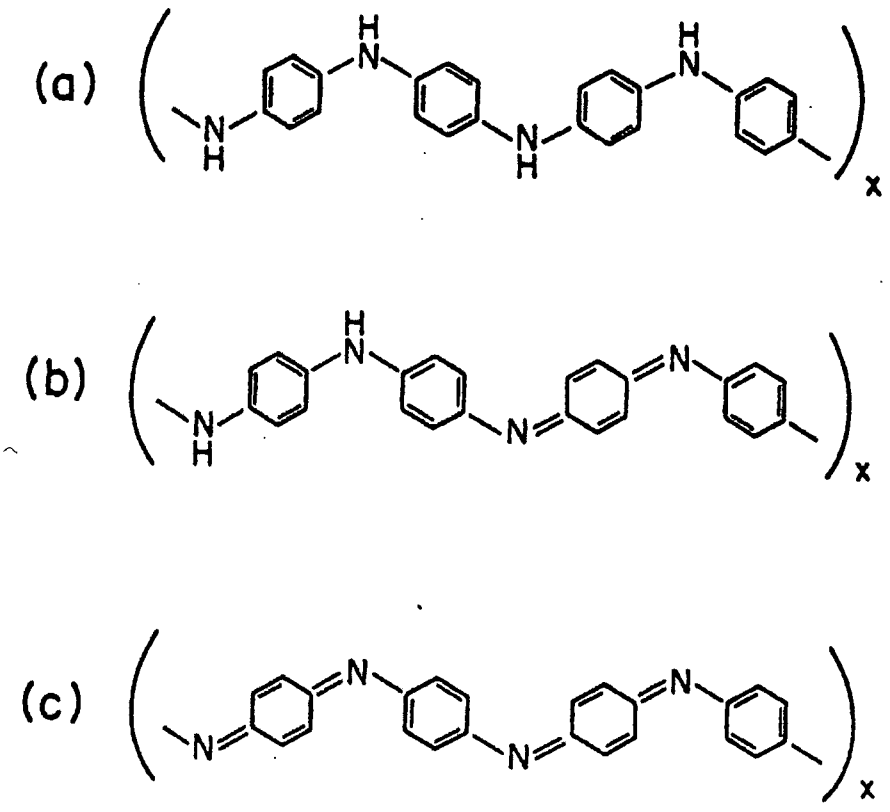

Figure 1.12. The three oxidation states of polyaniline: a) leucoemeraldine base
b) emeraldine base
c) pernigraniline base

a) The leucoemeraldine base (LEB) corresponds to the fully reduced form of polyaniline in which all the nitrogens are amine nitrogens and carry one hydrogen atom.

b) The emeraldine base (EB) is the half-oxidised form of polyaniline - half the amine nitrogens have been oxidised to produce imine nitrogens which no longer carry any hydrogen atoms.

c) The pernigraniline base (PNB) is the fully oxidised form of polyaniline - all the nitrogens are imine nitrogens.

The emeraldine base can further be processed into the conductive emeraldine salt form upon protonation in aqueous acid such as hydrochloric acid, figure 1.13.

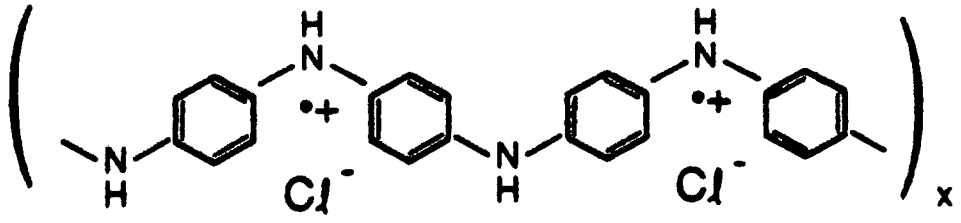

Figure 1.13. Emeraldine salt form of polyaniline

Each of these forms shall now be considered in further detail.

a) Leucoemeraldine Base

Bredas et al[17] have carried out geometry optimisations on LEB oligomers yielding the geometric structure shown in figure 1.14.

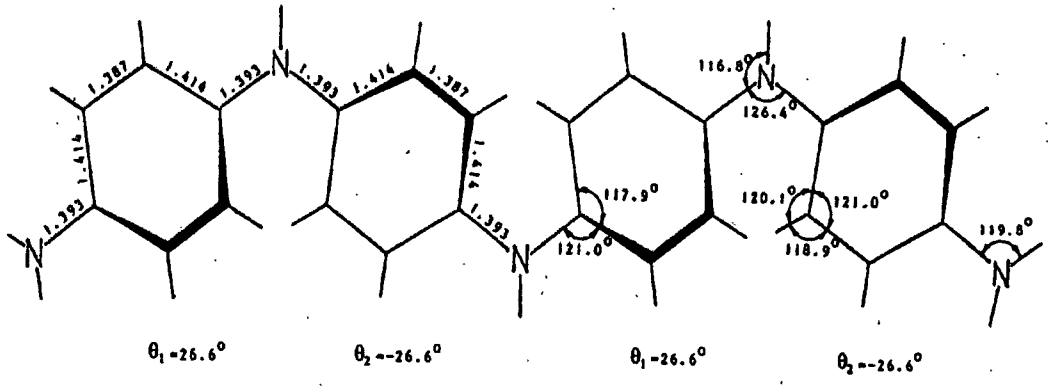

Figure 1.14. Geometric structure of LEB (after Bredas et al).

The calculations show that optimum geometry occurs when the benzenoid rings are twisted by a torsional angle of approximately 27° relative to the nitrogen-nitrogen plane. This torsional angle alternates along the chain so that neighbouring rings are oppositely oriented. Extrapolation of this result to the polymer chain yields a translational unit cell containing two ring-nitrogen units. These two units, however, are identical if rotational movement along the N-N plane is neglected. Therefore a subcell containing a single ring-nitrogen unit can be defined, containing 6 π-electrons per ring and 2 per nitrogen.

The electronic band structure of LEB based on Bredas' calculations takes the form of figure 1.15.

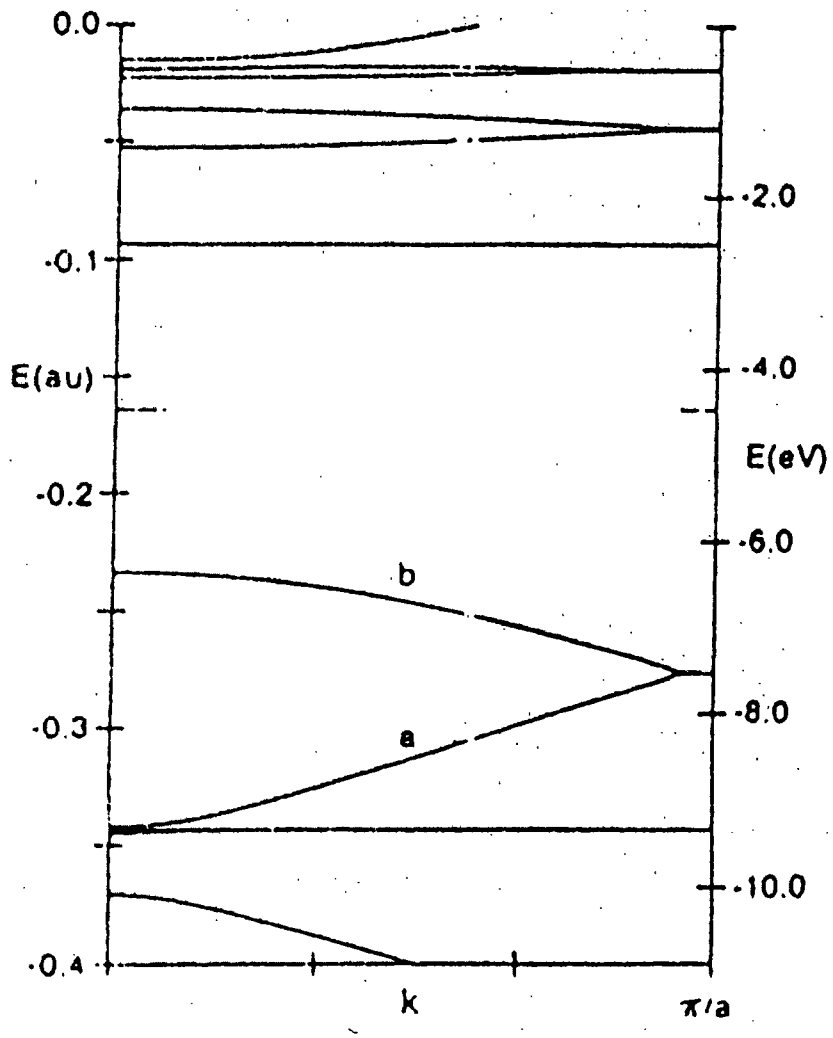

Figure 1.15: Electronic band structure of LEB.

Because of the rotational symmetry along the N-N axis, all the bands are degenerate by two at the end of the Brillouin zone. The upper occupied valence band consists of two branches a and b. The band gap is estimated to be large, with a value of approximately 3.8eV.

b) Emeraldine Base

Along the EB chain the rotational symmetry possessed by LEB is lost because a ring with quinoid geometry lies between the imine nitrogens. Therefore the translation unit

cell contains four ring-nitrogen units and the band structure contains twice as many electronic bands, figure 1.16.

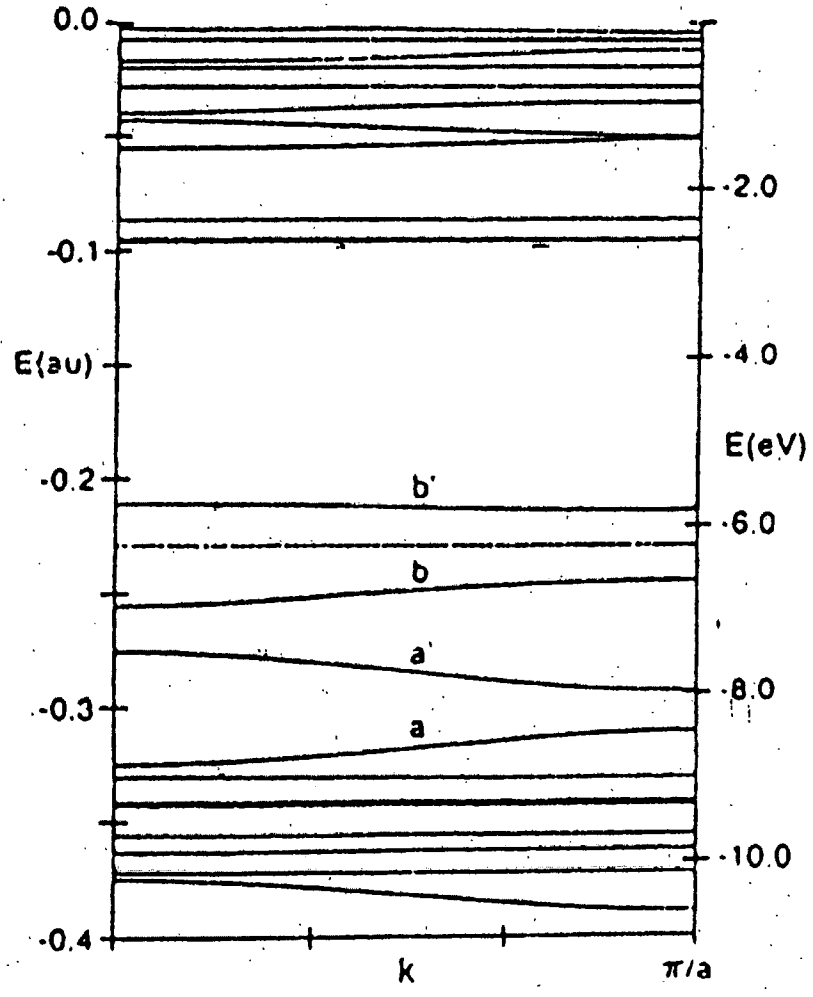

Figure 1.16: Electronic band structure of EB.

Comparison of figure 1.15 with figure 1.16 shows that the former upper occupied band of LEB is now split into four bands, labelled a, a′, b, b′. Because of the loss of symmetry of EB compared with LEB the degeneracy at the end of the Brillouin zone has disappeared. Also, the oxidation process has left EB with two less π-electrons per four ring-nitrogen units compared to LEB. Band b′ is therefore empty and is the lowest unoccupied band of EB. The band gap of EB is of the order of 1.4eV, and is related to both internal (Peierls-type) and external (chemical structure) effects.

An interesting feature of the band structure of EB is that the four branches, a, a′, b and b′ have different localisations. Branches a, a′ and b have contributions from atomic orbitals in the three benzenoid units, whilst b′ is mostly localised on the quinoid ring. This difference in localisation was first documented by Duke et al[18] and has led to a description of the electronic transition between the upper occupied and lower unoccupied bands in terms of a molecular exciton. Such an exciton involves the formation of a hole distributed over the benzenoid rings and an electron localised mostly on the quinoid ring.

c) Pernigraniline Base

Figure 1.17 shows the result of geometry optimisation calculations for the PNB form of polyaniline.

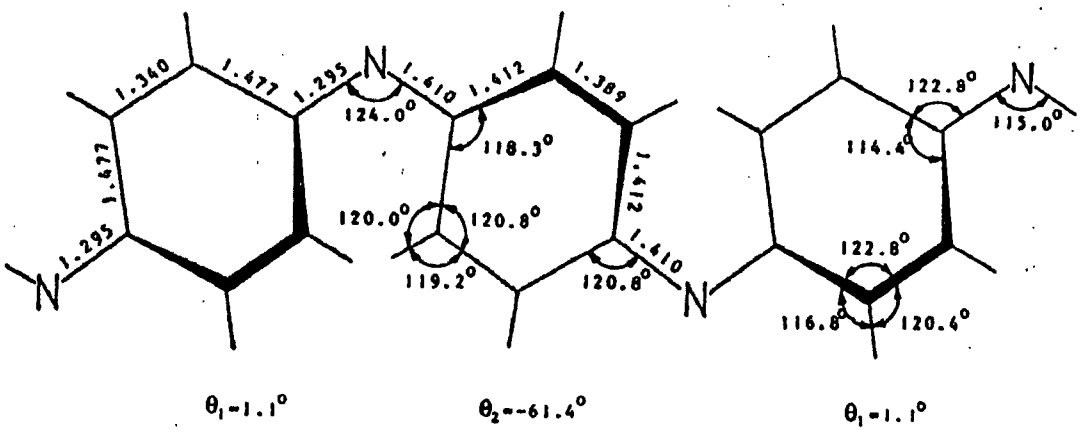

Figure 1.17. Geometric structure of PNB (after Bredas et al)

It is found that the most stable geometric structure occurs for a dimerised structure which exhibits a marked alteration between the benzenoid and quinoid character of the rings. It can be seen that the rings with quinoid character are only twisted by a very small amount (1.1°) relative to the N-N plane whereas the benzenoid ring has a torsional angle of approximately 61°, giving an angle between adjacent rings of 60°.

In principle it should be possible to use the results found for LEB and PNB to predict a geometric model for EB. In practice, however, this is found to be difficult to achieve due to both the more complicated repeat unit of EB and the difficulties in obtaining stable semi-oxidised oligomers.

The calculated electronic band structure of PNB is shown in figure 1.18.

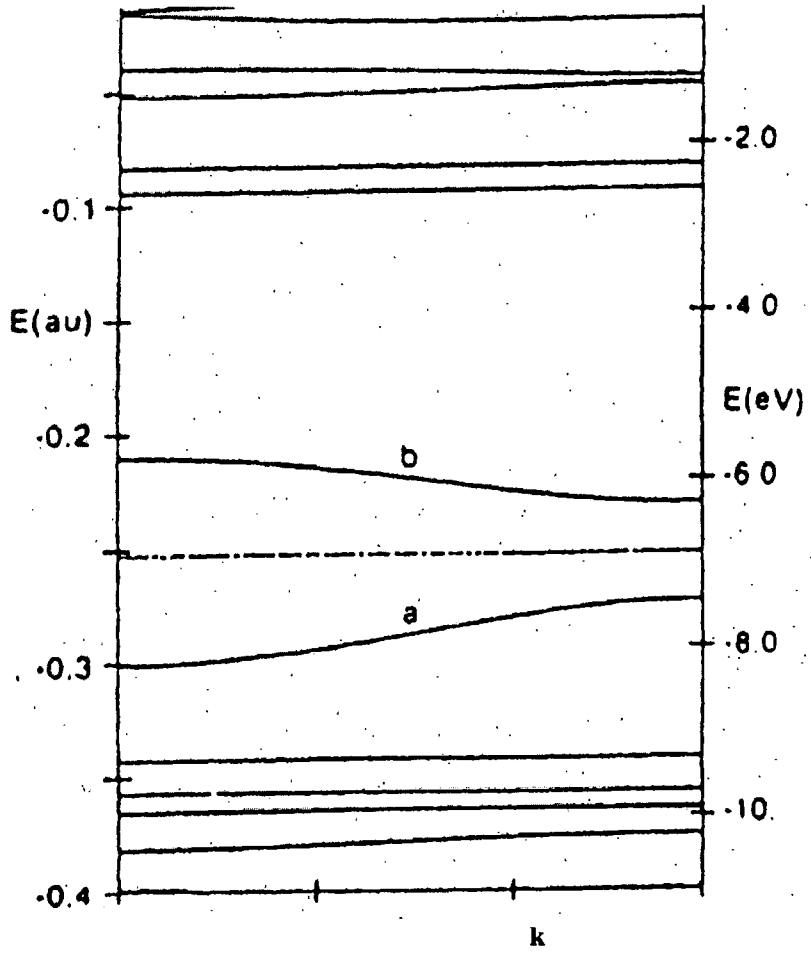

Figure 1.18: Electronic band structure of PNB.

The case is similar to that described for LEB, in that there are only two a and b branches, with branch a being the highest occupied band and branch b the lowest unoccupied band. This fully oxidised form is calculated to have an energy gap of approximately 1.4 eV which is internal in origin due to the Peierls-like distortion caused by bond length and ring torsional angle dimerisation.

d) Emeraldine Salt

The conversion of emeraldine base to emeraldine salt by protonation yields increases in conductivity of up to 12 orders of magnitude. Typical conductivity values of EB are 10^{-10} Scm^{-1} and values of approximately 100 Scm^{-1} are common upon doping. What is remarkable about this transition is that it takes place without any change to the number of electrons on the chains[19]. Figure 1.19 shows the changes in structure of EB following protonation.

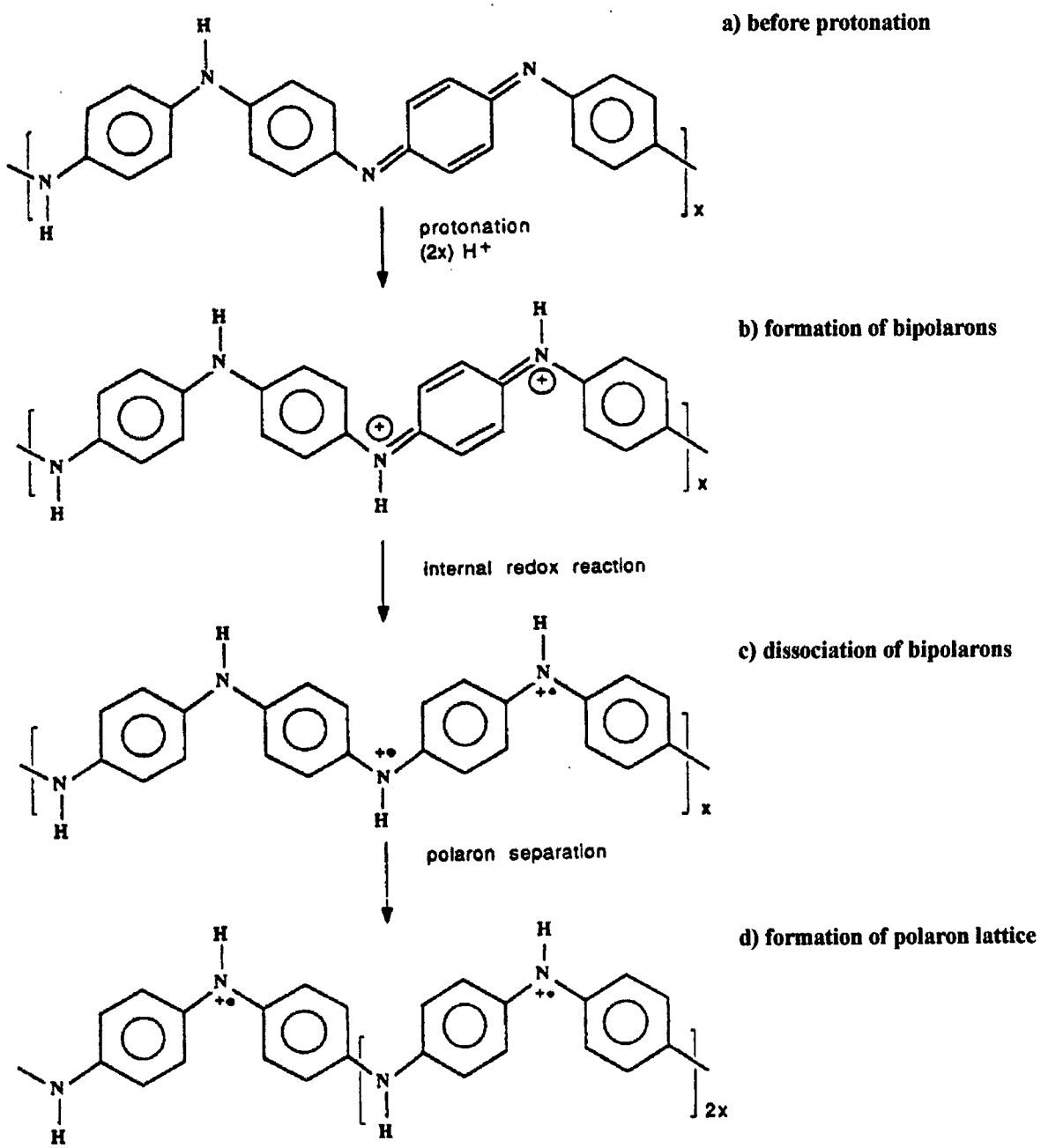

Figure 1.19: Protonation scheme: emeraldine base ⇒ emeraldine salt

It can be seen from the diagram that the process involves firstly the protonation of imine, -N=, sites, figure (b). These extra charges are localised on the quinoid element of the chain, and constitute a bipolaronic structure. This structure is energetically unstable[29] however, and therefore evolves to one consisting of polarons, figure (c). Due to the electrostatic repulsions between the positive charges these polarons then separate to produce a polaron lattice, figure (d).

The polaron lattice structure is the general representation of the salt form of emeraldine, but there has been contention as to whether the bipolaron structure will in fact be so unstable as to result in two polarons. Stafström et al[20] have investigated the electronic band structures in the case of bipolaron and polaron structures, yielding the band diagrams shown in figure 1.20.

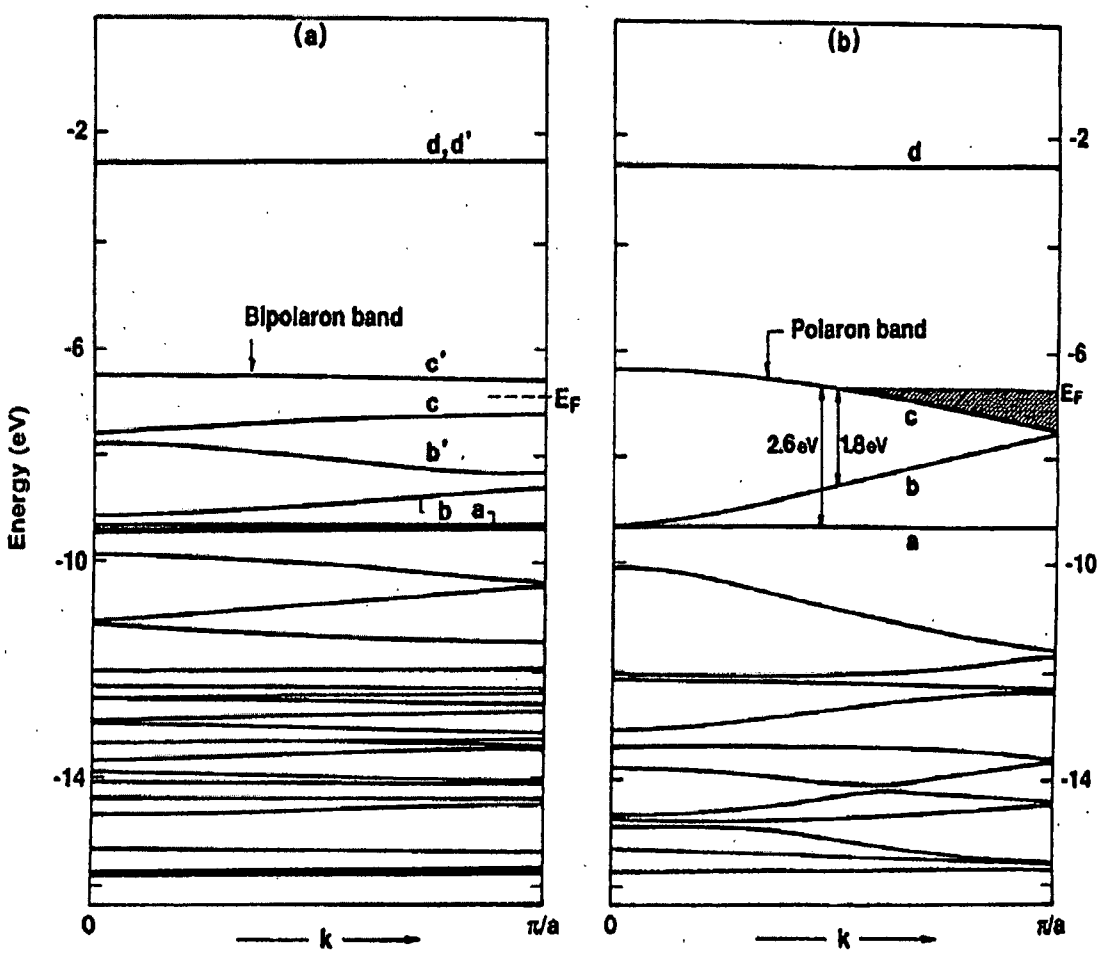

Figure 1.20. VEH band structure for bipolaron and polaron lattice structures of ES.

The unit cell of the bipolaron lattice is twice as big as that of the polaron lattice leading to twice as many bands in the first Brillouin zone. For the bipolaron structure band c corresponds to the highest occupied band and band d to the conduction band. The first unoccupied band however is c', the bipolaron band. For the polaron lattice the half-filled band c constitutes the polaron band. For both the bipolaron and polaron structures there is seemingly only one defect band in the gap, compared with two for other conducting polymers. The reason for this is that although two defect bands do indeed exist, the upper defect bands are almost degenerate with the conduction bands and are therefore indistinguishable from these bands.

The conflict between the proposed electronic structures of emeraldine salt has been resolved using the data from optical absorption spectra[20,21,22]. Strafström et al[20] have shown that transitions which would be expected for the bipolaron structure, such as that between the highest occupied band c and the bipolaron band c', are not in fact detected. Those expected for the polaron lattice however, are observed and are in good agreement with theoretical predictions. The transitions observed include:

a) direct optical transitions from band b to the polaron band at 1.8eV.
b) direct optical transitions from band a to the polaron band at 2.6eV.
c) electronic transitions from the polaron band to the conduction band at 4.1eV.

It is therefore generally accepted that the polaron band structure most readily describes the conducting form of emeraldine.

1.7 Conduction Mechanisms in Emeraldine Salt

The conduction mechanism(s) in polyaniline have been the subject of considerable debate which has led to a number of different possible mechanisms being suggested. For example, Cowan et al[23] have described a hopping model for the electrical conductivity of doped polyaniline, where the polymer is composed of fully protonated metallic regions surrounded by insulating regions. Similar conclusions have been made by other groups: Zuo et al[29] have performed conductivity measurements as a function of temperature and

protonation level. Their main conclusions were that the polymer is of a granular metal nature, whereby charge energy limited tunnelling (CELT) occurs between conducting islands. Other reports suggest that conductivity only takes place along individual chains[24]. This (quasi) one-dimensional nature of electronic transport along individual chains has been shown to be especially applicable to oriented samples: the conductivity along the direction of orientation is increased due to alignment of chains, and the conductivity perpendicular to this direction remains essentially the same. The conductivity mechanism perpendicular to chain direction is similar to that of an unoriented specimen - the carriers 'hop' between chains. This inter-chain hopping is generally assumed to be the reason for limiting the conductivity in polyaniline, due to the lack of inter-chain order[25].

Conduction mechanisms have been extensively studied by E R Holland[26] here at Durham University. In particular, the work has been concerned with the effect of temperature upon the conductivity in the region 10-300K. It was found that the conductivity increased monotonically with temperature, indicative of a disordered conductor in which charge carriers are localised. Curve fits to the experimental data suggests fluctuation induced tunnelling (FIT) as a possible conduction mechanism, as described by Sheng[32]. For such a regime the material is considered to consist of regions with extended "metallic" states separated by potential barriers. The electrons tunnel between the metallic islands, and the degree to which these electrons are able to tunnel is considered a limiting factor in the bulk conductivity of the material. Sheng suggested that the height of a tunnel barrier could be reduced by fluctuation of the voltage across the tunnel 'junction' due to the random thermal motion of electrons. Therefore the tunnelling current is dependent upon temperature, and the conductivity is of the form:

$$\sigma = \sigma_0 \exp(-T_1 / (T + T_0))$$

where T_1 depends upon the average barrier height or grain spacing and T_0 is the temperature where thermal fluctuations dominate the tunnelling current compared to elastic tunnelling.

A comparison between the experimental data and FIT-modelled conductivity for a 500% elongated emeraldine salt sample is shown in figure 1.21[26], for conductivity measured both parallel and perpendicular to the direction of elongation.

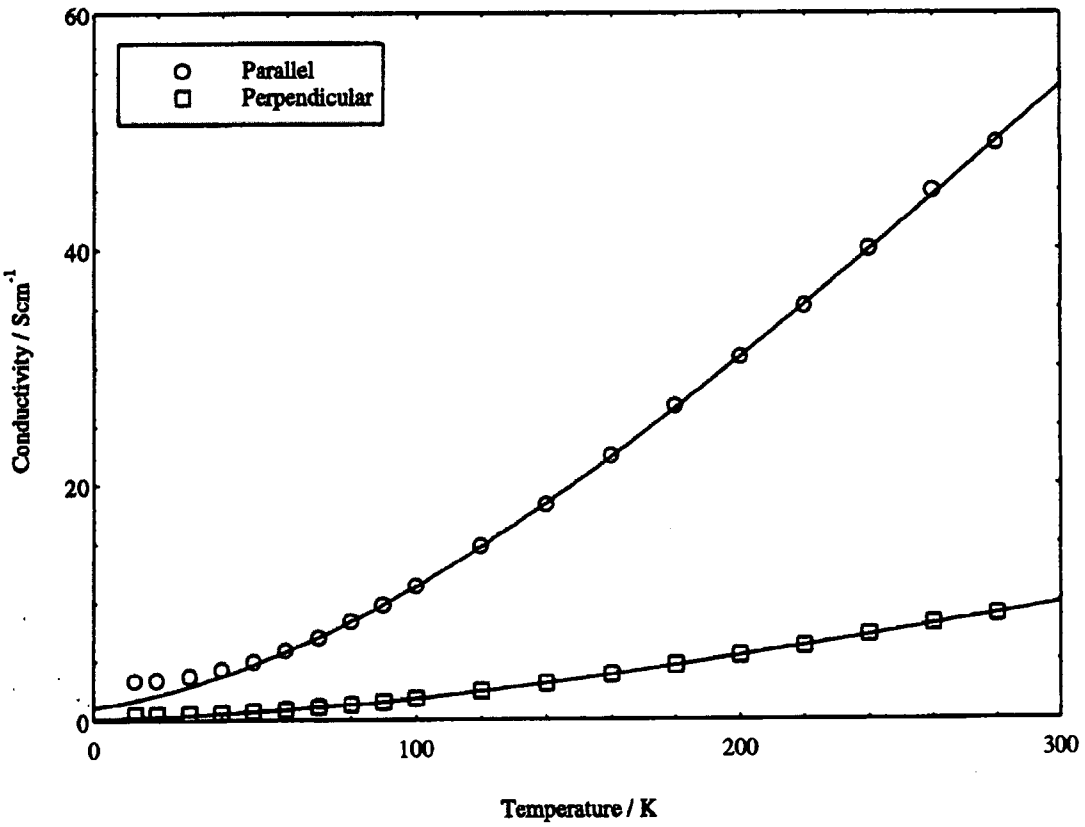

Figure 1.21: Comparison of experimental and theoretical conductivity for 500% elongated ES film using Fluctuation Induced Tunnelling model.

1.8 Summary

This chapter has introduced the main concepts relating to conducting polymers. The conductivity phenomenon in the most simple conjugated polymer, trans-polyacetylene, has been ascribed to the formation of solitons which are caused by the combining of its two degenerate states, thus forming a bond mismatch along the chain. Dimerisation of the chain results in the formation of an extra energy band between the valence and conduction bands.

For polymers with non-degenerate phases, bond alternation results in the formation of polarons or bipolarons. This again changes the electronic structure of the polymer by creating two energy levels which are symmetrical about the mid-gap.

Polyaniline has been shown to exist in three different states of oxidation. The geometrical and electronic nature of these forms has been described. Chemical doping of the emeraldine base form results in the conducting emeraldine salt. Such doping leads to the formation of polarons rather than bipolarons, as has been verified by optical studies. Furthermore, the possible mechanisms of electrical conduction in the emeraldine salt form of polyaniline have been discussed.

Increased knowledge of the structural properties can be probed by stretch-alignment of the polymer. This technique has been shown to change many of the physical and electronic properties of the polymer. The aim of this thesis is to probe further the effects of orientation, and to see how many of the properties of polyaniline are affected by high elongation ratios. A variety of experimental techniques have been incorporated in an attempt to achieve this goal, the main results of which are described in the following chapters.

References

1. J C Huang. *Advances in Polymer Technology*, (1995), **14**, no.2, 137-150.

2. S Dogan, U Akbulut, T Yalcin, S Suzer, L Toppare. *Synth. Met.* (1993), **60**, no.1, 27-30.

3. W K Lu, R L Elsenbaumer, B Wessling. *Synth. Met.* (1995), **71**, no. 1-3, 2225-2226.

4. H Shirakawa, T Ito, S Ikeda. *Polymer Journal,* **4** (1973), 460.

5. C K Chiang, C Z Fincher, Y W Park, A J Heeger, H Shirakawa, E J Louis, S C Gau & A G MacDiarmid. *Phys Rev Lett* **39** C (1977), 1098.

6. M Hatano, S Kambara, S Okamoto. *J. Polymer Science* **51**, 526, (1961).

7. M Hatano. *Kogyo Kagaku Zasshi* **65**, 723, (1961).

8. T Ito, H Shirakawa, S Ikeda. *J. Polymer Science Polym. Chem. Ed.* **12**, 11, (1974).

9. J C W Chien. *Polyacetylene: Chemistry, Physics and Material Science*, publ. Academic Press Inc., 1984.

10. W P Su, J R Schrieffer, A J Heeger. *Phys. Rev. Lett.* **42**, (1979), 1698.

11. W P Su, J R Schrieffer, A J Heeger. *Phys Rev B,* **22**, (1980), 2099.

12. R E Peierls. *'Quantum Theory of Solids'*, Oxford Univ. Press, p108 (1955)

13. S Lefrant *et al. Solid State Communications*, **29**, 191 (1979)

14. M J Rice. *Phys. Lett.* **71A**, 152 (1979)

15. W P Su, J R Schrieffer and A J Heeger. *Phys Rev B* **28** (1983) p1138.

16. R H Friend. *Physics and Chemistry of Electrons and Ions in Condensed Matter.* Publ. D Reidel, 1984. p625-651.

17. J L Bredas. *Proceedings of the Nobel Symposium on Conjugated Polymers and Related Materials*, ed. W R Salaneck, OUP (1992).

18. C B Duke, A Paton, E M Conwell, W R Salaneck and I Lundstrom. *Journal of Chemical Physics* (1987), **86**, 3414.

19. J-C Chiang and A G MacDiarmid, Synth Met **13**, (1986), 193.

20. S Stafström, J L Bredas, A J Epstein, H S Woo, D B Tanner, W S Huang and A G MacDiarmid, (1987), Phys. Rev. Lett. **59**, 1464.

21. A P Monkman and P N Adams, Synth. Met. **41-43**, (1991), 627.

22. A P Monkman and P N Adams, Solid State Comm, **78**, (1991), 29.

23. D L Cowan, V Priest, T R Marrero and D W Slaughter. *J Phys. Chem. Solids.* **51**, no.4, pp307-312, 1990.

24. H Y Hwang, S W Lee, I W Kim, H Lee. *Synth. Met.* **69** (1995) p225-6

25. A J Heeger. *Faraday Discuss. Chem. Soc.* **88** (1989) p1.

26. E R Holland. PhD Thesis, Durham University.

27. R R Chance, D S Boudreaux, J L Bredas and R Silbey in *Handbook of Conducting Polymers.* Ed. T A Skotheim, Publ. Dekker, New York, 825 (1986)

28. K Fesser, A R Bishop and D K Campbell. *Phys. Rev. B: Condensed Matter.* **27**, 4804 (1983)

29. A J Epstein, J M Ginder, F Zuo, H S Woo, D B Tanner, A F Richter, M Angelopoulos, W S Huang and A G MacDiarmid. *Synth. Met.*, **21**, 63 (1987)

30. G Natta, G Mazzanti and P Corradina. *Alti Accad. Naz. Lincei Rend. Sci. Fis. Mat. Nat.* **25**, 2 (1958)

31. D K Campbell and A R Bishop. *Phys. Rev. B.* **24**, 4859 (1981).

32. P Sheng. *Phys. Rev. B*, **21**, 2180 (1980).

CHAPTER 2: PREPARATION AND PROCESSING OF POLYANILINE

2.1 Introduction

This chapter describes the preparation and subsequent processing of the emeraldine base form of polyaniline. Techniques to increase the molecular weight of polymers have been the subject of considerable interest because of its effect on physical properties such as mechanical strength and electrical conductivity[1,2]. A method is described to obtain molecular weights in the region of 150 000 Daltons. The experiments to determine the effect of different preparation parameters upon molecular weights were performed by Dr. Phillip Adams at Durham University. Molecular weights were measured using gel permeation chromatography and ^{15}N n.m.r analysis[4]. The preparation of solvent-cast polyaniline films is described, and a method for obtaining stretch ratios of up to 700 per cent is reported. The effect of this elongation upon the electrical conductivity of doped samples is described.

2.2 Polymerisation mechanism for polyaniline

Exactly how aniline polymerisation takes place is still uncertain. It is likely that the radical cation species are produced as a result of oxidative attack on aniline monomers. These monomers then condense with the loss of protons to give the protonated, semi-oxidised emeraldine form of polyaniline as the reaction product[5]. Using aniline dissolved in hydrochloric acid and ammonium persulphate as starting reagents, the reaction stoichiometry should be:

$$4C_6H_7N.HCl + 5(NH_4)_2S_2O_8 \Rightarrow 2HCl + 5(NH_4)_2SO_4 + 5H_2SO_4 + 2(C_{12}H_9N_2.HCl)_x$$

The product is a polysemiquinone radical cation[6], where x is the number of protonated repeat units.

If aniline polymerisation does indeed follow the proposed mechanism then it is a difficult reaction to classify as it shows characteristics of both cationic chain polymerisation and condensation polymerisation reactions[7]. Cationic chain polymerisations are usually carried out at low polymerisation temperatures which favour propagation over competing reactions, and use solvents with a high dielectric constant which favours initiation and propagation leading to high molecular weight polymers. One of the characteristics of condensation polymerisation is that the molecular weight of the polymer rises steadily throughout the reaction, and therefore long reaction times are essential to obtain high molecular weights.

2.3 G.P.C. Analysis to Measure Molecular Weight

Gel permeation chromatography has been used previously in the molecular weight determination of polyaniline[6]. The technique is essentially a size exclusion process. The typical apparatus is shown in figure 2.1.

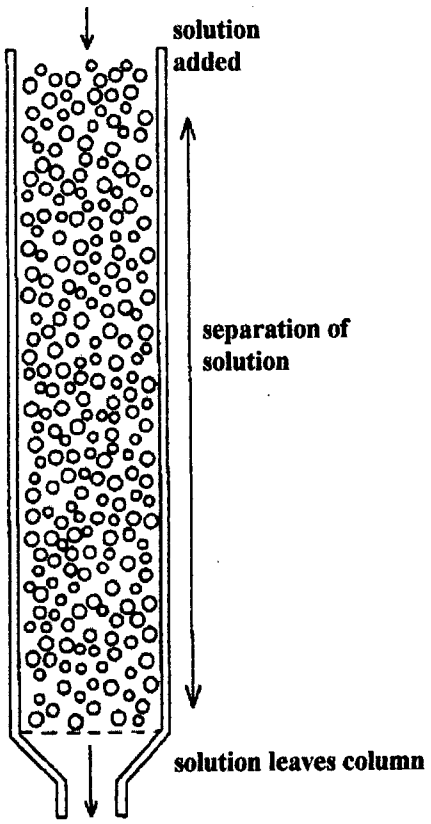

Figure 2.1: Illustration of g.p.c. column for molecular weight determination

The apparatus consists of a column packed with rigid porous beads. These beads are usually made of highly cross-linked polystyrene with a distribution of pore sizes. A continuous stream of solution, for which the molecular weight distribution is to be determined, flows through the column. As the polymer solution flows through the column the solvent will go either through or around the beads, depending upon the size of the molecules. The small molecules will pass through the pores in the beads and so their flow through the column will be impeded. Larger molecules, however, will flow around the beads, and therefore take less time passing through the column.

In practice two g.p.c. columns are used - one standard column and one containing the polymer for which the molecular weight is to be determined. The time spent in the column can then be compared with the standard to determine molecular weight distribution. For this analysis polyvinylpyridine dissolved in N-methyl-2-pyrrolidone (NMP) was used as molecular weight standard. The polyaniline samples were also dissolved in NMP.

2.3.1 G.P.C. Results

To measure the molecular weights of polyaniline a graph of log(molecular weight), M_p, versus retention volume for PVP standards is plotted. Here M_p is the peak molecular weight of the samples. The procedure for measuring molecular weights of polyaniline at 10 different reaction temperatures was as follows:

The standards were measured first, followed by the 10 samples. This was followed by the standards, then the samples once more, and finally the standards for a third time. For each of the three standards a graph of log M_p versus peak retention time was plotted and a straight line plot used to obtain an equation for the line, where y=log M_p and x=retention time. The average of the three values for each standard was taken and a similar equation obtained, as shown in table 2.1.

Run	Equation	Molecular weight value
1st	y=12.046-0.85338x	intermediate
2nd	y=12.320-0.88163x	maximum
3rd	y=12.117-0.86221x	minimum
average	y=12.239-0.87420x	average

Table 2.1: Equations used for deriving the molecular weights of polyaniline samples

The retention times (referred to as RT) are shown in table 2.2.

M_p/Daltons	log M_p	RT 1/ min	RT 2 / min	RT 3 / min	Average RT / min
1 000 000	6.000	7.17	7.24	7.43[1]	7.21
240 000	5.380	7.77	7.85	7.81	7.81
70 000	4.845	8.39	8.42	8.45	8.42
28 000	4.447	8.80	8.84	8.84	8.83
10 500	4.021	9.51	9.51	9.48	9.50
2 900	3.462	10.06	10.05	9.99	10.03

Table 2.2: g.p.c. Retention times for the three runs of PVP molecular weight standards
1. Value much higher than RT 1 and RT 2 therefore ignored in calculations

The peak molecular weights for the samples were calculated by taking the average of the two retention times and using the equation for the average molecular weight of the standards. The errors in M_p were estimated by taking the longer of the two retention times and calculating the molecular weight using the third of the equations in table 2.1, followed by the shorter of the two retention times and calculating M_p using the second of the equations. This yields an error of approximately 10% in the quoted values of peak molecular weight.

Figure 2.2 shows the g.p.c. trace for polyaniline prepared at -27.5°C.

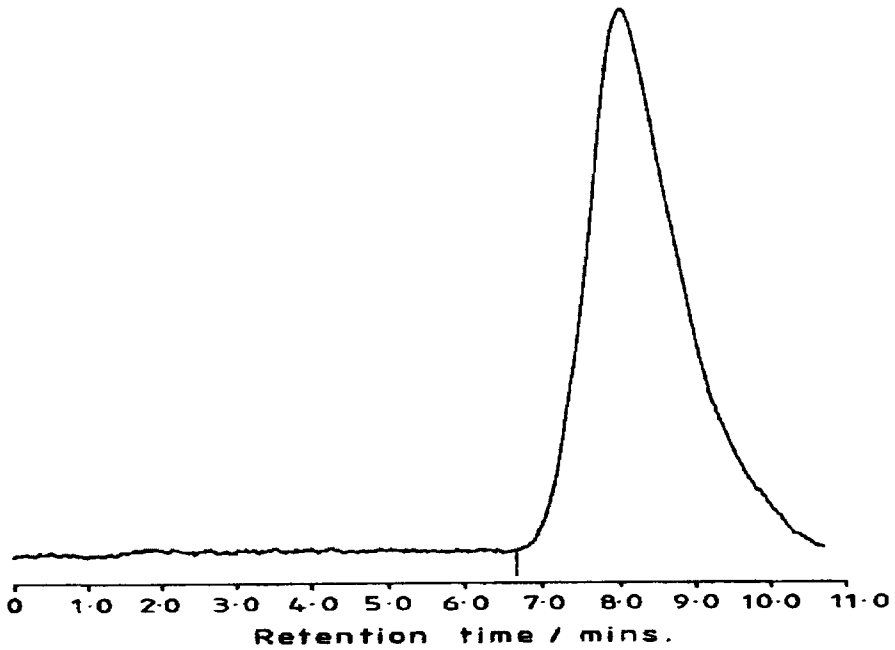

Figure 2.2: g.p.c. trace of polyaniline sample prepared at -27.5°C

The weight average, M_w, and number average, M_n, molecular weights were calculated by:

1. dividing the space under the chromatogram into equal segments,
2. measuring the heights from the baseline to the curve
3. calculating the corresponding molecular weight for each line

From these values, the molecular weights are determined by:

$$M_w = \frac{\sum h_i M_i}{\sum h_i} \qquad \text{and}$$

$$M_n = \frac{\sum h_i}{\sum h_i / M_i}$$

where h_i = height from the baseline to the curve on the chromatogram

M_i = molecular weight corresponding to that retention time.

The values of M_w, M_n and the polydispersity, (M_w/M_n), are shown in table 2.3 as a function of reaction temperature.

Reaction Temperature / °C	M_p / Daltons	M_w / Daltons	M_n / Daltons	Polydispersity M_w / M_n
-35.0	135 000	166 000	19 100	8.6
-30.0	138 000	176 000	27 500	6.4
-27.5	145 000	190 000	31 700	6.0
-25.0	153 000	209 000	43 500	4.8
-22.5	142 000	178 000	25 400	7.0
-20.0	133 000	154 000	24 600	6.2
-15.0	137 000	159 000	26 800	5.9
-10.0	107 000	148 000	28 400	5.2
0	86 000	122 000	20 400	6.0
+18	19 400	29 700	4180	7.1

Table 2.3: Peak, weight-average and number-average molecular weights, and polydispersity for polyaniline as a function of reaction temperature.

It can be seen from the table that the polydispersity has a minimum value of 4.8 for the sample with the highest molecular weight (T= -25°C), and a maximum of 8.6 for samples prepared at -35°C. It is therefore evident that there is a large distribution in molecular weights for any particular batch of polyaniline. Although the molecular weights reported later in the chapter are peak values, the fact that the samples are not monodisperse must be taken into account. This polydispersity is likely to have a large effect upon the mechanical and electronic properties, which at present cannot be eliminated. A definitive analysis of the molecular weight dependence upon such properties will not be possible until the polydispersity can be reduced. The work reported here is viewed as an intermediate stage of analysis, which is likely to improve as polydispersity is reduced.

2.4 Preparation of Polyaniline

The polyaniline investigated in this work was of considerably higher molecular weight than that used previously[20]. One of the problems when comparing results from experiments by different research groups is that the materials are of different molecular weights and different purities, thus leading to differences in structure and behaviour. To make this work self-contained, the exact preparation procedure for the polyaniline investigated for this thesis is reported. It is stressed, however, that the experimental work to determine the effects of different parameters upon molecular weight was not carried out by the author.

2.4.1 Preparation of low molecular weight polyaniline at room temperature

A typical method of producing polyaniline with average molecular weight of approximately 20 000 was as follows:

AnalaR aniline [9.313g (0.100 moles)] was added to AnalaR HCl (100g of 1M) solution and the pH adjusted to 1.0 by the addition of further HCl. AnalaR $(NH_4)_2S_2O_8$ [28.52g (0.125 moles)] was made up to 80g with distilled water and added to the reaction solution which was being stirred at room temperature. The reaction mixture was filtered and washed after 30 minutes with 10 x 200ml of distilled water. It was then deprotonated by stirring for 24 hours in 100ml of 33% aqueous ammonia solution, refiltered and washed with 8 x 200ml of water followed by 2 x 200ml of isopropyl alcohol. Finally it was dried under vacuum at 60°C to give a dark blue powder.

2.4.2 Preparation of high molecular weight polyaniline

The molecular weight of polyaniline depends on many parameters. In order to determine ways of obtaining the highest possible molecular weight, the following parameters were varied:

1. reaction temperature

2. solution pH at the start of the reaction
3. molar ratio of oxidant : aniline
4. oxidant addition time
5. total reaction time

The effects of these parameters will briefly be described.

1. Effect of temperature on molecular weight

In order to gauge the effect of temperature on molecular weight, the same synthetic procedure for preparing low molecular weight polyaniline was followed, but the reaction temperatures were varied between 0°C and -35°C. To prevent the mixture from freezing, lithium chloride was added during the process. Longer oxidant addition times of $14\frac{1}{2}$ hours and reaction times of 46 hours were used for all the reactions. The starting pH of the reaction mixture was adjusted to +1.0 after addition of the lithium chloride to the solution of aniline in hydrochloric acid. Table 2.4 shows the results for the reactions at different temperatures.

reaction temperature °C	weight % Li Cl	% yield of emeraldine base	% chlorine in emeraldine base	molecular weight (Daltons)
+18	0	93.0	0.42	19,400 ± 1000
0	0	89.6	0.23	86,000 ± 10,000
-10.0	8.65	92.1	0.41	107,000 ± 9000
-15.0	11.29	92.9	0.54	137,000 ± 9,000
-20.0	13.54	94.2	0.88	133,000 ± 10,000
-22.5	14.69	93.8	1.19	142,000 ± 9,000
-25.0	15.96	97.5	0.91	153,000 ± 9,000
-27.5	17.40	100.5	1.38	145,000 ± 9,000
-30.0	19.09	94.9	1.38	138,000 ± 7,000
-35.0	23.47	89.9	2.33	135,000 ± 7,000

Table 2.4: Values of salt concentration, percent yield, chlorine content and molecular weight for polyaniline samples prepared at various reaction temperatures[3].

Figure 2.3 shows graphically the effect of reaction temperature on molecular weight.

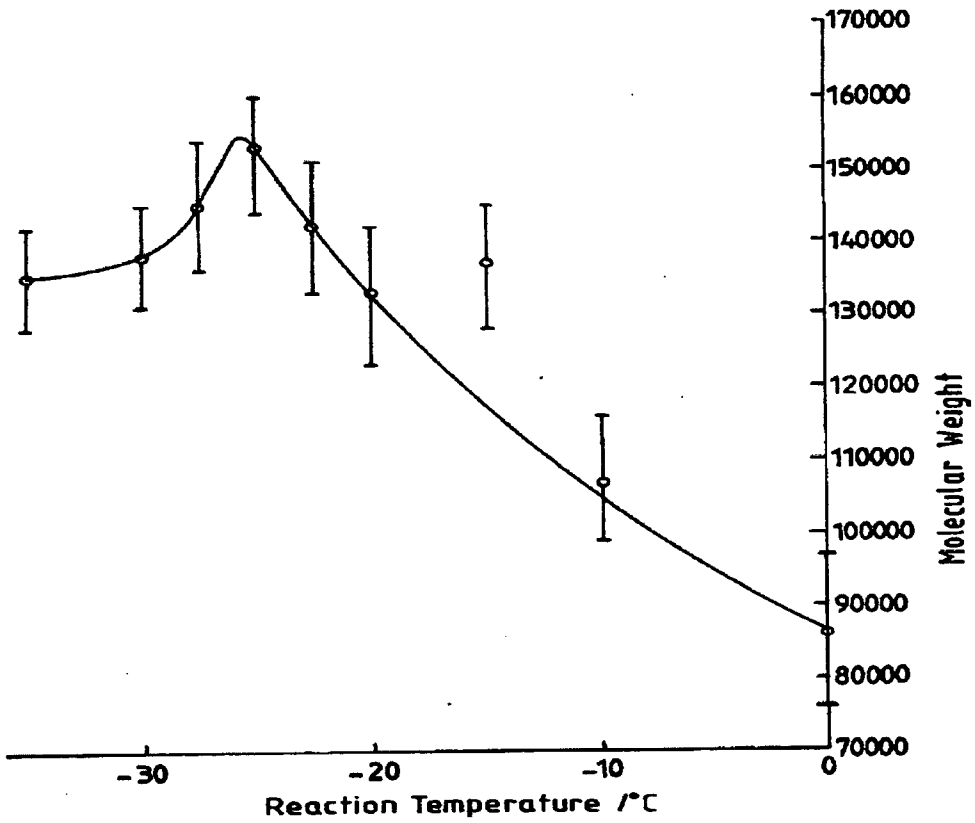

Figure 2.3 Effect of reaction temperature on molecular weight[3].

The graph shows that the highest molecular weight is obtained at -26 ± 1°C. This is approximately the same temperature that results in maximum yield, as can be seen from Table 2.4. The fact that the maximum yield is measured to be over 100% indicates that there may be a small amount of ring chlorination / sulphonation present.

2. Effect of solution pH at the start of the reaction

The effect of pH on the molecular weight was gauged by varying pH values from -0.1 to +3.0. Figure 2.4 shows the variation in molecular weight with these values of pH.

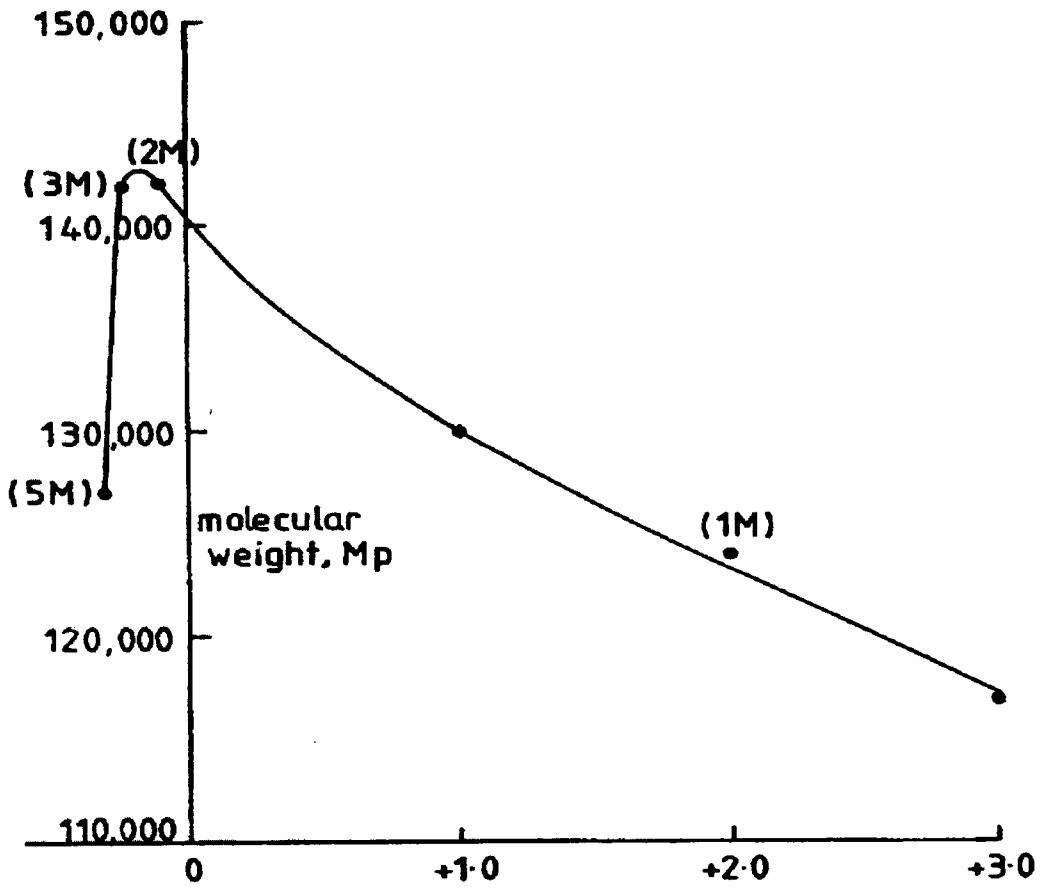

Figure 2.4 Effect of pH on molecular weight[3].

It can be seen from the graph that the highest molecular weight is obtained from aniline dissolved in 2-3 M HCl. However, it is found that the percent by weight of chlorine at the start of the reaction (i.e. ring chlorination) increases rapidly in anything stronger than 2M HCl. It is found in fact that the optimum starting pH as a function of ring chlorination is between +1.0 and +2.0.

3. Effect of molar ratio of oxidant to aniline

The variation in molecular weight with molar ratio of oxidant to aniline is shown in figure 2.5.

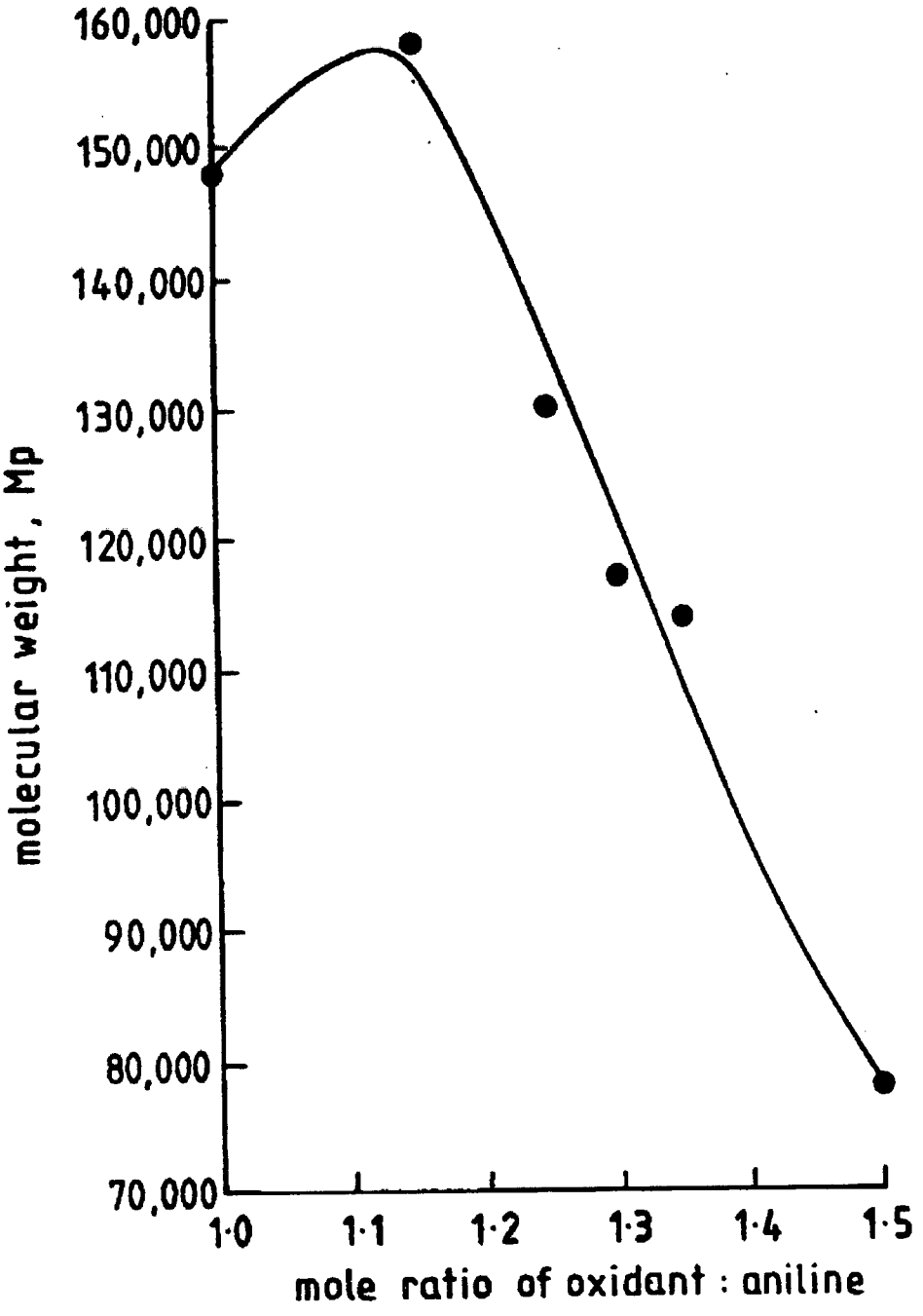

Figure 2.5 Graph of molecular weight versus molar ratio of oxidant:aniline for reactions at -26°C.[3]

The graph shows that the maximum molecular weight occurs with a ratio of between 1.10 and 1.15:1. It has also been found that the amount of ring chlorination rises steadily above a ratio of about 1.35:1 which corresponds to a decrease in yield, figure 2.6.

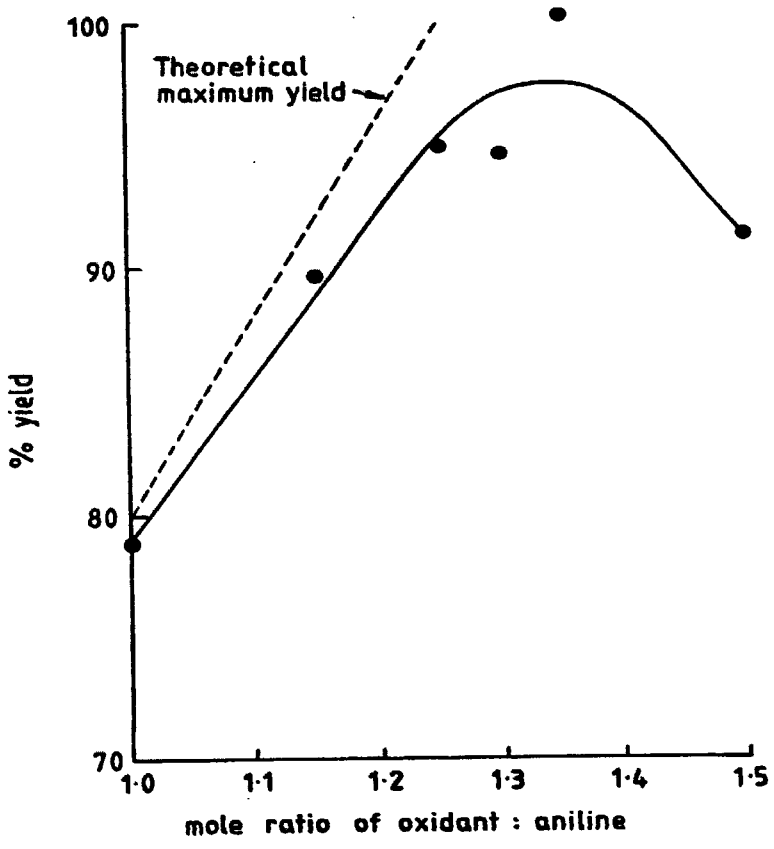

Figure 2.6. Graph of percent yield versus molar ratio of oxidant:aniline for reactions at -26°C.[3]

4. Effect of oxidant addition time

The oxidant addition times were varied from instantaneous addition to 36 hours at a temperature of -26°C. It was found that the molecular weight increased by about 25 per cent for oxidant addition time of 36 hours compared with instantaneous addition. The yield was also found to increase with increasing oxidant addition time.

5. Effect of total reaction time

The reaction times were varied from 3 to 90 hours at a temperature of -26°C, with the oxidant addition time remaining instantaneous in each case. It was found that the molecular weight and per cent yield increased only slightly with time, after most of the aniline had polymerised. It was also found that the rate of polymerisation is temperature

dependent, as shown by the low molecular weight and per cent yield for the reaction stopped after three hours, Table 2.5.

total reaction time / hours	% yield of emeraldine base	molecular weight (Daltons)
3	18.7	24,000
15	87.6	119,000
45	89.5	110,000
90	91.6	122,000

Table 2.5: Per cent yield and molecular weight for polyaniline samples prepared at -26°C as a function of reaction time (instant oxidant addition)[3].

2.5 Preparation of emeraldine base/NMP films

One of the major advantages of polyaniline over other conducting polymers is its processibilty in the 'conjugated' form. Angelopoulos et al[8,9] found that the emeraldine base form is soluble in the highly polar N-methyl-2-pyrrolidone (NMP), figure 2.7.

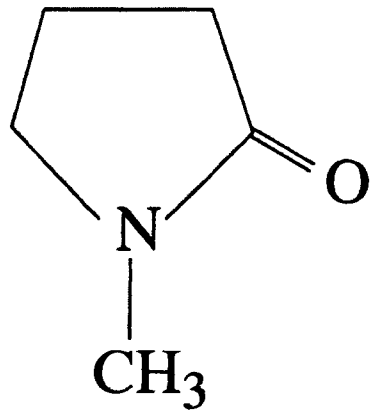

Figure 2.7. N-methyl-2-pyrrolidone

The degree of solubility of polyaniline in NMP is, however, dependent upon the weight ratio of the polymer to the solvent[10]. A solution made up of 2% polyaniline to 98% NMP will be very watery, whilst one of 15% polyaniline will be closer to a gel[2].

The preparation of polyaniline films involves the following steps:

a. dissolve the emeraldine base in NMP.
b. deposit a measured amount of the solution onto glass slides.
c. remove excess solvent by putting films in a vacuum oven until just dry.
d. peel films off glass slides.

An important consideration when preparing films of polyaniline is to ensure that the quality of these films is as high as possible. Homogeneity is a very desirable property. The ability to perform meaningful experiments on the samples is highly dependent upon the quality of the films. Therefore much of the initial work for this research was spent trying to perfect as much as possible the film quality.

The main controllable properties that were varied in order to prepare films of high quality were the following:

a. per cent weight solution of polyaniline in NMP.
b. weight of solution per cm^2 deposited onto glass slides.
c. temperature of vacuum oven.
d. degree of vacuum.

It was found that by following the steps below films of high homogeneity and thus suitable for further investigation could be formed:

EB powder (2.10g) was added to NMP (50g) in a boiling tube to give a 4% by weight polymer solution. The solution was then mixed in a Junke and Kenkel Ultra-Turrax homogeniser at 20 000 rpm to break down any lumps within the mixture. In order to remove further any smaller lumps the mixture was then placed in an Eppendorf Hermle Z320 centrifuge which was spun at 4000 rpm for 1 hour. The mixture was then decanted onto a number of glass slides which had been washed in water and acetone. Approximately 0.07 g/cm^2 was placed onto glass slides of dimensions 7cm x 4cm. The samples were then dried in a vacuum oven at 60°C under a vacuum of 20mm Hg. This

drying process lasted approximately 4 hours. The reason for using the values quoted above shall now be explained in more detail.

As mentioned earlier, the percentage weight of polyaniline to NMP has a substantial effect upon the viscosity of the solution formed. It was found that a 4% by weight mixture provided a solution which was of moderate viscosity allowing easy slide coverage and producing high quality films. The 4% mixture was also found to be the most successful EB/NMP mixture for orientation of the films. Furthermore, care had to be taken when homogenising the mixture to ensure that it did not gel as a result of heating. Although these gels are becoming increasingly interesting to polymer scientists[11,12], they are not suited to producing thin films. To dry the films a vacuum oven was maintained at a fairly low temperature and vacuum in order to remove slowly excess solvent from the samples. It was found that if either of these parameters was too high then it was much more difficult to control the removal of solvent, a factor which is essential to successful orientation. Also, if the vacuum or temperature is too high, the mixture will tend to 'bubble' whilst excess solvent is being removed. This creates small potholes with diameters of a few millimetres in the surface of the samples, thus losing the homogeneity and making further processing of the films (eg. orientation) very difficult to achieve.

The above procedure has described a method for obtaining emeraldine base / NMP films of high homogeneity with thicknesses of approximately 25 to 30 microns. Subsequent doping of these films by immersion in aqueous HCl transforms the samples to the conducting emeraldine salt form[19]. The formation of these films has been undertaken with subsequent orientation in mind. Thus, optimising film preparation and film orientation have been mutually inclusive events and a great deal of time was spent in finding the conditions which produced high quality films whilst at the same time maximising the potential for orientation. The steps outlined above have to some extent achieved this, but are by no means exhaustive. With more time there is little doubt that films of higher quality could be prepared and thus higher orientations achieved. A procedure for orienting the films is described in the following section.

2.6 Orientation of films

2.6.1 Stretch rig

This section describes a method for achieving elongations of EB films to the order of 700%. The main reason for orientation of the films is the increase in conductivity along the stretch direction compared to an unstretched (as-cast) sample.

To orient polyaniline films a stretch rig based on a design by Townsend[13] for the orientation of polyacetylene films was built. The apparatus is shown in figure 2.8.

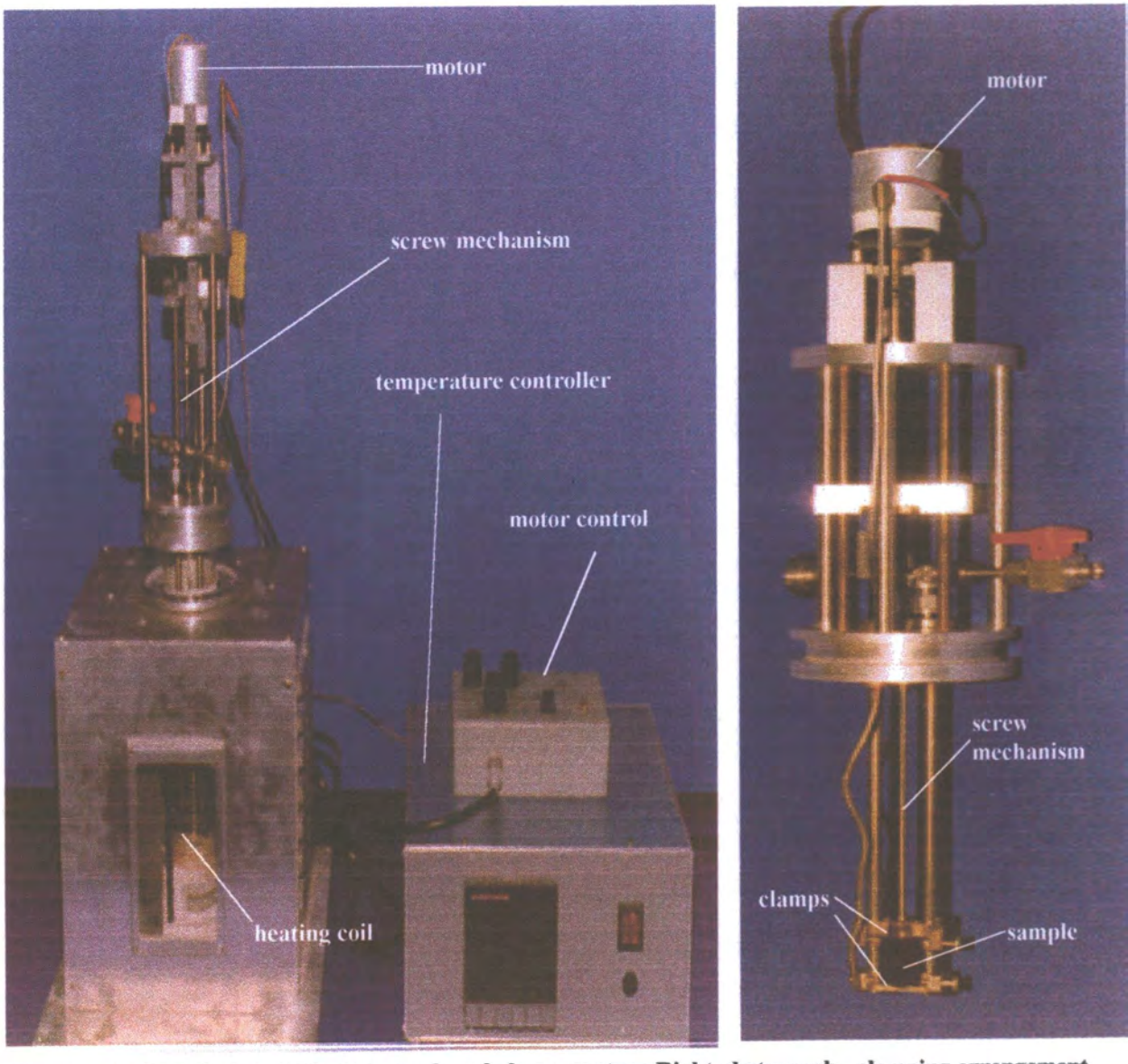

Figure 2.8: Stretch rig: Left photograph - whole apparatus ; Right photograph - clamping arrangement

To stretch an as-cast film, the ends of the sample are wound around two metal clamps. These clamps are firstly wound with insulating card to prevent the ends of the sample being at a higher temperature than the middle. The uppermost clamp is attached to a screw mechanism and a motor which allows it to be pulled vertically away from the lower roller, thus extending the sample. The rate of extension can be varied from 0 to 500 mm per minute by a motor control. The sample arrangement is mounted in a cylindrical glass vessel, around which a d.c. resistive coil is wound. The coil is kept in place by heating cement, with a narrow rectangular portion left uncovered to act as a viewing window. The coil allows the temperature of the specimen to be varied from room temperature to 300°C, using a Eurotherm Series 900 temperature controller. The temperature of the sample was measured using a thermocouple placed as closely as possible to the sample.

2.6.2 Manipulation of films to increase orientation

Methods to maximise orientation of EB films was the initial objective of this project. To achieve this a number of possible orientation parameters were varied. The parameters which were varied included film fabrication parameters which were mentioned in the previous section, temperature at which the samples were oriented, speed of orientation and dimensions of the samples. Initially, many samples were oriented under identical conditions to gauge the consistency of the results. A typical set of films prepared and oriented under identical conditions gave the following results, outlined in Table 2.6.

initial length l_1 (mm)	length at break l_2 (mm)	change in length, (l_2-l_1) (mm)	elongation to break $(l_2-l_1 / l_1) \times 100\%$
10	15	5	50
10	24	14	140
10	29	19	190
10	18	8	80
10	20	10	100

Table 2.6: Results of orientation of samples under identical conditions

It can be seen from the table that there is no consistency in the values obtained even if the orientation conditions remain the same throughout. This poses a considerable problem, but also suggests that there is something other than the parameters mentioned previously causing the samples to fracture. In fact, there are two main factors which lead to the apparent random fracturing of EB films. Firstly, it is clear that orientation of the films must be dependent upon the amount of NMP in the samples. The problem that arises is that it is impossible to achieve completely uniform removal of excess solvent from the samples in the vacuum oven. In practice it is usually found that the samples dry from the edges inwards. Thus, even when the edges of the films are just dry, the samples must stay in the vacuum oven until the remaining excess solvent is removed. The effect of this is to 'over-dry' certain portions of the EB films - in other words, more NMP is removed from the edges of the films than the middle. This behaviour can be seen by considering a thermogram of portions of film perimeters compared with film centres, figure 2.9.

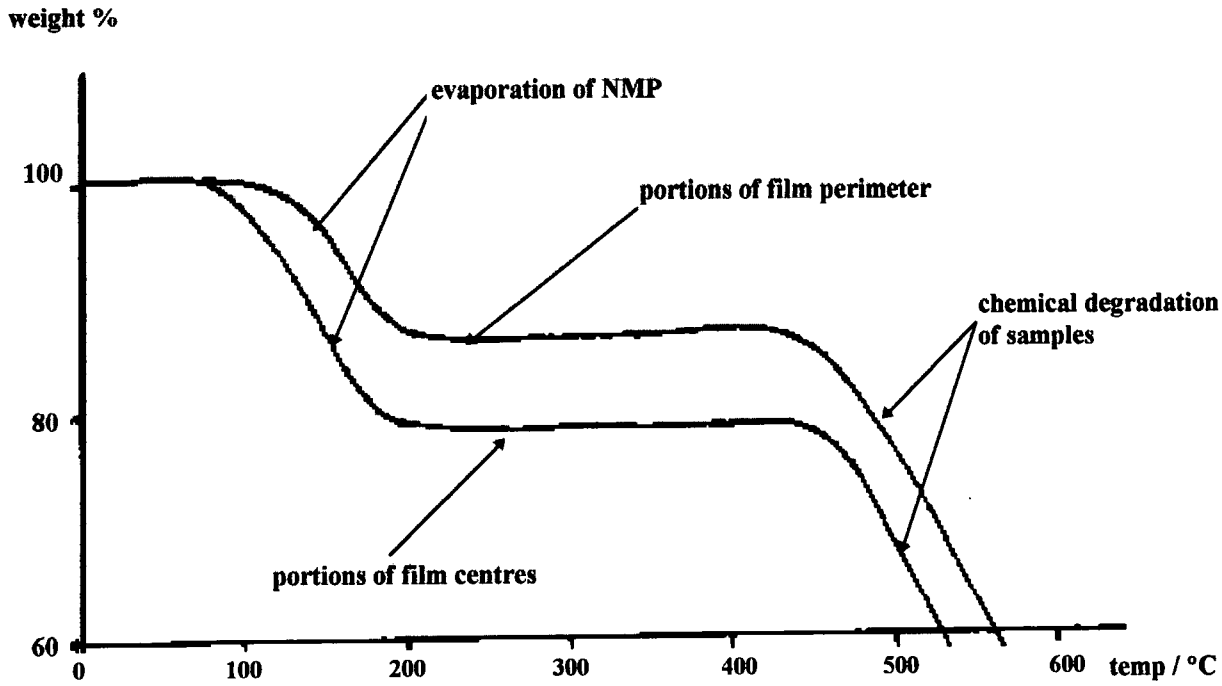

Figure 2.9: Thermograms to show differences in percentage of NMP for different portions of EB films.

The diagram shows the percentage weight loss of the samples as a function of temperature. The instrument used for this analysis was a Stanton-Redcroft TG-770, which allows samples to be studied over a temperature range from room temperature to 700°C. The evaporation of NMP from the samples occurs between approximately 100 and 200°C, as can be seen in the diagram. It can also be seen that the percentage weight loss of outer portions of films is indeed less than that of inner portions, thus revealing the differences in NMP content between different portions of the films.

Secondly, it was observed when stretching the films that in the majority of cases the films tended to tear from the edges rather than fracture. This was because although care was taken in making the edges of the films as even as possible, it was still not possible to remove completely tiny serrations. Therefore the edges were persistently the weakest part of the films. The problem was solved by folding the edges of the films before orientation was attempted. The beneficial consequence of this was two-fold: firstly, the problem of serrated edges is completely removed; secondly, orientation of the films causes a change in shape[20]. This change produces internal stresses which are predominant at the edges. It was found, however, that by having the edges folded the degree to which the shape is changed is reduced. Consequently, the likelihood of sample fracture at these points is also reduced.

2.6.3 Orientation procedure

To obtain consistent elongations up to 700% strain the following procedure was followed.

1. Prepare EB films as described in section 2.5.
2. Cut films to dimensions 6cm x 2.5cm.
3. Fold edges of film to dimensions shown in figure 2.10.
4. Set stretch rig heater to 110°C
5. When set temperature is reached, stretch sample at approximately 20mm/min.

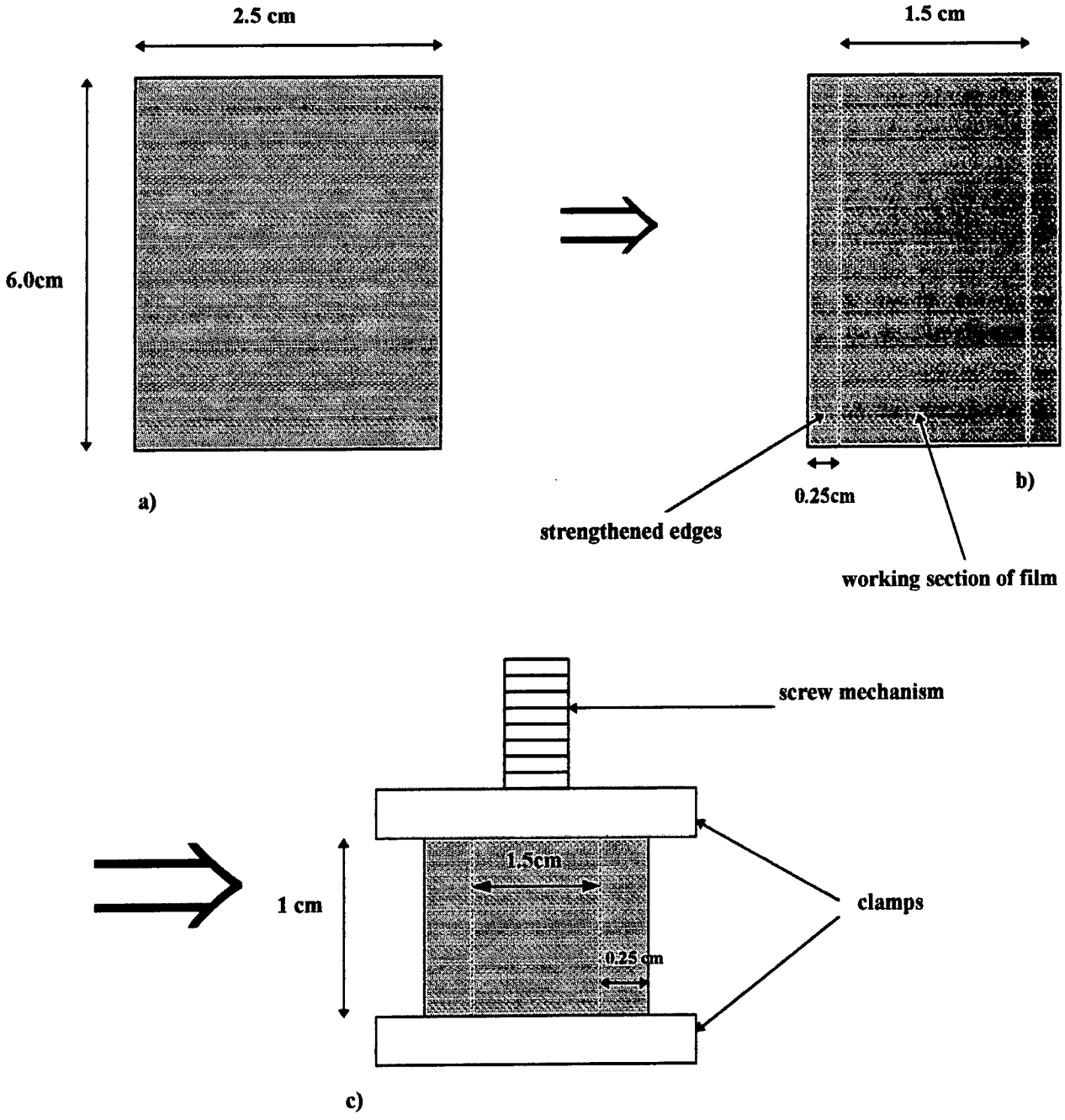

Figure 2.10: Manipulation of samples before orientation.
a) initial dimensions of film
b) edges folded
c) dimensions of sample in stretch rig

When the required elongation is reached, the samples are maintained under the applied stress and allowed to cool. They are then carefully removed from the stretching apparatus. The folded edges are cut off with a scalpel, resulting in the desired oriented films available for further investigation.

2.6.4 Doping the Samples

It is found that full doping of emeraldine base to emeraldine salt is achieved when 50% of all the nitrogens, i.e. the imine units, become protonated. The most common protonic acid for this purpose is aqueous HCl. Figure 2.11 shows the graph of conductivity versus acid concentration for the aqueous HCl doping of NMP cast films measured by Kromack et al[22].

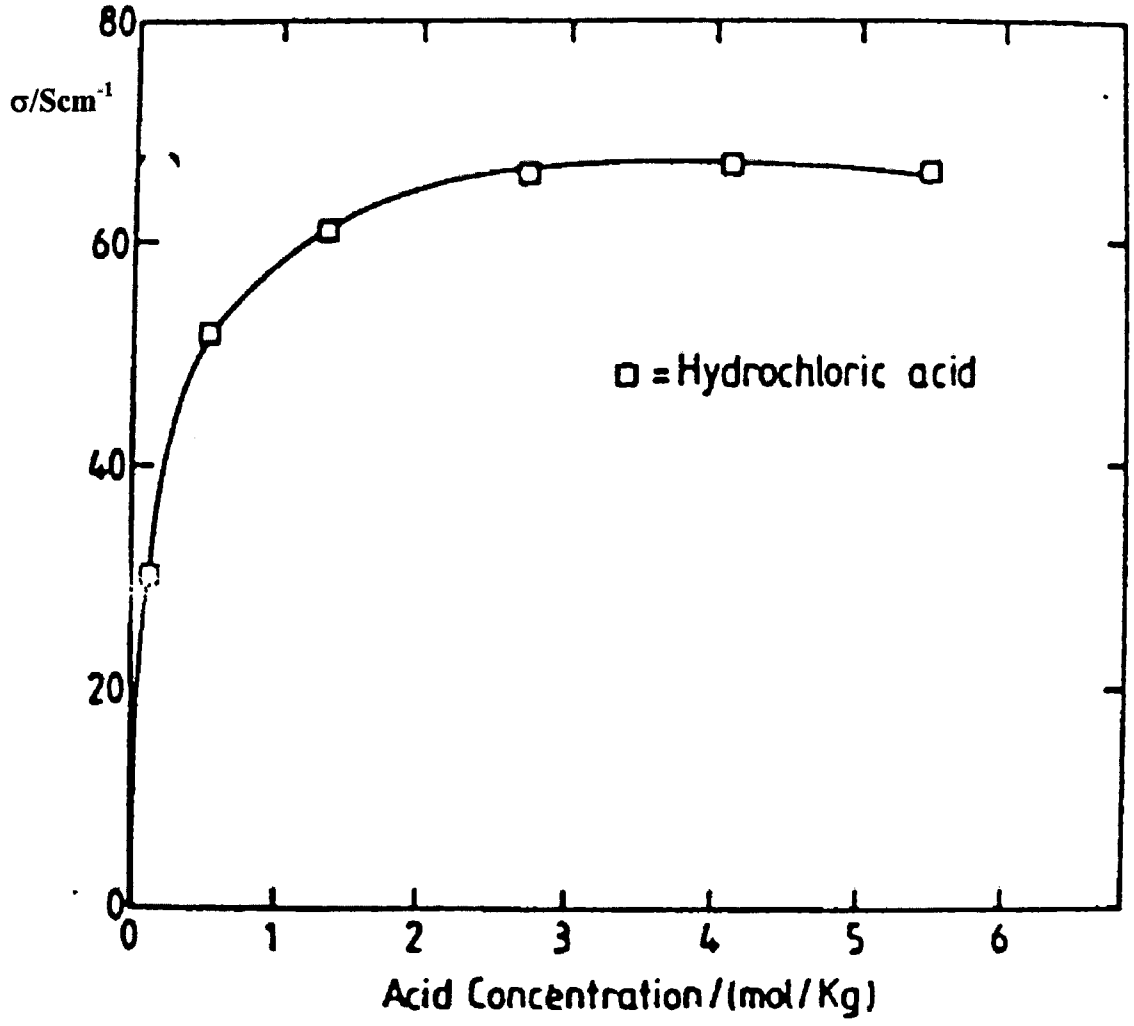

Figure 2.11: Effect of HCl dopant concentration on conductivity.

Thus, for full protonation HCl of at least 1M should be used.

For the measurements reported in this work the samples were immersed in 1M HCl for 4 hours. They were then 'dried' with filter paper and cut into the required dimensions for conductivity measurements.

2.7 Conductivity Measurements

2.7.1 Montgomery Technique to measure conductivity of oriented samples

A procedure for measuring the conductivity of anisotropic samples was first described by Montgomery[14], who made a mathematical calculation of the electric field distribution in a rectangular prism when a current is passed between neighbouring corners. The technique is particularly suited to the measurement of the conductivity of oriented polyaniline films as it provides a method for measuring simultaneously the components of conductivity parallel and perpendicular to the stretch direction. Furthermore, the paper deals specifically with the case when one of the dimensions of the sample is much smaller than the other two, as is the case for thin films.

Figure 2.12 shows a rectangular sample with dimensions l_1 and l_2, and of thickness t.

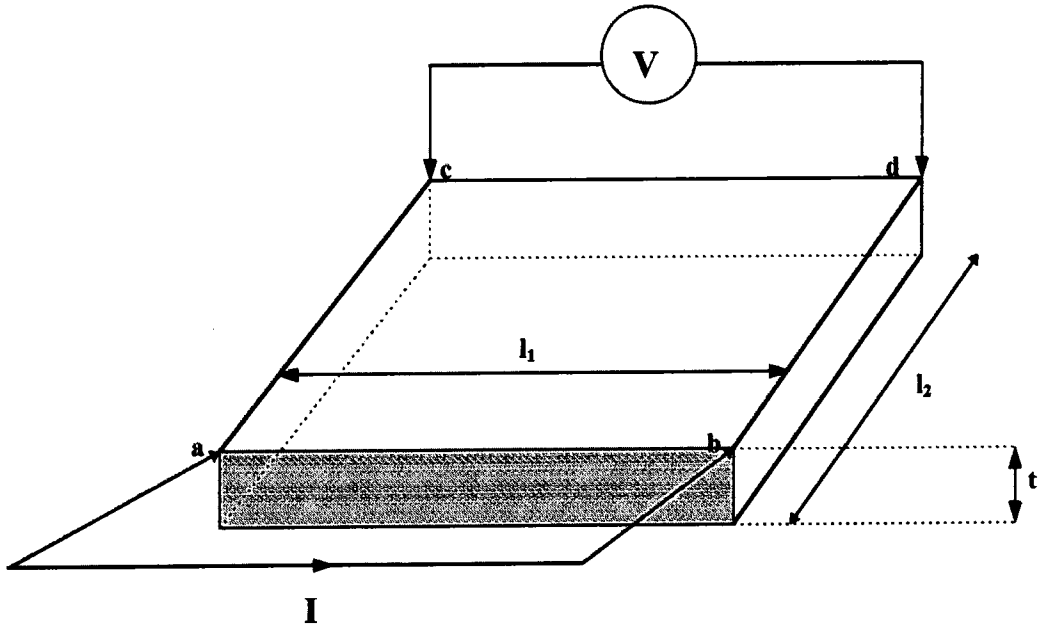

Figure 2.12: Electrical contact arrangement for conductivity measurements of polyaniline samples.

Consider the rectangular sample depicted above. The dimensions of the sample are l_1, l_2 and t, where t is the thickness of the sample. It is assumed that $t << (l_1 l_2)^{\frac{1}{2}}$.

When a current I is applied across points a and b, the associated voltage V across points c and d is measured. Thus, the resistance R_1 for the configuration depicted can be easily

evaluated. Similarly, another value of resistance R_2, can be obtained for the situation when all the voltage and current contacts are rotated by 90° from the positions shown in figure 2.12. The simplest case occurs for isotropic samples, where the conductivity of the material is given by:

$$\sigma = [HR_1t]^{-1}$$

The parameter H is a function of l_2/l_1. The dependence of H upon this ratio is shown in figure 2.13.

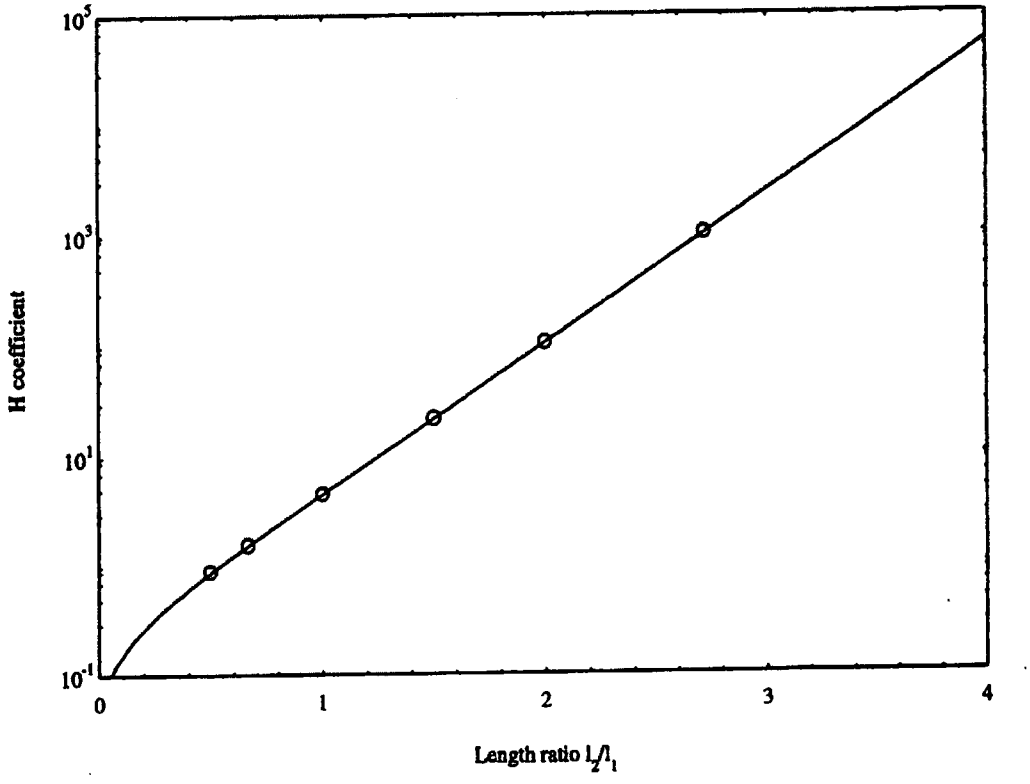

Figure 2.13: Relationship between H and ratio l_2/l_1 used for Montgomery measurement of electrical conductivity[14].

For the case of a square sample, i.e. $l_1=l_2$, H has the value 4.531.

For anisotropic samples the analysis is modified. The samples are arranged so that the direction of orientation is parallel to one side of the rectangle shown in figure 2.12. Two resistances R_1 and R_2 can again be obtained in the same manner as before, but in

this case one value will correspond to the conductivity parallel to the direction of orientation, and the other one perpendicular to this direction. In order to find these values of conductivity an effective dimension l_2'/l_1' must be defined, which is related to the ratio R_2/R_1. The relationship is shown in figure 2.14.

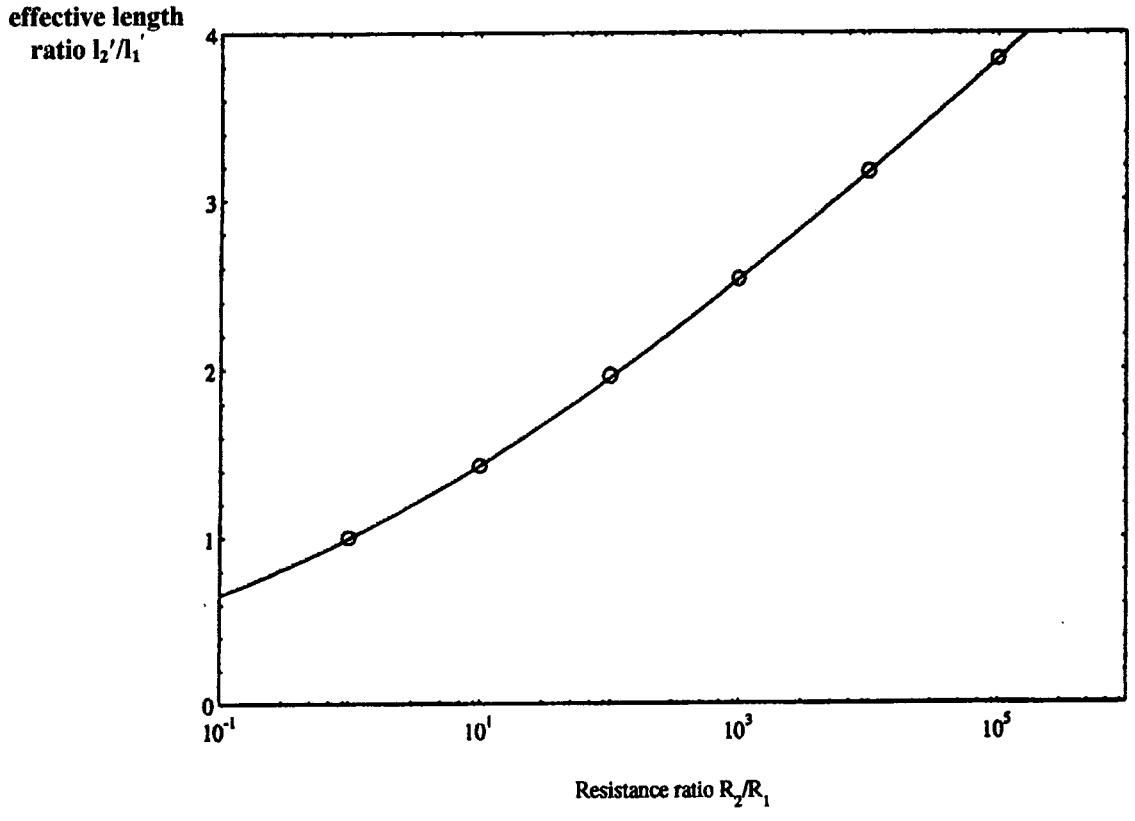

Figure 2.14: Variation of effective length ratio with resistance ratio for anisotropic samples. (From paper by Montgomery[14])

It is also necessary to evaluate a new value for H from the value obtained for l_2'/l_1', as described earlier for isotropic samples.

The conductivities in the directions parallel and perpendicular to orientation can then be evaluated by substitution of the appropriate quantities into the following equations:

$$\sigma_1 = H\,(l_2'/l_1')\,R_1 t$$

$$\sigma_2 = H\,(l_1'/l_2')\,R_2 t$$

Thus, measurements of the conductivity of doped emeraldine salt samples can be easily evaluated using the method described, and the effect of orientation upon the conductivity assessed.

2.7.2 Experimental

To measure the conductivity of ES samples a probe stage was built with four sprung gold probe tips arranged in a 6mm by 6mm square configuration. The reasons for using gold tips were twofold: firstly, gold does not react chemically with polyaniline at room temperature, and therefore degradation of the polymer does not occur; secondly, gold provides low contact resistance between the sample and the probe, thus minimising any disturbance to the measured values of conductivity which are inevitable when taking readings.

The test sample was cut into a square with dimensions as near as possible to the dimensions of the test probe. Its thickness was then carefully measured using a digital micrometer. The probe was connected to a Keithley 220 constant current source and a Keithley digital voltmeter (model 2000). The current was maintained at 1.0mA to minimise Joule heating which may lead to dedoping of the sample surface. All the connections were made via a four-way switch unit, which allowed 90° rotation of the voltage and current connections, thus allowing measurements of conductivity both parallel and perpendicular to the direction of orientation without having to disturb the sample.

2.7.3 Results

Table 2.7 shows the measured values of conductivity both parallel and perpendicular to the stretch direction for samples oriented between 0 and 700%.

% strain	$V_{//}$ / mV	$V_{\perp}$ / mV	t / cm	$\sigma_{//}$ / Scm^{-1}	$\sigma_{\perp}$ / Scm^{-1}	$\sigma_{//}/\sigma_{\perp}$
0	0.541	0.541	0.0040	102.2	102.2	1.00
100	0.106	0.876	0.0035	238.7	122.5	1.95
200	0.084	0.984	0.0033	267.6	126.1	2.12
300	0.054	1.032	0.0031	341.5	137.9	2.48
400	0.035	0.876	0.0030	468.9	175.9	2.67
500	0.018	1.117	0.0026	619.2	183.0	3.38
600	0.014	1.146	0.0025	698.6	192.6	3.63
700	0.045	0.948	0.0024	501.7	197.3	2.54

Table 2.7: Measured values of conductivity for stretch-oriented ES samples.

Figure 2.15 shows the measured values of conductivity plotted against % strain.

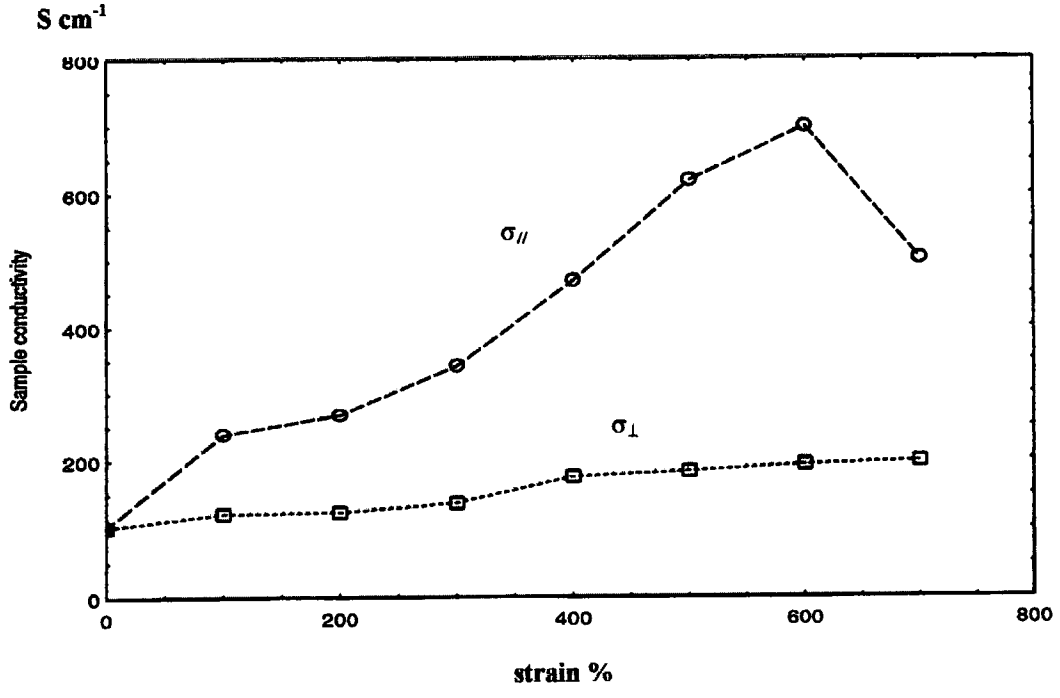

Figure 2.15: Variation in conductivity with elongation for ES films.

Figure 2.16 shows the electrical anisotropy $\sigma_{//} / \sigma_{\perp}$ as a function of strain.

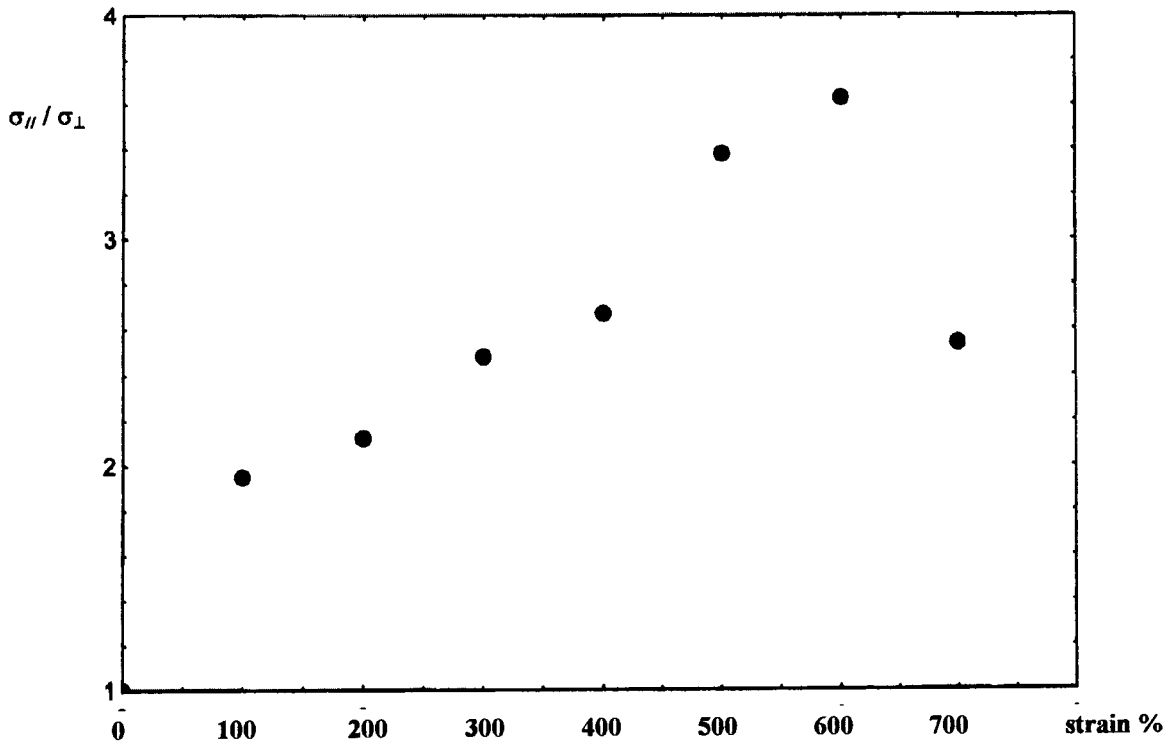

Figure 2.16: Electrical anisotropy versus strain for ES samples

The accuracy of the measurements is mainly limited by the degree of accuracy attainable in measuring the thickness of the samples. The thickness was measured using a digital micrometer which has a resolution of 1μm. It can be seen from table 2.7 that the thickness of samples varied from 40μm to 24 μm. This introduces a maximum error of approximately 5 per cent in the conductivity measurements. A further error is introduced by the necessity to evaluate the parameter H from the ratio of the dimensions of the sample, as described by Montgomery[14]. To minimise this error the curves were modelled numerically. The curve relating H to (l_2/ l_1) was found to be of the form[23]:

$$y = a + b \exp(x) + c (\exp(x))^2 + d (\exp(x))^3 + f (\exp(x))^4$$

and the appropriate values for the constants evaluated. This enables the values of H to be found to high accuracy (< 1%).

Thus the overriding source of error can be attributed to sample thickness.

It must be stressed that the conductivity measurements reported in this thesis are the highest measured values for each degree of elongation. Many samples stretched to 600% elongation, for example, exhibited conductivities substantially lower than 700 Scm^{-1}. A satisfactory explanation for this lack of consistency is difficult to make, but the most likely reason is due to inhomogeneous doping of the polymer. Uniformity of doping is affected by factors such as molecular weight, crystallinity and morphology of the polymer. A typical emeraldine base sample has a distribution of molecular weights, both crystalline and amorphous regions, and subtle differences in morphology (for example, density) from point to point. It is therefore not at all surprising that not only will different samples exhibit different conductivities, but also different parts of any one particular sample. This has indeed been shown to be the case for many conducting polymers[21] and is one of the major obstacles facing research groups in this field. However, in order to attempt to analyse quantitatively the results obtained, it is assumed that the values of conductivity quoted correspond to regions of the polymer where maximum doping has occurred.

2.7.4 Discussion and Analysis of Results

It can be seen from the previous diagrams that the increase in strain has a considerable effect upon the conductivity of polyaniline samples. The maximum value of conductivity was measured to be approximately 700 Scm^{-1}, with an anisotropy of almost 4. The conductivity in the direction of orientation is seen to rise almost linearly with percentage elongation up to 600%. Similar results have been found by other groups[15,16]. It is also observed, however, that the maximum measured conductivity does not correspond with the maximum strain of 700%. This is possibly due to the morphological variations mentioned earlier.

In contrast to these reports, however, the conductivity perpendicular to direction of orientation is also seen to increase slightly. This phenomenon cannot be explained satisfactorily from the available data. It is possible that the increase is due to the increased difficulty in aligning the probe with the samples, especially at high elongations. The probe may then measure a component of the parallel conductivity when it is positioned to measure perpendicular conductivity. It is assumed that this is the most

likely reason for the measured increase in perpendicular conductivity, and that in real terms the value remains essentially unaltered as a function of elongation.

These results can be compared with those of other groups. The results of Wan et al[15] show maximum measured conductivity of approximately 350 Scm^{-1} for a film elongated by 300%, figure 2.17. If it is assumed that the conductivity is indeed linearly proportional to the elongation, then simple extrapolation of Wan's data would give a conductivity of approximately 770 Scm^{-1} for a 600% strain sample. This is in fairly good agreement with the value of 700 Scm^{-1} for the samples made here at Durham.

The conductivity perpendicular to direction of orientation remains essentially constant, and it is therefore concluded that it is independent of strain. Again, this behaviour has been observed by other groups[15,16].

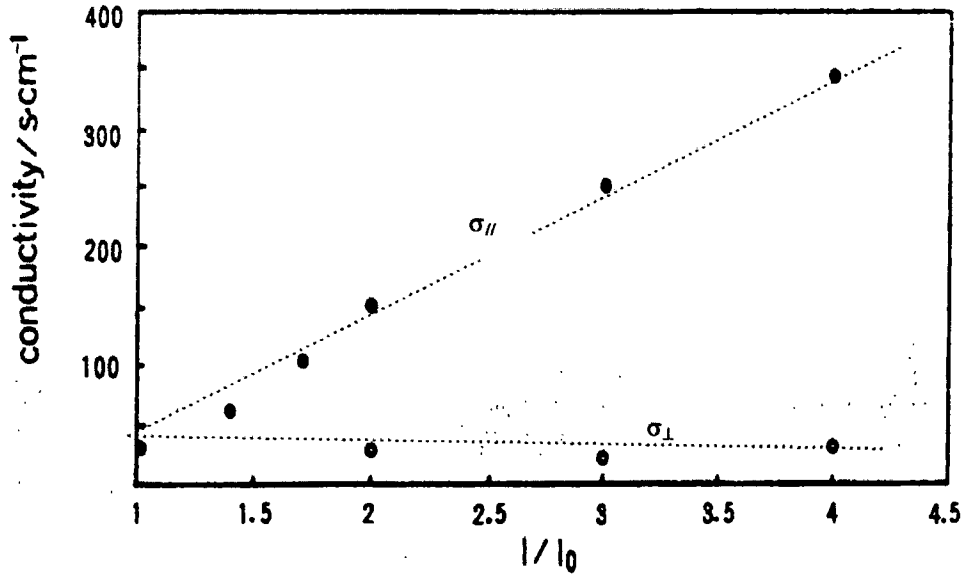

Figure 2.17 Variation of conductivity with strain (from the paper by Wan et al) Note: the definition of strain here is l/l_o, compared with the more usual definition of $\Delta l/l_o x100\%$. Thus, a value of 4 above is equivalent to 300% strain.

Wan et al have described a simple model of a series of chain resistance and interchain resistance to explain the enhanced conductivity of stretched polyaniline films[16]. The model is based on a number of experimental facts. For example, the temperature dependence of conductivity for conducting polymers shows semiconducting rather than metallic behaviour which obeys a variable range hopping model[17]. This has been

attributed to the contact resistance between conducting regions surrounded by insulating boundaries. Metallic behaviour is observed, however, if this resistance is removed by the shorted voltage compaction (VSC) method[18]. Thus, it is necessary to consider the interchain as well as intrachain contribution to conductivity. The paper shows that the enhanced conductivity is controlled mainly by the interchain conductivity and interchain coupling in stretched films. This can be seen by considering two equations for the conductivity. Wan et al found that the theoretical ratio of the conductivity of stretched samples, $\sigma'_{//}$, to unstretched, σ_o, was of the form:

$$[\sigma'_{//} / \sigma_o]_{theory} = f\ \sigma'_i / \sigma_i$$

where f is related to the interchain coupling of the system, σ'_i is the interchain contribution to conductivity in stretched samples, and σ_i is the interchain contribution to conductivity in unstretched samples. If we assume that the measured conductivity is linearly proportional to the degree of elongation of the samples, we have:

$$[\sigma_{//}]_{expt} = \sigma_o + (\alpha\ .\ \text{elongation})$$

Comparison of these two equations suggests a strong relationship between increase in conductivity for stretched films and increase in interchain coupling.

The above model provides a satisfactory explanation of the conduction mechanism in oriented polyaniline films. Conductivity measurements on samples stretched by up to 600% strain are commensurate with this description, and it can therefore be concluded that the increase in interchain coupling is one possible explanation for increases in conductivity along the stretch direction.

2.8 Summary

This chapter has described how emeraldine base polyaniline with molecular weight of the order of 150,000 Daltons was made. The effect of various control procedures during this preparation have been discussed. A method for producing homogeneous

EB/NMP films has been described and further manipulation of these films has allowed for elongations of up to 700% to be reproducibly attainable. The conductivity of these samples after doping in aqueous HCl has been measured and the relationship between conductivity and elongation assessed. Values of almost 700 Scm^{-1} for the conductivity in the direction parallel to elongation have been measured, but the conductivity has been found to vary at different points within a sample. Possible reasons for discrepancies in measured values of conductivity have been discussed.

References

1. S K Jeong, J S Suh, E J Oh, Y W Park, C Y Kim and A G MacDiarmid. *Synthetic Metals* **69**, (1995), pp171-172.

2. E J Oh, Y Min, J M Wiesinger, S K Manohar, E M Scherr, P J Prest, A G MacDiarmid and A J Epstein. *Synthetic Metals* **55-57**, (1993), p977-982.

3. P N Adams, P J Laughlin and A P Monkman. *Synthetic Metals* **76** (1996), 157.

4. P N Adams, D C Apperley and A P Monkman. *Polymer* **34**, no. 2, pp328-332 (1993)

5. E M Genies, A A Syed and C Tsintavis. *Mol. Cryst. Liq. Cryst*, **121**, (1985), 181-186.

6. A G MacDiarmid and A J Epstein. *Faraday Discuss. Chem. Soc.*, **88** (1989), 317-332.

7. E A Collins, J Vares and F W Billmeyer. *Experiments in Polymer Science* (1973) John Wiley and Sons, Inc.

8. M Angelopoulos, G E Asturias, S P Ermar, A Ray, E M Scherr, A G MacDiarmid, M Akhtar, Z Kiss and A J Epstein. *Mol. Cryst. Liq. Cryst.*, **160**, (1988), p151

9. M Angelopoulos, A Ray, A G MacDiarmid and A J Epstein. *Synth. Met.* **21** (1987) p21.

10. M Aldissi, *Advanced Materials*, 1993, vol.5, no. 1, pp60-62.

11. K Tzou and R V Gregory, *Synth. Met., Proceedings of ICSM*, 1992.

12. A G MacDiarmid, Y Min, E J Oh, E M Scherr, X Tang, J G Masters and A J Epstein. *Synth. Met. Proceedings of ICSM*, 1992.

13. P D Townsend, C M Pereira, D D C Bradley, M E Horton and R H Friend, *J. Phys. C*, **18**, (1985), L283.

14. H C Montgomery, *J. Appl. Phys.* **42** (1971) p2971.

15. H Y Hwang, S W Lee, I W Kim and H Lee. *Synth. Met.* **69** (1995) p225-226.

16. M X Wan, M Li, J C Li, Z X Liu. *Jour. Appl. Polym. Sci.* (1994), **53**, no.2 p131-139.

17. N F Mott and E A Davis, *Electronic Processes in Non-Crystalline Materials*, Clarendon Press, Oxford, 2nd ed., 1979. p34.

18. M Wan, Y Cao, J Li, W Zhou and S Li. Chin. *J. Polym. Sci.*, **9**, (3), p209 (1991).

19. M Wan, W Zhou, Y Li and J Liu. *Solid State Comm.* **81** no.4, pp313-316 (1992).

20. A J Milton, PhD Thesis, University of Durham, 1993.

21. *Polyacetylene* by J C W Chien. Publ. Academic Press Inc. (1987).

22. K R Kromack, M E Jozefowicz, J M Ginder, A J Epstein, R P McCall, G Du J M Leng, K Kim, C Li, Z H Wang, M A Druy, P J Glatkowski, E M Scherr and A G MacDiarmid. *Macromolecules*, **24**, 4157 (1991)

23. E R Holland. PhD Thesis. Durham University. (1995).

CHAPTER 3 MECHANICAL ANALYSIS

3.1 Introduction

This chapter reports the results obtained from a series of mechanical testing experiments with emeraldine base polyaniline films. The aim of the experiments was to observe the way in which the mechanical behaviour of the samples varied as a function of initial elongation (this shall be referred to as $e_{\%}$). Stress-strain relationships were obtained from samples with $e_{\%}$ varying from 0 to 700. The data was then analysed in an attempt to elucidate the effect of elongation upon the mechanical properties. The experiments were performed at BICC Communications Ltd., Helsby.

Due to the problems of inhomogeneous doping of emeraldine base to the salt form, and the brittle nature of salt samples, an investigation into the mechanical properties of ES films was not undertaken. Until homogeneous doping can be established it will be impossible to correlate the mechanical behaviour of ES samples with initial elongation.

3.2 Theory of Mechanical Properties

To analyse the mechanical behaviour of a substance, the material must be subjected to forces and the deformation of the material observed. The measured changes in the dimensions of the material as a function of the applied forces enable characterisation of their mechanical properties.

3.2.1 Stress and Strain

In general, the state of stress acting on a body must be defined using tensor notation[1]. The resultant strain can be a complicated process to describe, especially if the situation consists of a general type of deformation incorporating extension and compression in different directions. However, for the case of thin films, and especially when taking into account the nature of the stresses to which the films were subjected for this particular analysis, the situation can be greatly simplified. The main simplifications are as follows:

a. The stresses on the samples are considered to be tensile and one dimensional in nature, acting only in the vertical direction.
b. The change in the cross-sectional area of a sample is considered to be negligible.

The assumptions shall now be considered:

Figure 3.1 shows a typical elongated film under stress.

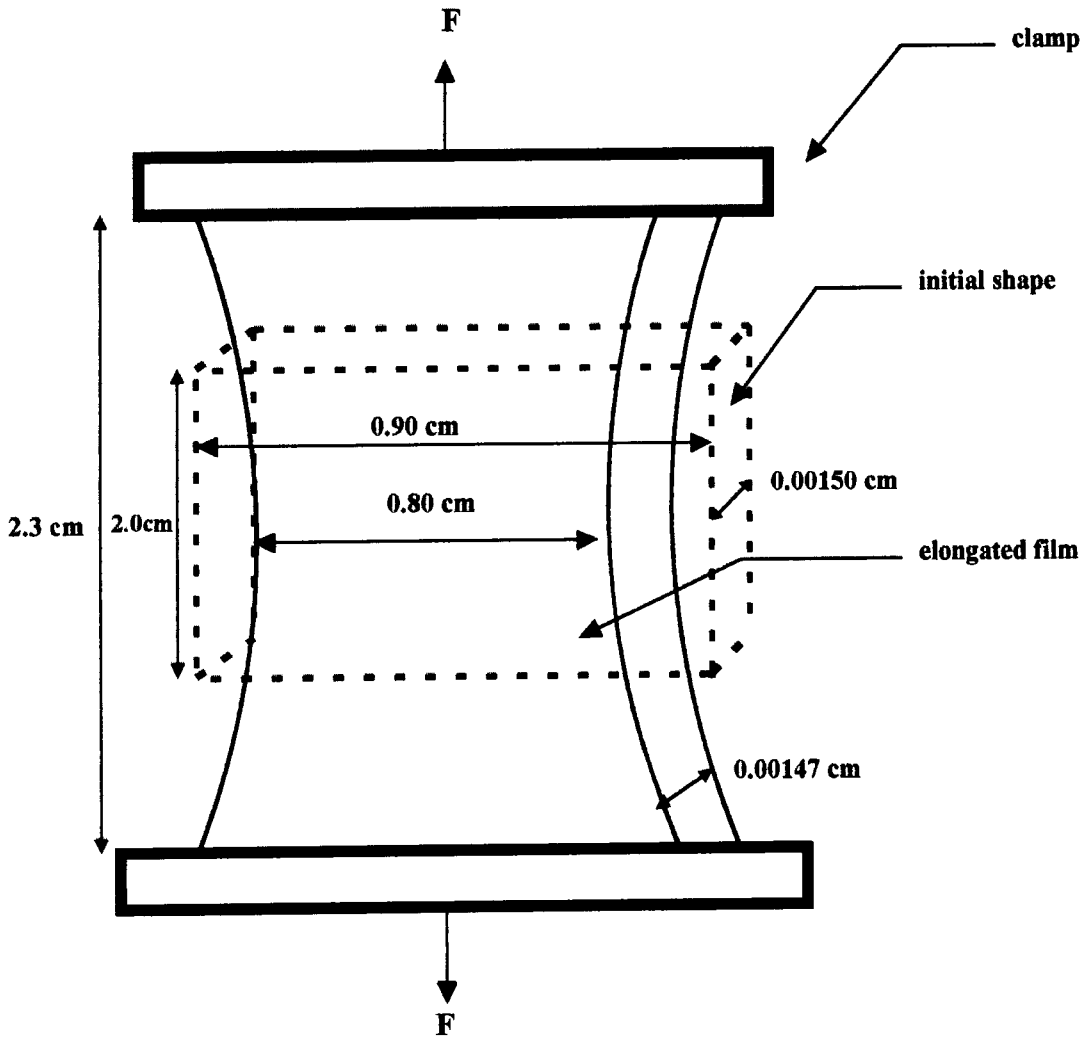

Figure 3.1. Thin film under stress.

The forces exerted by the extensometer are only applied in the vertical direction. These forces, however, cause the shape of the sample to change since the volume of the sample is conserved. To assess the reliability of the measurements an idea of the magnitude of

this change in dimensions of an extended sample is required. Table 3.1 shows the dimensions of a typical sample before and after mechanical testing.

	strain = 0%	strain = 15%
length / cm	2.0	2.3
width / cm	0.90	0.80
thickness / cm	0.00150	0.00147

Table 3.1. The dimensions of a typical sample before and after elongation.

For the situation above, the extensometer measures a force **F** acting on an unstretched sample. This is equivalent to a stress of ~7.4×10^6 **F**. The force acting on the sample extended to 15% strain will be equivalent to a real stress of ~8.5×10^6 **F** , whereas the measured stress will still be ~7.4×10^6 **F**, as the extensometer does not register the change in dimensions of the sample. This causes an error of approximately 12 per cent between the real and measured values.

It is important to note that the value of 0.80 cm for the width of a film after elongation is the minimum width of the specimen. The average width would be closer to 0.87 cm, indicating an error in the measured stress of approximately 4 per cent. This error margin is acceptable and we can therefore approximate the stress to that applied to a sample with unvarying lateral dimensions.

The consequence of the previous assumptions is that the expressions for the stress and strain can be extremely simplified. The quantities can be described in their most simple form by the well-known equations:

stress = force / cross-sectional area (X-sectional area constant)
strain = change in length / original length

These expressions, although not giving an exact representation of the mechanical state of a sample, are certainly adequate, and although a small error may be present, the effect of initial elongation on stress-strain behaviour can be reliably gauged.

3.2.2 Relationship between Stress and Strain

The relationship between stress and strain for polymeric materials is largely dependent upon the temperature of the sample and the speed at which the strain is increased. Figure 3.2 shows the dependency of stress-strain curves on temperature for a typical polymer.

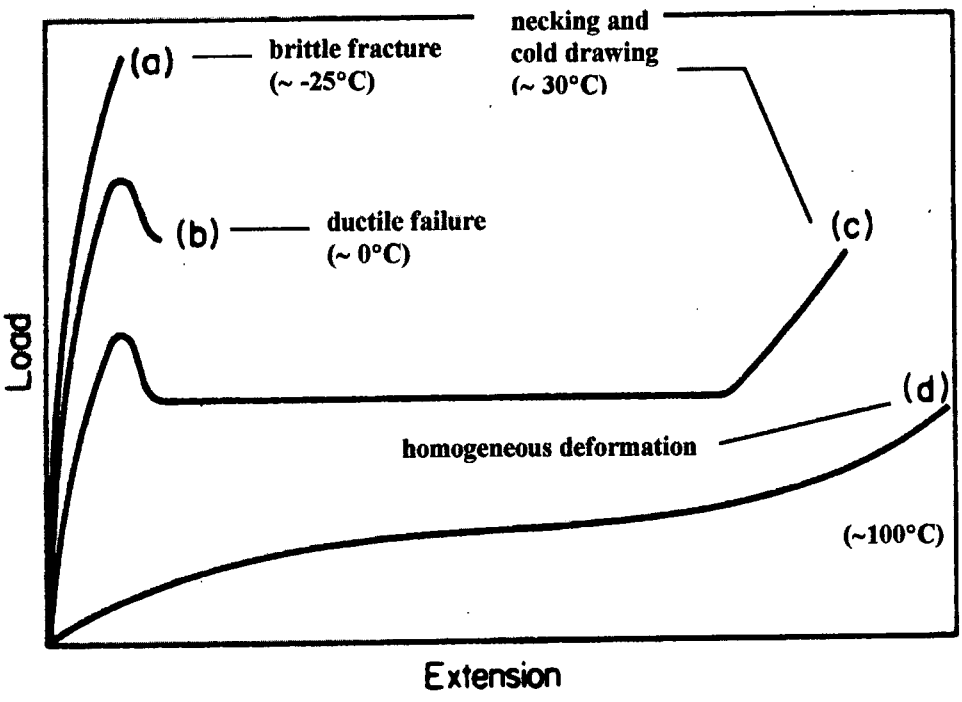

Figure 3.2 Effect of temperature on the stress-strain properties.

It can be seen from figure 3.2 that at low temperatures the load rises approximately linearly with increasing elongation up to the breaking point, at which point the polymer fractures in a brittle manner. At higher temperatures a yield point is observed and the load falls before failure, sometimes with the phenomenon of necking occuring[2]. This is ductile failure, which occurs at relatively low strains (~10-20%). As the temperature rises still further, strain hardening may occur, whereby the neck stabilises and cold-drawing occurs. In this case the extensions are large, as high as 1000% in some cases. At even higher temperatures homogeneous deformation is observed, with a very large extension at break.

3.2.3 Viscoelasticity in Polymers

The mechanical behaviour of polymers differs from other materials due to their dependence upon the rate of applied stress or strain. Whilst elastic solids such as metals obey Hooke's Law, with the behaviour independent of the applied stress or strain rate, the situation for polymeric materials is rather different. It is found that polymers may exhibit both elastic and viscous behaviour, and this behaviour varies as a function of the rate of applied stress and strain. Figure 3.3 shows the variations in mechanical behaviour for varying rates of stress and strain[1].

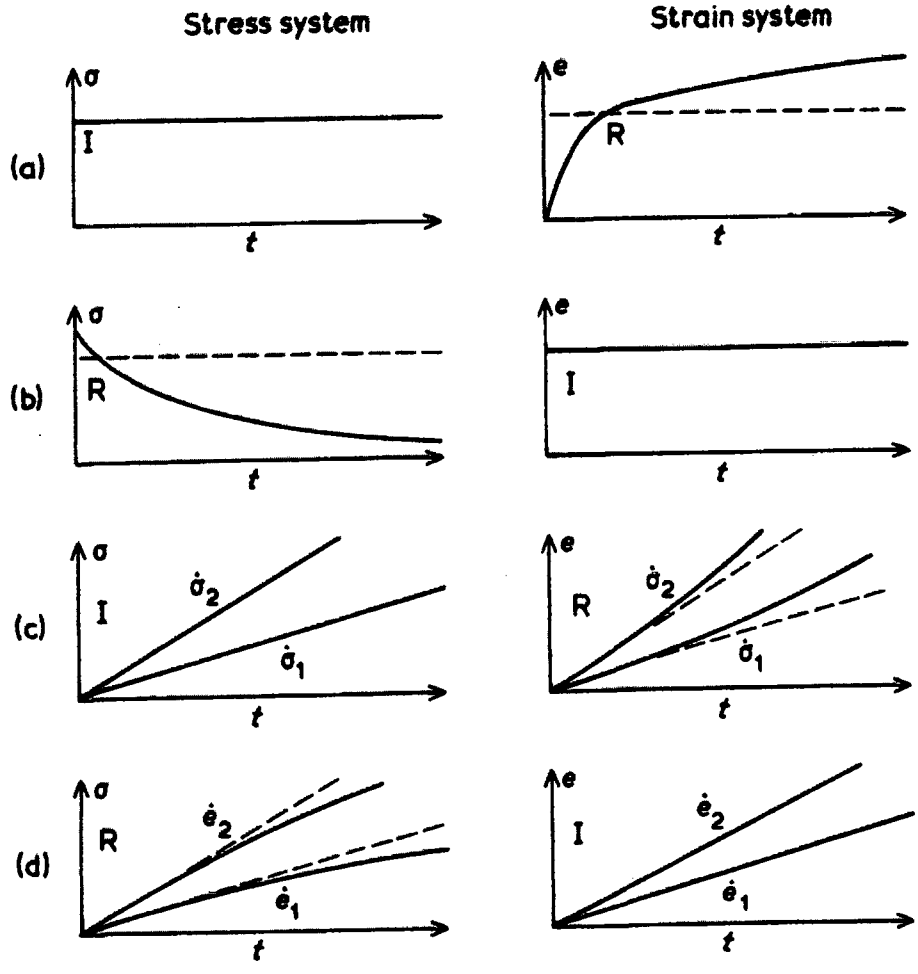

Figure 3.3: Mechanical behaviour of polymers: a) constant stress
b) constant strain
c) constant stress rate
d) constant strain rate

These shall now be considered individually.

a) Constant stress: At t=0 a constant stress is applied to the sample. It can be seen that the strain increases rapidly at first, and as t increases the rate of increase of strain slows down. This behaviour is termed creep.

b) Constant strain: If the strain is held constant the stress decays slowly with time. This behaviour is termed stress relaxation.

c) Constant stress rate: It can be seen from figure c that the increase in strain due to a constant stress rate is not linear, as would be expected for elastic solids. The slope of the curve is seen to increase with time. Furthermore, as the stress rate increases so too does the slope of the stress-strain curve.

d) Constant strain rate: Again, non-linear behaviour is observed if the rate of strain remains constant. The slope of the curve decreases with time. It is also seen that the slope increases for increased strain rates.

The deformation of a polymer can be described by a combination of Hooke's Law (elastic solid) and Newton's Law (viscous liquid). Mathematically these are described by the following equations:

$$\sigma = \mathbf{E}\,\mathbf{e} \;\Rightarrow \mathbf{d\sigma/dt} = \mathbf{E}\,\mathbf{de/dt} \quad \text{(Hooke's Law)}$$

$$\sigma = \eta\,\mathbf{de/dt} \quad \text{(Newton's Law)}$$

where E = Young's Modulus, η = viscosity.

These equations can be combined in a variety of ways to explain mechanical behaviour for the different circumstances mentioned above. A useful method of combining elastic and viscous behaviour is by using mechanical models, figure 3.4.

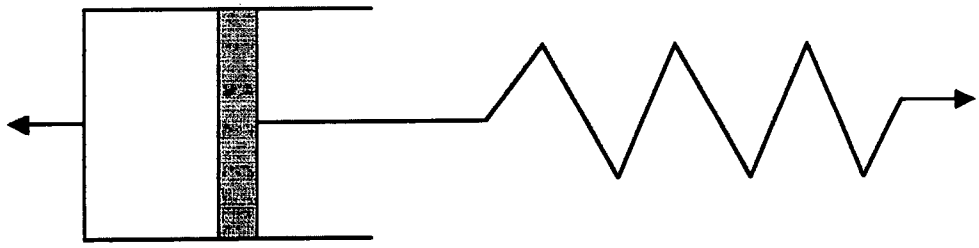

a) Maxwell Model

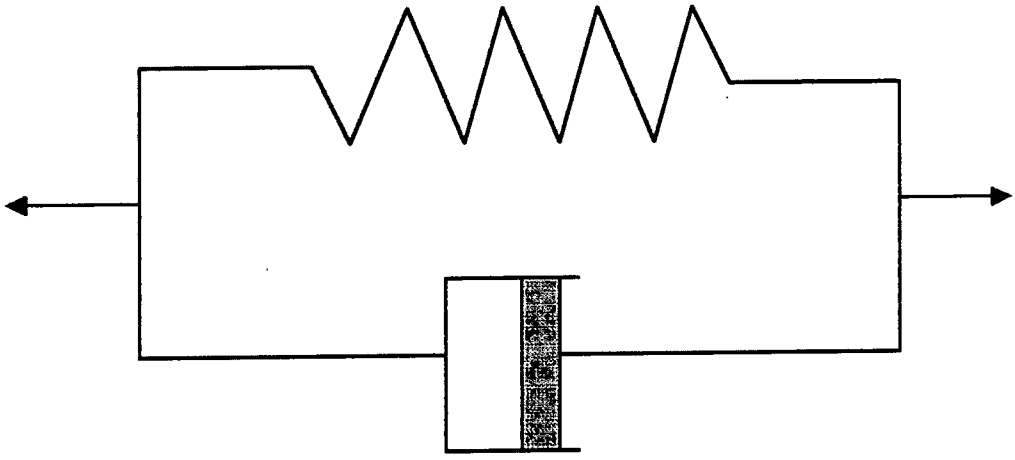

b) Voigt Model

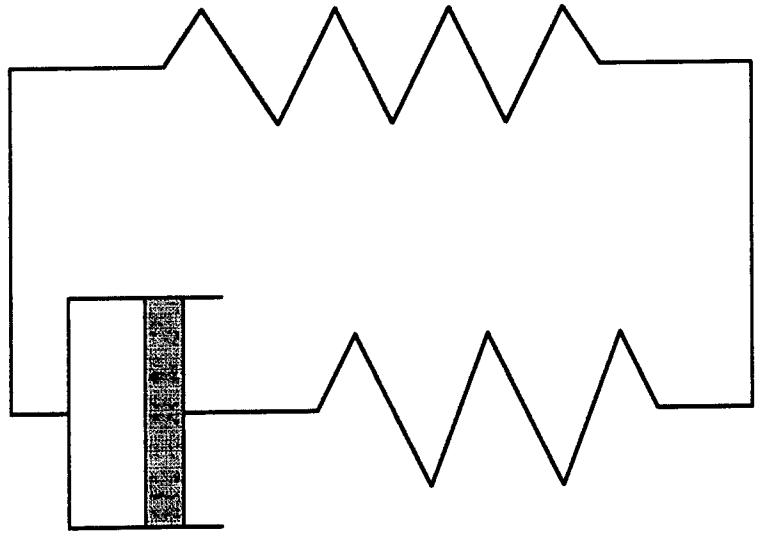

c) Standard Linear Solid.

Figure 3.4: Mechanical models for viscoelastic behaviour.

a) Maxwell model: This model consists of a spring and dashpot in series. A stress σ will produce a strain $e = e_1 + e_2$, where e_1 is the strain in the spring and e_2 the strain in the dashpot. The stress-strain behaviour for this model can then be shown to be given by:

$$\mathbf{de/dt = 1/E\ d\sigma/dt + \sigma/\eta}$$

This model describes stress relaxation in polymers to a first approximation, but does not explain creep.

b) Voigt model: The spring and dashpot are placed in a parallel arrangement for this model. Thus, the strain produced due to the spring, e_1, is equal to that due to the dashpot, e_2. The overall stress will be the sum of the spring and dashpot stresses, $\sigma_1+\sigma_2$. The stress and strain are then related by:

$$\mathbf{de/dt = \sigma/\eta - Ee/\eta}$$

This model is particularly effective in describing the creep behaviour of polymers where the stress remains constant, but is unsuccessful in describing stress relaxation.

c) Standard linear solid: This model consists of a Maxwell element and a spring in parallel, and has been used to try to explain both the creep and stress relaxation phenomena in one model. It is the simplest combination of the other two models, though much more complicated combinations[16] have been examined in order to model more accurately the behaviour.

3.2.4 Factors Affecting Stress-Strain Behaviour Of Polymers

a) Speed Of Test

Figure 3.5 shows the effect of the speed of testing upon the stress-strain curve for poly-methyl methacrylate[3].

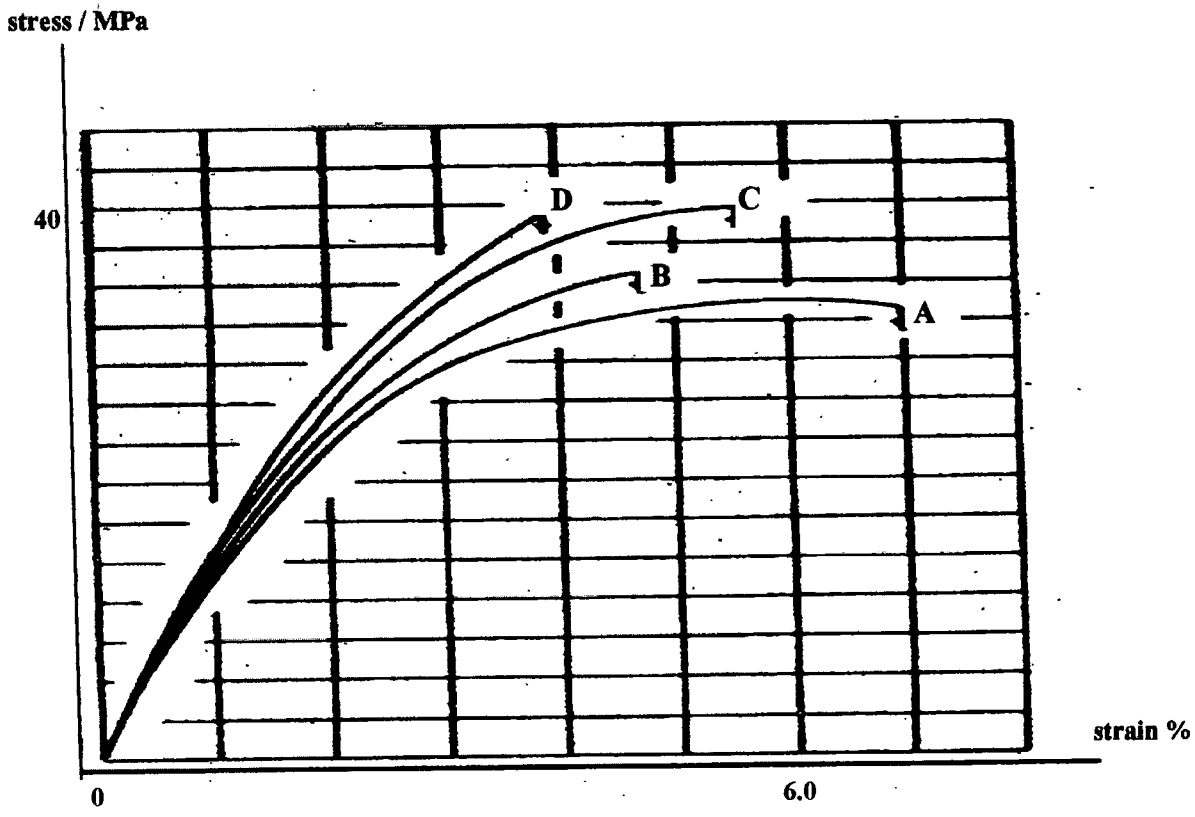

A) 0.5mm / min

B) 2.0mm / min

C) 8.0mm / min

D) 32.0mm / min

Figure 3.5 Dependency of stress-strain behaviour on test speed.

The diagram shows that as the rate of elongation increases, the tensile strength and modulus also increase. With rigid polymers the breaking strain decreases as the speed of testing increases.

It is thus evident that the stress-strain behaviour of polymers depends largely upon both the temperature and speed of testing. It can also be seen that the effect of an increase in the speed of testing is similar to the effect of a decrease in temperature.

b) Molecular Weight

It has been shown[4,5] that the stress-strain properties of polymers are affected by molecular weight and molecular weight distribution. The general conclusions of research into the effect of molecular weight are as follows:

a. At low molecular weights the breaking stress and modulus are low.
b. the properties increase as the molecular weight increases and then approach a maximum at high molecular weights.

The stress-strain properties of polyaniline[11] have been shown to have similar dependencies on molecular weight, as shown in figure 3.6.

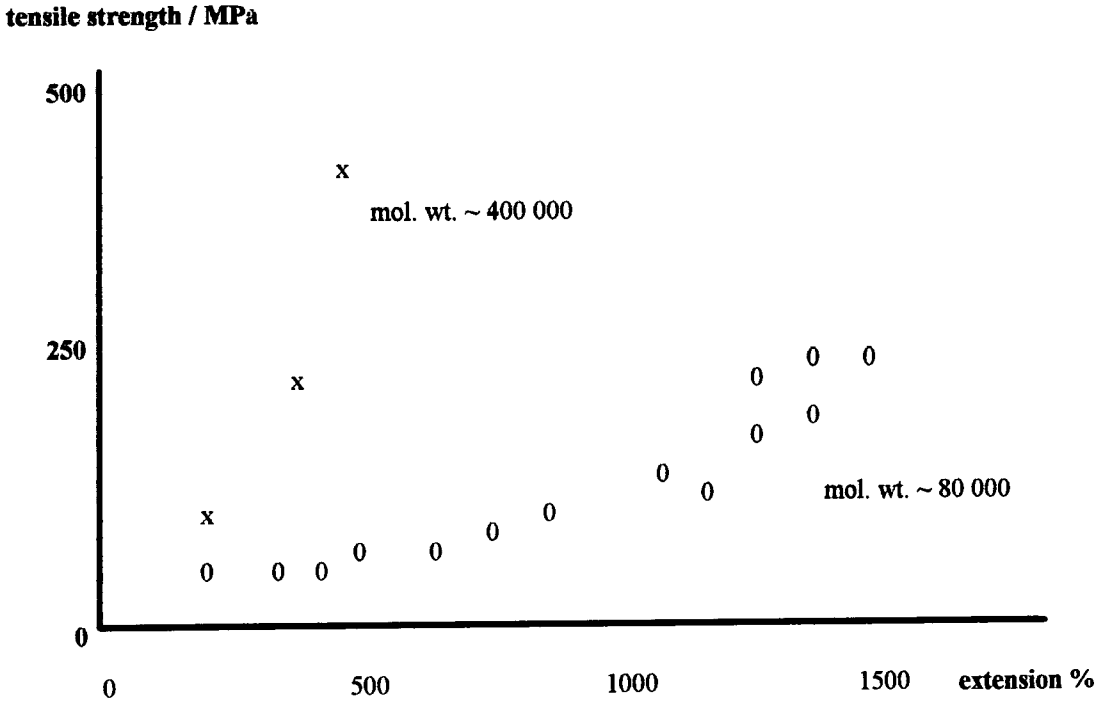

Figure 3.6: Tensile strength versus elongation for high and low mol. wt. PANi.

c) Crystallinity

Because polymers are semi-crystalline the crystalline structure, as well as the associated morphology, is complex[18]. These morphological variations determine the mechanical properties of the polymer. The morphological complexities make quantitative description of the properties very difficult. Polyaniline is known to be a complex polymer on the molecular scale[11,19]. The high polydispersity reported earlier in this work, for example, epitomise the problems encountered in attempting to produce a definitive description of mechanical and electrical behaviour. Such factors will have dramatic effects upon the morphology of individual crystalline regions and the surrounding amorphous state. For this reason little quantitative analysis has been reported concerning the effect of crystallinity upon the mechanical properties of complex polymer systems recently. However, for polymers with more simple repeat units and well-defined crystalline fraction, the mechanical behaviour has been interpreted in terms of crystallinity. The results are summarised below:

As the crystallinity of a polymer increases the polymer becomes more brittle. Usually the modulus of a crystalline polymer is high, but the elongation to break is low. An example of this type of behaviour is found for crystalline polypropylene[6]. It is important to distinguish between the effect of crystallinity and molecular weight on the mechanical properties of a polymer. When measuring the mechanical properties as a function of molecular weight, the fact that changes in molecular weight are likely to cause changes in crystallinity must be taken into account. Sperati, Franta and Sparkweather[12] found that the mechanical properties of polyethylene depend more upon changes in crystallinity rather than changes in molecular weight.

d) Orientation

Uniaxially stretch-oriented polymers are found to have mechanical properties which vary in different directions. The Young's modulus is found to be greater in the direction parallel to orientation compared with the direction perpendicular to orientation. The orientation of polymers has been reported to give the polymers increases in tensile strength of up to 500 per cent in the direction of orientation compared to the

perpendicular direction[7]. It has also been found that perpendicular to the direction of orientation the tensile strength may be reduced to as little as a third of the tensile strength of an unoriented specimen. This behaviour can be explained by the fact that in the direction parallel to orientation, stresses are exerted mainly on the primary bonds of the polymer chains. In the direction perpendicular to orientation however, the stresses act mainly on the weak secondary bonds between the chains. The elongation to break for oriented polymers is found to be less in the direction perpendicular to orientation than for its unoriented counterpart. In the direction of orientation however, the stress-strain curve often shows a yield point, and the elongation to break can be much greater than for the unoriented material[7].

e) Solvents

Solvents are known to change the mechanical behaviour of polymers. Plasticisers, for example, have the effect of lowering the glass transition temperature of a sample. The properties of films cast from solution may depend upon the solvent even if all or nearly all the solvent is removed from the films before mechanical tests are performed. The stress-strain behaviour of cellulose nitrate[8], for example, is found to be strongly dependent upon the solvent used to prepare the film. This dependency can be attributed to changes in crystallinity or crystal morphology induced by the solvent used. The tensile strength of rubber[9] has been found to vary depending on the solvent used to cast the samples. This variation has been attributed to differences in molecular morphology, a factor which depends upon how effective the solvent is at dissolving the material.

3.3 Experimental Procedure

This section describes the procedure used to obtain the stress-strain information for polyaniline samples with varying degrees of elongation.

3.3.1 Extensometer

A Nene strain gauge using a software package called Retrofit was employed to carry out the mechanical testing of the polyaniline samples. A diagram of the extensometer is shown in figure 3.7.

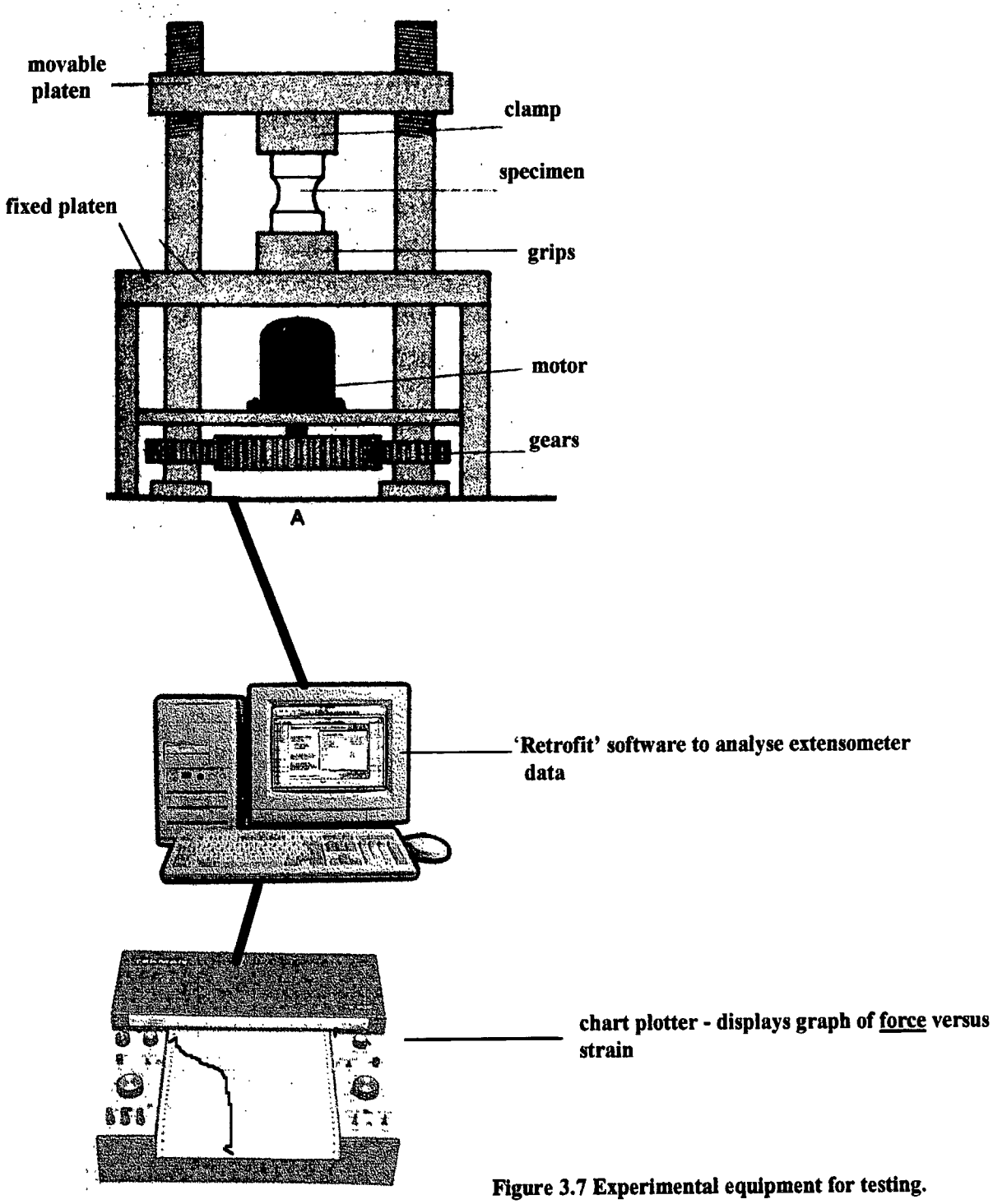

Figure 3.7 Experimental equipment for testing.

There are a number of ways of varying the stress or strain applied to a material in order to obtain information relating to the mechanical behaviour. The main methods are constant load, constant load rate and constant elongation rate. For this analysis the constant elongation rate has been used; the samples were subjected to a 20 mm/minute strain rate and the variation in load required to produce this strain was measured. The reason for this choice was fairly arbitrary, although it does allow for a comparison with the results obtained by other groups who have used a similar regime.

3.3.2 Clamping the samples

It is of upmost importance to ensure that the clamping of the samples is undertaken with considerable care. Therefore the test machine grips are designed to transfer load smoothly into the test piece without producing local stress concentrations. Nonuniform loading causes bending of the sample in addition to tension, which means that stress in the sample will not be uniform. To avoid this, hydraulic gripping devices incorporating swivel joints[10] are used in the linkage that carries the load to the test piece, figure 3.8.

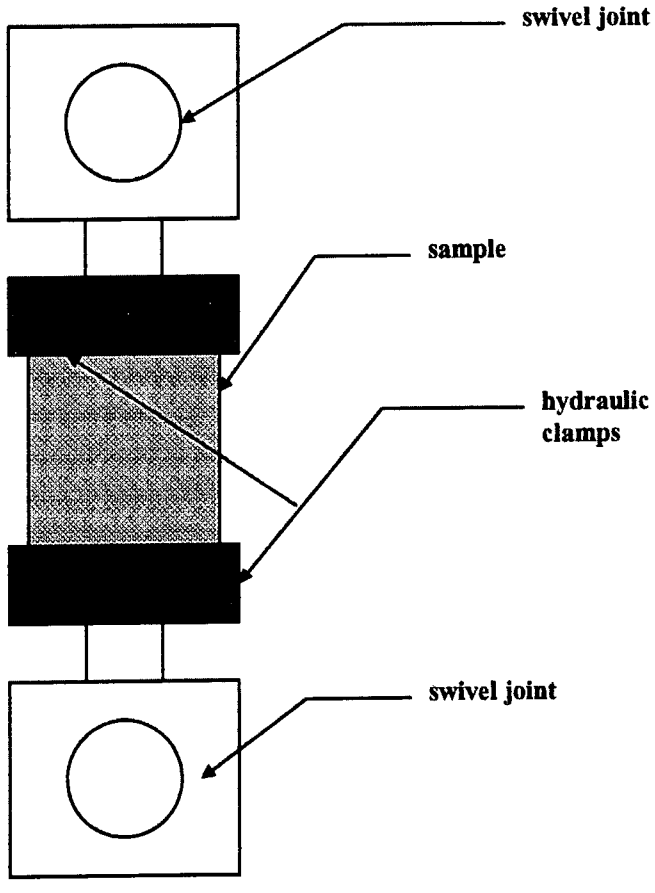

Figure 3.8: Clamping arrangement for mechanical testing

3.3.3 Data Accumulation

The data measured by the extensometer is actually a measurement of the load on the sample as a function of extension. Data for each sample were rescaled so that a plot of stress versus extension could be obtained in order to compare mechanical behaviour. Once accomplished, stress-strain scans for approximately fifty samples with varying degrees of elongation were taken. It was important to observe the samples as they were being tested so that the scans for any samples which teared due to edge imperfections, or snapped at the clamps, could be ignored. Approximately thirty scans were suitable for further analysis.

3.4 Results

Figures 3.9 to 3.16 show the normalised scans obtained from the strain gauge for thirty-three emeraldine base samples tested with $e_{\%}$ varying from 0 to 700.

Table 3.2 shows the mechanical properties of the samples as a function of $e_{\%}$.

Figure 3.9 Stress versus Strain - e%=0

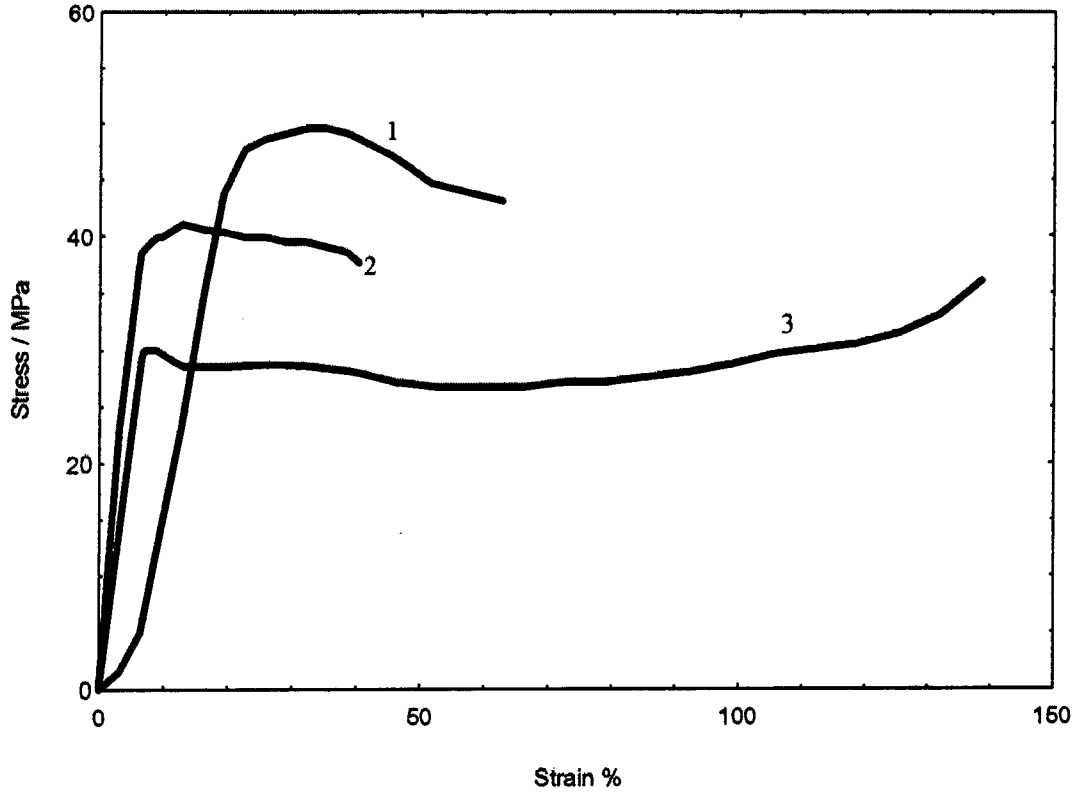

Figure 3.10 Stress versus Strain - e%=100

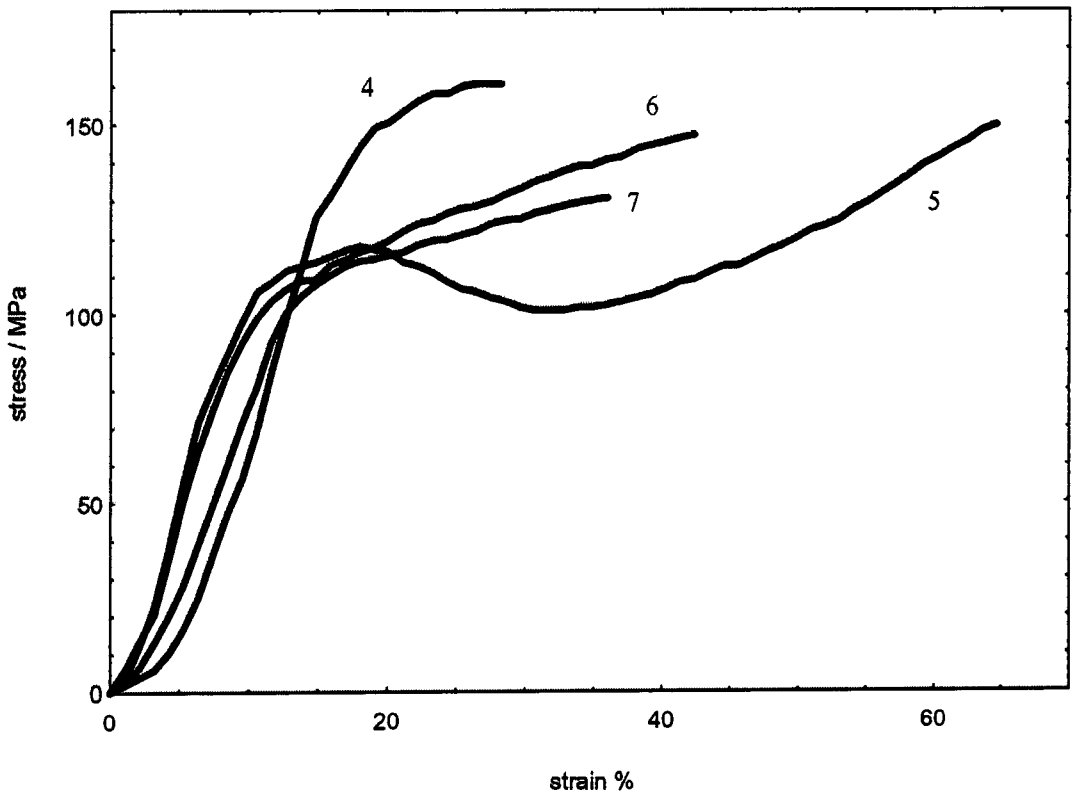

Figure 3.11 Stress versus strain - e% = 200

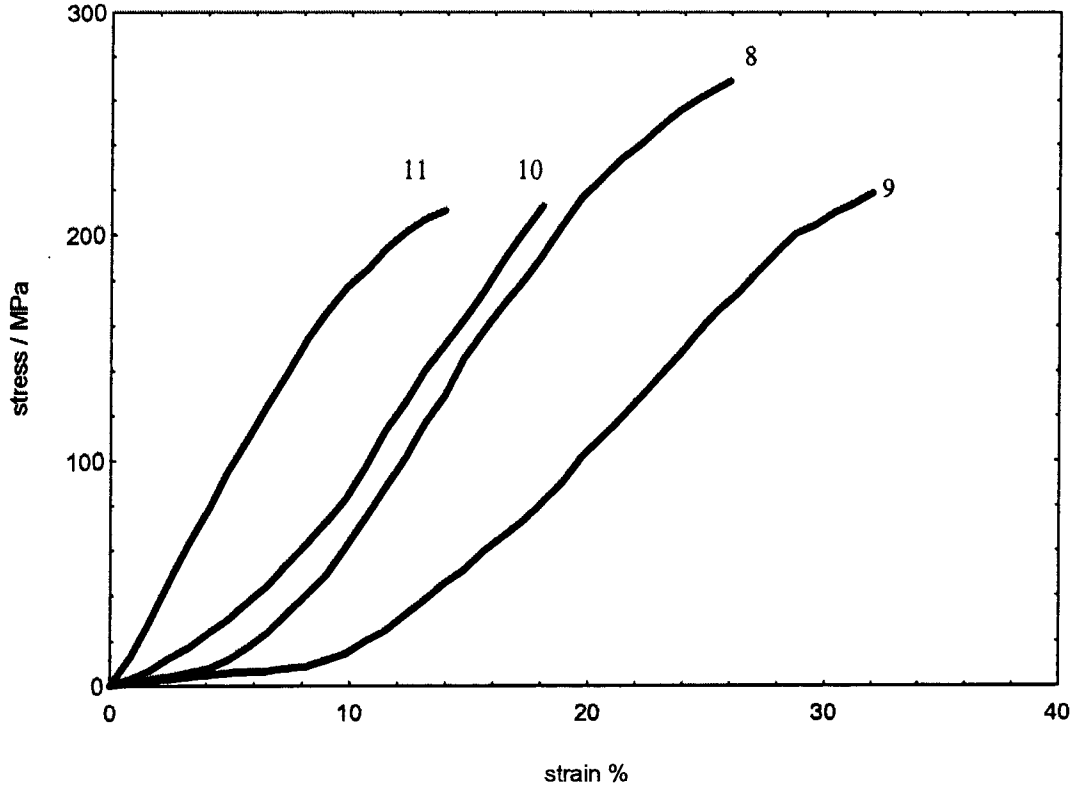

Figure 3.12 Stress versus strain - e% = 300

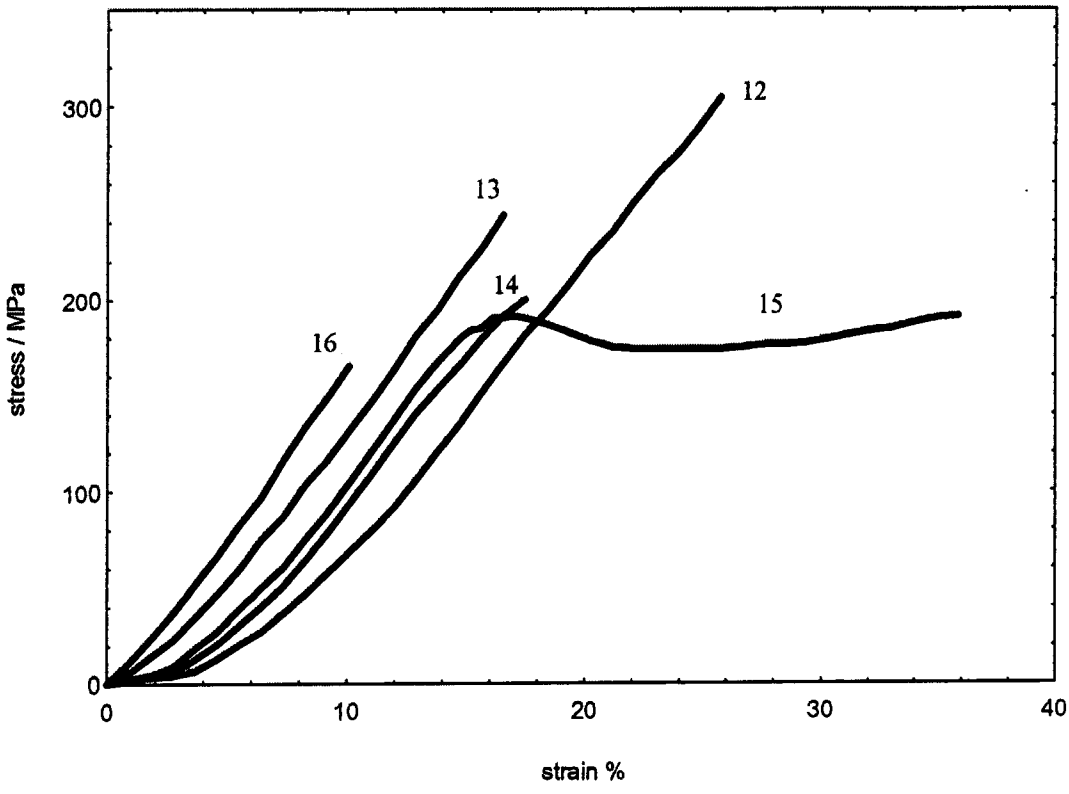

Figure 3.13 Stress versus strain - e% = 400

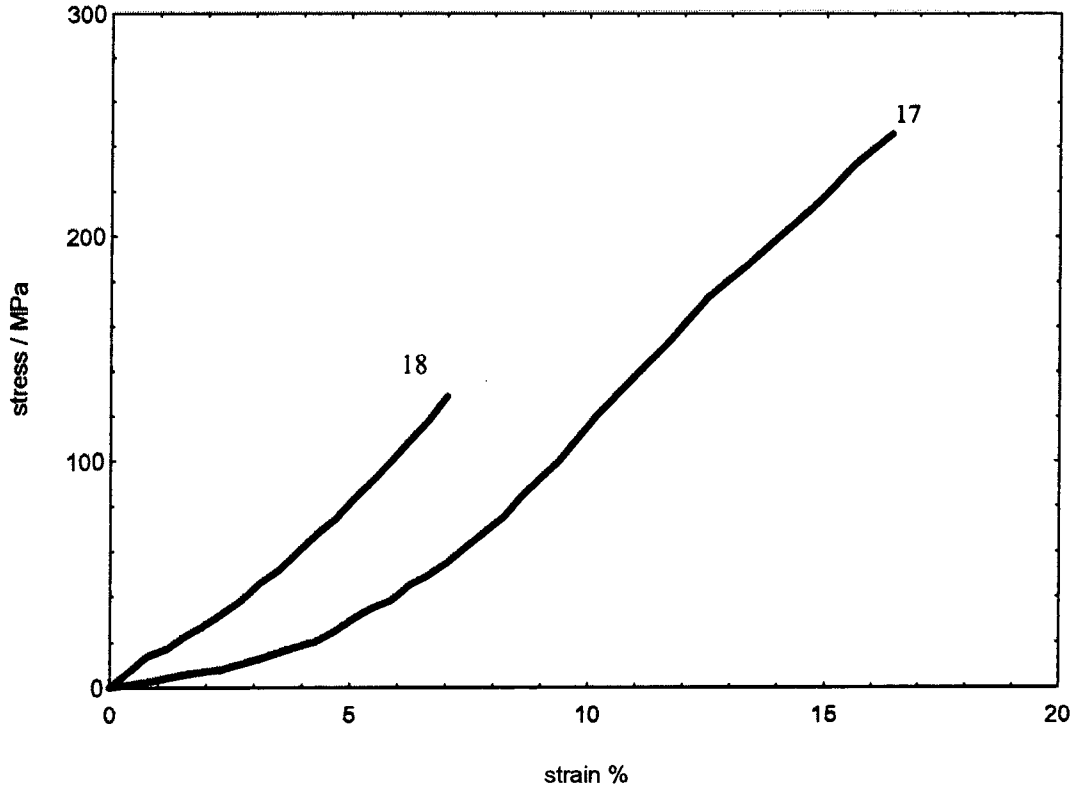

Figure 3.14 Stress versus strain - e% = 500

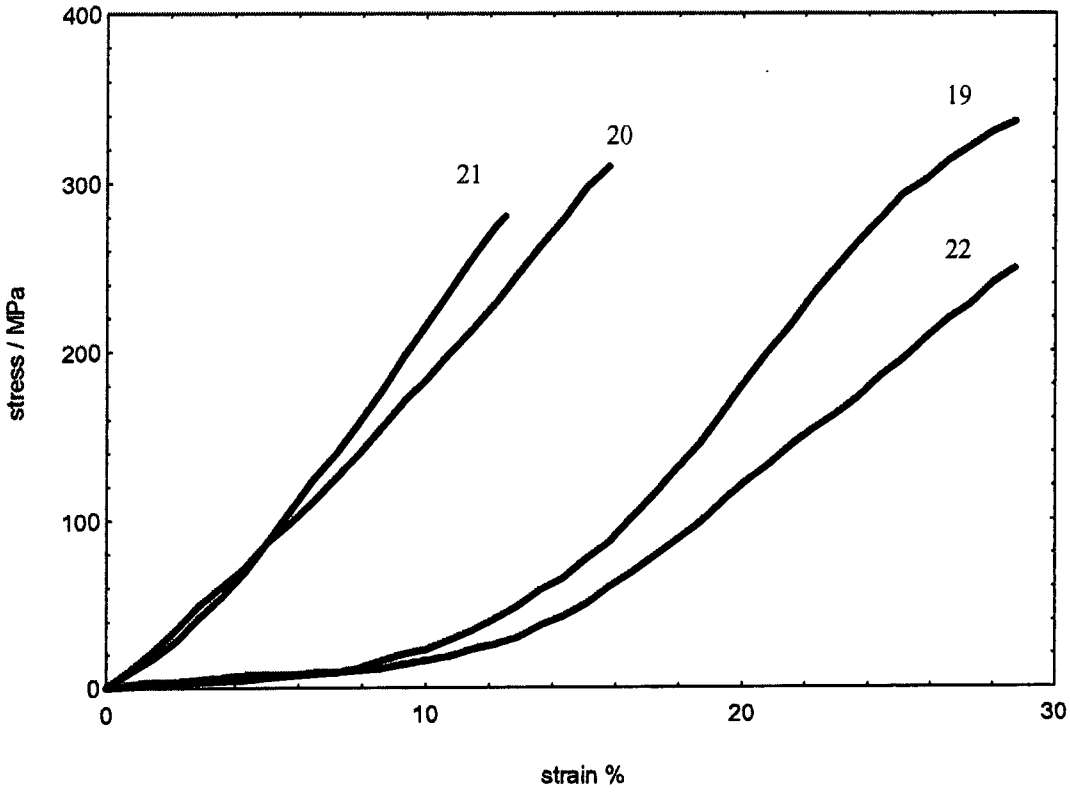

Figure 3.15 Stress versus strain - e% = 600

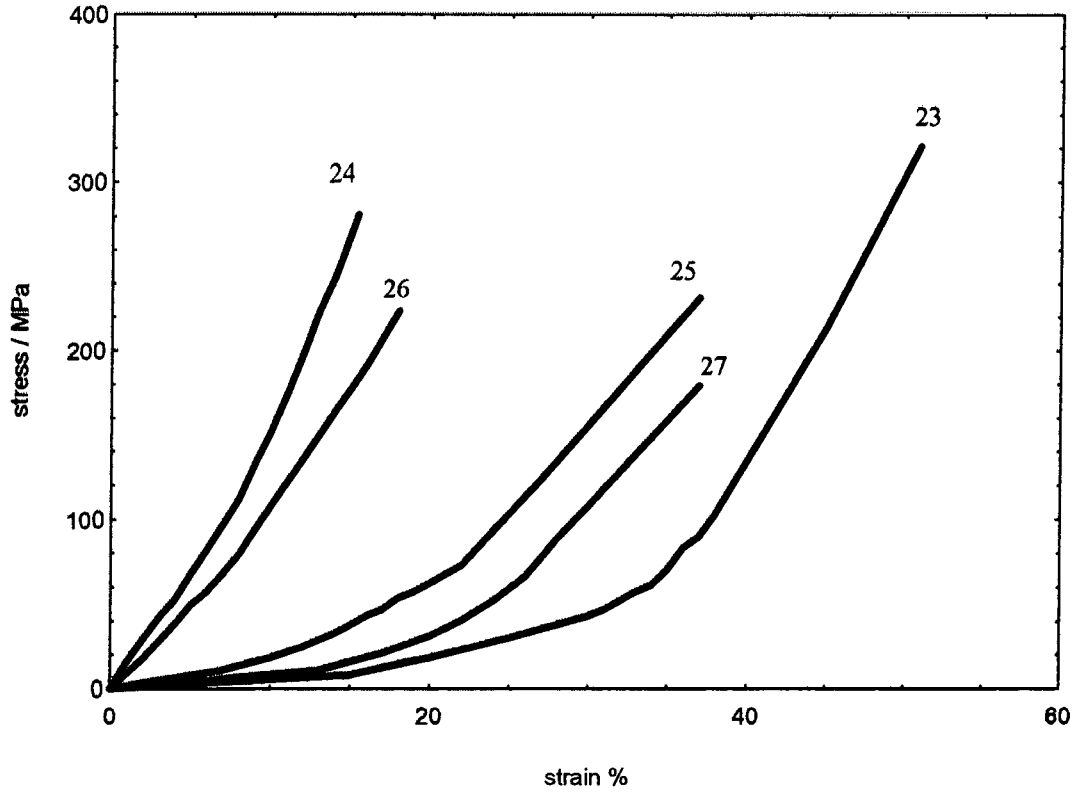

Figure 3.16 Stress versus strain - e% = 700

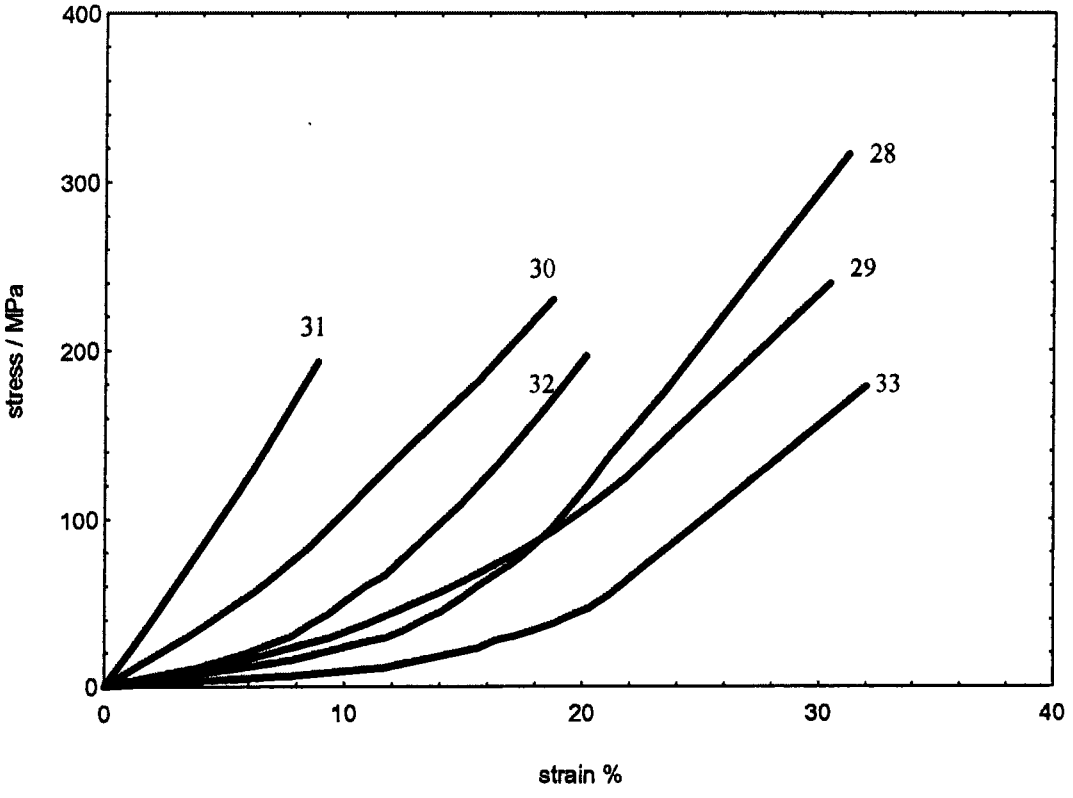

Table 3.2: Variation of mechanical properties with initial elongation.

sample no.	**initial elongation $e_{\%}$**	stress at break/MPa	strain at break %	Young Modulus/ GPa
1	**0**	43.4	64.6	0.33
2	**0**	37.3	41.5	0.98
3	**0**	35.7	139.5	1.44
4	**100**	163.6	29.9	0.96
5	**100**	152.7	67.0	1.25
6	**100**	148.9	43.8	1.09
7	**100**	133.2	36.5	1.04
8	**200**	271.2	25.8	0.99
9	**200**	217.6	32.0	-
10	**200**	212.8	18.1	1.49
11	**200**	210.9	13.7	1.90
12	**300**	307.8	25.1	-
13	**300**	245.4	16.4	1.71
14	**300**	199.6	17.2	-
15	**300**	194.1	34.4	1.60
16	**300**	166.2	10.3	1.76
17	**400**	250.8	16.5	1.86
18	**400**	131.7	7.2	2.04
19	**500**	342.7	28.5	1.49
20	**500**	318.3	15.9	2.35
21	**500**	285.3	12.5	2.00
22	**500**	256.6	28.7	-
23	**600**	339.3	50.6	-
24	**600**	287.8	15.1	2.41
25	**600**	238.9	36.2	-
26	**600**	227.1	17.3	1.47
27	**600**	183.5	36.6	-
28	**700**	315.7	31.6	-
29	**700**	238.6	30.5	-
30	**700**	231.5	18.6	1.41
31	**700**	204.2	9.0	2.28
32	**700**	200.6	20.2	-
33	**700**	184.0	31.7	-

3.5 Discussion of Results

Initial inspection of the stress-strain relationships for emeraldine base appear to show little relationship with initial elongation. Figures 3.9 to 3.16 show a large degree of variation in the mechanical behaviour of the samples tested. The stress-strain relationships of the samples show behaviour ranging from elastic solid behaviour (eg. samples 10, 13, 20, 31), where the stress remains approximately proportional to strain, to necking and cold-drawing behaviour (eg. samples 3, 15). This necking phenomenon has also been observed in PET[15] for unoriented and low $e_{\%}$ samples. The inconsistencies mentioned have made quantitative analysis of the mechanical response to applied strain very difficult, especially in relation to initial elongation. All controllable factors remained the same during synthesis and orientation, so the only conclusion that can be drawn is that any disparity is due to factors such as the variation in morphology at the molecular level which will vary from sample to sample and cannot be controlled. Because of these inconsistencies it was not possible to model the mechanical behaviour of the samples using the methods described in section 3.2.3.

The behaviour of breaking stress, breaking strain and modulus shall now be treated individually.

3.5.1 Effect of initial elongation on breaking stress

The breaking stress varies from 36 MPa ($e_{\%}$=0) to 340 MPa ($e_{\%}$=500). This indicates an increase in tensile strength to the order of 900 per cent upon orientation. With the exception of $e_{\%}$=0 and $e_{\%}$=100, the initial elongations are spread in what appears to be a random manner as a function of breaking stress. It is evident, however, that the breaking stresses of all the oriented samples are more than their unoriented counterparts.

Figures 3.17 and 3.18 show graphically the variation in breaking stress with $e_{\%}$. The errors in the average values were evaluated by the usual standard deviation technique.

It is apparent from these graphs that on average an increase in the breaking stress takes place as $e_{\%}$ increases up to approximately 500 (the value for $e_{\%}$=400 was overlooked as

the results for only two samples were suitable for analysis). For samples elongated above 500% there is a slight decrease in average breaking stress. The increase in mechanical strength with initial elongation is due to increased alignment of the polymer chains. The strong intramolecular bonds become more dominant parallel to the direction of orientation, thus increasing the stress required to cause fracture. The slight decrease in breaking stress for $e_{\%}>500$ is intriguing, but can possibly be explained by the fact that samples with such high extensions may have developed more points with high stress concentrations during the initial elongation process. This behaviour is consistent with 700% elongation being the maximum obtained value for EB samples to date. Furthermore, the samples with higher elongations are thinner than their unoriented counterparts. This enlarges the percentage variation in thickness at different points in the samples, thus making the samples more likely to fracture at lower extensions.

MacDiarmid et al[17] have also measured the mechanical properties of EB films. They report increases in tensile strength of approximately 500% for films stretched to $e_{\%}=1300$, with a highest measured value of 231 MPa. For $e_{\%}=700$ they report tensile strengths of approximately 100 MPa. It can be seen from figure 3.18 that the average values reported in this chapter for $e_{\%}$ up to 700 are higher than those of MacDiarmid. One possible explanation for this is differences in the molecular weight of the samples for different groups.

Similar experiments have been performed on other polymeric materials which allow comparison with these EB values. Akagi et al[13] found that the tensile strength of trans-polyacetylene films increased approximately linearly with $e_{\%}$, with a maximum breaking stress of approximately 800 MPa for films stretched to 700%. This value indicated a 7-fold increase compared with unoriented samples. The tensile strength of poly-p-phenyleneterephthalamide (KEVLAR) is approximately 3.9 GPa. The highest measured value of breaking stress for polyaniline samples was 342 MPa for $e_{\%}=500$, which although lower than the values for these two polymers is of comparable magnitude.

Figure 3.17: Graph of breaking stress versus initial elongation for EB films

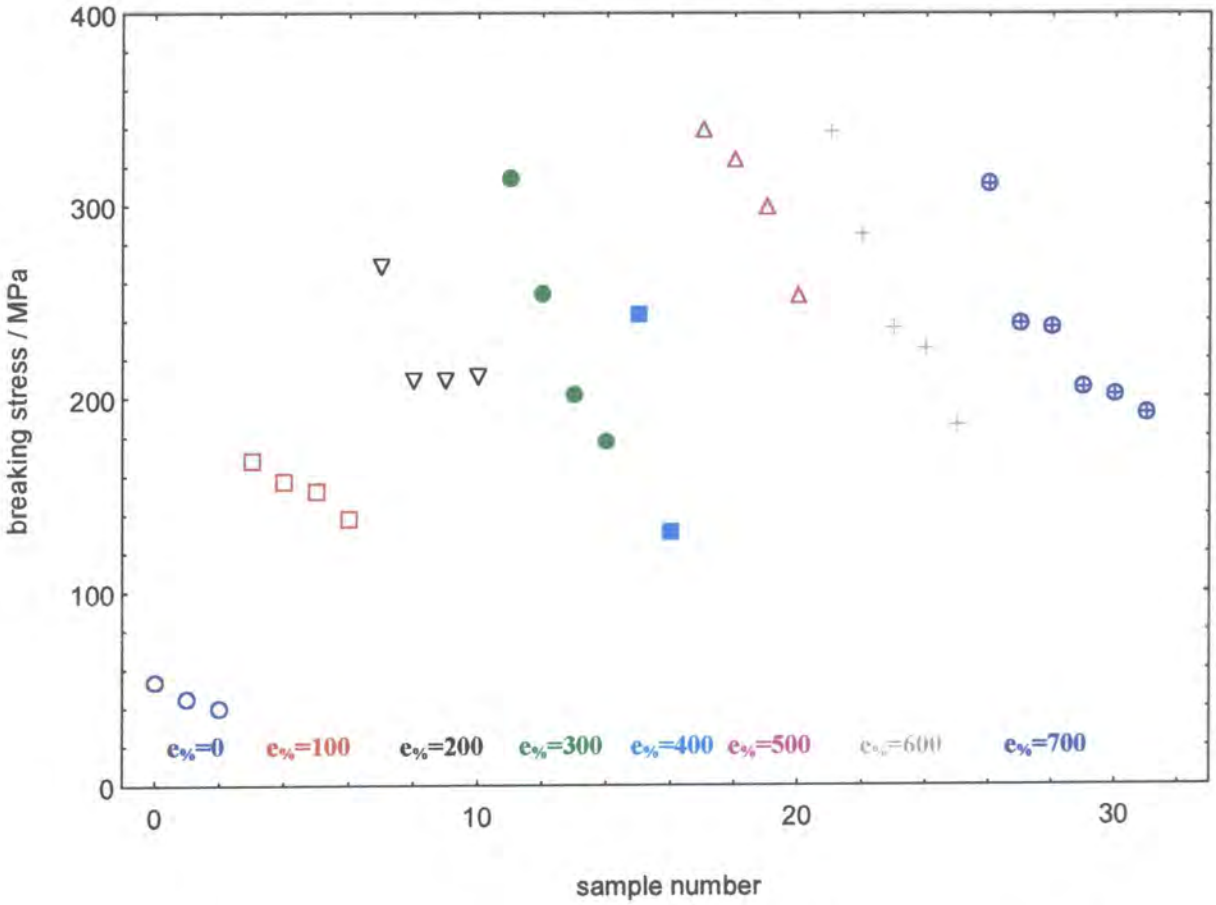

Figure 3.18: Graph of average breaking stress versus initial elongation for EB films

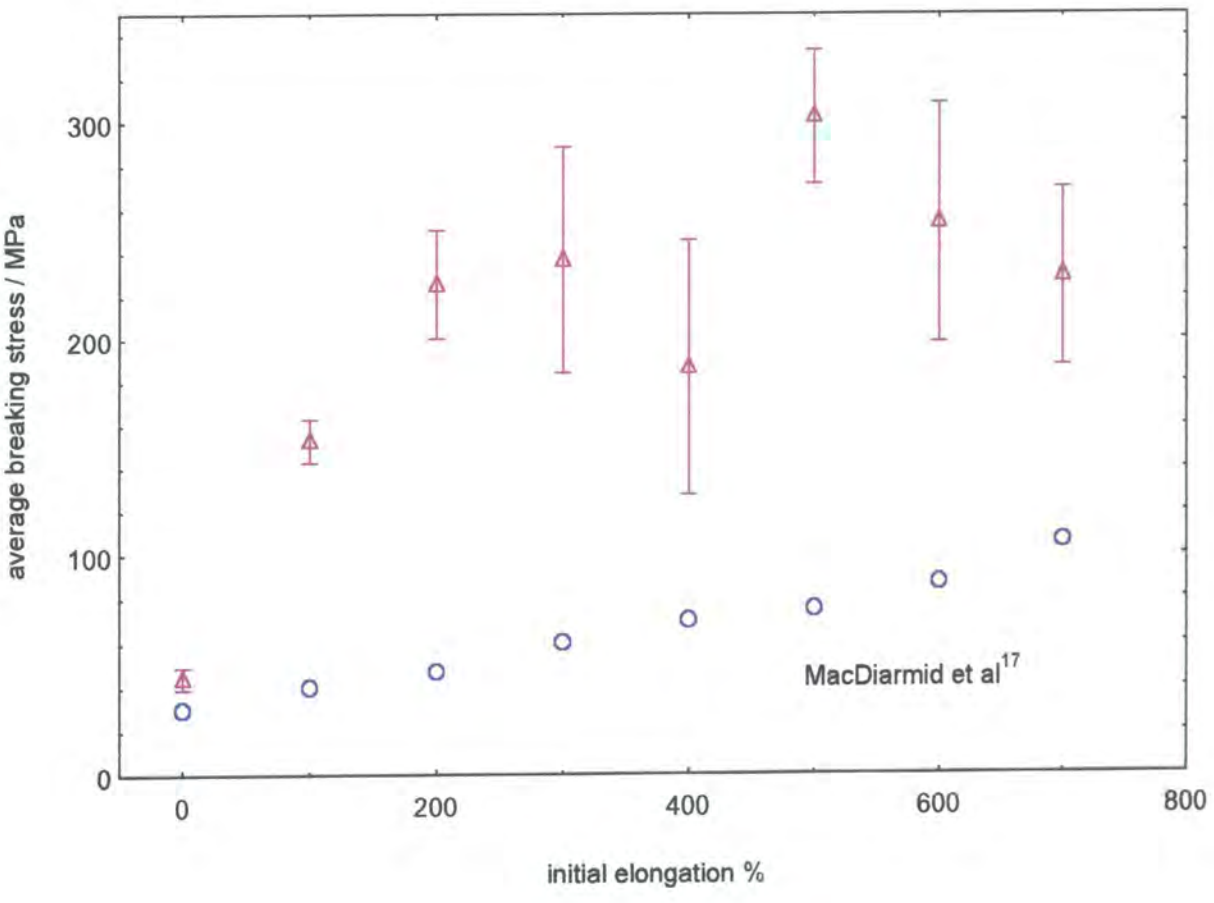

3.5.2 Behaviour of breaking strain as a function of initial elongation

Figures 3.19 and 3.20 show graphically the variation of breaking strain with $e_{\%}$. The graphs show an initial decrease in average breaking strain up to $e_{\%}$=200-300%. For the samples tested with higher initial elongations the breaking strain appears to be independent of $e_{\%}$. One possible way of explaining this behaviour is by considering the relative crystallinity of the samples, and how elongation affects crystallinity. The crystallinity of base samples measured by X-ray diffraction techniques is higher for 300% elongated samples compared with unoriented samples ($\chi_{300\%}/\chi_{unoriented} \sim 1.6$). The crystallinity of samples elongated to 600% has been measured to be approximately the same as the value for 300%. Increases in crystallinity lead to the samples becoming more brittle and therefore lowering the extension to break. It is therefore possible that the reason for these trends may indeed be due to the crystallinity changes. Similar behaviour has also been seen in oriented polystyrene[7]. A clearer picture would perhaps have been obtained had it been possible to make crystallinity measurements on individual samples before testing them mechanically. Unfortunately it was not viable to do this.

Figure 3.19: Graph of breaking strain versus initial elongation for EB films

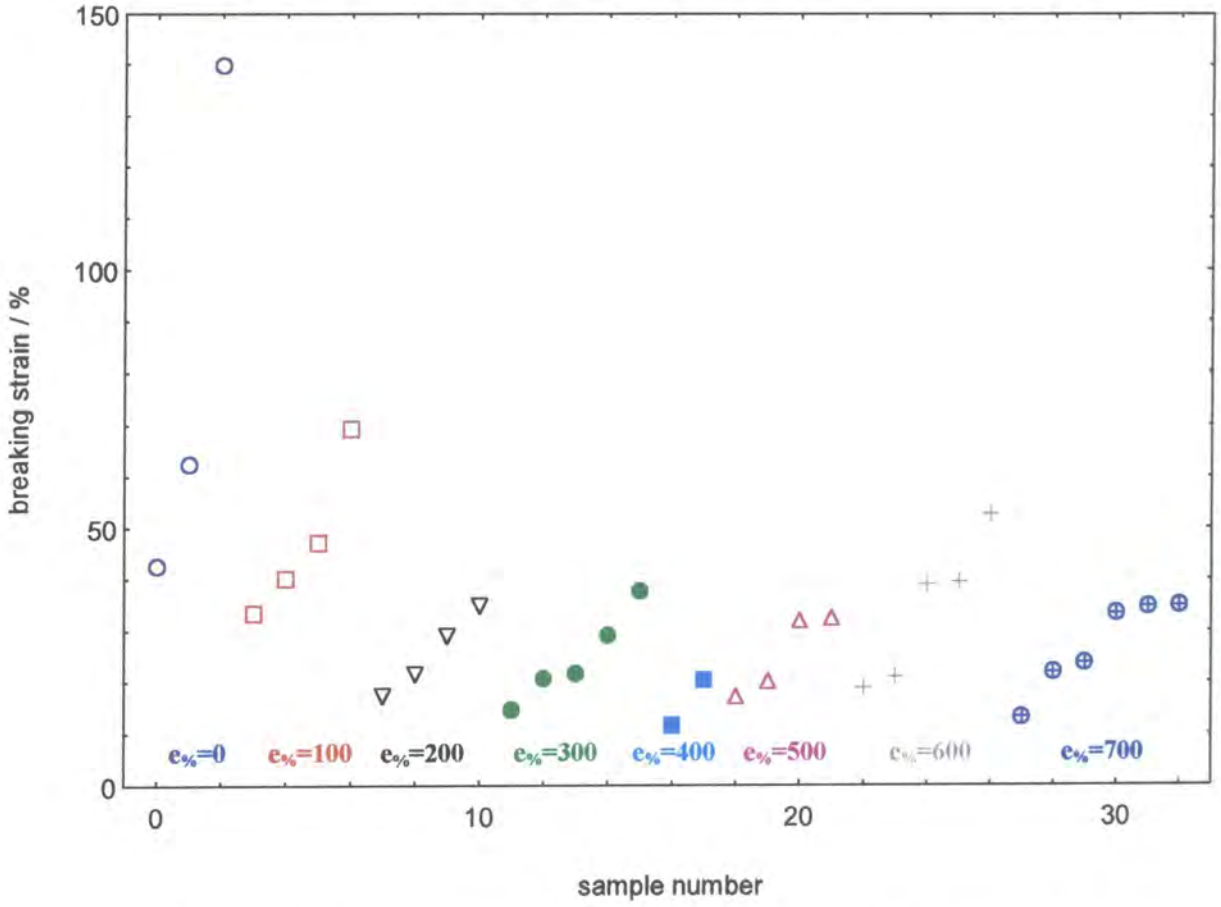

Figure 3.20: Graph of average breaking strain versus initial elongation for EB films

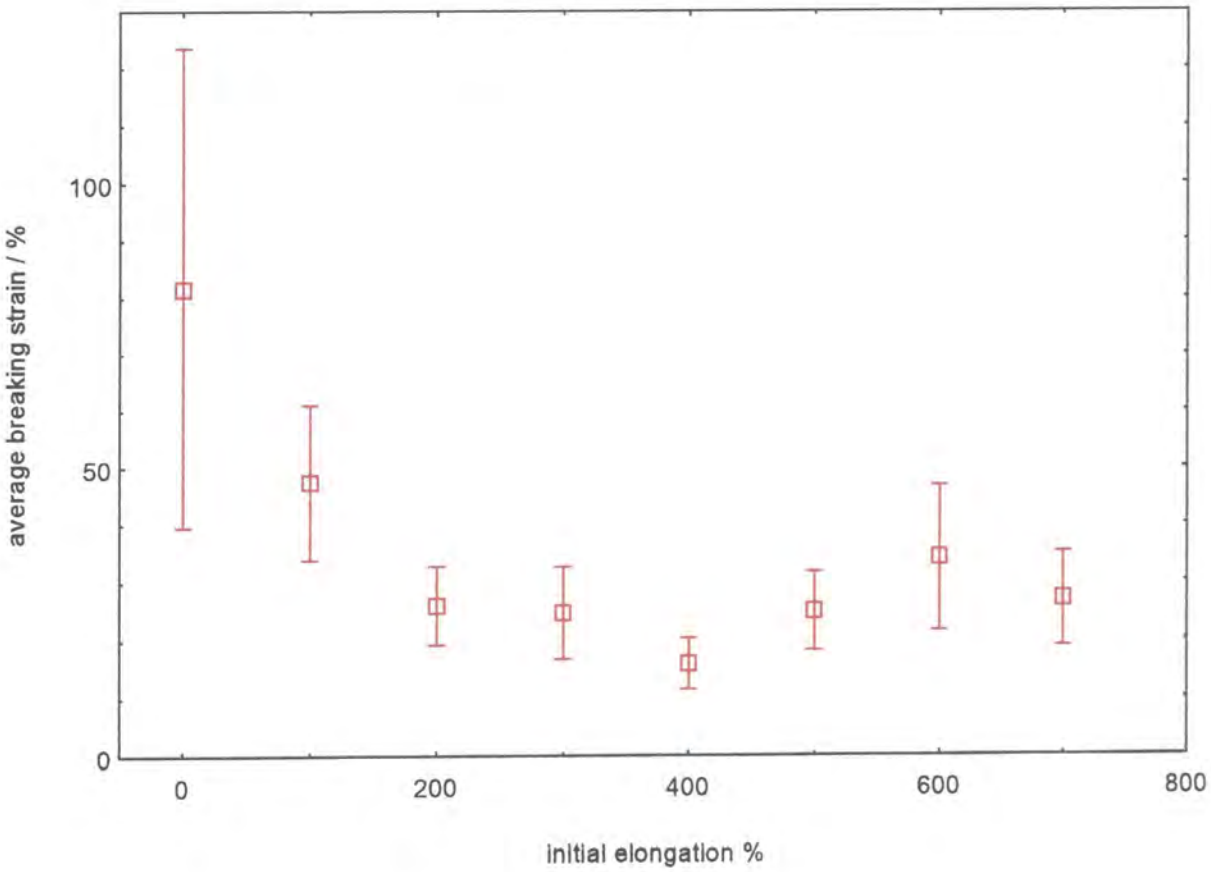

3.5.3 Behaviour of Young Modulus as a function of initial elongation

Values of the Young modulus vary from 0.33 GPa for unoriented samples to 2.41 GPa for $e_{\%}$=600. The moduli for a number of samples were not calculated as the variation of stress with strain was not linear. For the moduli which were obtainable there does seem to be improved grouping as a function of $e_{\%}$ compared with the breaking stress and breaking strain measurements, especially for $e_{\%}$=100 and $e_{\%}$=300. This can be seen by the graphical representations shown in figures 3.21 and 3.22.

It can be seen from these diagrams that the average modulus firstly increases approximately linearly with $e_{\%}$ up to ca. 400%, and then remains constant. This increase is almost two-fold. Again this behaviour could be attributed to the changes in crystallinity with orientation.

The Young modulus for trans-polyacetylene[13] also displays linear behaviour but does not show a plateau region as was found for the EB samples. The modulus of 700% trans-PA was found to be approximately 80 GPa, which compares favourably with that of Kevlar (~132 GPa). However, the values for polyaniline are much lower than this.

Figure 3.21: Graph of Young Modulus versus sample number for EB films

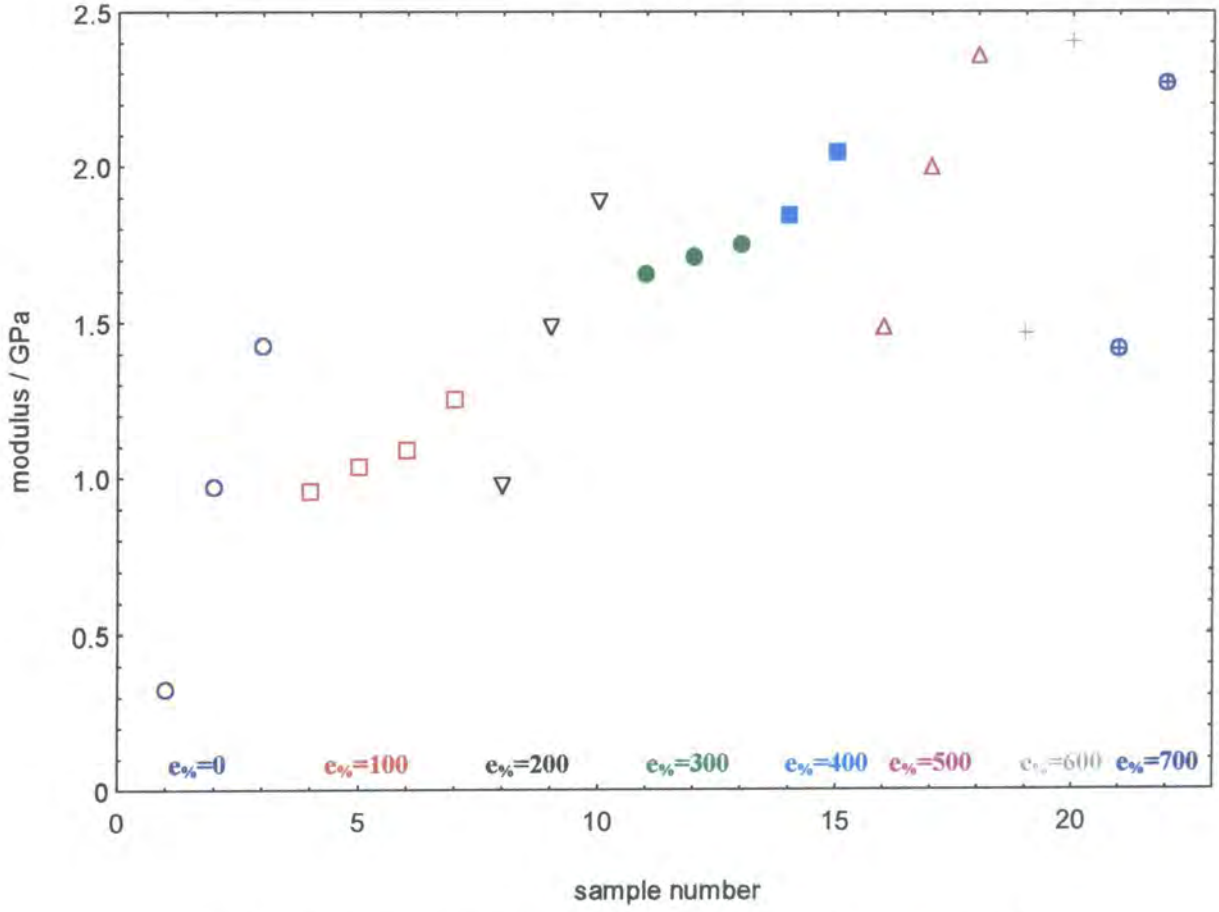

Figure 3.22: Graph of average modulus versus initial elongation for EB films

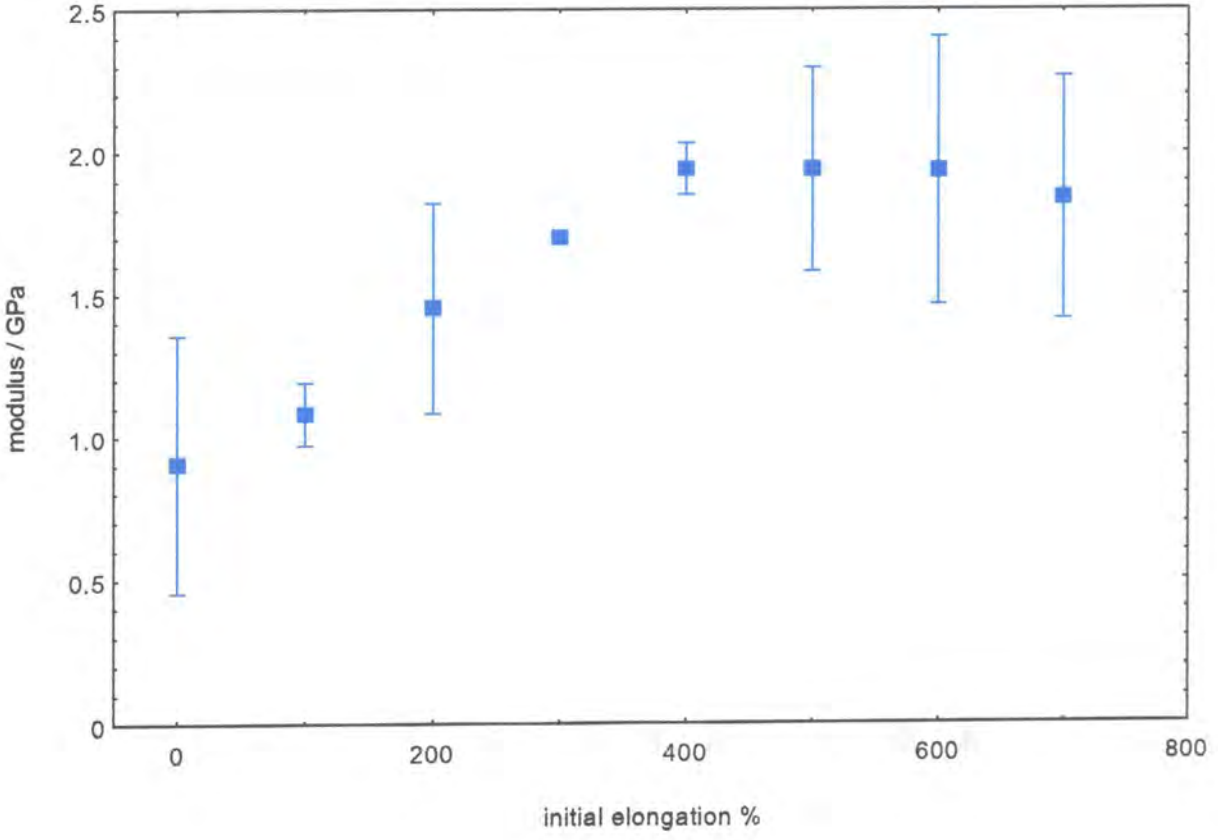

3.6 Interpretation of Mechanical Behaviour -Crystallinity Considerations

It will be shown in the next chapter that orientation of emeraldine base films at elevated temperature affects their crystallinity. The crystallinity of $e_{\%}$=300 samples is found to be higher than that of unoriented samples. However, the crystallinity of 600% elongated samples is almost identical to that of 300% samples. Fischer et al[14] considered the possibility of the initial increase in crystallinity with elongation being due to molecular rearrangement caused by the elevated temperature (~110°C) rather than the stretching itself. However, they found that the crystallinity of an annealed sample was the same as one which had not been annealed. Therefore the initial change in crystallinity must be closely linked with the orientation of the molecules themselves. The measurements of crystallinity are explained in Chapter 4, and possible reasons for the negligible change in crystallinity above 300% elongation discussed. However, in relation to the mechanical properties of EB the behaviour appears to be linked with crystallinity. The average behaviour of breaking stress can still be explained by the fact that elongating the samples to values above 300% will still align the molecules, but in an essentially amorphous fashion. This alignment would cause the uniaxial stress exerted by the strain gauge to act mainly on the strong intra-molecular bonds, and as $e_{\%}$ increases so too will the effect of these bonds. The weaker inter-molecular van der Waal's bonds will predominate perpendicular to the direction of orientation. Because of the small dimensions of the samples it was not possible to measure mechanical properties perpendicular to the direction of orientation.

3.7 Summary

The mechanical behaviour of oriented emeraldine base samples has been studied. The experiments have revealed little relationship between the specific values of initial elongation and the mechanical properties measured. However, it is possible that the trends observed may be linked to the crystallinity of the samples. There is a notable increase in breaking stress for increasing values of $e_{\%}$, which has been interpreted in terms of increased alignment of polymer chains along the direction of elongation. The variations in breaking strain and Young modulus are both consistent with variations in crystallinity. The diversity in the quantitative results for different samples may be

indicative of different samples having subtle differences in morphology and therefore variations in crystallinity.

Unfortunately it was not possible to measure crystallinity values for individual samples, and therefore difficult to quantify the relationship between crystallinity and mechanical properties. It is likely that mechanical testing with samples of known crystallinity would enhance our understanding of these properties but further work would be required to achieve this goal.

References

1. *Introduction to Polymers*, R J Young , publ. Chapman & Hall 1987.

2. *An Introduction to the Mechanical Properties of Solid Polymers*. I M Ward & D W Hadley, publ. John Wiley & Sons, 1993.

3. J K Knowles and A G H Dietz. *Trans. Am. Soc. Mech. Eng.*, **77**, 177 (1955)

4. E H Merz, L E Nielsen, , R Buchdahl. *Ind. Eng. Chem.*, 43, 1396 (1951).

5. J A Yanko. *J. Polymer Science*, 3, 576, (1948)

6. P W O Wijga, *Physical Properties of Polymers*. Monograph No. 5, Soc. Chem. Ind., p 35, New York, Macmillan Co. 1959.

7. R G Cheatham and A G H Dietz. *Modern Plastics*, **29**, 113 (Sept., 1951).

8. G G Jones and F D Miles. *J. Soc. Chem. Ind.*, **52**, 251 (1933).

9. A S Novikov, T V Dorokhina, and P I Zubov. *Rubber Chem. and Technol.*, **31**, 27 (1958).

10. *Encyclopaedia Britannica, Macropaedia*, Vol. 11, Edition 15, Publ. Helen Hemingway Benton, 1973-74.

11. E J Oh, Y Min, J M Wiesinger, S K Manohar, E M Scherr , P J Prest, A G MacDiarmid, A J Epstein. *Synthetic Metals*, **55-57**, 977-982 (1993).

12. C A Sperati, W A Franta, H W Starkweather Jr. *J. Am. Chem. Soc.*, **75**, 6127 (1953)

13. K Akagi, M Suezaki, H Shirakawa, H Kyotani, M Shimomura and Y Tanabe, *Synth. Met.* **28**, D1-D10, 1989.

14. J E Fischer, Q Zhu, X Tang, E M Scherr, A G MacDiarmid and V G Cajipe. *Macromolecules* **27**, pp 5094 - 5101. (1994)

15. C L Chang, W Y Chiu, K H Hsieh and C-C M Ma. Journal of Applied Polymer Science, **50**, no.5, pp855-862 (1993).

16. *Viscoelasticity*. W Flugge. Publ. Blaisdell Publishing Company, 1963.

17. A G MacDiarmid, Y Min, J M Weisinger, E J Oh, E M Scherr and A J Epstein. *Syn. Met.*, **55-57**, 753 (1993)

18. L Mandelkern in "*Physical Properties of Polymers*" 2nd ed. Publ. American Chemical Society. (1993)

19. Y Wei, G W Jang, K F Hsueh and E M Scherr, A G MacDiarmid and A J Epstein. *Polymer*, **33**, no. 2. 314 (1992)

CHAPTER 4 - X-RAY DIFFRACTION

4.1 Introduction

This chapter reports the results of X-ray diffraction experiments performed on polyaniline samples of varying degrees of elongation. Experiments have been performed on both emeraldine base and emeraldine salt samples in an attempt to determine the effects of both elongation and protonation on sample morphology. The experimental data were gathered and corrected by Dr. Jo Jutson at BICC Communications Ltd., Wrexham Technology Centre, Wrexham. This analysis also included the peak deconvolution routines, described later.

4.2 Theory of X-ray diffraction

The physical basis for X-ray diffraction is the interference effects produced by phase differences between rays elastically scattered from different atoms in the crystal[1,2]. The X-rays are scattered from electrons in the atoms which in turn are accelerated by the electric field vector of the X-ray photons. This produces the emission of secondary X-rays with the same wavelength and phase of the incident radiation. Thus, each atom in the sample may be considered to be a source of secondary spherical waves whose strength is governed by the scattering power of the atom. This scattering power is known as the *atomic form factor*, a quantity which is proportional to the atomic number of the atom.

In practice the sample is irradiated by a collimated beam of monochromatic X-rays with wave vector $\underline{k}$. The scattered rays in the directions of constructive interference may be considered as parallel beams of wave vector $\underline{k}'$, where $|\underline{k}| = |\underline{k}'|$. A schematic of this is shown in figure 4.1.

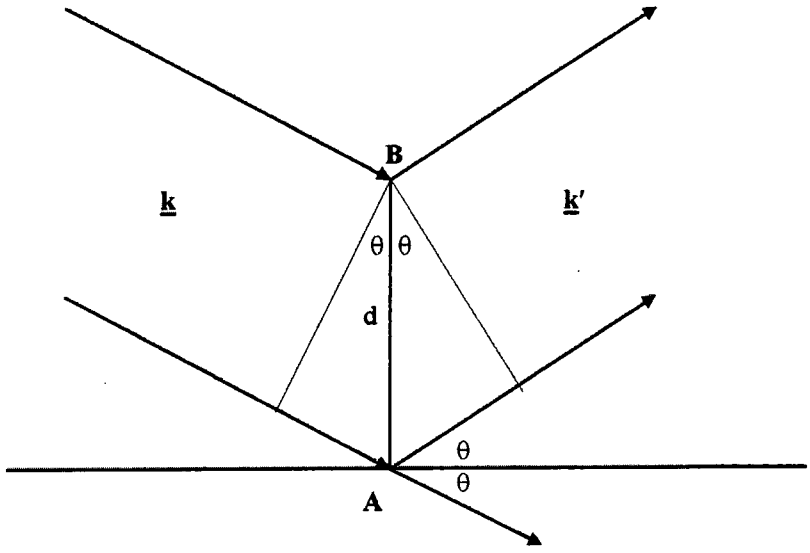

Figure 4.1: The scattering of an incident plane wave $\underline{k}$ by two centres A and B.

The scattered spherical wave leaving atom A in the direction $\underline{k}'$ is written:

$$(\varphi f / r') \, e^{\,i\,(k'r' - \omega t)}$$

where φ is the amplitude of the incident beam,

f is the atomic form factor,

r′ is the distance to the detector (photographic plate or Geiger counter) measured from A.

The scattering amplitude from B may be written:

$$(\varphi f / r_B) \, e^{\,i\,(k'r' - \omega t + \Delta)} \qquad \text{where } \Delta = \underline{\rho} \,.\, \underline{\Delta k}$$

This analysis may be generalised to account for any atom j which is at a distance $\underline{\rho}_j$ relative to atom A and at a distance $\underline{r}_j$ from the detector. This atom produces a signal amplitude at the detector equal to

$$(\varphi f / r_j) \, e^{\,i\,(k'r' - \omega t)} \, e^{\,i\,(\underline{\rho} j \,.\, \underline{\Delta k})}$$

Thus the signal amplitude at the detector and in the $\underline{k}'$ direction arising from the complete sample becomes

$$\sum_{\text{all atoms}} (\varphi f / r_j)\ e^{\,i\,(k'r'-\omega t)}\ e^{\,i\,(\rho j\,.\,\Delta\underline{k})}$$

The only term in this equation that can produce diffraction effects is

$$\sum_{\text{all atoms}} e^{\,i\,(\rho j\,.\,\Delta\underline{k})}$$

because atoms in different positions produce scattered waves with different phases.

This analysis leads to the well known condition for diffraction, which can be conveniently described in terms of the reciprocal lattice base vectors $\underline{A}$, $\underline{B}$ and $\underline{C}$ by the equation:

$$\Delta\underline{k} = n_1\,\underline{A} + n_2\,\underline{B} + n_3\,\underline{C} \qquad \text{where } n_1, n_2 \text{ and } n_3 \text{ are integers.}$$

Hence, for a family of planes (hkl) in the real lattice, the condition for constructive interference in crystal diffraction becomes:

$$\Delta\underline{k} = h\,\underline{A} + k\,\underline{B} + l\,\underline{C}$$

Referring back to figure 4.1, if 2θ is the angle separating incident and diffracted beams then

$$|\,\Delta\underline{k}\,| = 2\,|\,\underline{k}\,|\sin\theta = 2\pi / d_{hkl} \quad \Rightarrow\ 2\,d_{hkl}\sin\theta = \lambda$$

where λ is the X-ray wavelength,
d_{hkl} is the interplanar spacing, and
2θ is the diffraction angle.

4.2.1 Ewald Sphere Construction

As can be seen from the equation relating the change in wave-vector to the reciprocal lattice vectors, each diffracted beam is associated with a particular family of crystal planes. This can be simply described in terms of the Ewald sphere construction, figure 4.2.

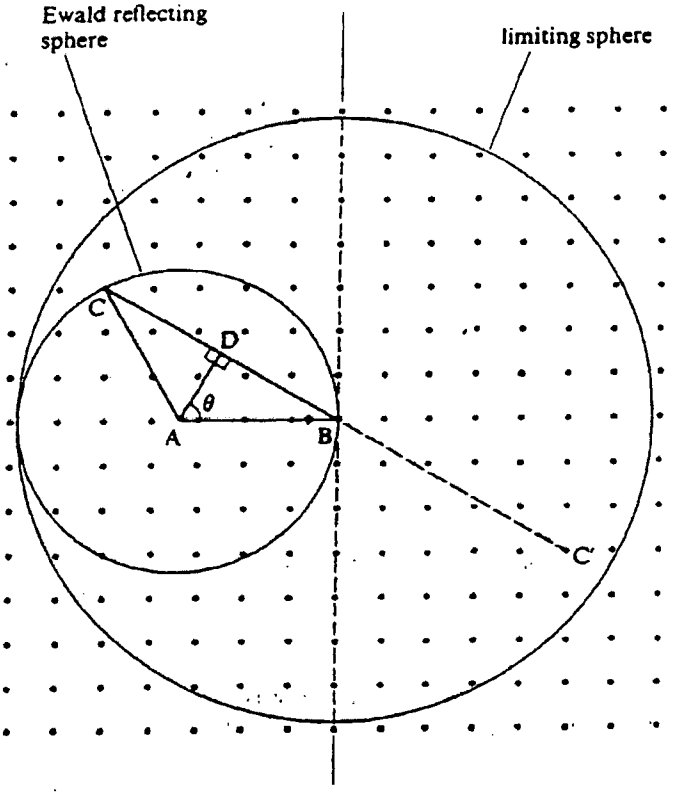

Figure 4.2: Ewald sphere construction to show the condition required for diffraction

The incident radiation has wave vector $\underline{k}$, which is arranged to end on the origin of the reciprocal lattice. Using the origin of $\underline{k}$ as centre, a sphere of radius $|\underline{k}| = 2\pi/\lambda$ is constructed. Wherever the surface of the sphere passes through a point of the reciprocal lattice then it can be shown[2] that diffraction conditions for this set of planes are satisfied. Normally however, a single crystal in an arbitrary orientation is unlikely to have any set of planes oriented in an appropriate position to satisfy the diffraction conditions. Consequently, the moving crystal technique[3] is employed; a method involving rotation of the crystal into appropriate orientations to cause diffraction. Rotating the crystal is equivalent to rotating the Ewald sphere around B, thus bringing other lattice points into

contact with its surface and satisfying the diffraction conditions. This is the basis of the diffractometer used for this work.

A diffraction pattern obtained from a sample enables important information relating to crystal structure of the sample to derived. Values for crystallinity, d-spacing and crystallite size can be determined[4] by analysis of the position, intensities and widths of the resulting Bragg peaks.

4.3 X-Ray Diffraction by Polymers

X-ray diffraction has been extensively used in the structural characterisation of polymers for many years, and serves as a very useful tool for polymer investigation. Although polymer molecules possess the ability to crystallise[5], they differ from most other crystalline solids in that they are normally only semi-crystalline. Evidence for this comes from the fact that the density of a 'crystalline' polymer is normally between that expected for a fully crystalline polymer and that for an amorphous polymer. Furthermore, flat-plate X-ray diffraction patterns from melt-crystallised polymers are usually in the form of rings superimposed on a diffuse background[5], figure 4.3.

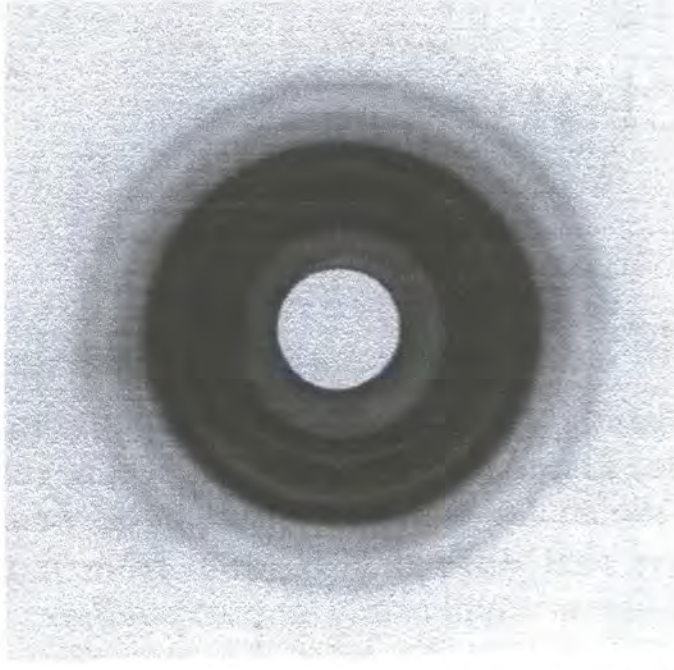

Figure 4.3. Flat-plate X-ray diffraction pattern obtained by an isotropic sample of melt-crystallised polypropylene.

The background indicates the presence of an amorphous phase and the rings indicate a second phase consisting of small randomly oriented crystallites. The X-ray analysis described in this chapter allows one to probe crystallinity and to compare the amorphous phase to the crystalline phase, particularly in relation to elongation ratios. Similar experiments have been performed on polyethylene[6] and polypropylene[7], enabling comparisons to be made later in the chapter.

4.3.1 Crystallisation Mechanisms in Polymers

For a polymer molecule to crystallise it is necessary that the polymer chains are principally linear[17]. Non-linear molecules have many more conformations than linear and therefore reduce the probability of crystallisation occurring. Limited branching will not completely prevent crystallisation but may severely limit it.

4.3.2 *Fringed Micelle* Model for Semi-Crystalline Regions

The packing of molecules in semi-crystalline polymers was originally described by the *fringed micelle* or two-phase model[18], figure 4.4.

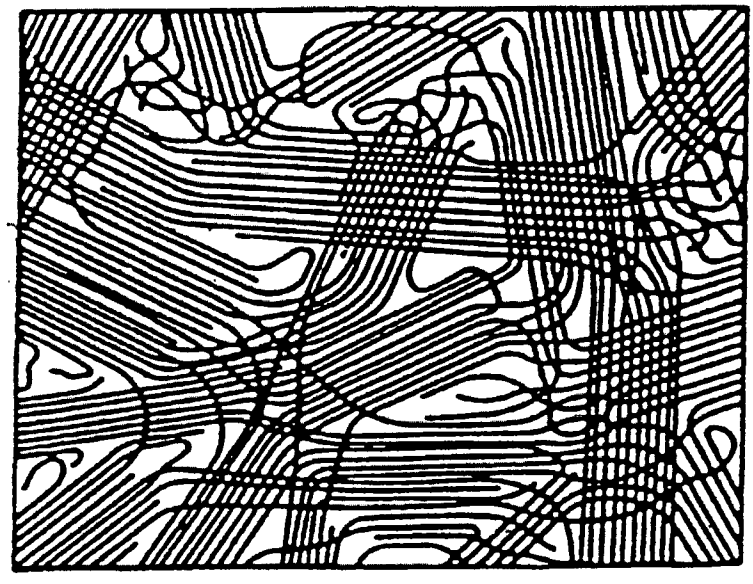

Figure 4.4. Fringed micelle model for a semi-crystalline polymer

This comprises local order (crystalline regions) surrounded by disordered (amorphous) regions. In the amorphous regions the chains are randomly oriented and tangled, with

relatively low density. The crystalline regions on the other hand are highly oriented and are of relatively higher density.

Since the chain segments in crystalline regions are held together by van der Waals forces which only act at close distances, polymers with sterically hindering substituent groups are much more likely to be amorphous than those with no side groups, figure 4.5.

poly(methyl methacrylate) (PMMA)

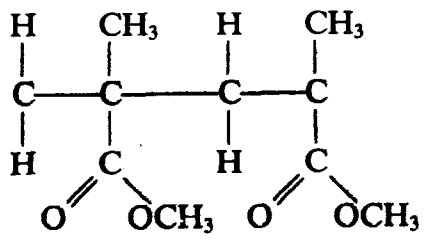

Figure 4.5. a) poly (methyl methacrylate). Typical crystallinity: 2 - 5%
Substituent side groups reduce probability of crystallisation - vdW's forces ineffective

polyethylene (PE)

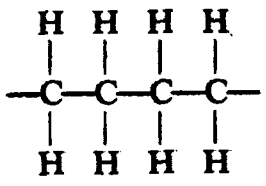

b) polyethylene - typical crystallinity - 50%

Another concern relating to crystallisation is the arrangement of molecules within a particular crystallite. The most likely arrangements of single crystals are depicted in figure 4.6. It is found that model (c) cannot generally be correct since this requires the amorphous density to exceed that of the crystal at the interface[22,23]. The probability for adjacent re-entry is found to be >2/3 compared with the probability of random re-entry whose value is <1/3. It is therefore assumed that types (a) and (b) are predominant folding regimes, with a small contribution from type (c).

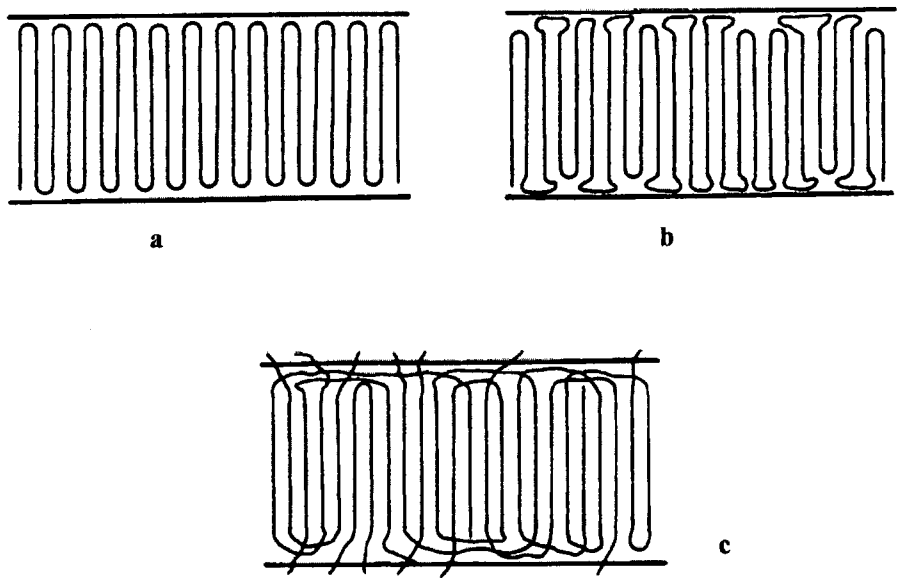

Figure 4.6. Illustration of the different types of folding suggested for polymer single crystals: a) adjacent re-entry with sharp folds; b) adjacent re-entry with loose folds; c) random re-entry.

4.4 Polyaniline X-ray diffraction - Review

X-ray diffraction experiments have been performed by a number of research groups[8,9,10] on emeraldine base and emeraldine salt samples in both the unstretched and stretched forms. This section gives a brief summary of the main results from these experiments.

4.4.1 Emeraldine Base

The results for emeraldine base films obtained by Milton[11] are depicted in figure 4.7. It is clear from these scans that crystalline structure increases with elongation. This increase in crystallinity was found to be approximately linear. Similar trends have also been found by other groups[12,19]. The crystalline peaks were found to be approximately compatible with an orthorhombic unit cell with dimensions a = 5.7Å, b = 7.8Å.

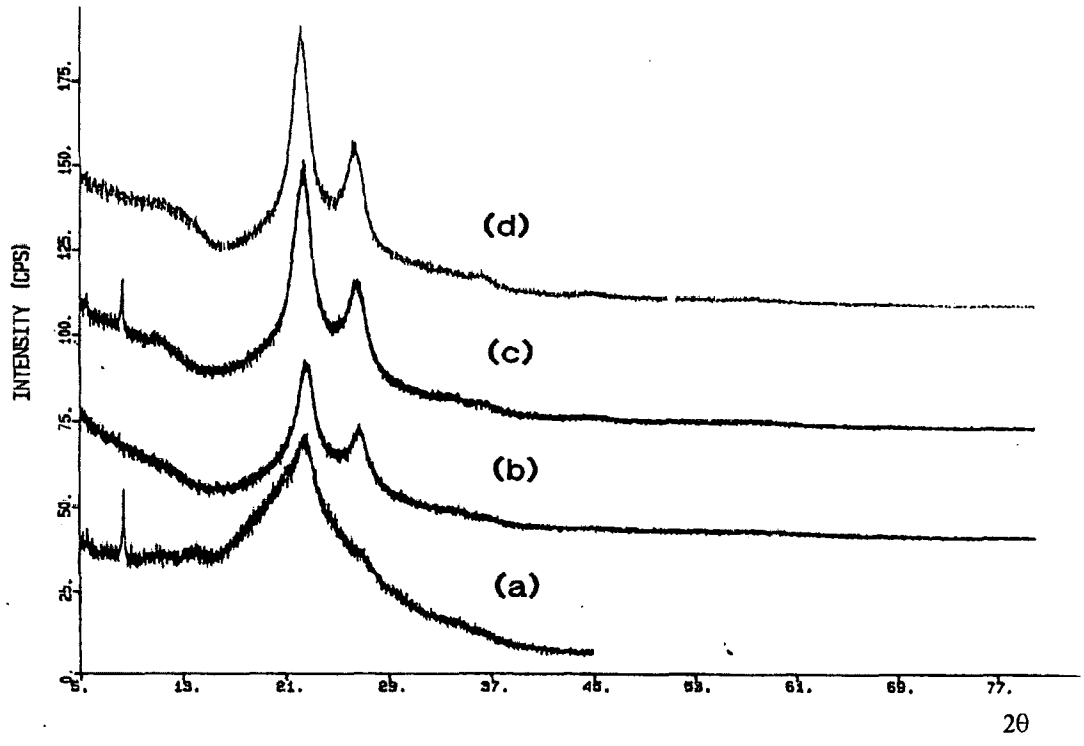

figure 4.7. Diffractometer scans for stretched EB films.
(a) 0% strain, (b) 100% strain, (c) 180% strain, (d) 230% strain.

4.4.2 Emeraldine Salt

Figure 4.8 shows a set of scans for EB and ES films with varying degrees of elongation.

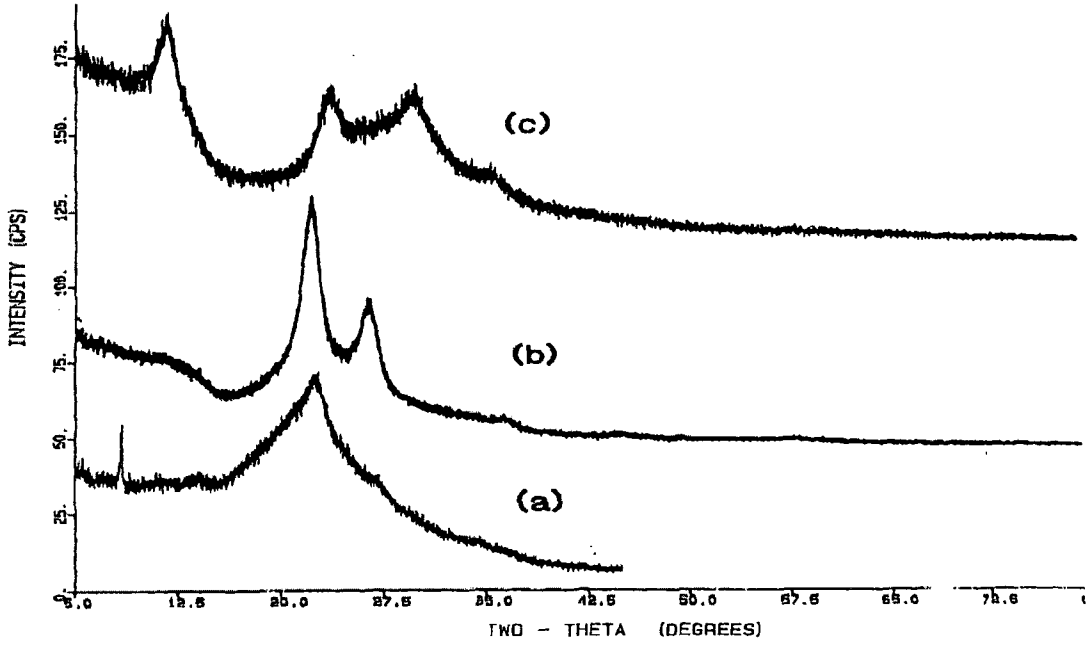

Figure 4.8. Diffractometer scans for ES stretched films (a) 0% strain EB; (b) 230% strain EB; (c) 240% strain ES. (After Milton)

The scan shows an obvious change in crystal structure upon doping and changes in d-spacings are also evident. Because of the decrease in intensity of the Bragg peaks for ES and the high background scattering, values for lattice parameters were not attainable from these scans.

Similar findings to the above have also been reported for other polymers such as poly(o-toluidine)[8] and poly(3-alkylthiophene)[13].

4.5 Experimental Techniques

4.5.1 The Diffractometer

The X-ray diffraction experiments were run on a D500 Siemens Diffractometer with the following specifications:

Radiation: Cobalt K-alpha
Wavelength of radiation: 1.788Å
2θ region covered: 3° to 50°
Step time: 60 seconds.

4.5.2 Analysis of Data

The data from the diffractometer was analysed by computer using a software package called DIFFRAC.AT. This includes a profile fitting routine which is used to separate the amorphous and crystalline peaks. The fitting program performs, in the sense of least squares, a profile fitting to the raw data file by a function of the type:

$$f(x) = P1(x) + P2(x) + \ldots\ldots\ldots + Pn(x) + bkg(x)$$

where bkg(x) is a straight line. The software fits the Pi(x)'s, i=1,2,....,n, to one or a mixture of the functions below:

Let h=h(i), b=b(i), p=p(i), X=x-p(i)

1. GAUSS: $Pi(x) = h \exp(-bX^2)$

2. LORENTZ (CAUCHY): $Pi(x) = h / (1 + bX^2)$

3. VOIGT (Pseudo-V)

   $Pi(x) = hg$ if $X^2 < \ln 2 / b$

   $= hc$ otherwise

   where $g = \exp(-bX^2)$ and $c^{-1} = 2((1 - \ln 2) + bX^2)$

4. PEARSON 7 sep: $Pi(x) = (Cauchy)^{s(i)}$ where i = 1,2,....n

5. PEARSON 7 com: same as 4 with common exponent s

6. SPLIT P7 sep: $Pi(x) = (Cauchy)^{s(i)}$ if $x<0$

   $= (Cauchy)^{t(i)}$ $x>0$

7. SPLIT P7 com: same as 6 with common exponent s,t

8. VOIGT 2 (Pseudo-V): Pi(x) = 0.5 Gauss + 0.5 Lorentz

   where Gauss = $h \exp(-b \ln(2X^2))$

9. VOIGT 3 (Pseudo-V): Pi(x) = a Gauss + (1-a) Lorentz

   where Gauss = $h \exp(-b \ln(2X^2))$

The crystallinity is calculated relative to the crystallinity of polyethylene. In the absence of a polyethylene sample with 100% crystallinity measurements are relative to a preselected polyethylene standard. The peak profile shape used for polyethylene is Split P7 which most closely matches the polymer shape and indeed diffraction peak shapes for most materials. In practice it has been found that other profile functions do not give a fit. Since the crystallinity determinations are relative there are no specific instrumental corrections for deconvolution. In the case of the polyaniline samples, where the

crystalline peaks are very small and broad, the undoped samples were fitted by Split P7 but the doped could only be fitted assuming Gaussian shaped peaks.

It is thus important to note that data is relative. It is more appropriate to view the results as a comparison of the different samples to give a ranking in order of crystallinity, d-spacings, crystallite size etc.

The goodness of a profile fitting is related to the differences between calculated and observed intensities (I_{obs} - I_{calc}) for the n fitted data points. Three possible ways for characterising this goodness are:

Normal.mean error : $(\Sigma (I_{obs} - I_{calc})^2 / n)^{1/2}$

Reliability : $(\Sigma (I_{obs} - I_{calc})^2 / \Sigma I_{obs}^2)^{1/2} \times 100$

RI (%) : $|\Sigma (I_{obs} - I_{calc}) / \Sigma I_{obs}| \times 100$

For all the samples Normal.mean error was less than 2 counts per second, Reliability % was less than 3 and RI% less than 1. From these values the estimated error in d-spacings may be evaluated.

4.5.3 Estimation of Crystallinity

The crystallinity of a sample is calculated by comparing the integrated areas of the amorphous and crystalline peaks. In practice this procedure is not as trivial as might at first be expected. Consider a typical Wide Angle X-ray Scattering (WAXS) curve for a semi-crystalline polymer, figure 4.9.

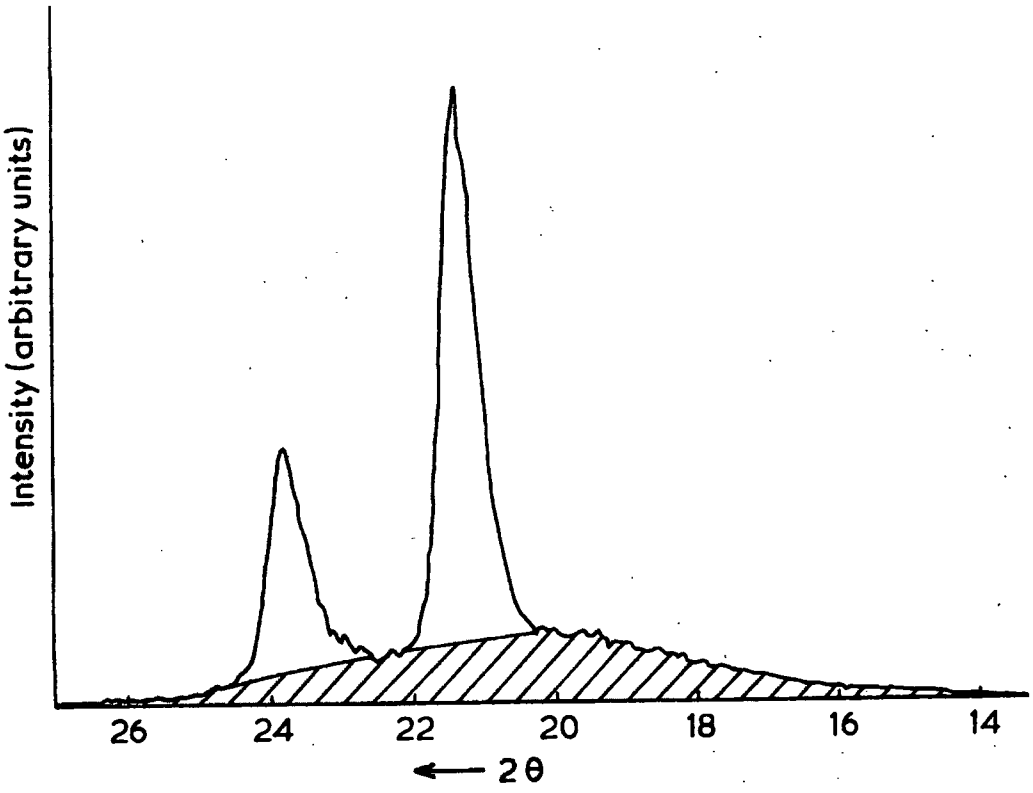

Figure 4.9. WAXS curve for polyethylene. The intensity of scattering is plotted as a function of 2θ; the amorphous hump is shaded.

The relatively sharp peaks are due to scattering from crystalline regions and the broad underlying hump is due to scattering from non-crystalline areas. In principle, it should be possible to determine the degree of crystallinity from the relative areas under the crystalline peaks and the amorphous hump. In practice however, it is often difficult to resolve the curve into areas due to each phase. The shape of the amorphous hump can be determined from the WAXS curve for a completely amorphous sample, obtained by rapidly cooling a molten sample. However, for many polymers this can prove difficult or even impossible to do so the amorphous scattering can only be estimated. Also, corrections should be made for disorder in the crystalline regions (for example, the fold edges of figure 4.6) which can give rise to a reduction in the sharp peaks. The ever-improving software technology is enabling these and similar anomalies to be very accurately gauged and accounted for. It is believed that the use of the DIFFRAC.AT software will allow reliable manipulation of the results.

4.5.4 Focussing of Diffractometer

The diffractometer employs Bragg-Brentano para-focussing geometry[14], as shown in figure 4.10.

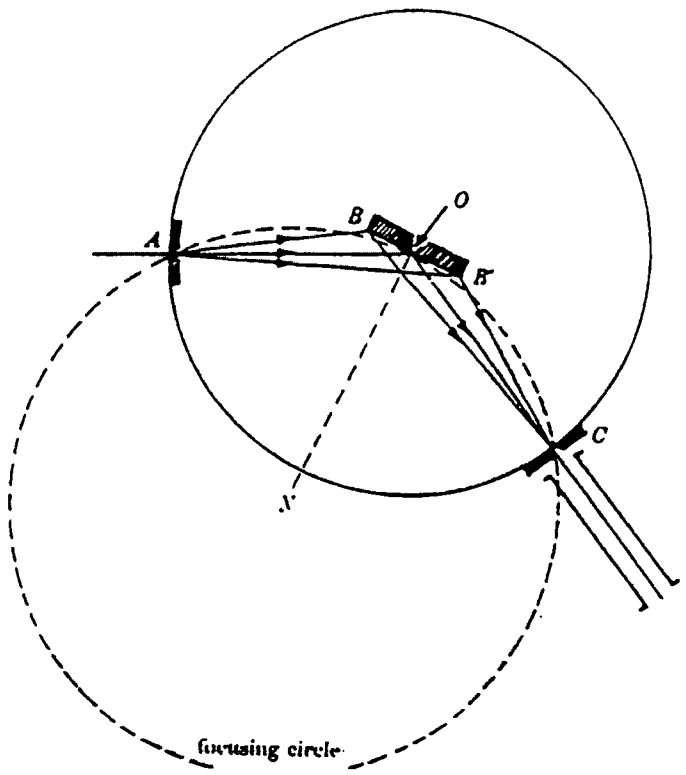

Figure 4.10. Bragg-Brentano focussing geometry

The X-rays diverge from point A and strike the sample which moves along the perimeter of the focussing circle. The detector is mounted on an arm which is pivoted at 0. The specimen is rotated at half the angular speed of C so that the normal to the sample, ON, always bisects AOC. This arrangement enables the condition for diffraction to be satisfied, as characterised by the Ewald sphere construction. Because the sample is flat and therefore tangential to the focussing circle, it is not possible to achieve undistorted focussing. This obstacle can, however, be overcome by the use of a suitable slit and monochromator arrangement to reduce the vertical divergence of the X-ray beam, figure 4.11.

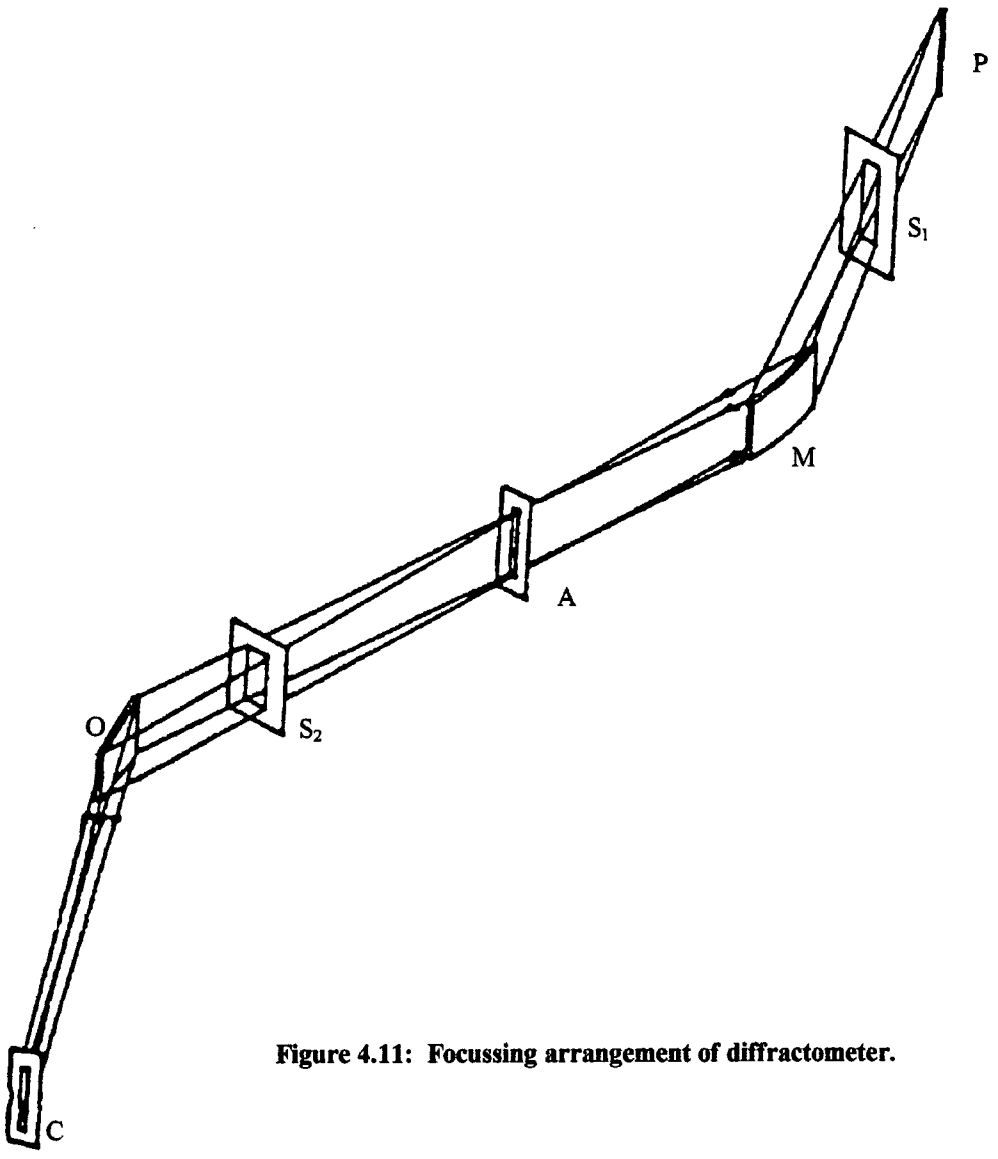

Figure 4.11: Focussing arrangement of diffractometer.

The arrangement consists of the following:

P: X-ray tube focus

M: monochromator

O: specimen axis

C: counter entrance slit

The focus of the monochromator is at A, at which point another slit is placed to filter further the beam. The monochromator has the effect of reducing the vertical divergence

of the X-ray beam since only incident beams of slight divergence will be reflected. The typical angular beam using this arrangement is ca. 0.5°.

4.6 Experimental Results

The X-ray diffraction data is presented in this section. The analysis contains the results for both doped and undoped samples, with elongations varying from 0 to 600%. Also included in this section are profile fittings to separate the amorphous and crystalline peaks using the methods described earlier.

Figure 4.12. Diffractometer scans for elongated EB films

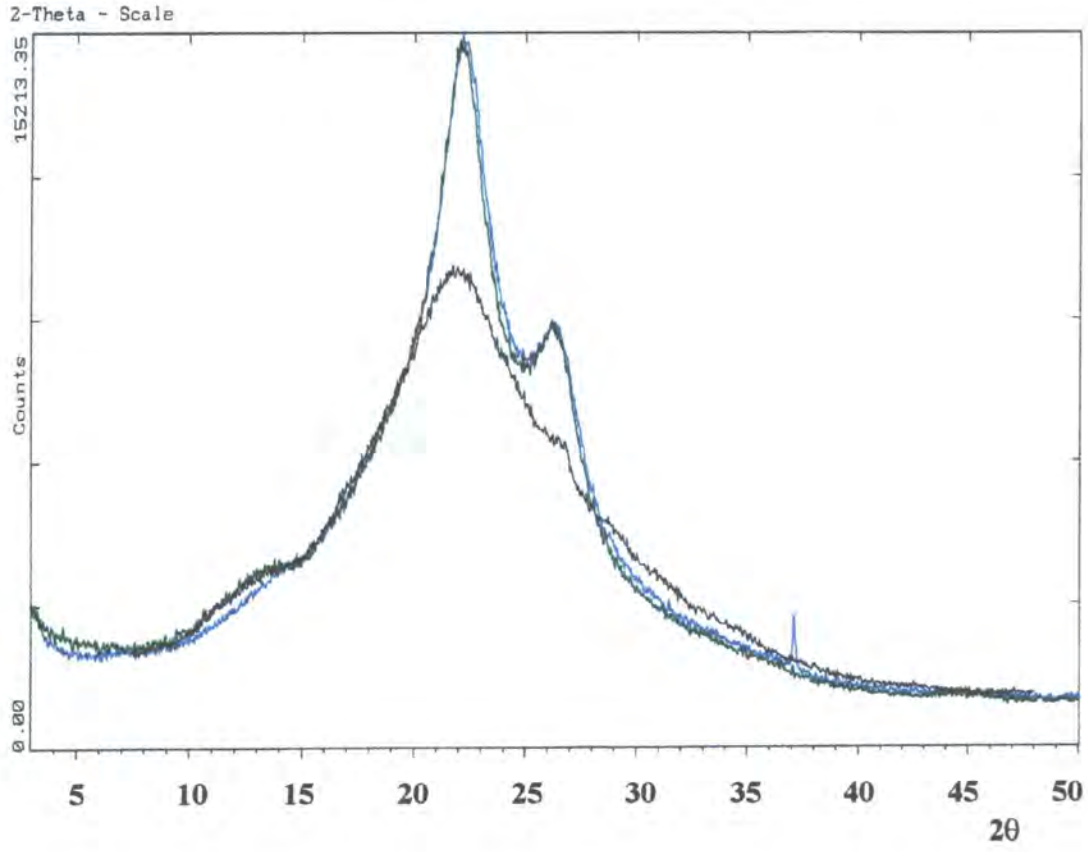

black curve: 0% initial elongation,
green curve: 300% initial elongation,
blue curve: 600% initial elongation.

Figure 4.13. Diffractometer scan for 0% elongated EB film.

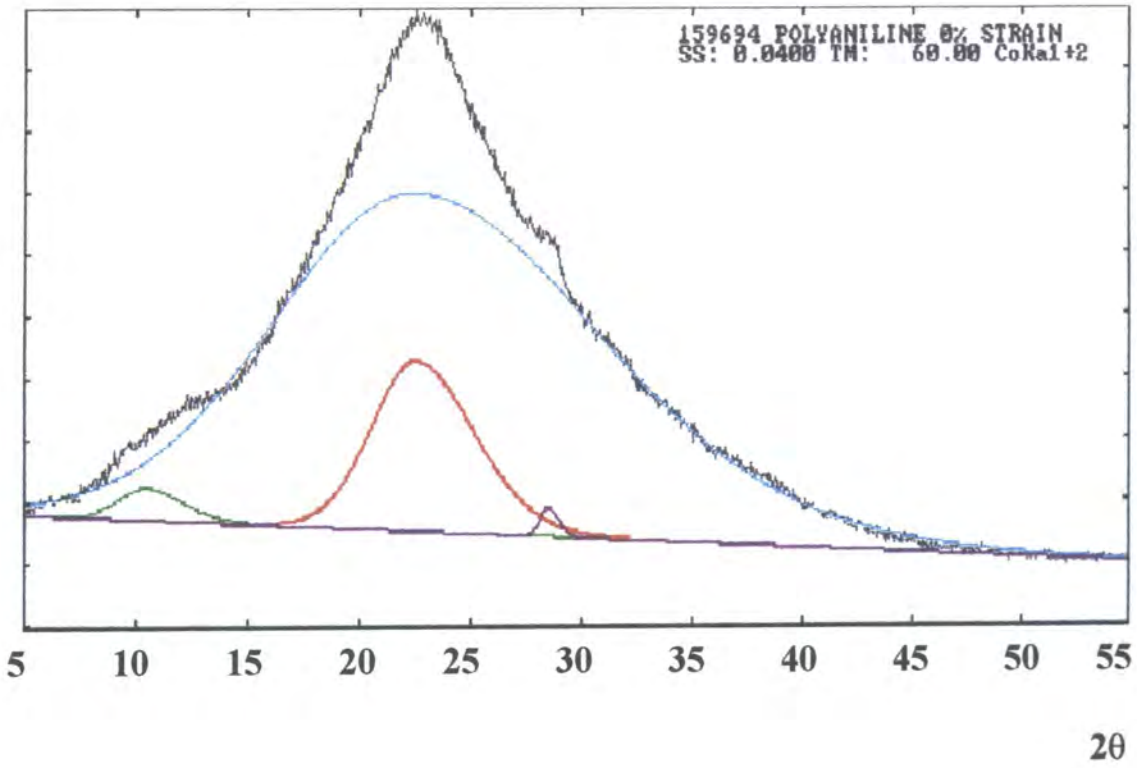

Figure 4.14. Diffractometer scan for 300% elongated EB film.

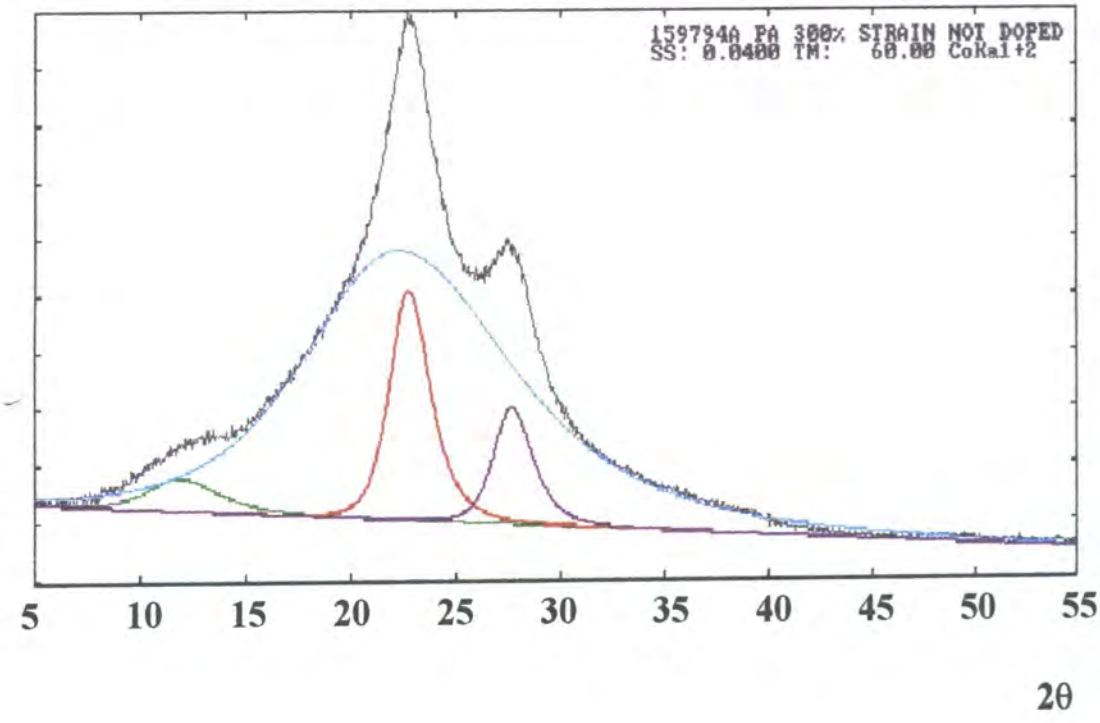

Figure 4.15. Diffractometer scan for 600% elongated EB film

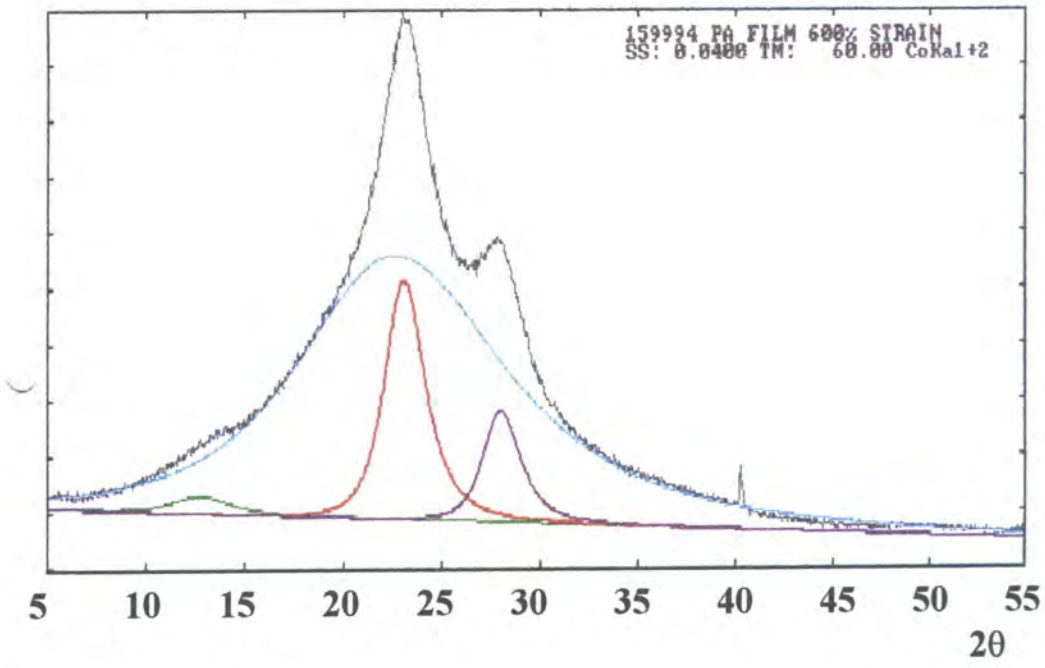

Figure 4.16. Diffractometer scans for elongated ES films. (—— 0 %, —— 300%. —— 600%)

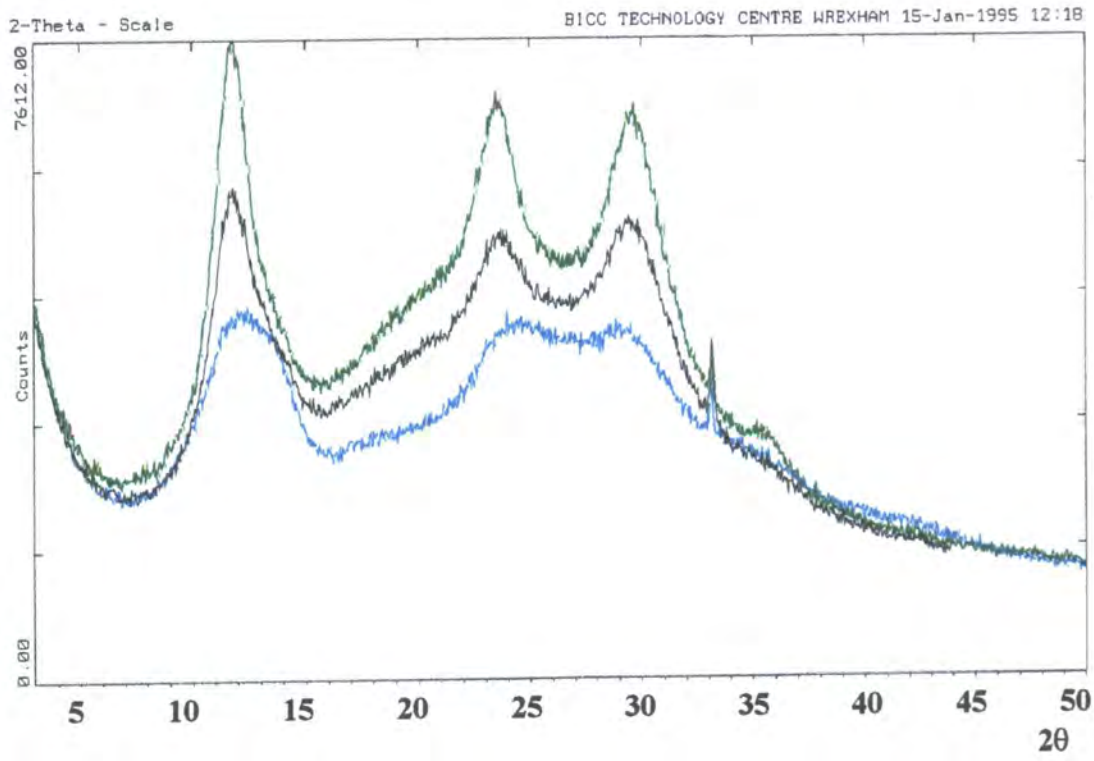

Figure 4.17. Diffractometer scans for 0% elongated ES films

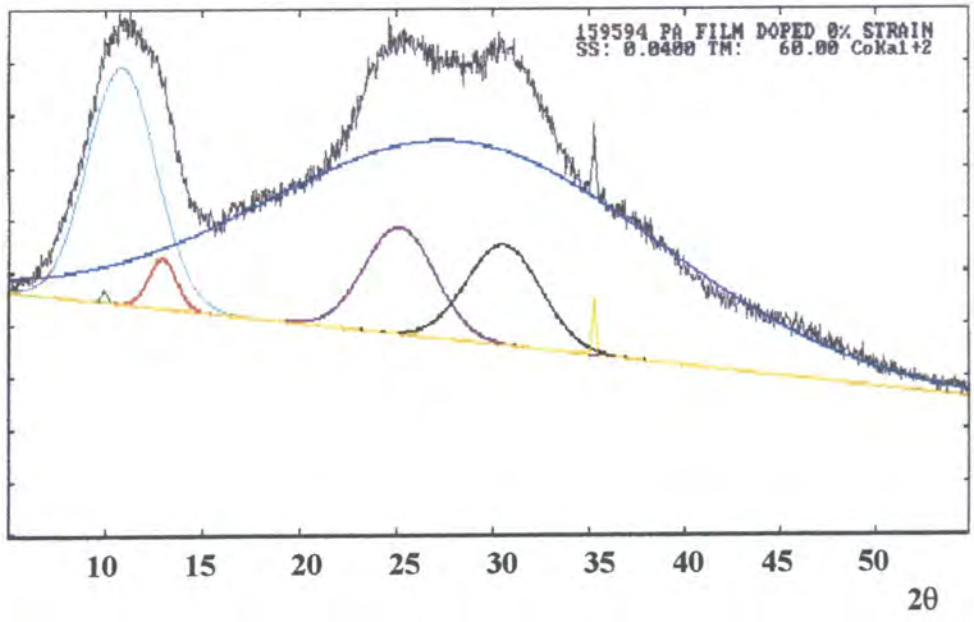

Figure 4.18. Diffractometer scans for 300% elongated ES films

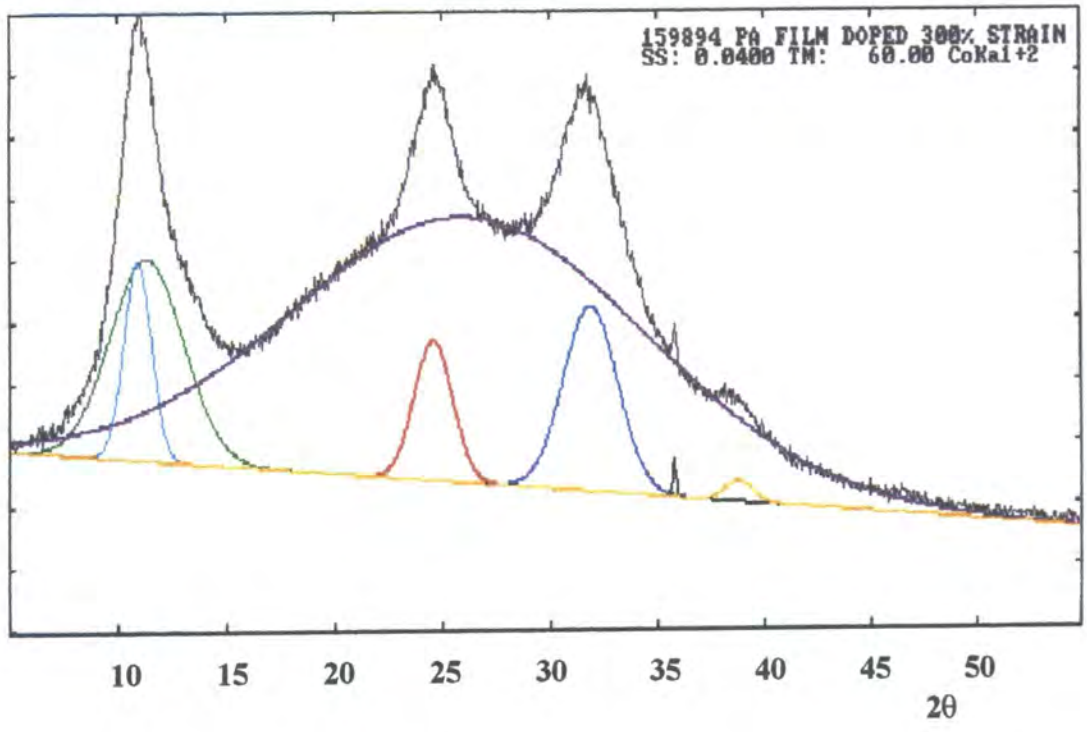

Figure 4.19. Diffractometer scan for 600% elongated ES film

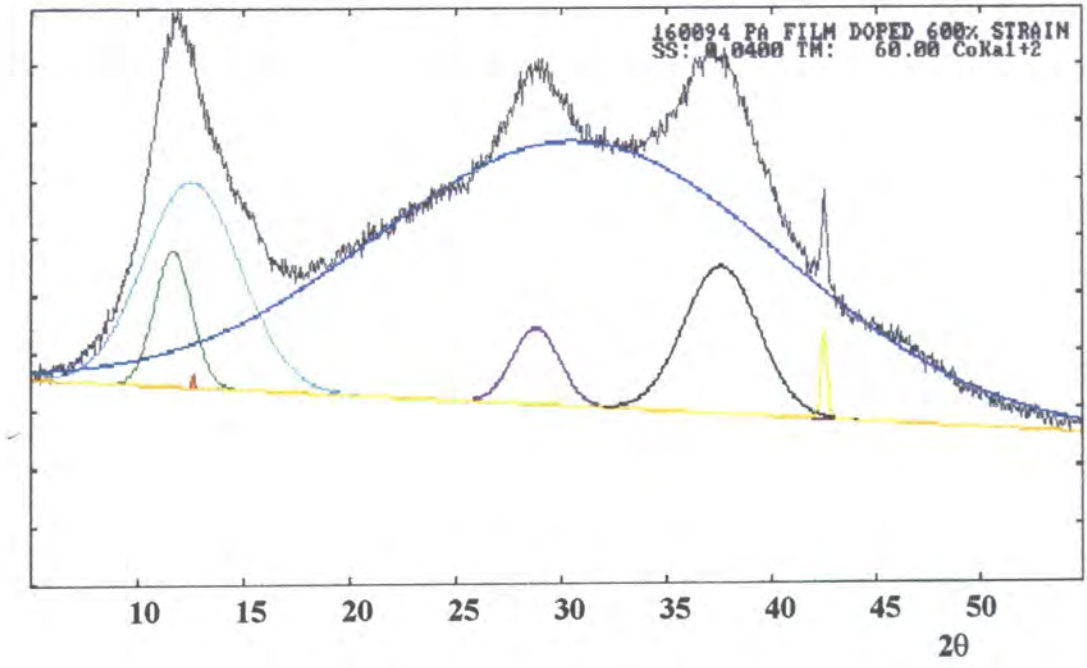

4.7 Discussion of Results

4.7.1 EB films

The diffractometer scans 4.12-4.15 give information which enable determination of the effect of film elongation on the crystallinity, d-spacings, lattice parameters and crystallite size for undoped samples. These shall now be treated individually.

4.7.1(a) Crystallinity

Table 4.1 shows the measured values of crystallinity as a function of strain.

Strain %	Crystallinity %
0	14.4
300	22.5
600	22.0

Table 4.1. Values of crystallinity for EB samples with elongations from 0% to 600%.

Table 1 shows that an initial increase in crystallinity occurs for 300% elongated emeraldine base samples. However, the crystallinity of a 600% elongated sample is approximately the same as that of a 300% sample. An increase in elongation above about 300% does not seem to affect the crystallinity of the polymer by any substantial amount. Previous measurements[11,12] on crystallinity as a function of elongation imply a linear increase but there is no evidence for this above 300% strain from these measurements. One explanation for this behaviour could be that the samples used for these experiments are of considerably higher molecular weight than before[15]. This may reduce the likelihood of further increases in crystallinity at higher elongation ratios due to the higher density of molecules and therefore the increased difficulty for molecules to arrange themselves into suitable positions to crystallise. It has also been suggested[20] that the reason for increased crystallinity during stretch-alignment is the morphological changes due to the elevated temperatures under which the process is carried out. However, comparison between the crystallinity of annealed and non-annealed EB

samples has proven that this is not the case - there was no observed change for the two situations.

Crystallinity measurements of ca. 14% for unstretched EB samples are higher than previously reported. Annis and Specht[9] report 5% crystallinity for their samples, indicating a considerable disparity between values reported by different groups. This discrepancy cannot yet be satisfactorily explained, suffice to say that it is important to appreciate that crystallinity values are relative rather than absolute, and may vary depending on the analysis techniques employed to derive the values.

4.7.1(b) d-spacings

Table 4.2 shows the measured d-spacings for the amorphous and crystalline peaks for EB samples as a function of elongation. The typical error in the calculated d-spacings for polymers is approximately 0.02 Å (polyethylene). It is assumed that the errors for polyaniline are of the same order.

Strain %	peak type	d-spacing / Å	d-spacing / Å
0	crystalline	4.75	3.89
300	crystalline	4.67	3.92
600	crystalline	4.65	3.91
0	amorphous	4.78	-
300	amorphous	4.75	-
600	amorphous	4.73	-

Table 4.2. d-spacing versus elongation for EB

The d-spacings for the amorphous peaks, which give the average spacing between polymer chains in the amorphous region, decreased slightly as the elongation increased. The d-spacings for the crystalline peaks show a similar trend to the crystallinity measurements mentioned earlier. There is a relatively large change in d-spacing from 0% strain to 300% strain, but above this the values remain approximately unchanged.

Once again this illustrates that the overall effect of elongation on crystalline parameters above values of about 300% is small.

4.7.1(c) Lattice Parameters

The scans for 300% and 600% strain EB films show two discernible crystalline Bragg peaks. These have been previously ascribed to the (110) and (200) planes according to an orthorhombic unit cell structure for ordered EB chains[11,21]. The lattice parameters a and b were calculated from these two peaks and are shown as a function of strain in Table 4.3.

Strain %	a / Å	b / Å
0	7.78	5.99
300	7.84	5.82
600	7.82	5.79

Table 4.3. Lattice parameters as a function of elongation for EB.

This shows the characteristic change of lattice parameters from 0% to 300%, followed by negligible change above this value. The values do compare reasonably well with those obtained by Jozefowicz & Epstein[8] (a=7.65-7.8, b=5.7) for unstretched EB, though no comparisons can be made for highly oriented films, since the results published in this thesis are the only ones available for 600% strain.

4.7.1(d) Crystallite size

The widths of the Bragg peaks enable calculation of the average crystallite size in the direction perpendicular to the plane, assuming the c-axis to be in the direction of elongation. A software package called Win-Crysize was used to perform this calculation. To correct for the effect of instrumental factors on the peak profile and width the data was compared with data from a standard sample which has a) similar transparency to the sample under investigation, b) diffraction peaks in the same region

and c) crystalline fraction large enough to not give line broadening due to crystallite size. For polymers hexamine is used. These values of crystallite size for EB are shown in Table 4.4.

Strain %	crystallite size/Å (200) plane	crystallite size/Å (110) plane
0	<60	<60
300	66	64
600	64	71

Table 4.4. Crystallite size as a function of elongation for EB

The crystallite size for the undoped unstretched sample was too small for calculation. Those for the 300% and 600% strain samples are of a similar size, again indicating that elongation above 300% strain has little effect on crystallinity.

4.7.2 ES Films

The diffractometer scans for emeraldine salt samples are shown in figures 4.16-4.19. A notable difference from the EB scans is that more Bragg peaks are evident. There are at least four discernible peaks in each of the ES scans compared to two for the EB. Another feature of these peaks is that they are significantly less intense than the EB peaks and have a higher background scattering. Thus it is not possible to determine an accurate crystal structure. It is, however, still possible to make measurements concerning crystallinity and d-spacings for doped samples. These shall be treated below.

4.7.2(a) Crystallinity

Strain %	Crystallinity %
0	29.6
300	27.5
600	26.4

Table 4.5. Crystallinity versus elongation for ES samples

Table 4.5 shows the relative crystallinity of ES samples for 0%, 300% and 600% elongation. The crystallinity for salt samples is higher then those for base. The effect of elongation was a small decrease in crystallinity. This trend is not clear from the diffraction patterns obtained but while the stretched samples appear to have more crystalline peaks they also have larger amorphous peaks. Again this emphasises the importance of regarding the crystallinity values obtained as relative and not absolute. In addition, the unstretched samples have very broad crystalline peaks due to the small crystallite size, which merge into the amorphous peak.

4.7.2(b) d-spacings

Strain %	peak type	d-spacings / Å					
0	crystalline	-	8.49	7.39	4.23	3.56	-
300	crystalline	8.76	8.53	-	4.39	3.49	2.92
600	crystalline	8.81	8.37	-	4.37	3.48	-
0	amorphous	3.79	-	-	-	-	-
300	amorphous	4.14	-	-	-	-	-
600	amorphous	4.12	-	-	-	-	-

Table 4.6. Strain versus d-spacing for ES polyaniline

The amorphous d-spacings for the salt samples are lower than those for their base counterparts. The same trend is shown for the crystalline peaks. It can be seen from the table that there is approximately a 10% increase in d-spacing for 300% elongated films compared with unoriented, with very little change when increasing from 300% to 600% elongation. An analogy cannot, however, be drawn for the crystalline peaks, where for some of the peaks an increase in d-spacing is observed between 300% and 600% elongation, and for others a decrease. One way of accounting for this is by recognising that no two samples have identical morphologies and so these trends could be due to the individual morphology of each sample.

Lattice parameters and crystallite size were not calculated for the doped samples since it was not clear which were the (110) and (200) peaks. However, it was clear from the variation in peak breadths that crystallite size increased with elongation.

The measured d-spacings can be compared with those measured by Pouget et al[21]. These authors have suggested two different possible structures for polyaniline depending upon synthesis conditions. Class I is that for which the base form is essentially amorphous, and is formed when the polymer is obtained from solution in protonated form. Class II is that for which the base is partially crystalline and is obtained when the polymer is formed in the unprotonated form by using a suitable solvent such as NMP. Thus the salt form of this, termed ESII, is formed by immersion in HCl. The measured d-spacings for the ESI structure measured by Pouget are outlined in table 4.7, and those for ESII in table 4.8.:

d / Å	intensity	indexation (hkl)
9.57	strong	0 0 1
5.94	strong	0 1 0
4.26	strong	1 0 0
3.51	very strong	1 1 0

Table 4.7: Measured d-spacings for ESI polyaniline structure (after Pouget et al[21])

d / Å	intensity	indexation (hkl)
7.88	medium	0 1 0
4.38	weak	0 1 2
3.49	strong	2 0 0

Table 4.8: Measured d-spacings for ESII polyaniline structure (after Pouget et al[21])

Comparison of these tables with table 4.6 confirm that ESII is indeed the most likely structure for the samples tested here, although the differences between the d-spacing for the (010) plane cannot be satisfactorily explained. It is likely that the differences are due to the different software packages used to analyse the data.

An interesting comparison with semi-crystalline polyaniline can be found with low density polyethylene (LDPE), figure 4.20, which also possesses an orthorhombic crystal structure.

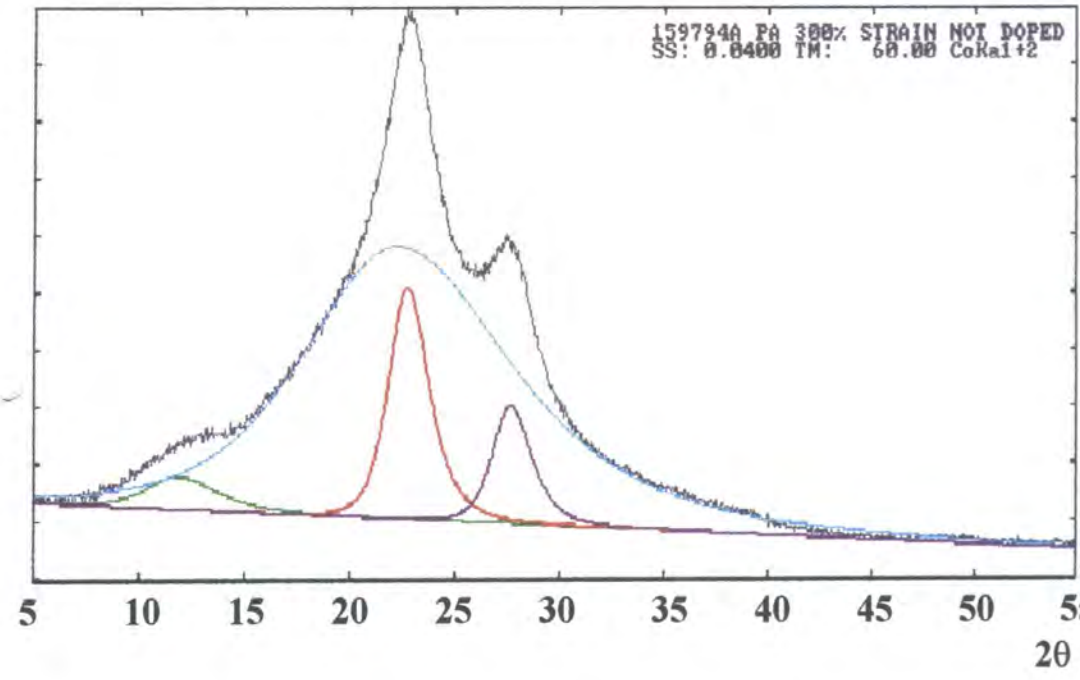

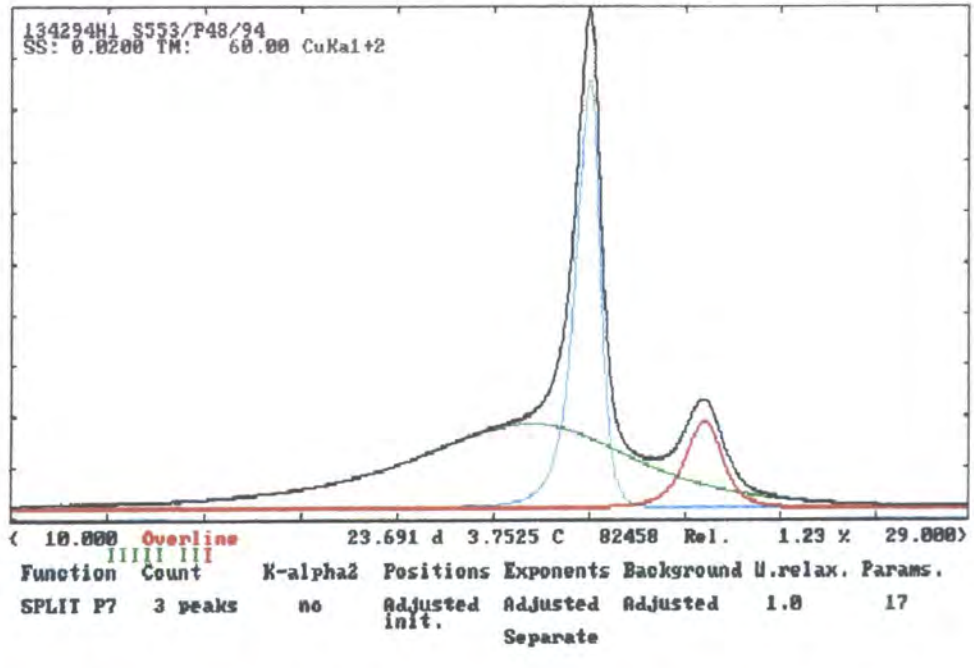

Figure 4.20. Comparison of diffractometer scans for 300% elongated EB and LDPE

	% crystallinity	crystallite size/Å		d-spacing / Å	
		(110)	(200)		
LDPE	22.5	95	150	4.86	4.37
300% PANi	22	64	66	4.67	3.92

Table 4.9. Comparison of crystallinity, crystallite size and d-spacing for LDPE and 600% PANi.

It can be seen from Table 4.9 that the crystallite size for LDPE is much larger than that for 300% EB. This can be accounted for by the fact that the complex stereochemistry of the polyaniline chain make it difficult for the chains to assume the appropriate conformations to allow crystallisation to be energetically favourable, compared with the simple structure of LDPE[6].

4.8 Summary

X-ray diffraction techniques have allowed the crystalline fraction of oriented polyaniline films to be investigated. Films elongated by up to 600% have been analysed both in the base and salt forms to investigate the effect of orientation on crystallinity. The diffractometer scans have enabled the crystallinity, d-spacings, lattice parameters a and b, and crystallite size to be calculated. Possible unit cell structures have not, however, been determined because not enough discernible Bragg peaks are evident to allow this.

The crystallinity of base samples has been found to initially increase with elongation but then to remain constant above 300% elongation. Similar trends are followed for the d-spacings, lattice parameters and crystallite size. This indicates a change in crystal structure between 0% and 300% strain, but negligible apparent change above this elongation.

For the salt samples, although the values for crystallinity and d-spacing do vary with strain, the variation is irregular and it is therefore difficult to account quantitatively for the effect of elongation upon crystal structure. It may be that the irregular nature of the ES data is due to the variations in morphology for different samples. These

morphological differences appear to be more prominent in the ES samples due to the large structural changes upon protonation.

In order to get a more definite picture of the effect of elongation upon crystal structure it would be advantageous to take diffractometer scans for a larger variety of elongations, perhaps at 100% elongation intervals. It would then be possible to determine more accurately how elongation affects structure. It would also be of interest to compare the effect of orientation with the effect of heating upon the X-ray structure of the samples, and to see whether high molecular weight polyaniline is affected more by heat than the samples tested by other groups. This is the subject of ongoing research here at Durham[16].

References

1. G Hildebrandt. *The Discovery of the Diffraction of X-rays in Crystals - a Historical Review.* Crystal Research and Technology. **28**, no. 6, 747 (1993)

2. H P Myers. *Introductory Solid State Physics.* Publ. Taylor & Francis Inc. (1990)

3. G E Bacon. *X-ray and Neutron Diffraction.* Publ. Pergamon Press. (1966)

4. J P Eberhart. *Structural and Chemical Analysis of Materials.* Publ. John Wiley and Sons. (1991)

5. R J Young. *Introduction to Polymers.* Publ. Chapman & Hall (1981).

6. C P Lafrance, M Pezolet and R E Prudhomme. *Macromolecules* **24,** 4948 (1991)

7. C P Lafrance and R E Prudhomme. *Polymer.* **35,** no. 18, 3927 (1994)

8. M E Jozefowicz, A J Epstein, J-P Pouget, J G Masters, A Ray, Y Sun, X Tang and A G MacDiarmid. *Synthetic metals*, **41-43,** 723 (1991)

9. B K Annis, E D Specht, N Theophilou and A G MacDiarmid. *Polymer*, **32,** no7 1160 (1991)

10. Y B Moon, Y Cao, P Smith and A J Heeger. *Polymer Comm.* **30**, 196 (1989)

11. A.J. Milton. PhD Thesis. Durham University, 1993.

12. E M Scherr, A G MacDiarmid, S K Manohar, J G Masters, Y Sun, X Tang, M A Druy, P J Glatkowski, V B Cajipe, J E Fischer, K R Kromack, M E Jozefowicz, J M Ginder, R P McCall and A J Epstein. *Synth. Met.* **41-43**, 735 (1991)

13. J Mardalen, E J Samuelsen and O R Gautun. *Synth. Met.* **41-43,** 598 (1991).

14. H P Klug and L E Alexander. *X-ray Diffraction Procedures for Polycrystalline and Amorphous Materials.* Publ. Wiley-Interscience, (1974)

15. P N Adams, P J Laughlin and A P Monkman. *Synth. Met*, **76**, 157. (1996).

16. L Abell. University of Durham. Personal Communication.

17. B Wunderlich. *Macromolecular Physics*, **2** Publ. Academic Press, London.

18. F Bueche. *Physical Properties of Polymers.* Publ. New York Interscience (1962)

19. M Wan, M Li, J Li and Z Liu. *Journal of Applied Polymer Science,* **53**, 131 (1989)

20. J E Fischer, X Tang, E M Scherr, V B Cajipe and A G MacDiarmid. *Synthetic Metals*, **41-43**, 661-664 (1991)

21. J P Pouget, M E Jozefowicz and A J Epstein, X Tang and A G MacDiarmid. *Macromolecules*, **24**, 779 (1991)

22. C M Guttman, E A DiMarzio and J D Hoffman. *Polymer*, **22**, 1466 (1981)

23. J D Hoffman. *Polymer*, **24**, 3 (1983)

CHAPTER 5: POLARISED REFLECTANCE ANALYSIS OF POLYANILINE

5.1 Introduction

The reflectance spectra of unoriented and oriented emeraldine base and emeraldine salt samples have been measured and analysed. With the use of polarisers it has been possible to compare the optical characteristics of polyaniline both along the direction of orientation and perpendicular to this direction. Thus the optical anisotropy of the samples can be assessed and related to other bulk properties of the material. Reflectance measurements have been taken in the energy range 4000 cm^{-1} (0.5 eV) to 45000 cm^{-1} (5.6 eV). The large energy range has allowed for a Kramers-Kronig analysis of the data, thus enabling the determination of a number of optical constants of the samples.

5.2 Uses of Reflectance Spectroscopy

Compared with transmission spectroscopy, reflectance spectroscopy is a fairly new experimental technique. The first reported measurements were made by Taylor in the early 1920s.[1] The technique is particularly applicable to measuring the optical properties of oriented films as it is not possible to produce oriented samples of polyaniline which are thin enough to allow for transmission measurements. Reflectance techniques have therefore been used extensively on a wide variety of materials not suited to transmission spectroscopy in an attempt to understand better electronic behaviour.[2]

5.3 Theory of Reflectance Spectroscopy

By illuminating a material with electromagnetic radiation, transitions of electrons may occur from occupied states to unoccupied states. If the energy of the radiation is known then it is possible to analyse quantitatively the initial and final electron states and hence probe the band structure of the material. When dealing with reflectance spectroscopy, a

beam of monochromatic light is shone on the sample and the fraction of incident light that is reflected is measured. By varying the energy of the incident light it is possible to determine the energies at which the sample absorbs radiation and to interpret this data in terms of the theoretical models for the electronic transitions.[3]

5.3.1 Definitions of Optical Properties

The optical properties of a substance are determined by its refractive index. For absorbing media this is a complex quantity - the real term denoted n and the imaginary term k, which is often termed the extinction coefficient. These quantities are usually determined indirectly, by, for example, transmission or reflectance measurements. The radiation intensity, I, which is proportional to the square of the amplitude of the incident radiation, decreases with distance through the sample. This decrease is exponential and of the form:

$$I = I(0)\, e^{-\alpha z}$$

where z is the distance travelled through the sample and α is termed the absorption coefficient. The absorption coefficient is related to the extinction coefficient k by the equation:

$$\alpha = \frac{2k\omega}{c} = \frac{4\pi k}{\lambda} = 4\pi k\nu$$

where ω is the angular frequency of the incident radiation, and ν, the wavenumber, is defined as reciprocal wavelength.

5.3.2 The Dielectric Function

The dielectric function describes the response of a substance to an electromagnetic field. It is very closely related to the electronic band structure, and is therefore useful in determining the overall electronic band structure of a material. The dielectric function is

also a complex quantity for absorbing media which can be written as a function of energy in the form:

$$\varepsilon(\nu) = \varepsilon_1(\nu) - i\,\varepsilon_2(\nu)$$

A complex dielectric function is interpreted as implying that the electric field and electric polarisation vectors are out of phase by an angle $\tan^{-1}(\varepsilon_2/\varepsilon_1)$.

In order to determine the dielectric function it is necessary to relate it to the measured reflectivity of a sample. This is achieved in the following manner:

Reflection from an absorbing medium is accompanied by a corresponding change of phase[20]. Therefore the amplitude of reflectance, r, can be expressed in the complex form:

$$r = \sqrt{R}e^{i\theta}$$

where θ is the phase change upon reflection.

According to the Fresnel equation at normal incidence, r can be expressed in terms of the complex refractive index (n - ik) by the equation:

$$r = \frac{n - ik - 1}{n - ik + 1}$$

Then n and k can be solved in terms of R and θ by the equations[8,9]:

$$n = \frac{1 - R}{1 + R - 2\sqrt{R}\cos\theta}$$

$$k = \frac{2\sqrt{R}\sin\theta}{1 + R - 2\sqrt{R}\cos\theta}$$

Furthermore, the real and imaginary parts of the dielectric function can be found by the relationship between the dielectric function and the refractive index, namely:

$\varepsilon(\nu) = [n(\nu) - i\,k\ (\nu)]^2$

yielding:

$\varepsilon_1(\nu) = n^2 - k^2$

$\varepsilon_2(\nu) = 2\,n\,k$

From the real and imaginary parts of the dielectric function, the optical conductivity, $\sigma(\omega)$, and the loss function, -Im $(1/\varepsilon)$, can be calculated. The loss function is a measure of the amount of energy absorbed by the sample as a function of incident energy. These are related by the following:

$\sigma(\omega) = \omega\,\varepsilon_0\,\varepsilon_2$

$$-\mathrm{Im}\left(\frac{1}{\varepsilon}\right) = \frac{\varepsilon_2}{\varepsilon_1^2 + \varepsilon_2^2}$$

Thus, a method is required to determine the energy-dependent phase change from the reflectance data. Subsequently the optical constants may be derived. This is achieved using the Kramers-Kronig relations which enable calculation of the phase change, and are discussed in the next section.

5.3.3 Kramers-Kronig Relations

The Kramers-Kronig technique for determining optical constants was first introduced by Kramers[4] in 1929, and then further developed by Kronig[5] in 1931. The basis for the analysis is the Principle of Causality, which states that there can be no effect upon a system before the cause. The condition of causality imposes some general relationships between the real and imaginary parts of any causal function[3]. In particular, it implies that for an optical function consisting of both real and imaginary parts, if the variation of the real part with frequency is known then the variation of the imaginary part with frequency may be calculated implicitly.

The Kramers-Kronig equation relates the reflectance from a sample to the change in phase of the incident radiation, and may be expressed in the form:

$$\theta(\nu_0) = \frac{\nu_0}{\pi} \int_0^\infty \frac{\ln R(\nu)}{\nu^2 - \nu_0^2} \, d\nu$$

By simple integration by parts, it is often quoted in the form:

$$\theta(\nu_0) = \frac{1}{\pi} \int_0^\infty \ln \frac{\nu + \nu_0}{\nu - \nu_0} \frac{d}{d\nu} \ln \sqrt{R(\nu)} d\nu$$

It can be seen from these equations that the phase shift at any point ν_0 depends on the reflectance at that point and also on all other values of reflectance from 0 to infinity. Of course it is not possible to take measurements over an infinite frequency range, and therefore in regions where experimental data is unattainable, suitable extrapolation techniques must be introduced. Extrapolation techniques have been the subject of some interest[6,7], but their importance has perhaps been overlooked in some cases, especially where relative rather than absolute measurements are of interest. However, it can be seen from the above equation that only a limited portion of the whole spectral range makes significant contribution to $\theta(\nu_0)$. The major contributions come from:

a) regions near ν_0, where the function $\ln[(\nu + \nu_0) / (\nu - \nu_0)]$ is strongly peaked.

b) regions where the reflectance is changing rapidly, and hence $d/d\nu \ln \sqrt{R(\nu)}$ is large.

It is therefore reasonable, and of little consequence to the overall outcome, to use a fairly arbitrary smooth extrapolation of the reflectance at low and high frequencies. Roessler[6] has devised a method for measuring the exact phase change upon reflection without the need for extrapolation between the frequency limits of the experimental data. His method has subsequently been implemented for Kramers-Kronig analyses of a number of materials[8,9]. This method, however, relies upon the region of measured reflectance containing two points of transparency, where the phase change can be taken as zero. It will be shown in the results section that this is not the case for polyaniline samples, and the method is therefore not applicable in this case.

5.4 Optical Properties of Polyaniline

The optical behaviour of polyaniline has been studied both through transmission and reflectance spectroscopy. These shall now be treated separately.

5.4.1 Transmission Spectra of Polyaniline

Monkman and Adams[10,11] have measured the optical transmission spectra of both emeraldine base and emeraldine salt samples, by spin-coating thin films onto quartz substrates. The results are shown in figure 5.1:

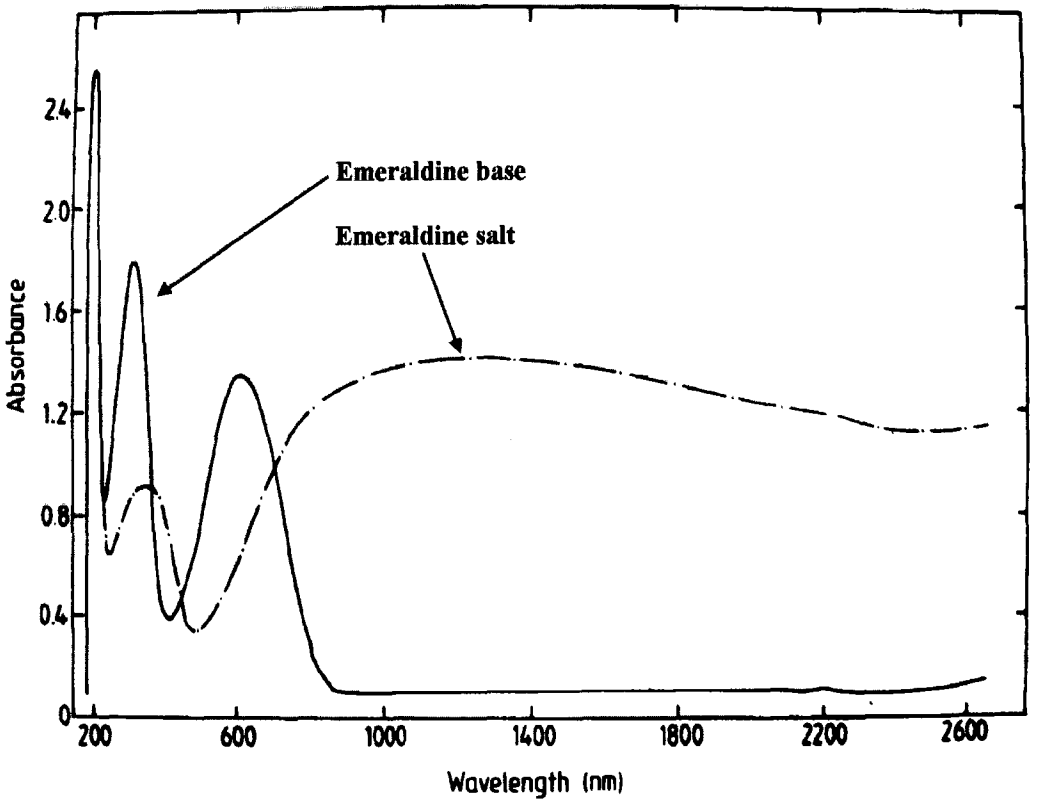

Figure 5.1: Optical transmission spectra of EB and ES polyaniline films

The emeraldine base spectrum reveals absorptions at 320 nm (3.9 eV), corresponding to the π-π^* transition of the benzenoid rings along the polymer backbone, and 620 nm (2.0 eV), which is ascribed to the formation of self-trapped excitons in the quinoid rings.

Similar results have also been reported by other groups[12,13]. The emeraldine salt spectrum shows a substantial modification of the optical behaviour. The band previously observed in EB at 320 nm shows a large decrease in intensity, and shifts to 360 nm. The exciton absorption is no longer observed and instead is transformed into a broad band which remains almost constant above approximately 1000 nm, attributed to metallic behaviour in this region.

5.4.2 Reflectance Spectra of Polyaniline

The reflectance spectra of polyaniline have been measured by Monkman and Adams[10], and McCall et al[14] on both unoriented and oriented samples. The spectra obtained for free-standing films display electronic transitions corresponding to those reported for the transmission measurements. The results for emeraldine salt have been compared to those for metallic polyacetylene[15], and similarities in the spectra are evident.

The polarised reflectance spectra of polyaniline stretched to 250% have been measured[10], figure 5.2. The authors report optical anisotropy in both the EB and ES forms. For the base samples, the reflectance minima are seen to coincide at ca. 450nm. However, the onset of the reflectance peaks at ca. 750 nm differ by about 50 nm, indicating alignment of the polymer chains along the stretch direction. For the salt samples the reflectance minima were observed to occur at different energies depending on the direction of polarisation, with the reflectance minimum for parallel polarisation occurring approximately 70 nm below that for perpendicular polarisation. Although the reason for this shift is not clearly understood, it is hoped that polarised reflectance measurements on highly oriented samples (ca. 600%) will enable the optical behaviour to be further probed, and the mechanisms elucidated.

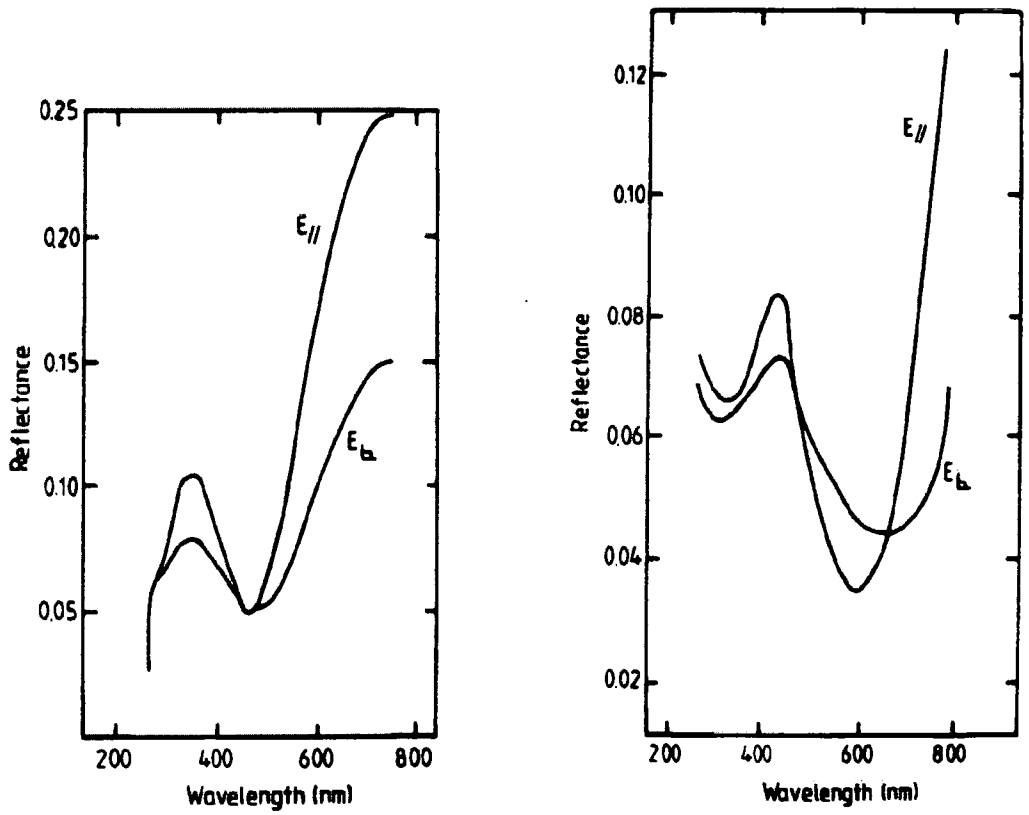

Figure 5.2: Optical anisotropy in a) emeraldine base, and
b) emeraldine salt oriented films.

5.5 Experimental Procedure

Reflectance data was recorded using a Perkin Elmer Lambda 19 UV/VIS/NIR spectrophotometer. A schematic of the instrument is shown in figure 5.3. The Lambda 19 is a double-beam, double-monochromator, all-reflecting optical system, which is computer-controlled using the UVCSS software program[16]. The instrument is essentially designed for transmission spectroscopy. In order to take reflectance measurements the sample compartment was installed with specially designed reflection mountings, figure 5.4. The reflection mountings allow for minor adjustments to the horizontal alignment of the sample in order to maximise the amount of light reflected back to the detector assembly.

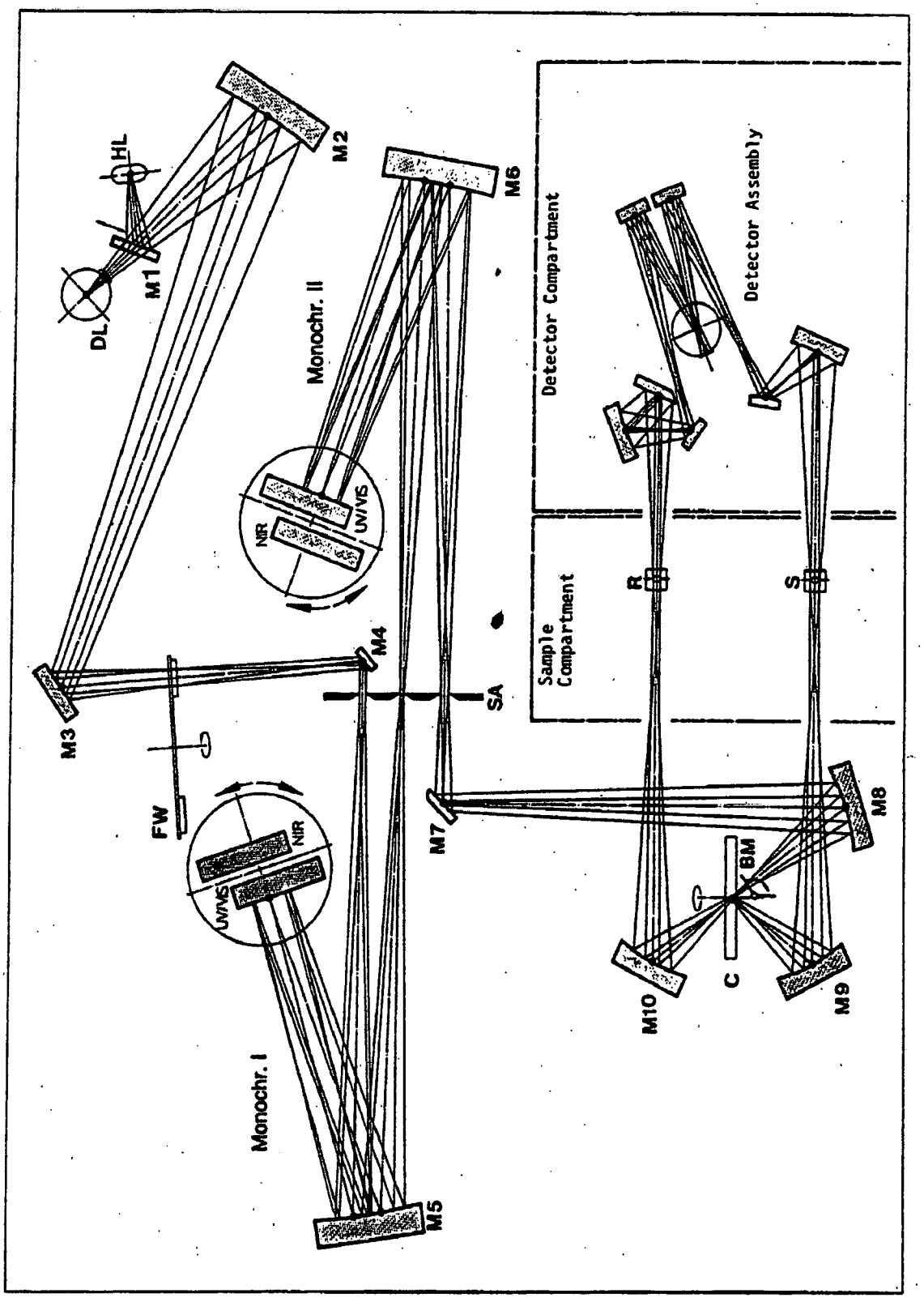

Figure 5.3: Schematic diagram of the optical system of Lambda 19 spectrophotometer

Figure 5.4: Mounting to allow for reflection from polyaniline samples.

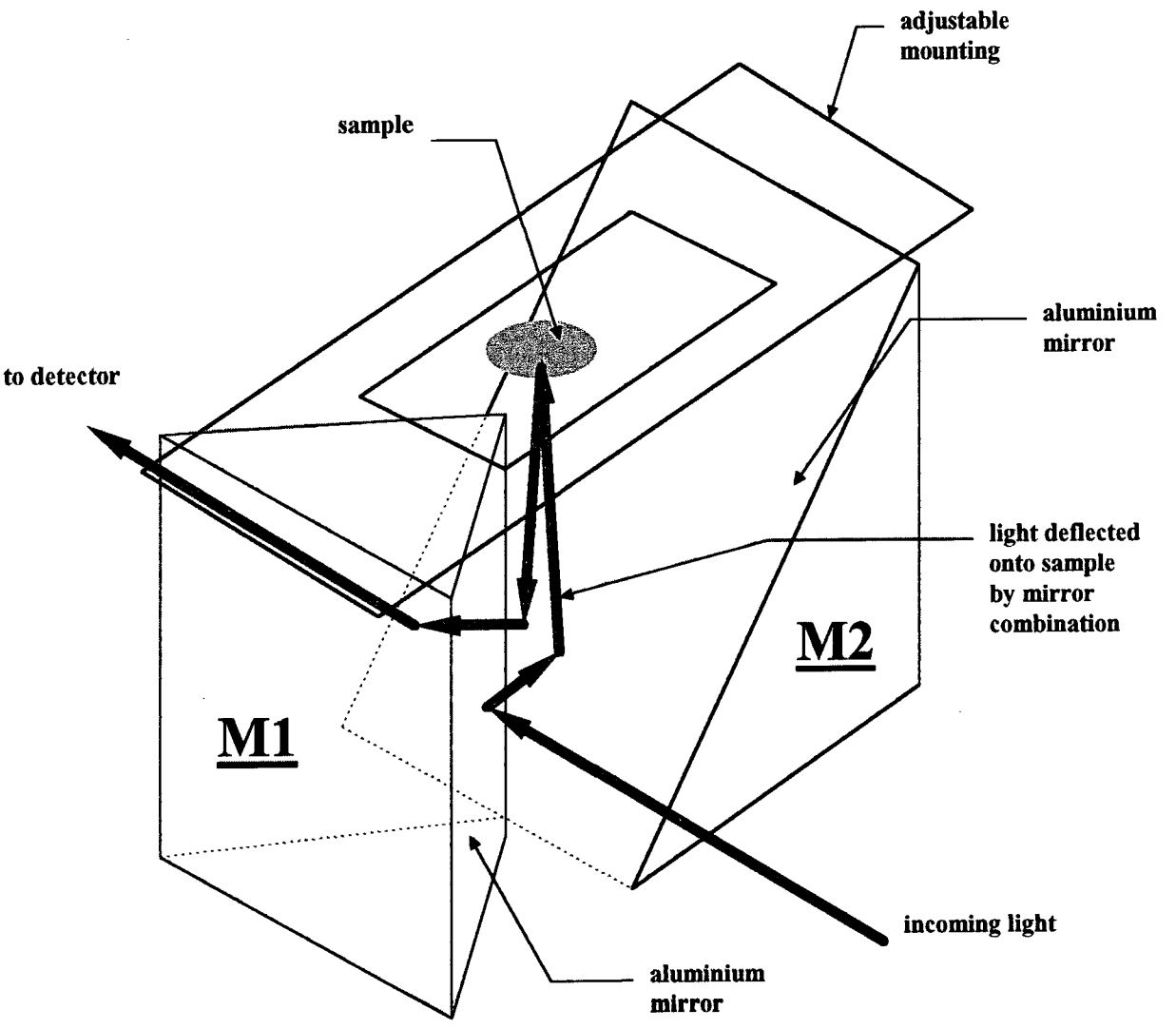

The incident light is converted from the horizontal to vertical direction by deflection from M1 onto the 45° sloping mirror, M2. Light reflected from the sample is then deflected again from M2 to M1, and onwards towards the detector. The mirrors can be finely adjusted to make the light coming to and from the sample as close to vertical as possible, but because of the design of the mountings there must be a small deviation from precisely vertical reflections.

5.5.1 Polarisation Measurements

In order to compare the optical behaviour of oriented samples along and perpendicular to the direction of orientation, Glan Taylor polarisers were used. These are air-spaced calcite polarisers with spectral range 0.44-5.65 eV, depicted in figure 5.5.

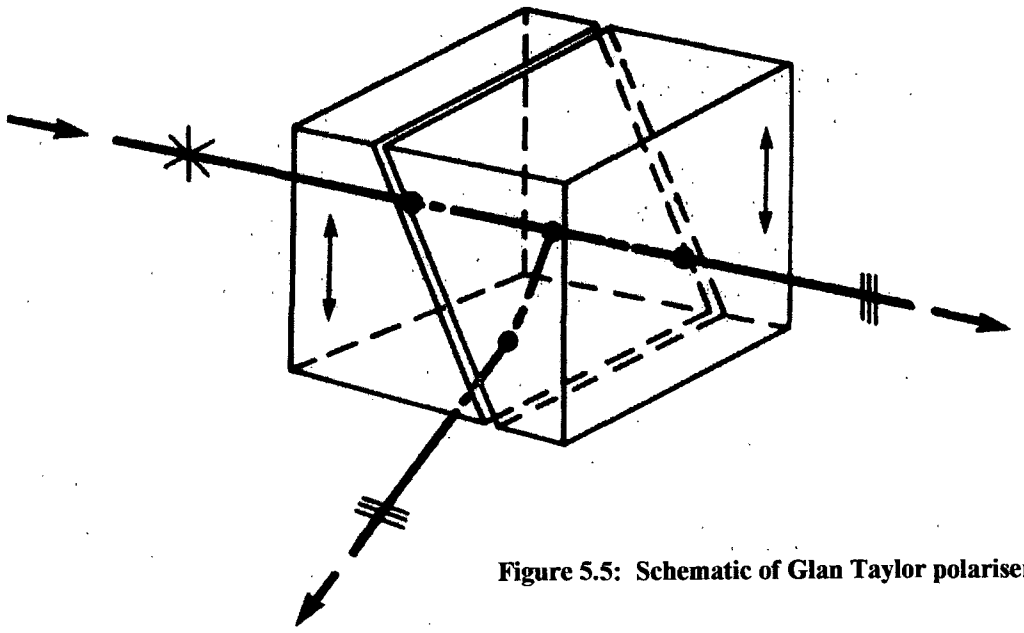

Figure 5.5: Schematic of Glan Taylor polariser.

It can be seen that at the air-gap the parallel vector of the incoming radiation is reflected internally, whilst the perpendicular vector is transmitted through the air-gap and remains undeviated.

5.5.2 Sample Preparation

The samples were prepared in the manner described in Chapter 2. Because of the nature of the experiment, great care was taken to ensure that the surface quality of the samples was as high as possible. Those samples with any obvious surface imperfections were disregarded. It has been observed during this period of research, and by other groups[14], that orientation often causes undulations to appear on the surface of the samples, figure 5.6. Because of the importance of keeping the samples as flat as possible, sticking tape was used to hold them in a flat position. The samples were then glued to glass substrates to increase further their rigidity.

Figure 5.6: EB film stretched to 600% elongation, revealing undulations of the surface.

5.5.3 Background Correction of Spectrophotometer

The Lambda 19 is a two beam instrument which takes measurements by comparing the intensity of light at the two detectors. Therefore a background correction on a material of known reflectivity must be undertaken. Because of its very high reflectivity over a large energy range, aluminium is usually used to serve this purpose. The spectrometer measures the reflectance from two aluminium mirrors which are initially placed in both the sample and reference beam. Therefore, when the reflectance of the polyaniline

samples are subsequently measured, they are not absolute values but relative to aluminium.

Aluminium has the reflectance spectrum depicted in figure 5.7[2].

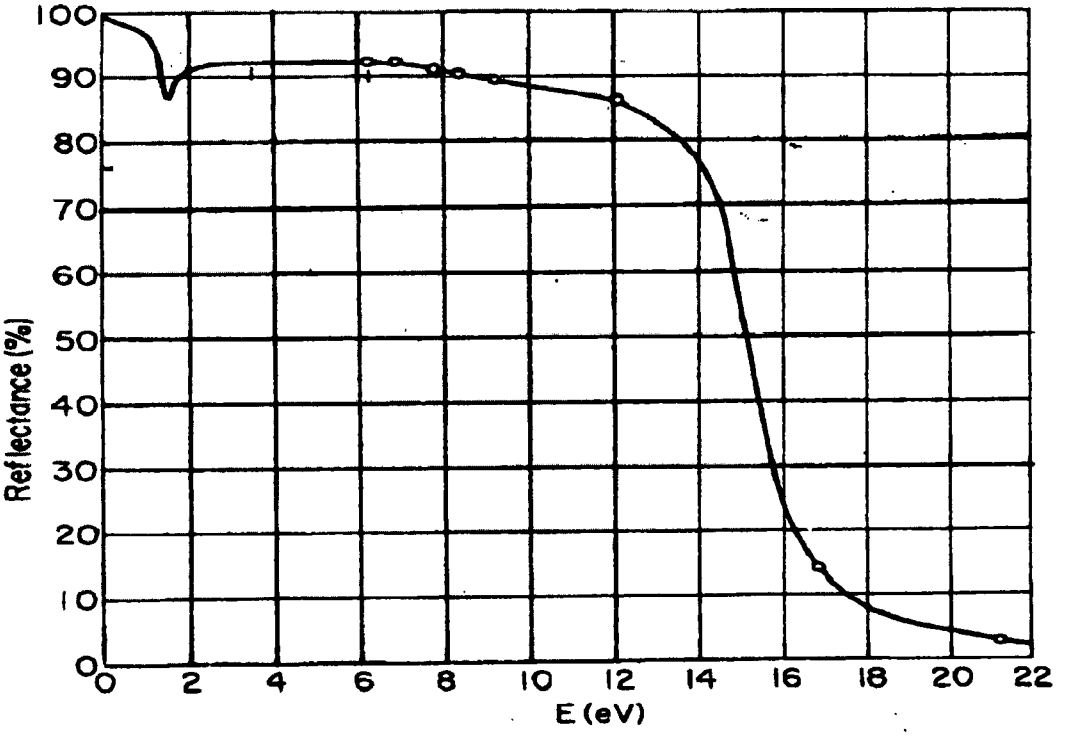

Figure 5.7: Absolute Reflectance spectrum of aluminium

It can be seen that aluminium reflects approximately 90 per cent of incident light in the region 1-7 eV. Therefore a correction factor must be applied to the results obtained to find the absolute values for polyaniline. The absolute percentage reflectance is thus given by:

$$R_{absolute} = (R_{measured} \times R_{aluminium}) / 100 \ \%$$

For the data obtained, a computer program was written to model the reflectance of aluminium[17] and the subsequent transformation applied. The results reported later in the chapter are therefore absolute values of reflectance.

5.5.4 Extrapolation Techniques

The extrapolation techniques outside the energy limits for the Kramers-Kronig analysis took the following format:

For the low energy region (E<0.5 eV) the reflectance was assumed to fall off with a gradient determined by the measured reflectance gradient between 8000cm^{-1} and 4000cm^{-1}. In the region around 50 000 cm^{-1} it is evident from the reflectance data that the onset of another peak in R is occurring. The exact position, intensity and width of this peak is not known. Therefore a smooth peak was defined using a mixture of Gaussian and Lorentzian curve fitting procedures. Above this peak the reflectance was assumed to fall off as $1/\omega^2$ up to 100 000 cm^{-1} and as $1/\omega^4$ above this value, as described elsewhere[3,14]. The effect of the extrapolation was checked by recalculating the reflectance from the values of n and k obtained from the Kramers-Kronig analysis, and an excellent match between the two sets of data was found.

In summary, to evaluate the optical constants for a particular sample the following steps were followed:

1. measure reflectance (relative to aluminium) using spectrophotometer
2. compensate for reflectance of aluminium using appropriate transformation
3. add extrapolated data to accumulated data
4. determine phase change (θ) as a function of wavenumber using Kramers-Kronig equation (a computer program was written to perform this task[31])
5. determine frequency dependent n and k from their relation with θ and R
6. determine frequency dependent optical functions from their relation with n and k

5.6 Reflectance Results

This section presents the results obtained on emeraldine base and emeraldine salt samples, both polarised and unpolarised, elongated to 0%, 300% and 600%.

Figure 5.8 shows the unpolarised reflectance spectra of emeraldine base films:

Figure 5.8: Reflectance spectra of emeraldine base films.

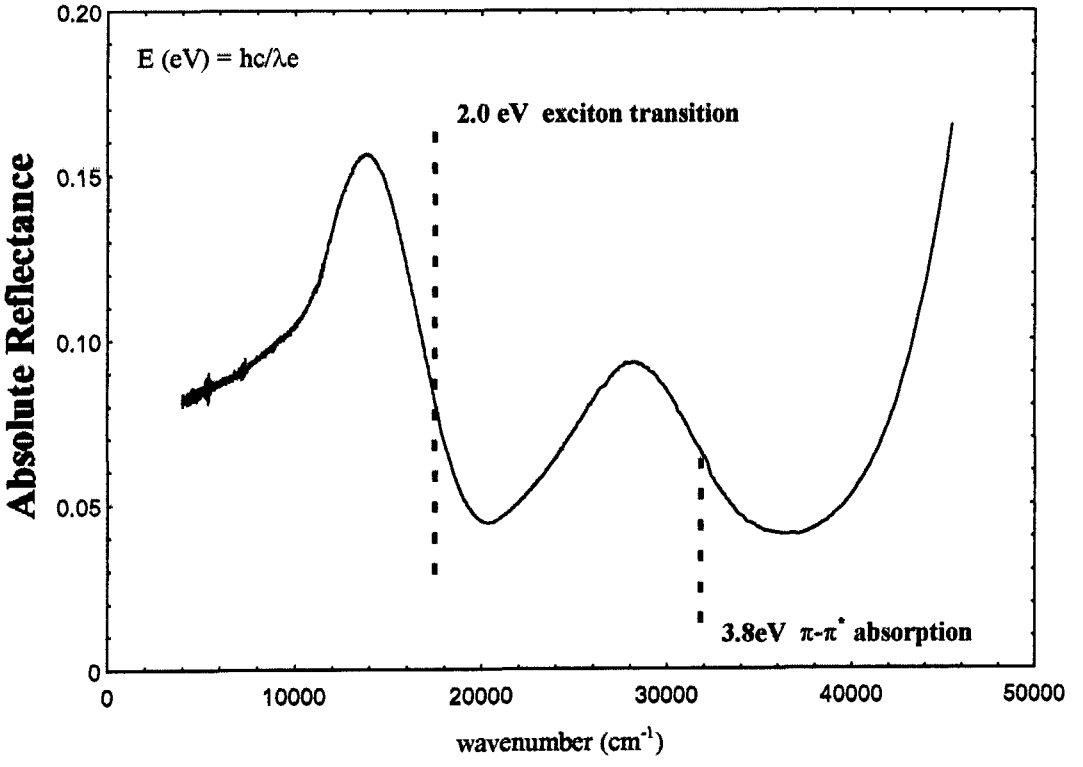

The data reveal two absorption bands centred at approximately 2.0 and 3.8 eV. The 3.8 eV transition is due to the π-π^* band gap absorption. The 2.0 eV feature results from an intra-chain exciton transition from the highest occupied levels centred on the benzenoid rings to the lowest unoccupied level centred on the quinoid rings. These measurements coincide with previous absorption measurements[10] and agree with theoretical calculations[18,19].

Figure 5.9 shows the unpolarised reflectance spectra of emeraldine salt films.

Figure 5.9: Reflectance spectra of emeraldine salt films.

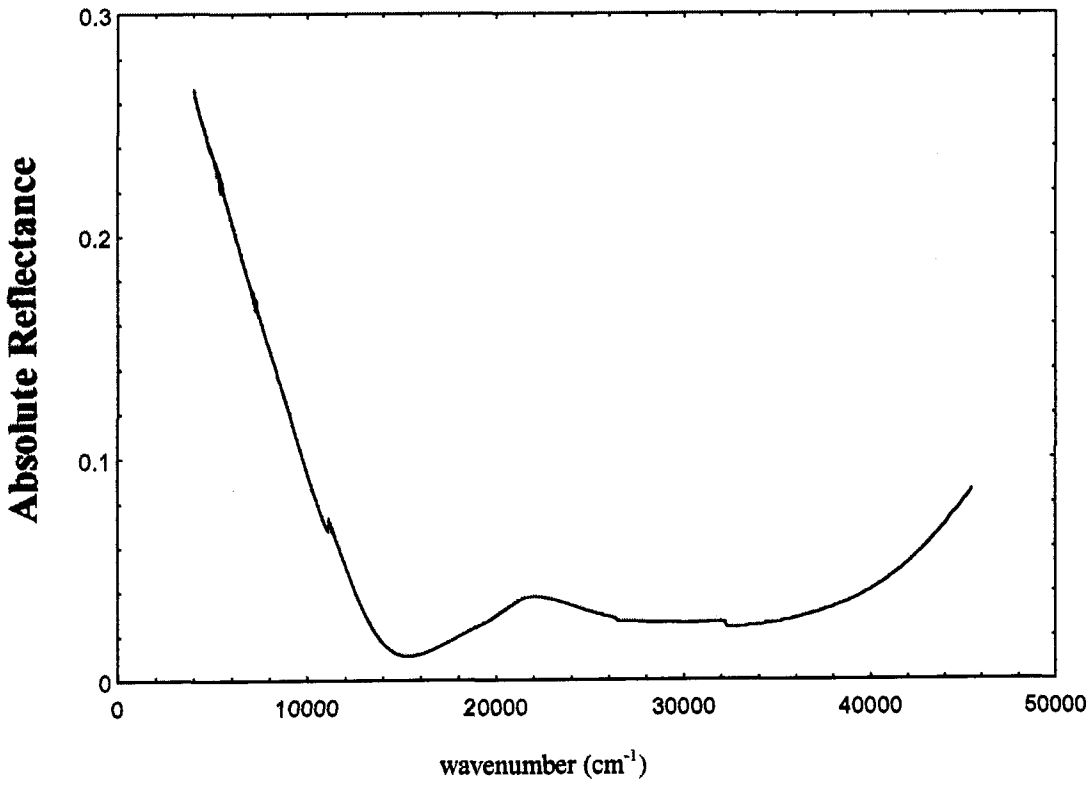

It can be seen that for the salt films the reflectivity is high in the NIR with maximum values of over 0.3. The reflectance then decreases to a minimum at ca. 16000 cm^{-1}. Another broad reflectance minimum is centred at ca. 32000 cm^{-1}. These trends are consistent with polaron formation upon protonation, thus allowing for new electronic transitions from the lower-lying energy bands.

The polarised reflectance spectra of oriented emeraldine base and emeraldine salt are shown in figures 5.10-5.13. A qualitative comparison of the parallel and perpendicular reflectance ratios as a function of elongation are shown in figures 5.14 and 5.15.

Figure 5.10 300% Emeraldine Base Polarised Reflectance Spectra

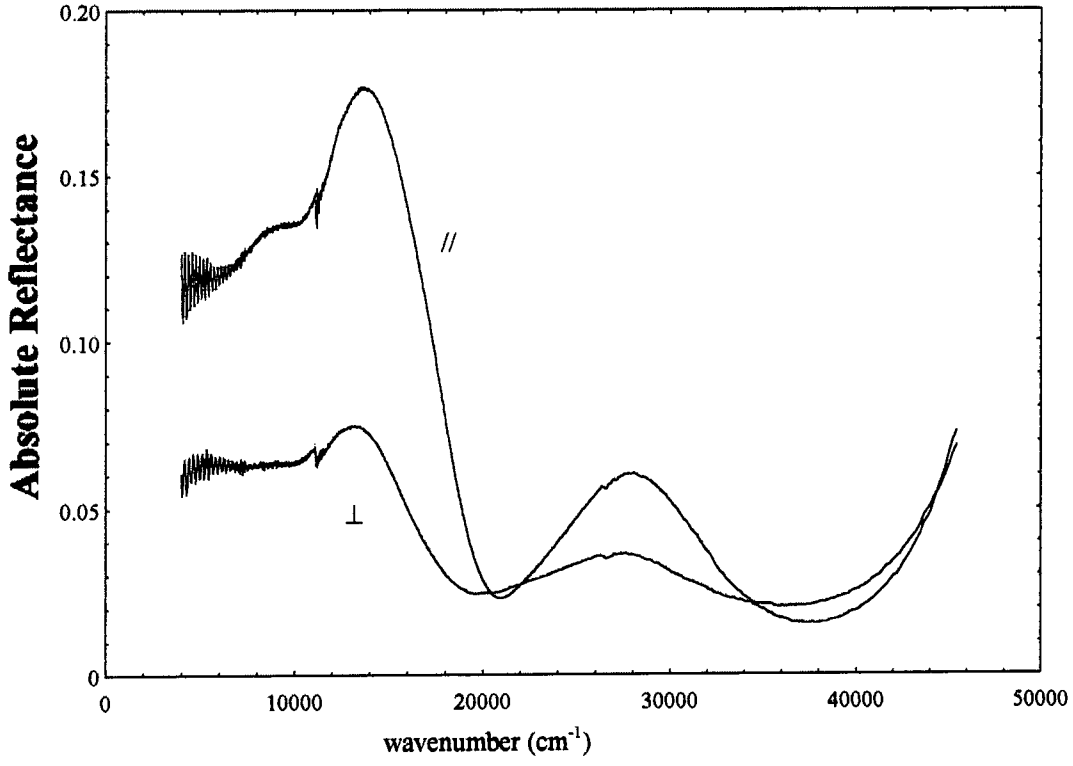

Figure 5.11 600% Emeraldine Base Polarised Reflectance Spectra

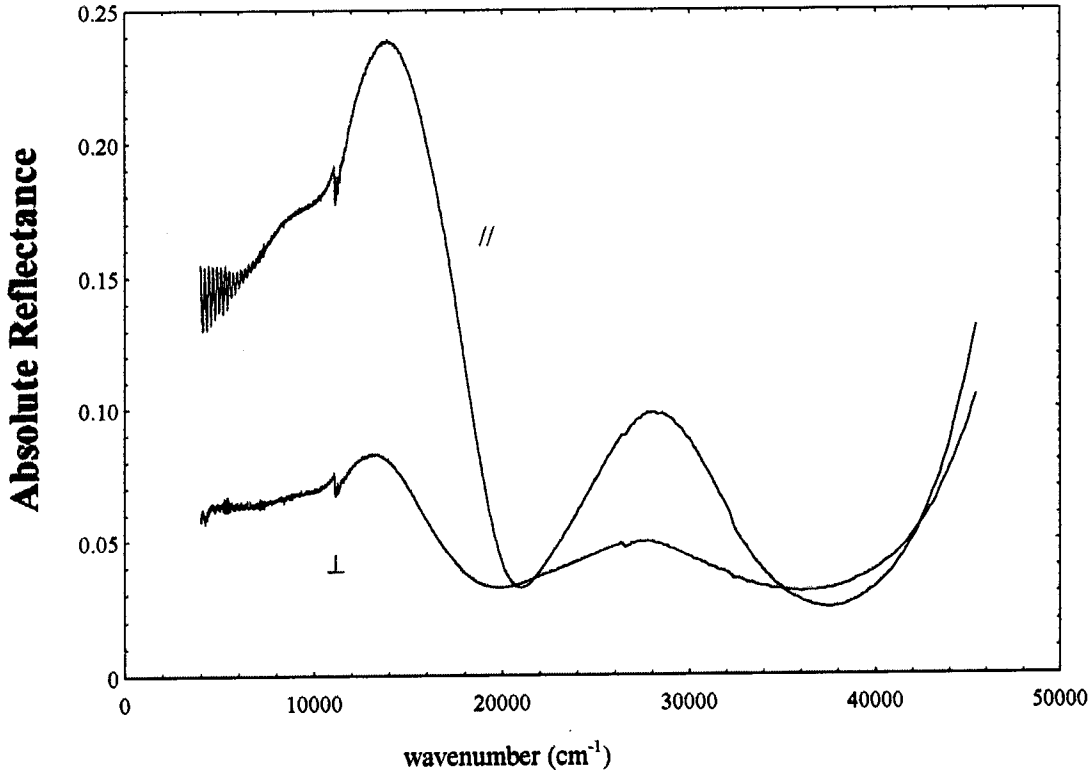

Figure 5.12 300% Emeraldine Salt Polarised Reflectance Spectra

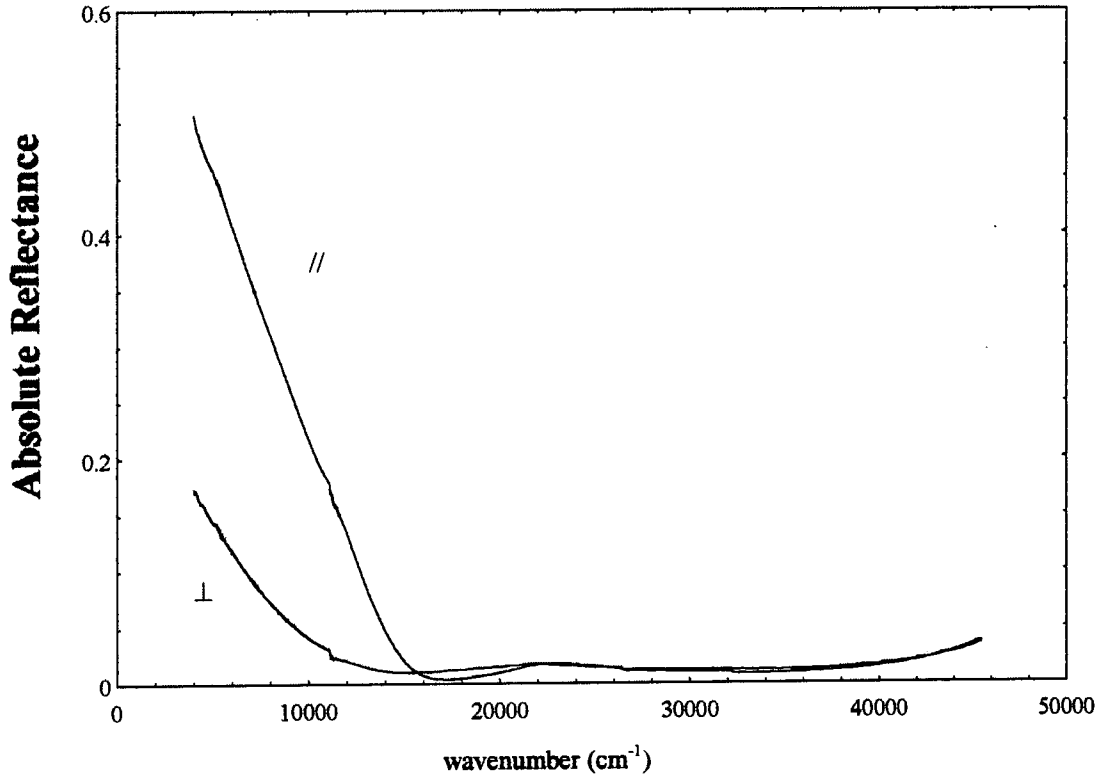

Figure 5.13 600% Emeraldine Salt Polarised Reflectance Spectra

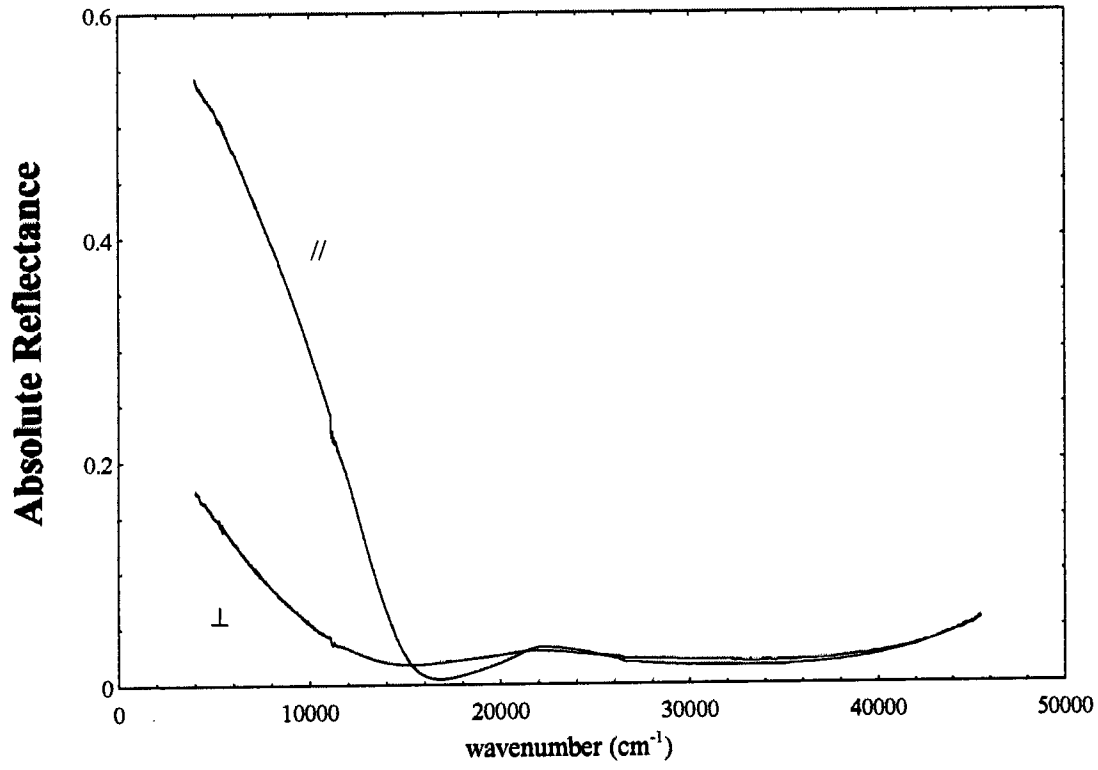

Figure 5.14: Optical anisotropy for EB films

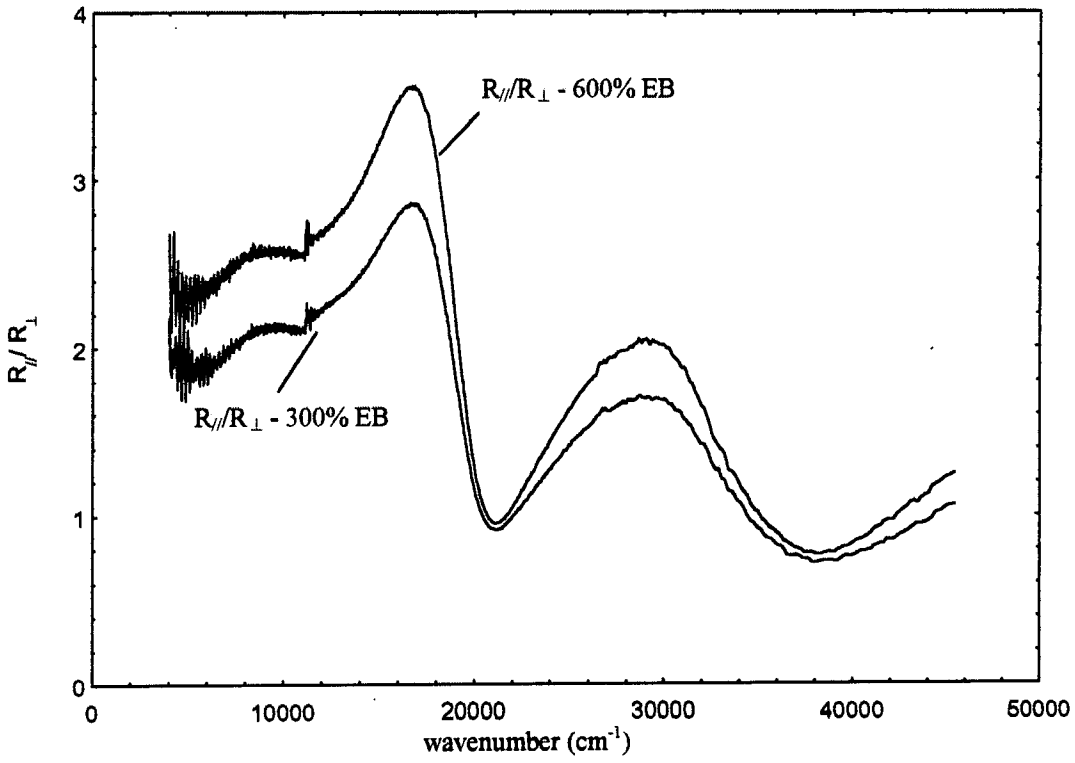

Figure 5.15: Optical anisotropy for ES films

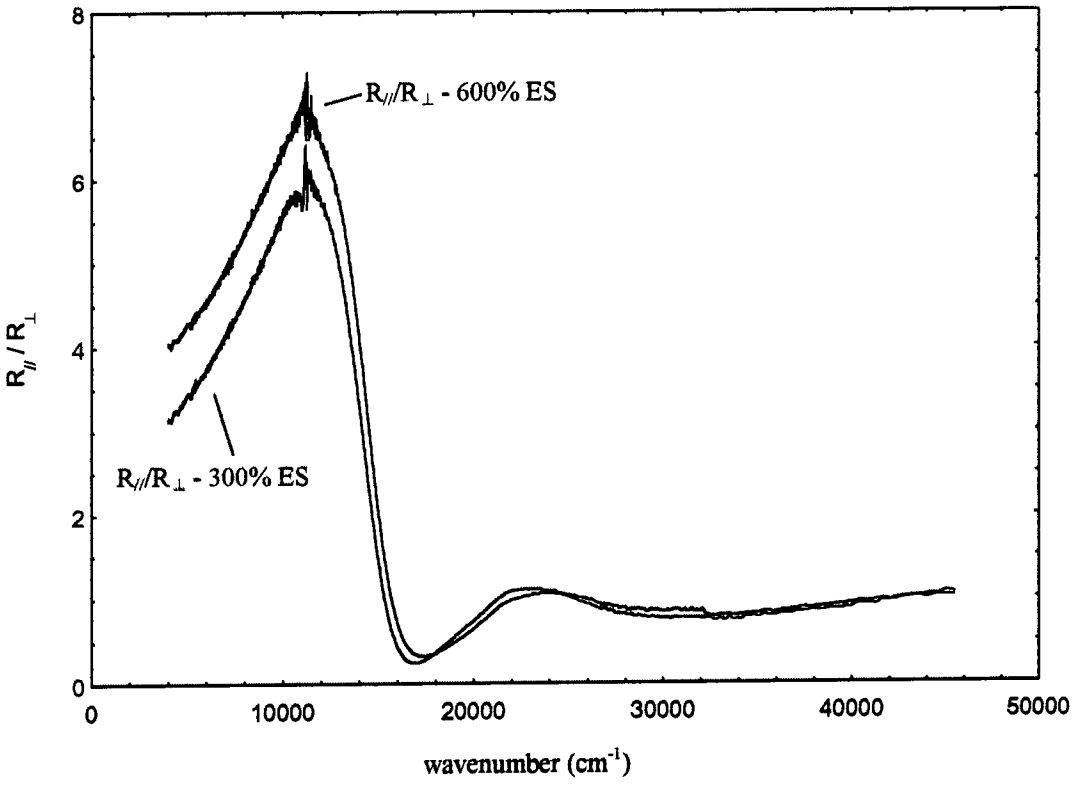

5.7 Discussion

The results presented here are those for which maximum anisotropy was observed in reflectance. This was achieved by adjusting the position of each particular sample in the spectrophotometer. The reflectance varied by approximately 4 per cent as the samples were moved. This suggests that the spectrophotometer is actually taking an average reading of reflectance, due to the radiation being incident on a substantial area of each sample (ca. 1 cm diameter). It is emphasised, however, that due to the constraints of time, reflectance measurements were only taken on one sample at each elongation. Further work will be required to make a detailed analysis of the variation in reflectance behaviour from sample to sample.

5.7.1 Emeraldine Base

a) Reflectance Anisotropy

Inspection of the polarised reflectance spectra for emeraldine base reveals significant anisotropy for light polarised parallel to the orientation direction compared with light polarised perpendicular. For 300% EB, a maximum anisotropy of approximately 2.8 is seen at ca. 2.0 eV; i.e. the exciton transition mentioned previously. Another maximum in optical anisotropy is observed at the π-π^* transition, whose value of $R_{//}/R_{\perp} \sim 1.6$ is lower than that for the exciton transition.

The reflectance spectra of 600% EB show slight increases in anisotropy compared with the 300% samples. For the exciton transition, $R_{//}/R_{\perp} \sim 3.5$ and for the π-π^* transition an optical anisotropy of ~ 2.0 is observed.

An explanation for the anisotropy in reflectance at the exciton transition having higher values than at the π-π^* transition can be found by considering the work of Duke et al[26] and Pomfret[27]. Duke suggests that the exciton transition involves an electron being promoted to a quinoid ring from the two neighbouring benzenoid rings. The defect is therefore spatially extended over more than one ring - electroabsorption (EA) measurements[27] have estimated the exciton to be spatially extended by ca. 4Å. The π-π^*

transition, on the other hand, is considered to be localised to the benzenoid ring - EA measurements estimate the spatial extent to be ca. 2.5Å which is the approximate diameter of such a ring. The idealised situation is shown in figure 5.16.

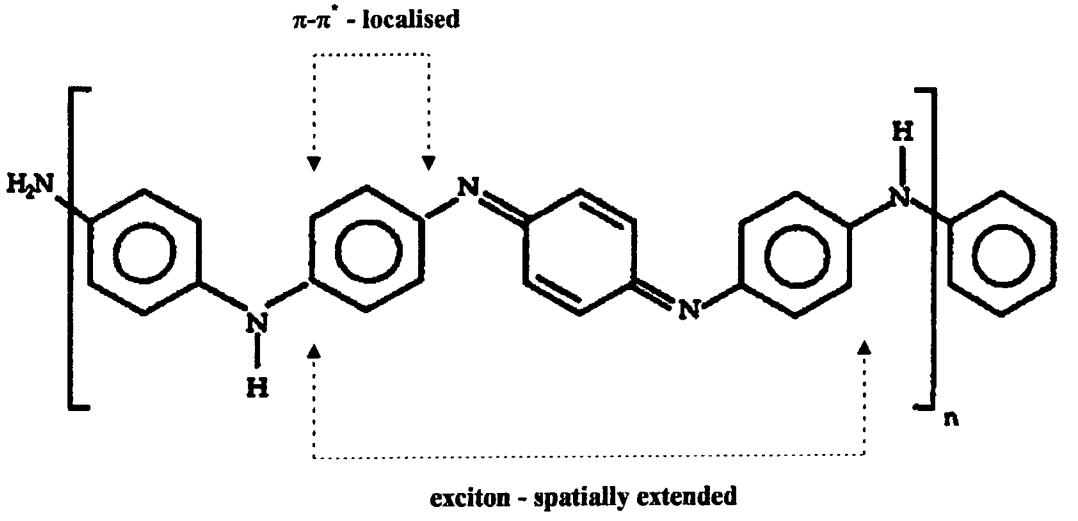

Figure 5.16: Schematic of spatial extent of electronic transitions for EB

For a perfectly aligned EB chain, it can be seen that the ground state exciton will be oriented along the direction of molecular orientation. The π-π^* transition, however, will continue to have a range of possible orientations due to the range of orientations of the benzenoid ring. For partial alignment the same trends will be evident but less pronounced.

b) Optical constants

The values of n, k, ε_1 and ε_2 derived from the Kramers-Kronig analysis for emeraldine base are shown in figures 5.17 to 5.24.

Figure 5.17 n and k for 300% EB films - parallel polarisation

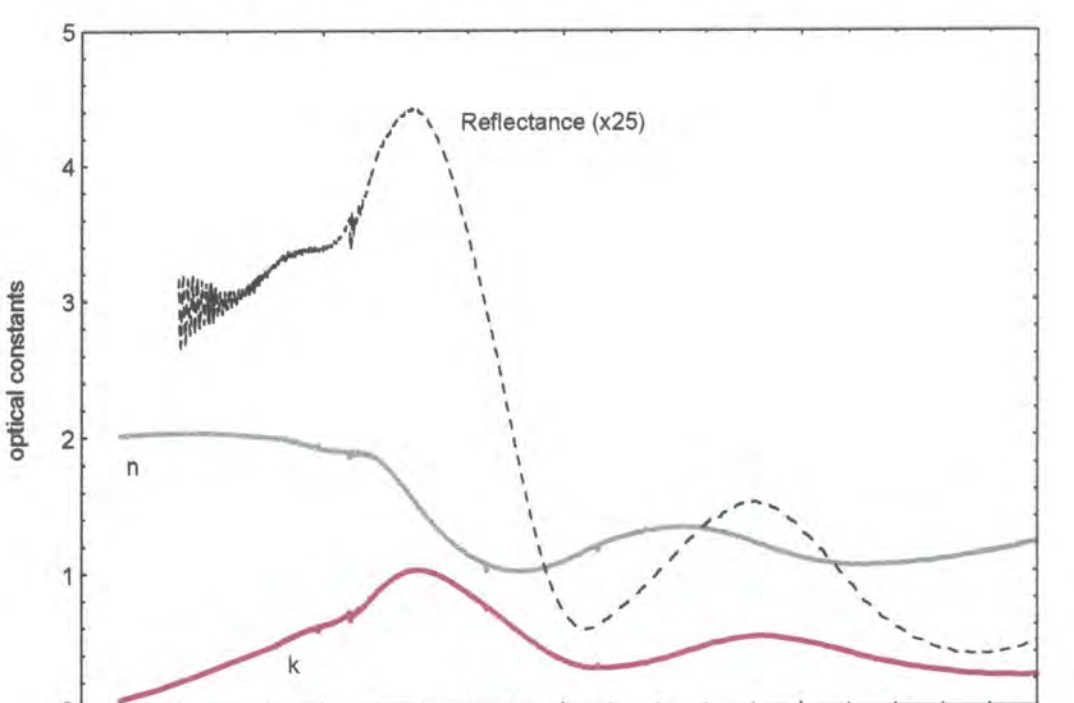

Figure 5.18 ε_1 and ε_2 for 300% EB films - parallel polarisation

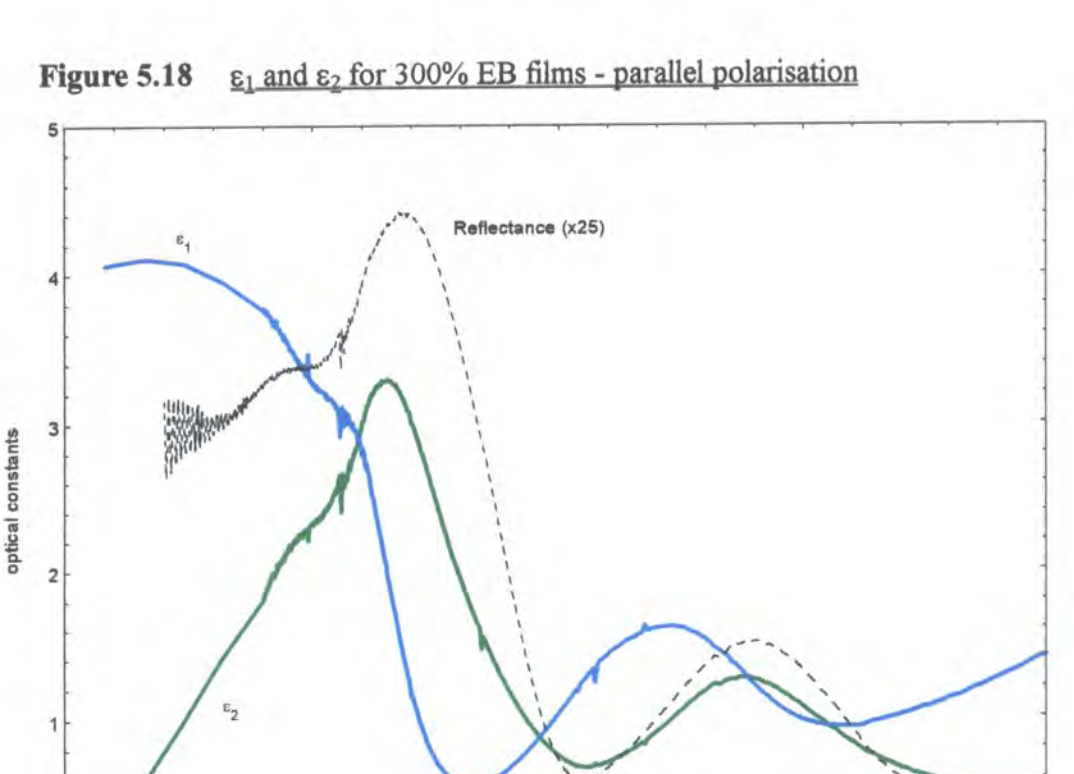

Figure 5.19 n and k for 300% EB films - perpendicular polarisation

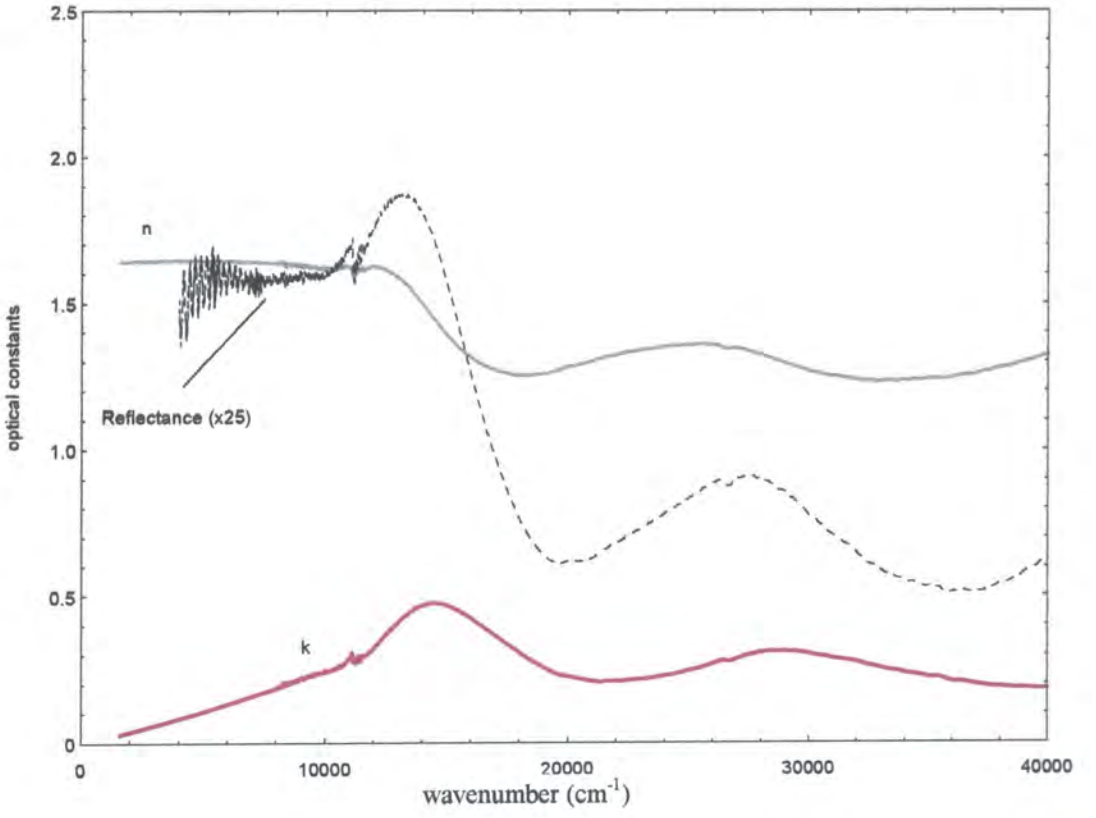

Figure 5.20 ε_1 and ε_2 for 300% EB films - perpendicular polarisation

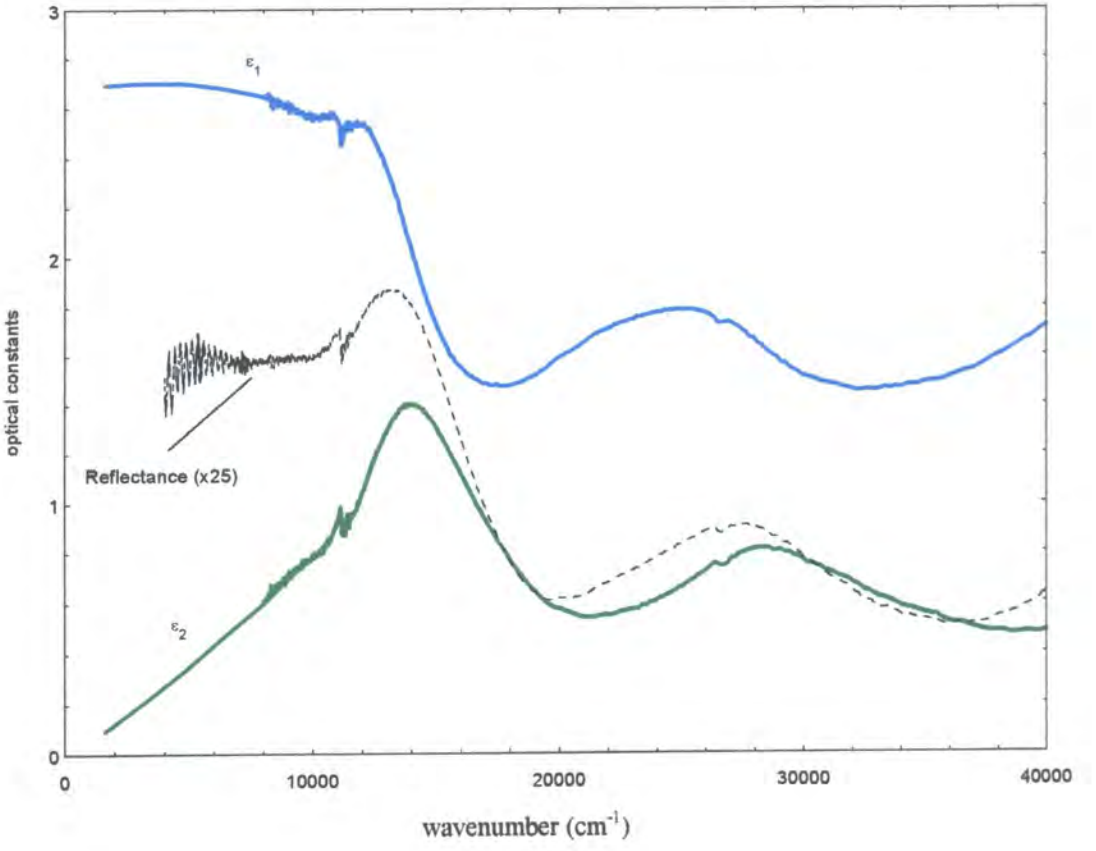

Figure 5.21 n and k for 600% EB films - parallel polarisation

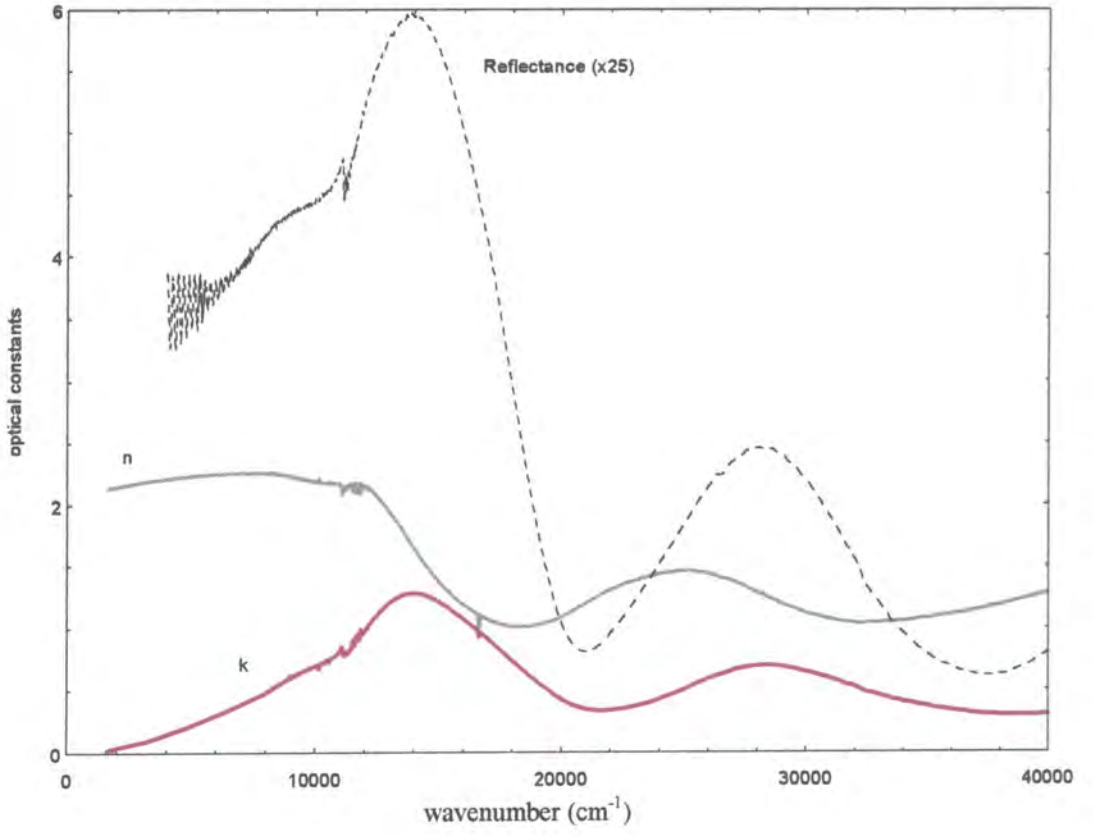

Figure 5.22 ε_1 and ε_2 for 600% EB films - parallel polarisation

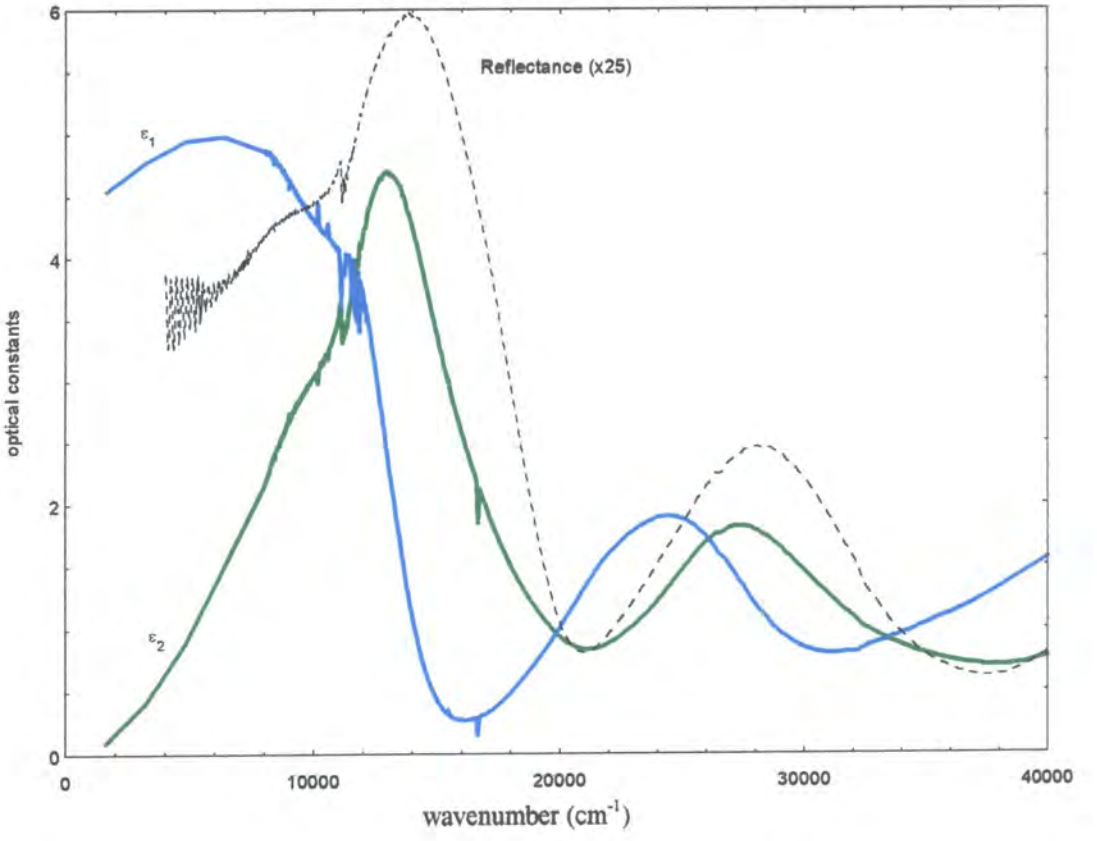

Figure 5.23 n and k for 600% EB films - perpendicular polarisation

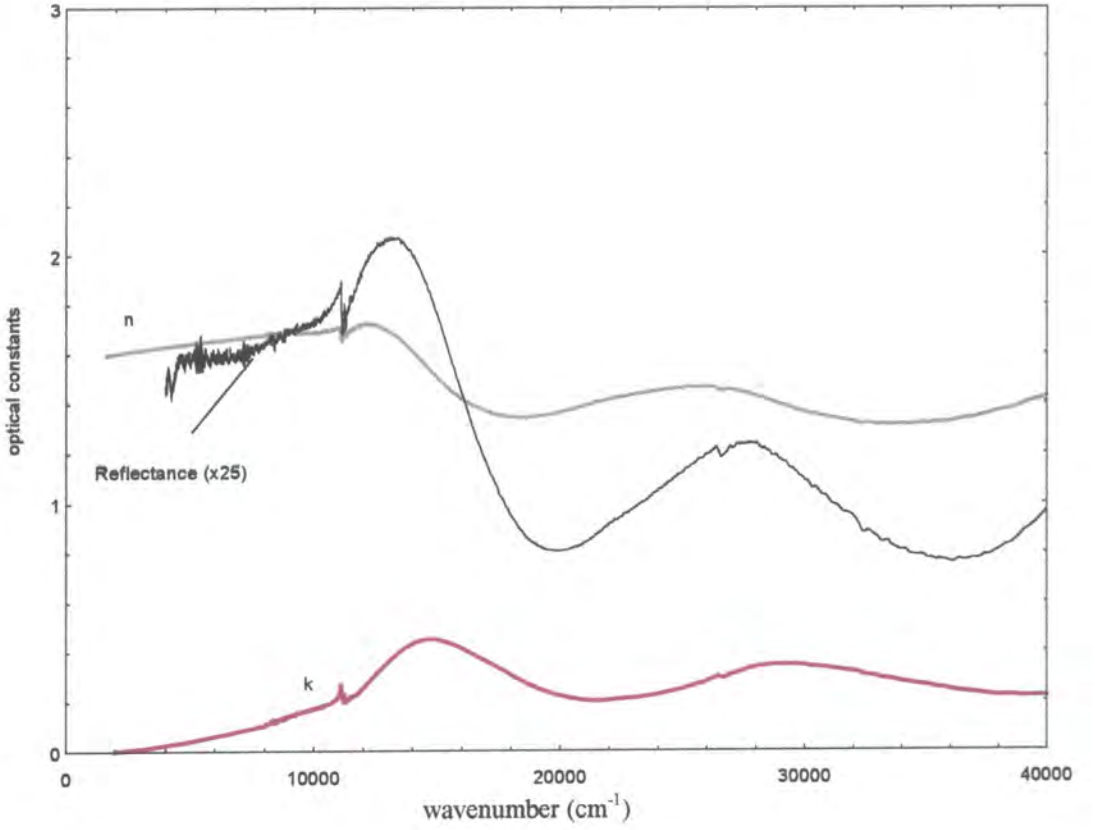

Figure 5.24 ε_1 and ε_2 for 600% EB films - perpendicular polarisation

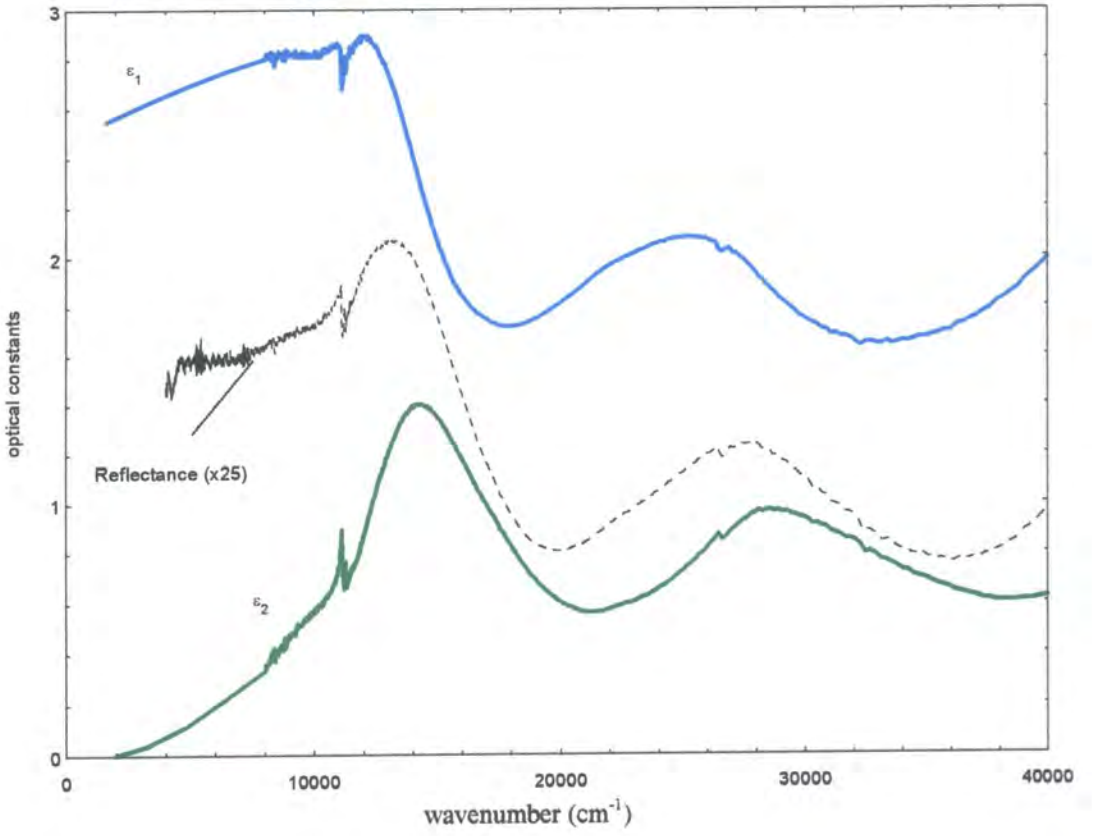

General features: 300% EB // polarisation: The refractive index has a value of approximately 2 at the low energy region of the spectrum. The value decreases to almost 1 at the exciton transition, with an associated increase in the extinction coefficient (k_{max}~1) corresponding to absorption in this region. Similar trends are observed at the π-π^* transition (n:1.3→1, k:0.3→0.5). The average fall off of refractive index with increasing wavenumber is consistent with the samples becoming more transparent to high energy radiation. The real part of the dielectric function is seen to decrease (ε_1:4.0→0.6) at the exciton transition and again at the π-π^* transition (ε_1:1.6→0.9). The minima in ε_1 coincide with the maximum oscillator strengths of the transitions mentioned. In other words, the atoms are no longer polarised but the electrons are promoted to higher energies by the incident radiation. The imaginary part of the dielectric function is associated with the frequency-dependent optical conductivity of the samples. Thus, the shape is similar to that of the reflectance spectrum indicating maxima in optical conductivities in the regions of highest absorption. The peak-to-trough differences in ε_2 are ε_2:3.3→0.7 (exciton) and ε_2:1.3→0.5 (π-π^*).

Table 5.2 shows the changes in n and k for emeraldine base samples stretched to 300% and 600% for electric vector polarised parallel and perpendicular to the direction of orientation.

	n_{max}	n_{min}	n_{max}-n_{min}	k_{max}	k_{min}	k_{max}-k_{min}
300% EB// (exciton)	2.03	1.00	**1.03**	1.01	0.29	**0.72**
300% EB⊥ (exciton)	1.64	1.25	**0.39**	0.47	0.21	**0.26**
600% EB// (exciton)	2.25	1.01	**1.24**	1.28	0.34	**0.94**
600% EB⊥ (exciton)	1.72	1.34	**0.38**	0.45	0.20	**0.25**
300% EB// (π-π^*)	1.32	1.04	**0.28**	0.51	0.23	**0.28**
300% EB⊥ (π-π^*)	1.35	1.23	**0.12**	0.31	0.18	**0.13**
600% EB// (π-π^*)	1.46	1.04	**0.42**	0.70	0.30	**0.40**
600% EB⊥ (π-π^*)	1.46	1.32	**0.14**	0.35	0.22	**0.13**

Table 5.1: Changes in optical constants as a function of elongation.

The following trends are apparent:

Δn for the exciton transition for 300% EB is higher (~ 2.6x) for $E_{//}$ than for $E_{\perp}$. For 600% EB the corresponding Δn ratio is ~ 3.3. Similar trends are followed for the π-π^* transition as a function of elongation (ratios of 2.3 and 3 for the two transitions).

It is evident from Table 5.1 that the k ratios ($\Delta k_{//}/\Delta k_{\perp}$) increase with increasing elongation, indicating increased alignment of the polymer chains with increased elongation. The ratio $k_{//}/k_{\perp}$ is defined as the dichroic ratio, D. Fraser[28] defined a fraction f of a chain as being perfectly aligned for a partially oriented polymer film. The value f is related to the dichroic ratio by the equation[29]:

$$f = \frac{D-1}{D+2}$$

The values of f for EB at the energies of the exciton transition and π-π^* transition are shown in figure 5.25 as a function of elongation.

Fig. 5.25 Fraction of orientation for electronic transitions in elongated EB films

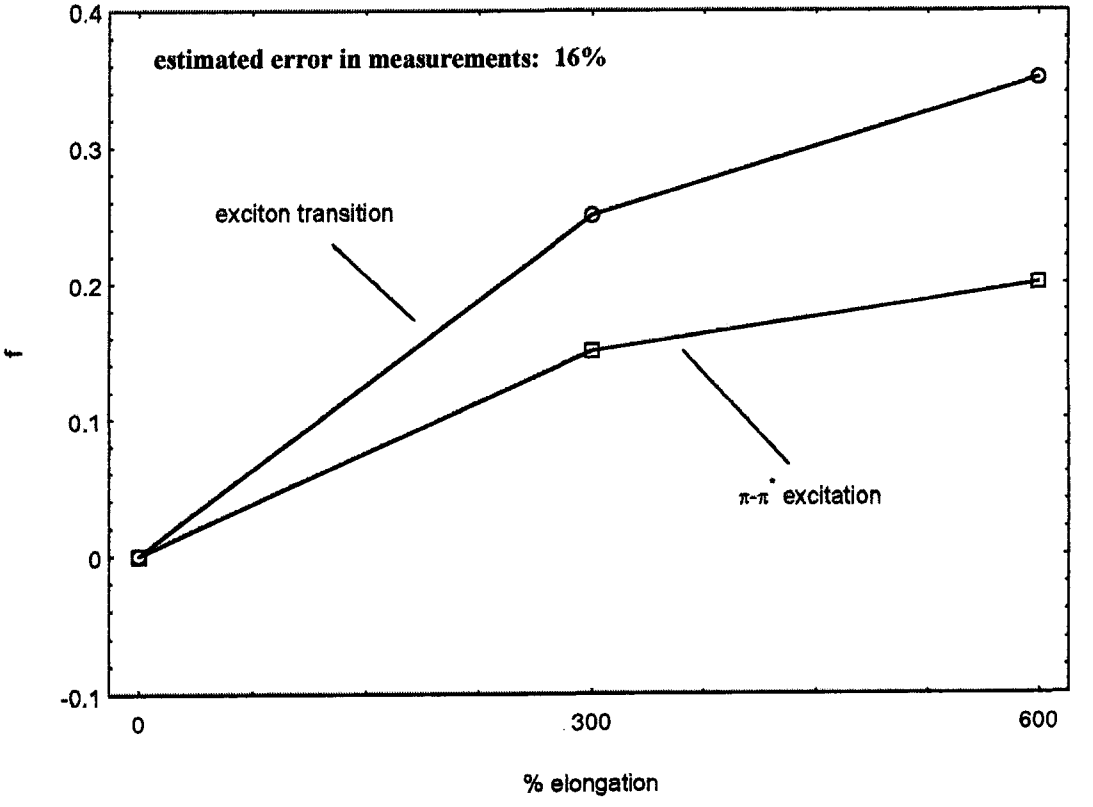

It can be seen that the average alignment increases with elongation for both the exciton and π-π^* transition. The diagram also reveals the observations made by Duke et al[26] and Pomfret[27] that due to the spatial extension of the exciton defect, the defect is more sensitive to orientation than the π-π^* transition.

c) Absorption Coefficient

The absorption coefficients ($\alpha=4\pi k\nu$) for oriented emeraldine base samples are shown in figures 5.26-5.27.

Figure 5.26 Absorption Coefficient for 300% EB films

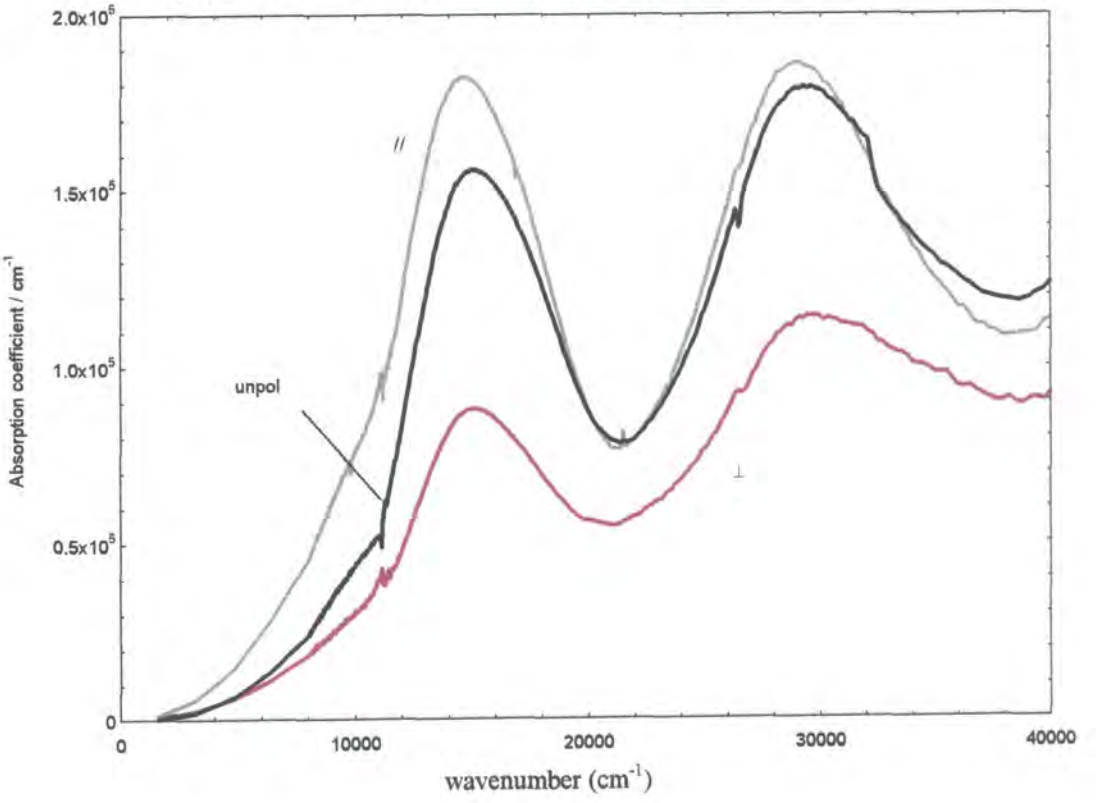

Figure 5.27 Absorption Coefficient for 600% EB films

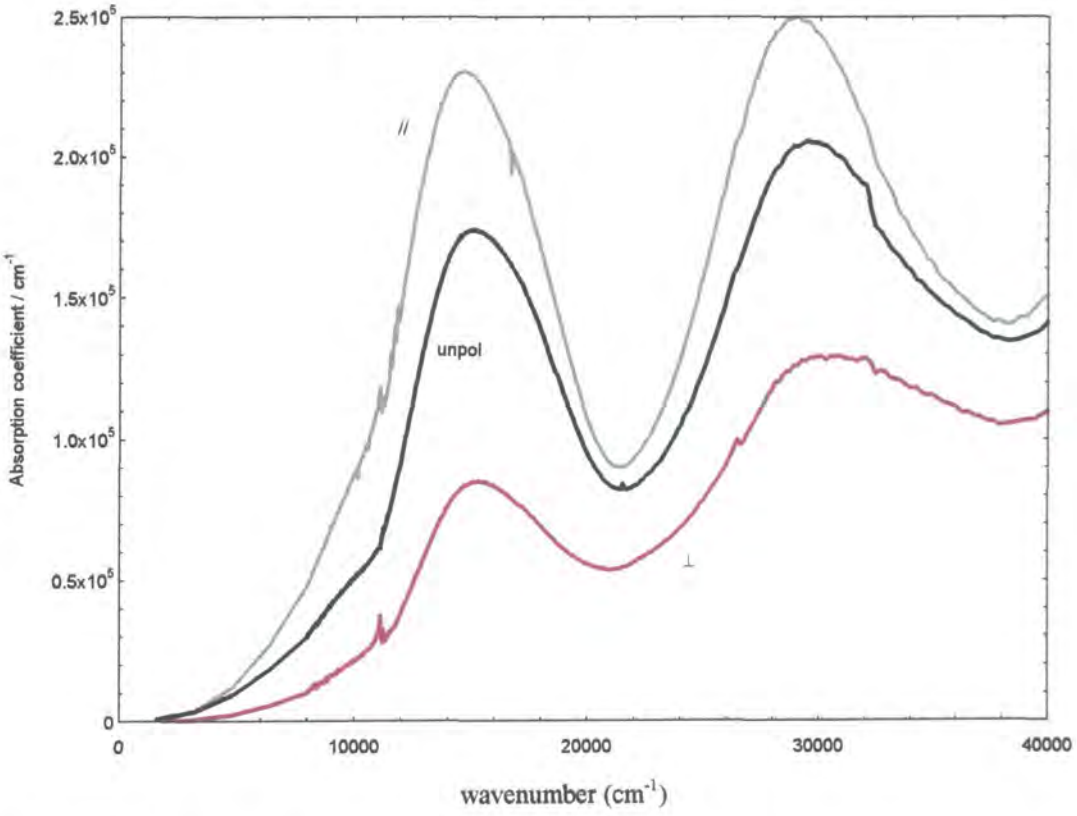

For 300% EB with parallel (perpendicular) polarisation the absorption coefficient has maxima of 182 000 cm^{-1} (86 000 cm^{-1}) at 680nm, and 186 000 cm^{-1} (114 000 cm^{-1}) at 350 nm. For 600% elongated samples the maxima have values of 230 000 cm^{-1} (85000cm^{-1}) and 250 000 cm^{-1} (130 000 cm^{-1}). These values correspond well with those of other groups[14]. It can be seen that these maxima correspond to the transitions mentioned previously. The anisotropies in α for 300% elongated films are 2.1 (exciton) and 1.6 (π-π^*). For 600% elongated films the corresponding anisotropies are 2.7 and 1.9. Thus energy is being absorbed more along the direction of elongation compared to perpendicular. Furthermore, as the elongation is increased the absorption ratio increases slightly. This indicates increased alignment of polymer chains as the elongation is increased.

Figure 5.28 shows the variation in absorption coefficient anisotropy for the EB samples.

Figure 5.28 Anisotropy in absorption coefficient for EB films

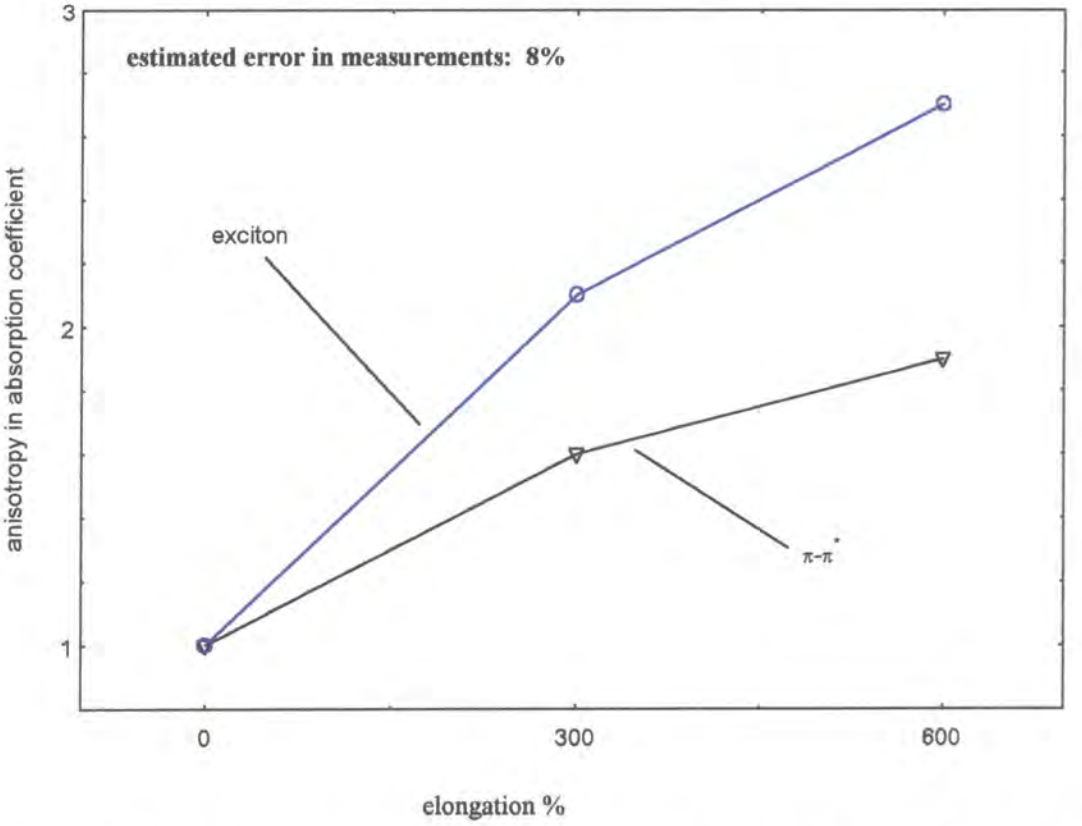

It is seen that the change in anisotropy as a function of elongation is not quite linear, but decreases slightly from linear behaviour as elongation is increased. The behaviour is again consistent with the spatial extent of the transitions mentioned previously.

5.7.2 Emeraldine Salt

a) Reflectance anisotropy

Referring back to figure 5.15 it is seen that there is a slight increase in reflectance anisotropy (ca. 11 per cent) for 600% elongated ES samples compared with 300% samples. The anisotropy difference is not, however, as large as that for base samples (ca. 25 per cent). It is thus evident that a degree of structural relaxation occurs upon doping of the samples. In addition to this, as was mentioned in Chapter Two, section 2.7.3, a major problem often encountered when dealing with doped samples is the homogeneity of doping. Because of this area of uncertainty, the theoretical values of, for example, d.c. conductivity, may be higher than experimental values. Furthermore, it was reported that the measured d.c. conductivity of emeraldine salt samples varied from sample to sample and indeed at different regions for a particular sample. This problem is inherent in the field of characterisation of electronic properties of samples which must be doped following synthesis[21].

b) Optical constants

The values of n, k, ε_1 and ε_2 derived from the Kramers-Kronig analysis for emeraldine salt are shown in figures 5.29-5.36.

Figure 5.29 n and k for 300% ES films - parallel polarisation

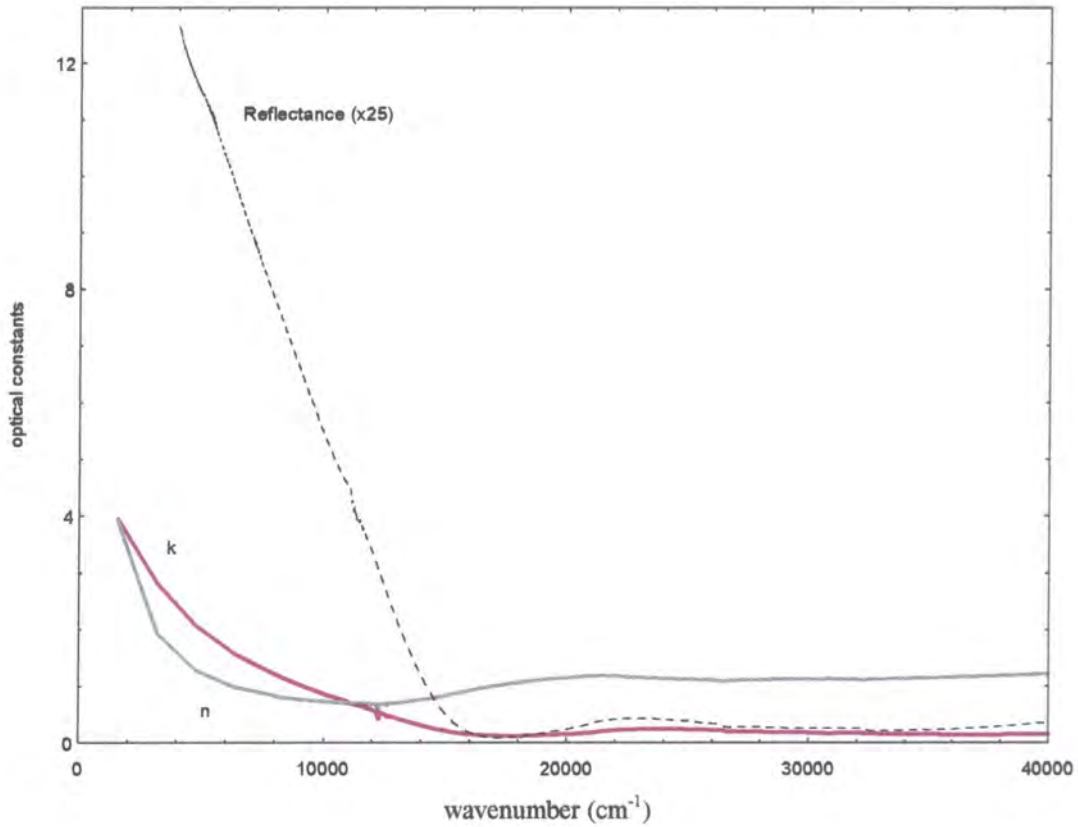

Figure 5.30 ε_1 and ε_2 for 300% ES films - parallel polarisation

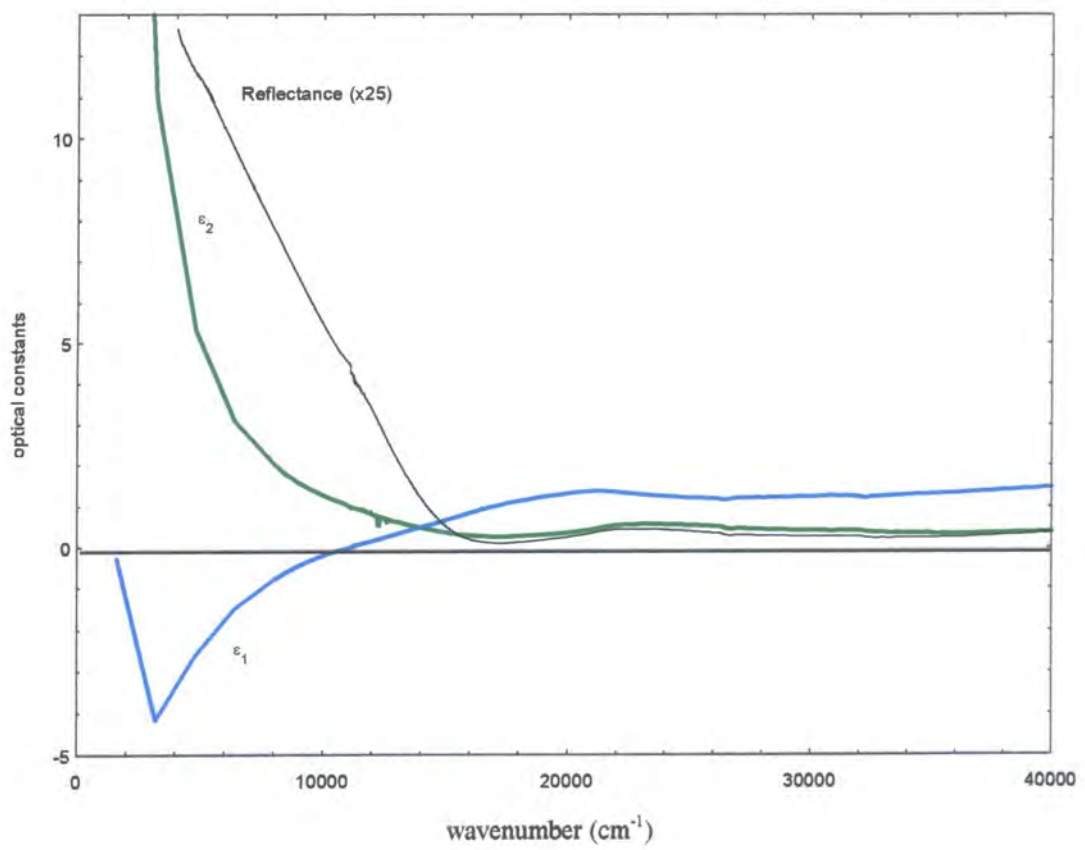

Figure 5.31 n and k for 300% ES films - perpendicular polarisation

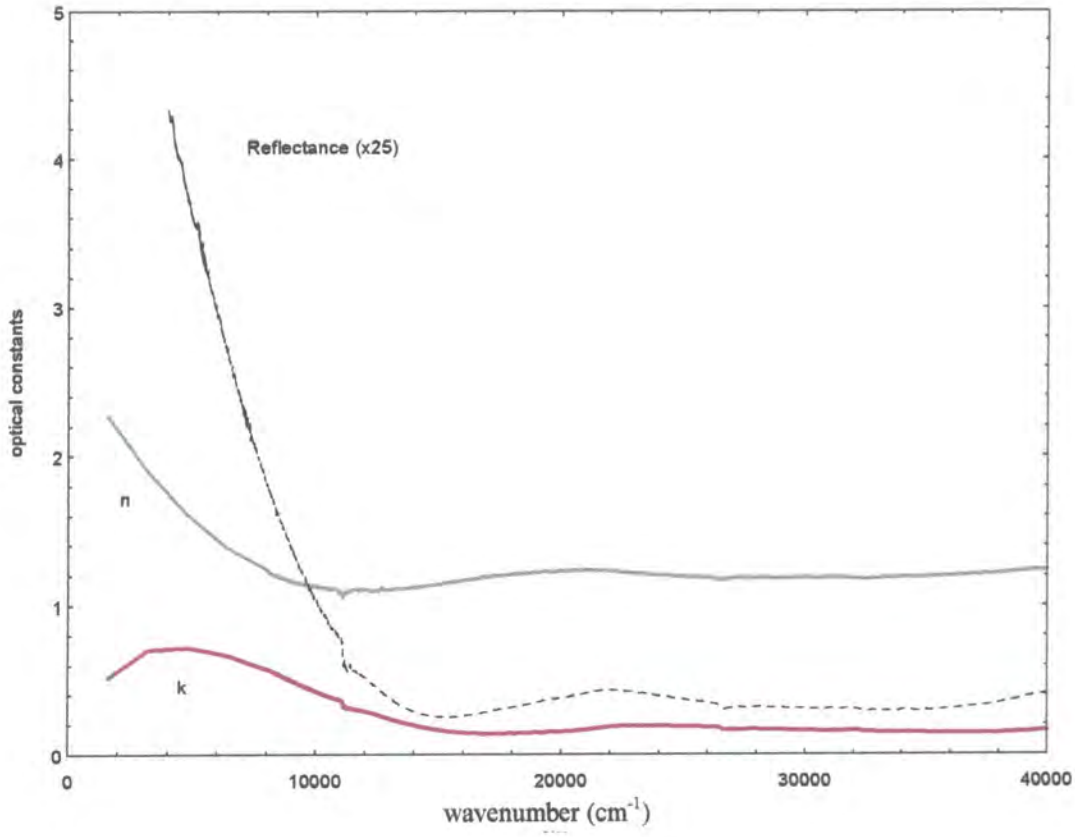

Figure 5.32 ε_1 and ε_2 for 300% ES films - perpendicular polarisation

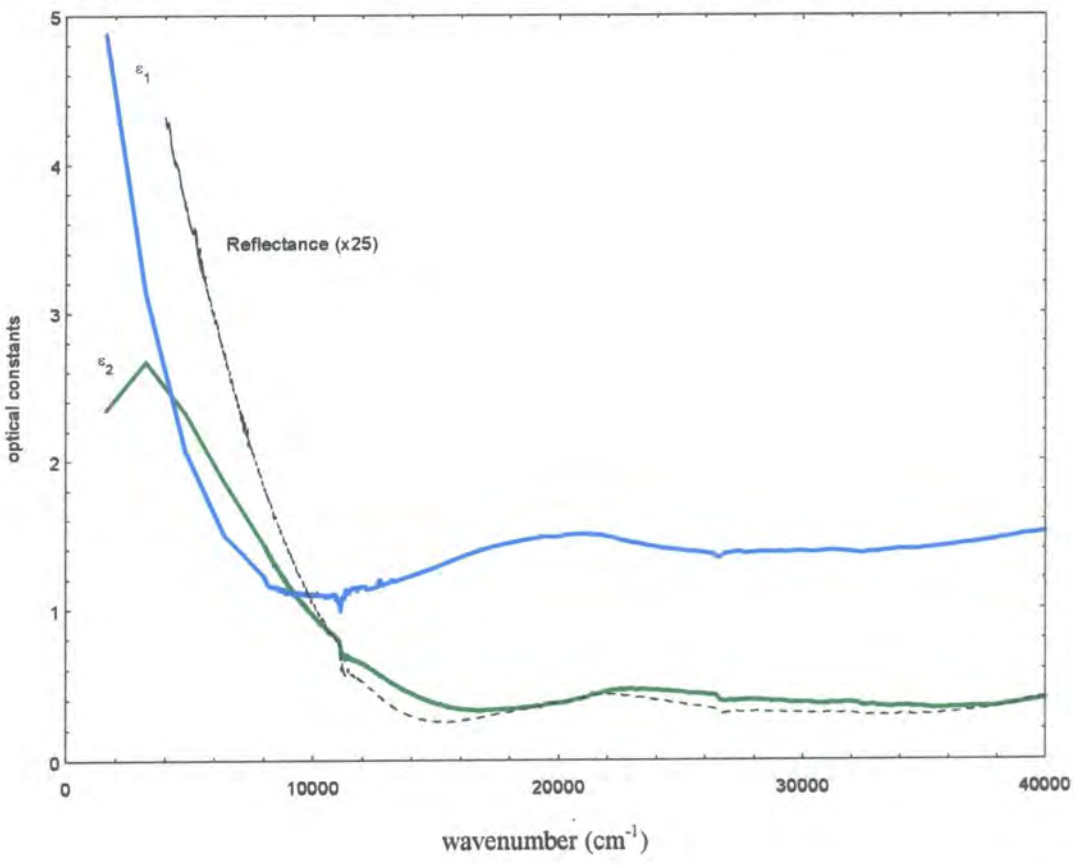

Figure 5.33 n and k for 600% ES films - parallel polarisation

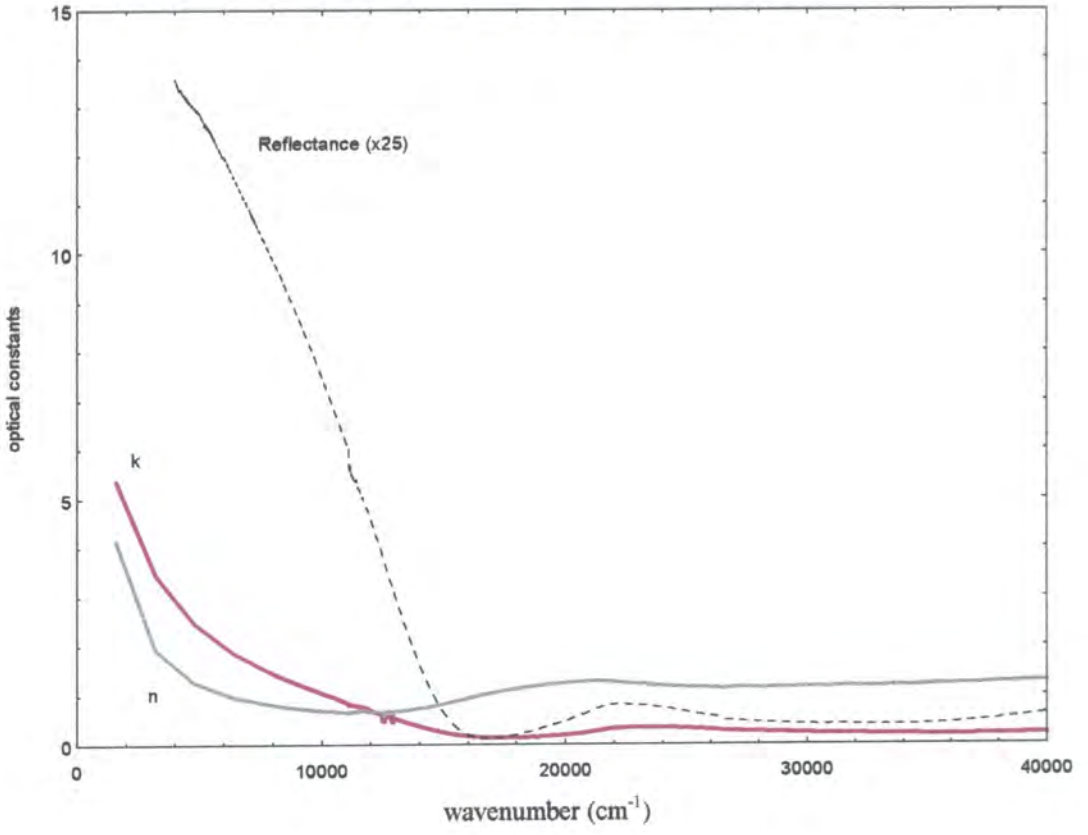

Figure 5.34 ε_1 and ε_2 for 600% ES films - parallel polarisation

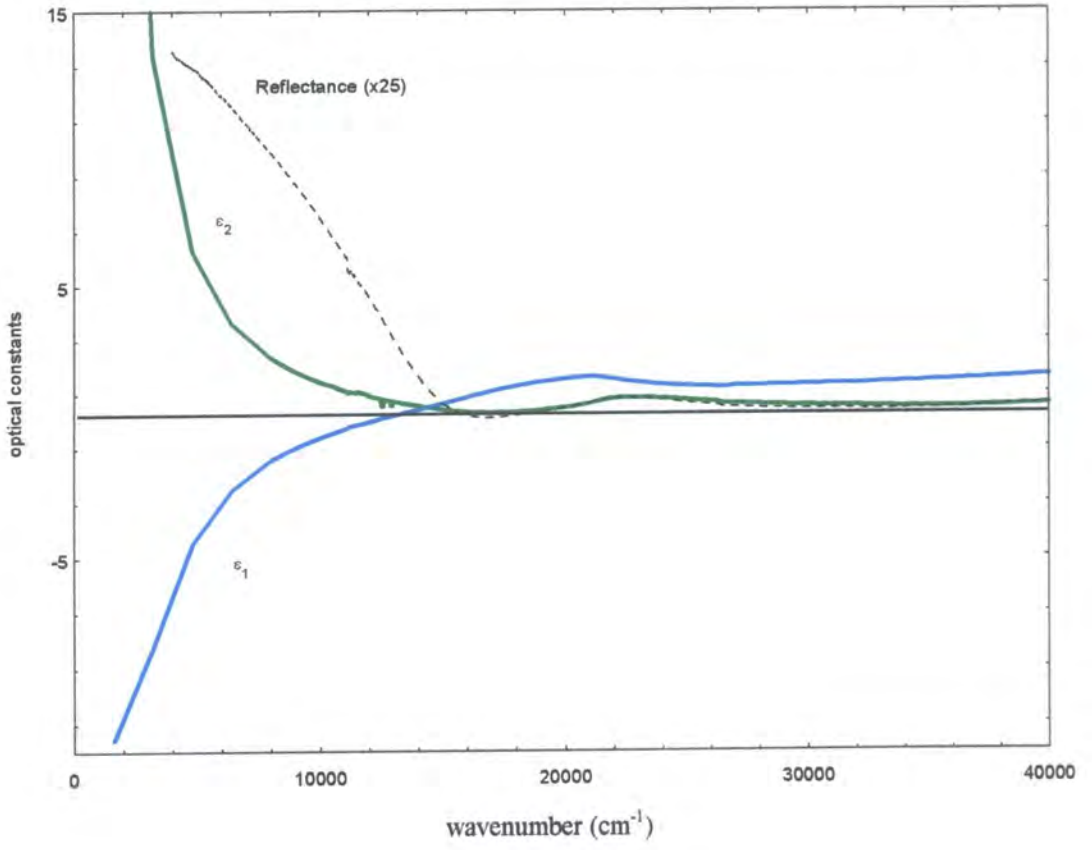

Figure 5.35 n and k for 600% ES films - perpendicular polarisation

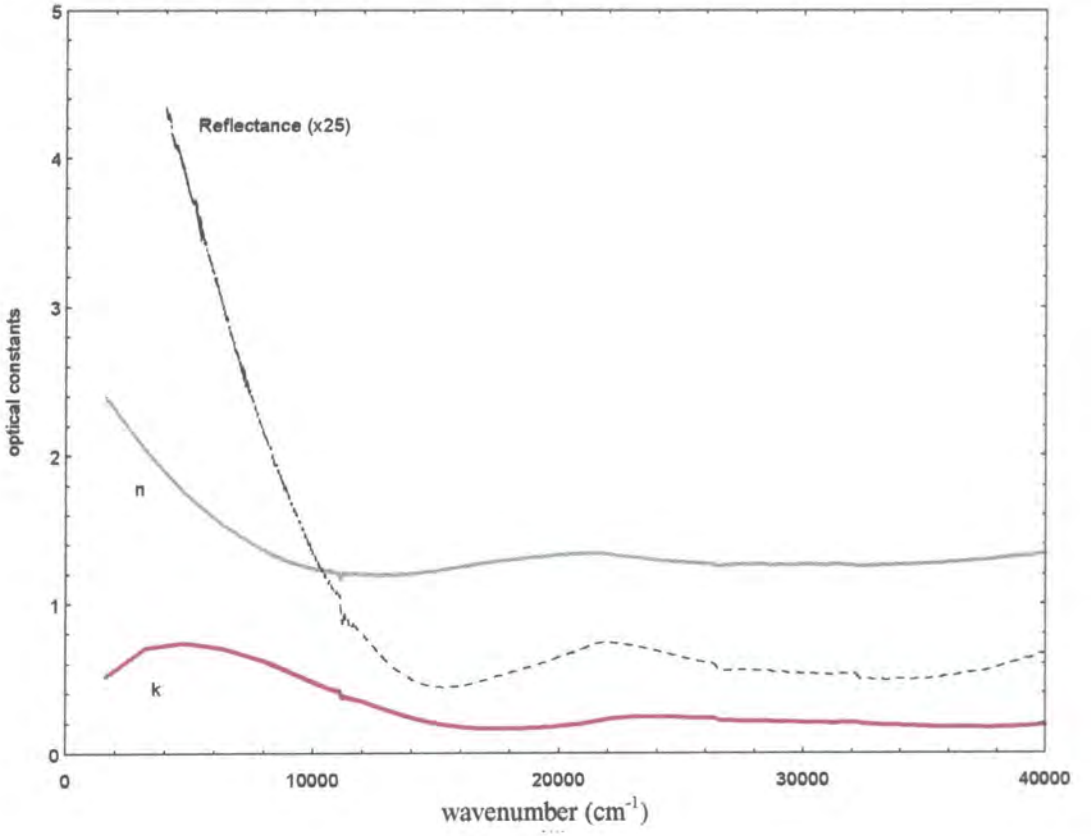

Figure 5.36 ε_1 and ε_2 for 600% ES films - perpendicular polarisation

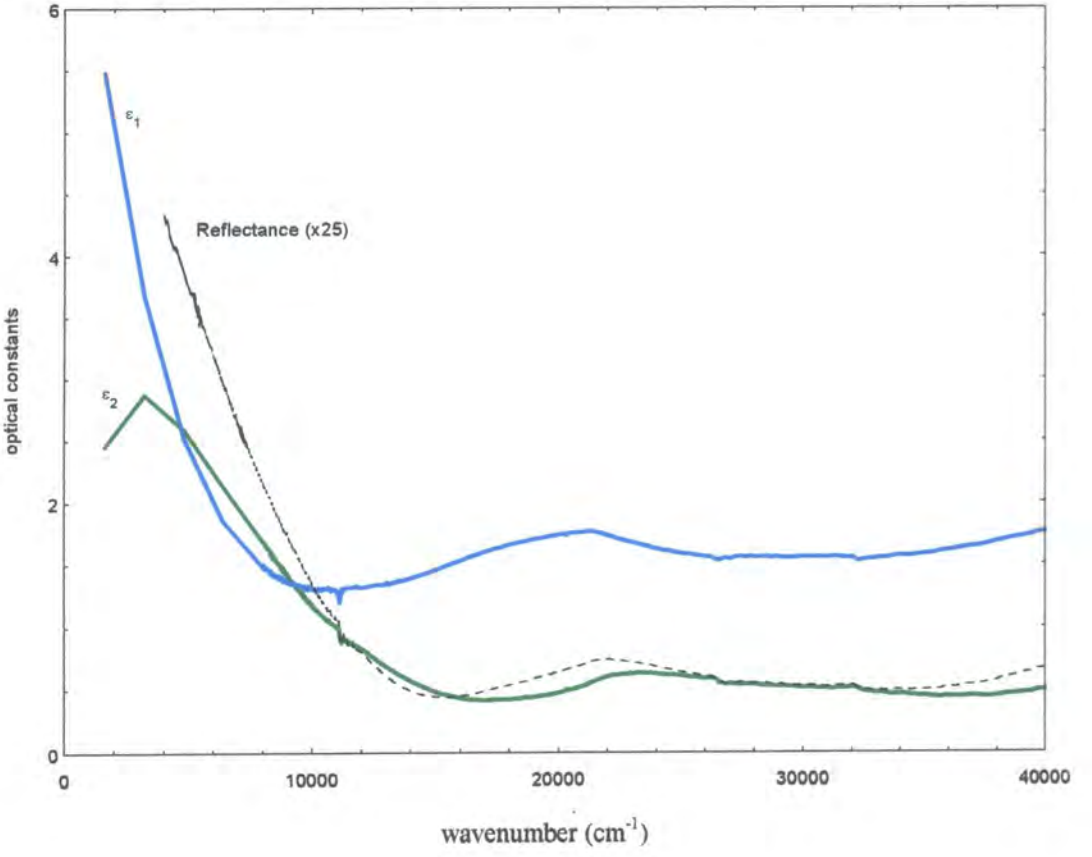

It can be seen that for the electric field polarised parallel to the direction of elongation n has a low energy value of approximately 4 for both the 300% and 600% elongated samples. The value of n decreases to approximately 1 as the energy increases and remains at approximately this value for the remainder of the spectra. The differences in n for 300% and 600% elongated samples is very small. The extinction coefficient has values higher than the corresponding values of refractive index in the low energy region, with a crossover of n and k at approximately 1.5 eV, after which k remains lower than n for the remainder of the spectrum.

For perpendicular polarisation of the incident E-field n has a low energy value of approximately 2.3 for both 300% and 600% elongations. This decreases to a value of approximately 1.2 above 1.5 eV. The extinction coefficient remains below n at all frequencies with a low energy peak at approximately 0.6 eV.

The real part of the dielectric function for parallel polarisation is negative up to approximately 1.5 eV, indicative of metallic behaviour. This is the region where $n<k$, and therefore $\varepsilon_1 = n^2 - k^2$ is negative. The point where ε_1 crosses the energy axis is often termed the screened plasma energy. This shall now be described in more detail.

A conducting material may be considered as a plasma of mobile electrons in the field of lattice ions. If a fluctuation in the density of total net charge occurs in any small region electrons will flow in or out of the region to restore balance. The process will go into reverse as too many electrons leave the region, and an oscillation will occur. Although this oscillation will usually decay due to damping, if the incident electric field has the same frequency as the oscillation then the oscillation will continue and strong absorption will take place. This energy is termed the screened plasma frequency, where the screening arises from the positive ion core background[30].

For perpendicular polarisation the real part of the dielectric function remains positive ($n>k$ at all energies). The low energy value of ε_1 is in the region of 5 for both 300% and 600% elongated films, which then decreases to approximately 1.2 as the incident

energy is increased. The positive values of ε_1 are consistent with less delocalisation perpendicular to the direction of elongation compared with parallel to this direction.
The imaginary part of the dielectric function is large for parallel polarisation at low energies. This behaviour is indicative of high absorption due to intra-band electronic transitions. ε_2 then decreases towards zero as the energy increases, with a small peak in the region of inter-band absorption, consistent with the formation of the polaron lattice. For perpendicularly polarised light ε_2 is again highest in the low energy region, but not as high as the corresponding value for parallel polarised light. As the incident energy is increased ε_2 again decreases. This behaviour is consistent with the changes in optical conductivity reported in section 5.10.2(d). There appears to be very little difference between the values of ε_2 for 300% elongated samples compared with those elongated to 600%.

c) Absorption coefficient

The absorption coefficients for oriented emeraldine salt samples are shown in figures 5.37-5.38.

Figure 5.37 Absorption Coefficient for 300% ES films

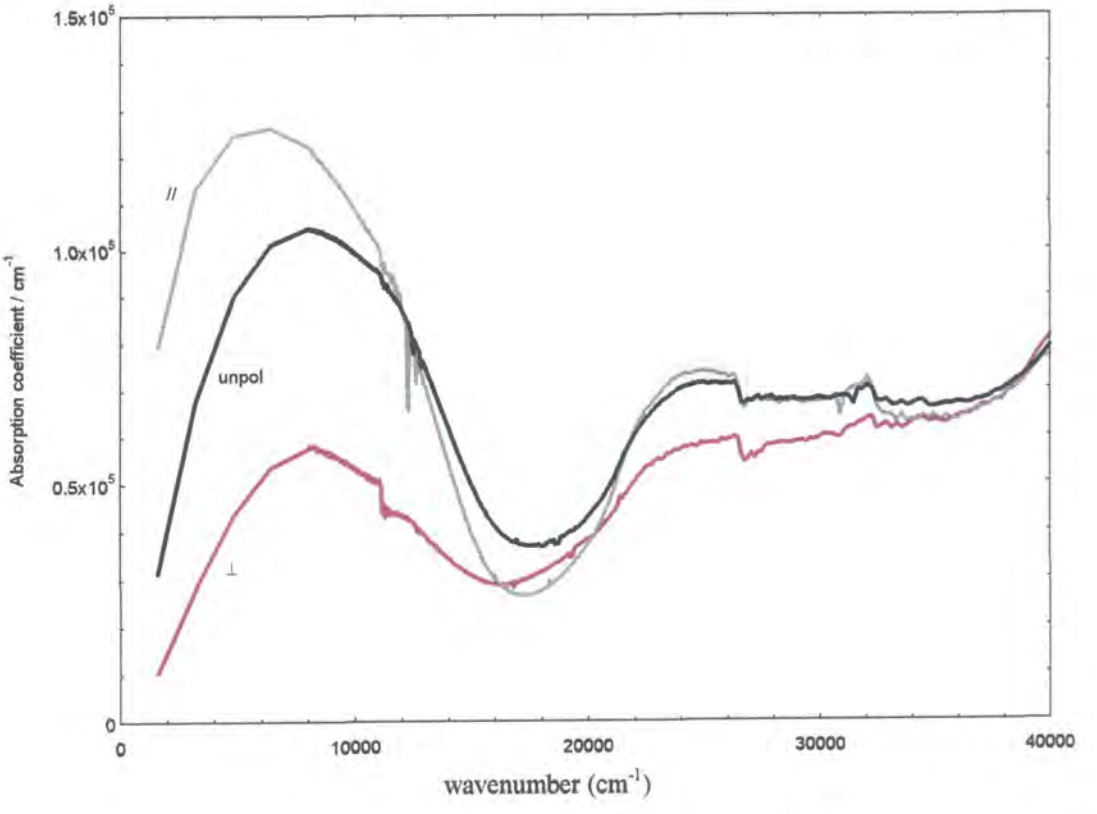

Figure 5.38 Absorption Coefficient for 600% ES films

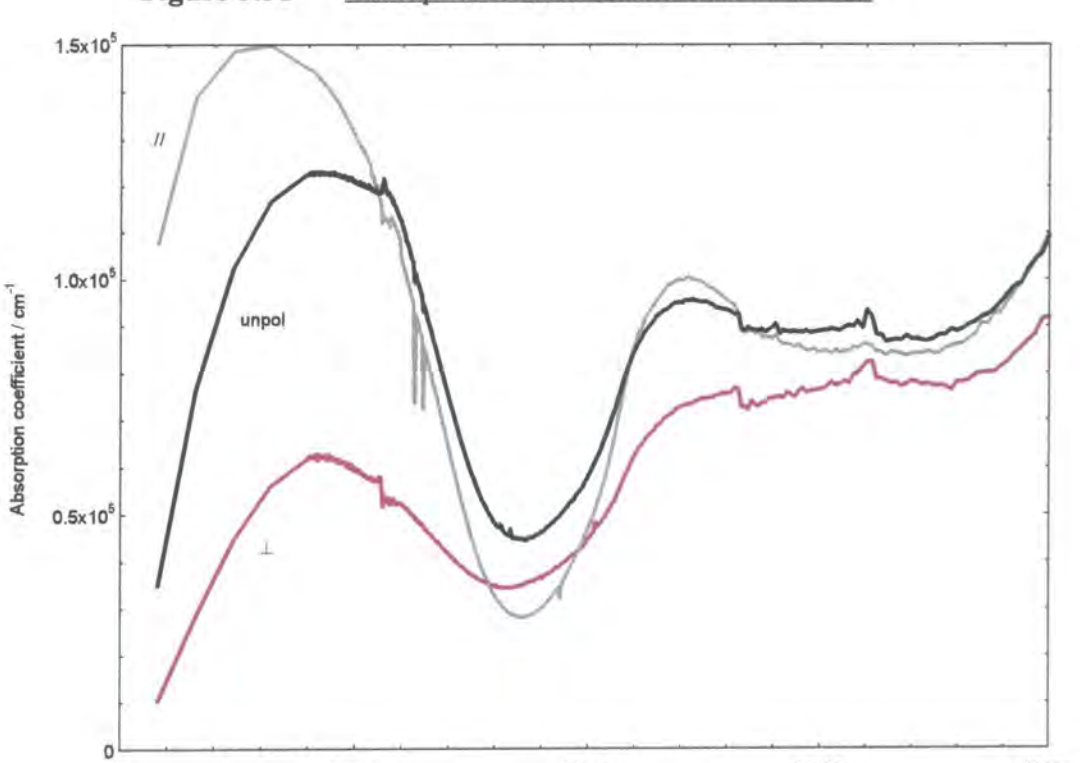

The absorption coefficient for 300% ES films with parallel (perpendicular) polarisation reveal maximum values of 125 000 cm^{-1} (58 000 cm^{-1}) and 73000 cm^{-1} (60 000 cm^{-1}). For 600% elongated films the maxima have values of 150 000 cm^{-1} (63 000 cm^{-1}) and 100 000 cm^{-1} (76 000 cm^{-1}). Absorption therefore increases slightly as a function of elongation. The anisotropies in absorption coefficient also increase with elongation, but this increase is only to the order of approximately 10 percent. The anisotropy in absorption coefficient is again consistent with increased delocalisation parallel to direction of elongation compared with perpendicular.

d) Optical Conductivity

The frequency-dependent optical conductivity $\sigma(\omega)$ is given by the equation:

$\sigma(\omega) = \omega\varepsilon_0\varepsilon_2 \equiv 2\pi c\nu\varepsilon_0\varepsilon_2$ where ν is the wavenumber.

This is shown in figures 5.39-5.40 for emeraldine salt samples.

Figure 5.39 Optical conductivity for 300% elongated ES samples

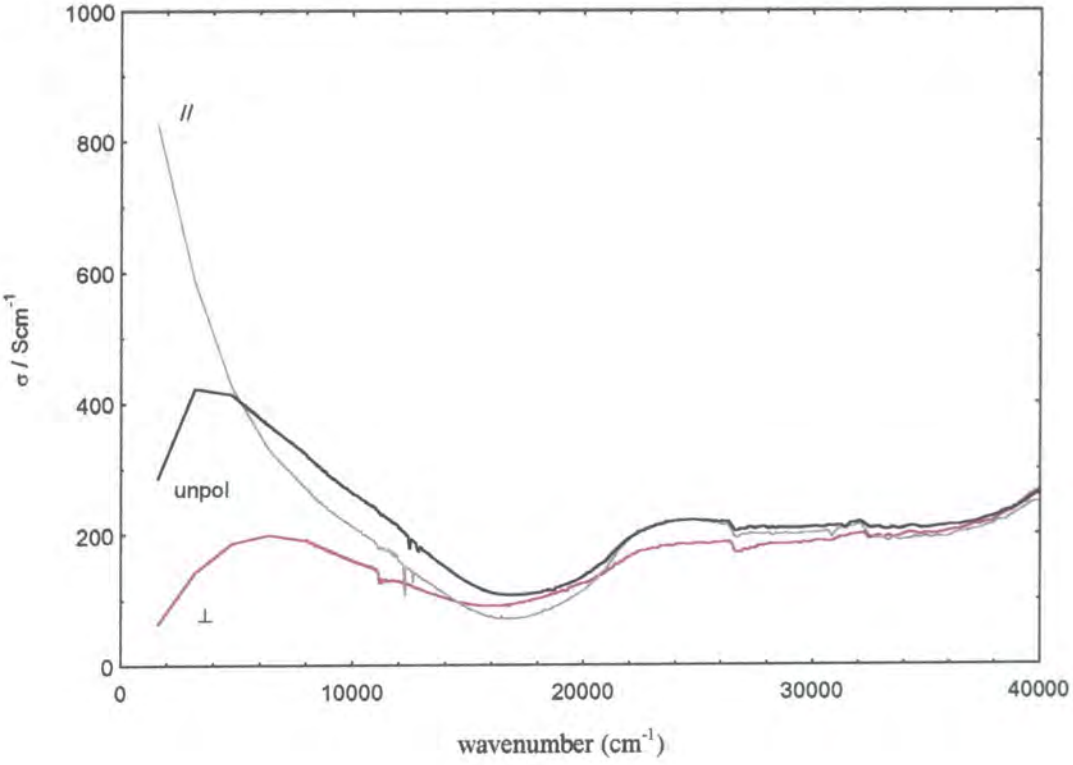

Figure 5.40 Optical conductivity for 600% elongated ES samples

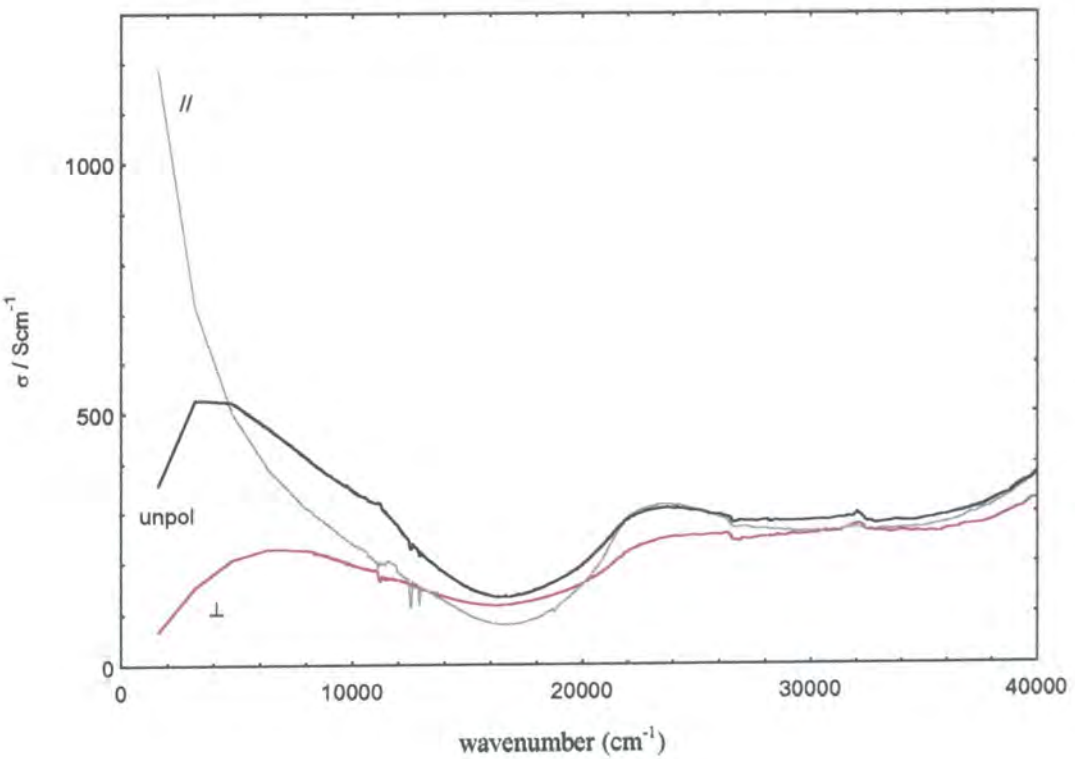

It can be seen that there is a large degree of anisotropy in the optical conductivity for light polarised parallel to the direction of elongation compared to light polarised perpendicular. For light polarised parallel to elongation direction the following features are observed: At low energies (< ~ 2eV) the optical conductivity increases with decreasing energy, due to intraband excitations. At approximately 2.7 eV interband transitions take place. The results can be compared with the VEH band structure of emeraldine salt, as described in chapter 1, section 1.6(d). The band structure is reproduced in figure 5.41:

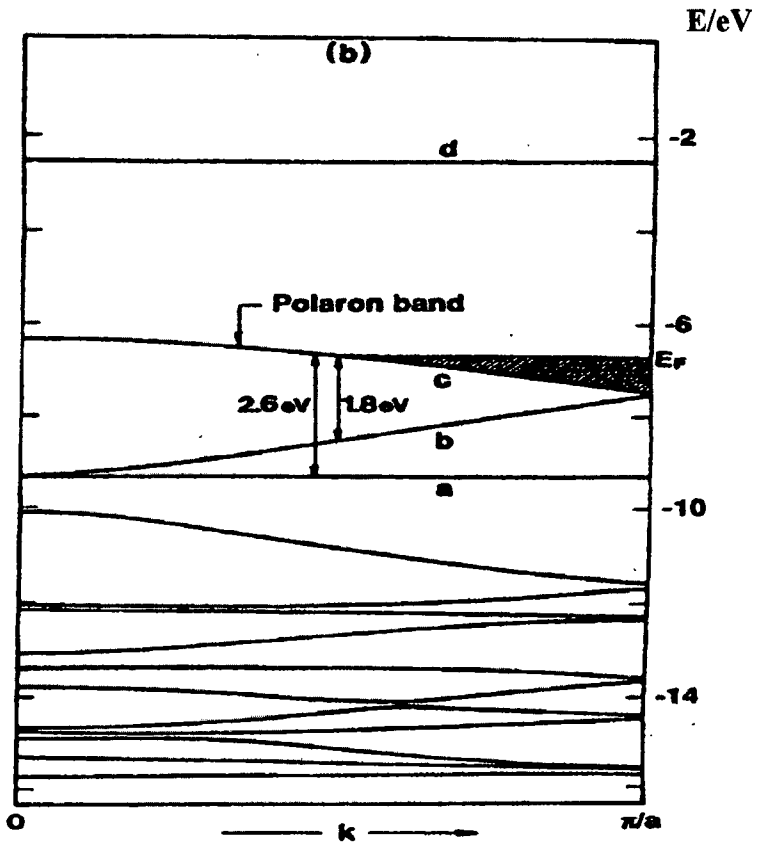

Figure 5.41: VEH band structure for polaron lattice structure of emeraldine salt.

It is evident from the band structure calculation that the interband transition is from band a to band c, the polaron band. Similar results have been made by other groups[22] using polyaniline protonated with camphor sulphonic acid. This group have modelled the optical conductivity of PANi-CSA using the 'localisation modified Drude model'. The data reported in this chapter does not go to low enough energies to allow for such modelling to be done, but it is evident that the optical conductivity (parallel polarisation)

in the region 0.5 to 5.6 eV is very similar to that for PANi-CSA, indicating almost metallic behaviour.

The optical conductivity perpendicular to direction of elongation tends to low values towards d.c. It is impossible to determine the exact value from the graphs because of the limited spectral range of the reflectance measurements, but the results seem to be qualitatively consistent with the d.c. conductivity reported in chapter 2.

Again it is evident that there is very little change in the optical conductivity for 300% elongated samples compared with 600%. The low energy value of $\sigma(\omega)$ for 600% ES films (parallel polarisation) is higher than that for 300% films. Due to the limited spectral region of reflectance measurements these values will be more dependent on the extrapolations than for other regions of the spectrum. It is therefore more suitable to look at the trends and general shapes of the curves rather than the values themselves in these regions.

e) Loss Function

Figures 5.42 and 5.43 show the loss function (-Im $(1/\varepsilon)$) obtained from the Kramers-Kronig analysis of the reflection data for ES films.

For parallel polarisation there is a well defined peak in the loss function for both 300% and 600% elongated films. The peaks occur at approximately 12 800 wavenumbers which is close to the energy at which ε_1 crosses the energy axis, i.e. the screened plasma energy. Thus, because the peak in loss function corresponds to the true plasma energy[20], it is not necessary to distinguish between the two for this analysis. The maximum in the loss function indicates where maximum energy is absorbed by the material. It is evident that the value for parallel polarisation is higher than that for perpendicular polarisation, indicating an over-damped response to the incident radiation for the latter polarisation direction. The loss functions for 300% elongated films are very similar to those for 600% films, commensurate with the similar values of the real and imaginary parts of the dielectric function mentioned previously.

It is evident from figures 5.42 and 5.43 that the plasma frequency, measured from the peak in the loss function, has higher values for parallel polarisation than perpendicular. This behaviour is indicative of increased carrier concentration along the direction of elongation[3]. A quantitative description of this behaviour is seen by considering the relation between plasma frequency and carrier concentration:

$$\Omega_p = \left[\frac{4\pi ne^2}{m^*}\right]^{1/2}$$

where Ω_p is the plasma frequency,
n is the number of electrons per unit volume with effective mass m^*.

It is seen that as Ω_p increases, so does n. Thus, there are more metallic carriers for higher values of Ω_p, which is revealed by the increased conductivity parallel to the orientation direction compared with perpendicular.

Figure 5.42: Loss function for 300% elongated ES films

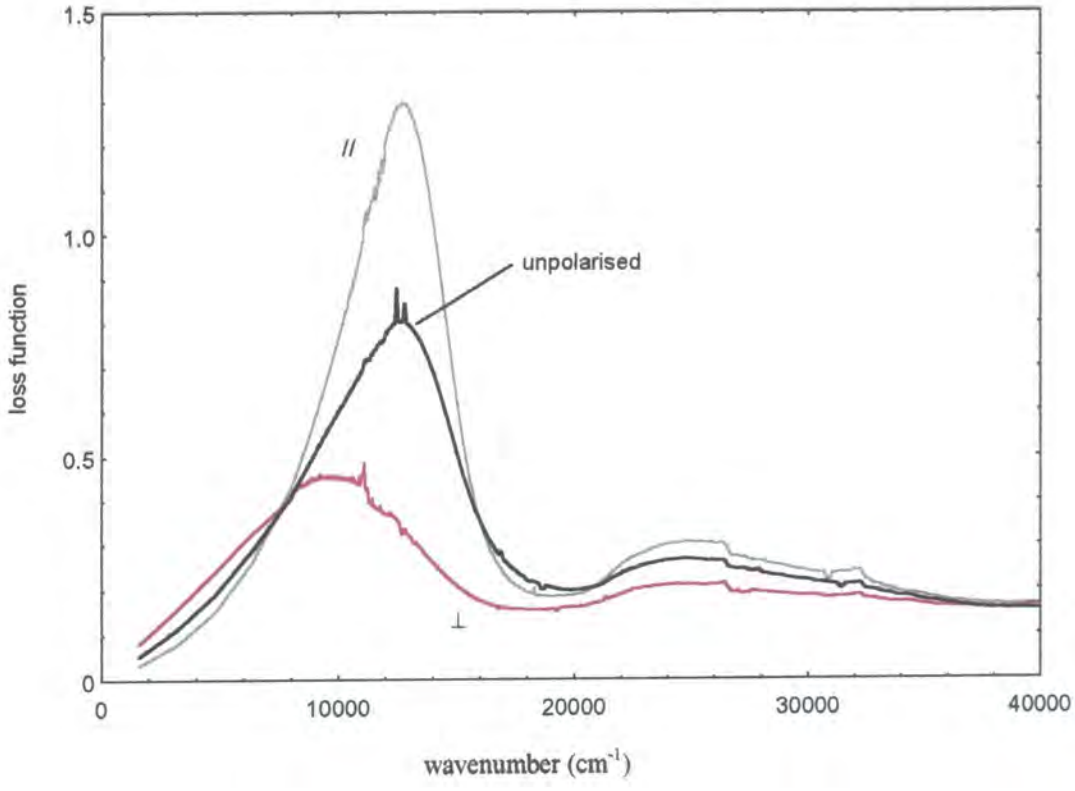

Figure 5.43: Loss function for 600% elongated ES films

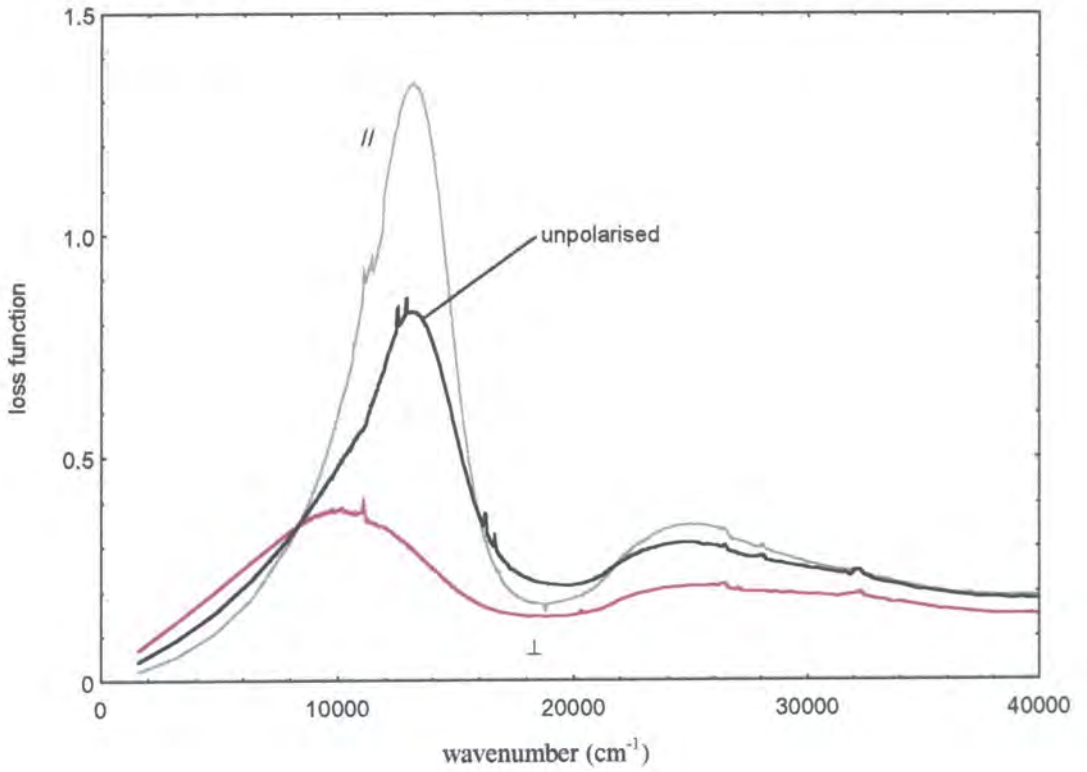

f) Effective Number of Carriers, N_{eff}

The effective number of carriers can be calculated from knowledge of the plasma frequency[3]. The plasma frequency has previously been described by the equation:

$$\Omega_p = \left[\frac{4\pi ne^2}{m^*}\right]^{1/2}$$

The number of effective carriers is given by:

$$N_{eff}(\omega) = \frac{2m^*V}{\pi e^2}\int_0^{\omega}\sigma(\omega')d\omega'$$

where V is the unit cell volume.

Comparison of these equations enables the effective electron mass, m^*, to be eliminated by the relation:

$$\frac{e^2}{m^*} = \frac{\Omega_p^2}{4\pi n}$$, thus giving:

$$N_{eff}(\omega) = \frac{8nV}{\Omega_p^2}\int_0^{\omega}\sigma(\omega')d\omega'$$

If it is initially assumed that one free carrier exists per unit cell[23] (i.e. idealised situation) then the product (nV) is unity, yielding:

$$N_{eff}(\omega) = \frac{8}{\Omega_p^2}\int_0^{\omega}\sigma(\omega')d\omega'$$

Thus, by integrating the optical conductivity and measuring the plasma frequency from the peaks in the loss function, the number of effective carriers can be determined as a function of frequency. Table 5.2 shows the measured peak values of the loss function for emeraldine salt samples.

elongation (%)	polarisation	Ω_p (cm^{-1})	$8/\Omega_p^2$ [$x10^{-8}$] (cm^2)
0	unpolarised	11900	5.6493
300	parallel	12850	4.8449
300	perpendicular	9680	8.5377
600	parallel	13300	4.5226
600	perpendicular	10000	8.0000

Table 5.2: Plasma frequencies measured from -Im(1/ε) for ES films.

The number of effective carriers for each situation are shown in figures 5.44 and 5.45.

Figure 5.44: Number of effective carriers for 300% elongated ES

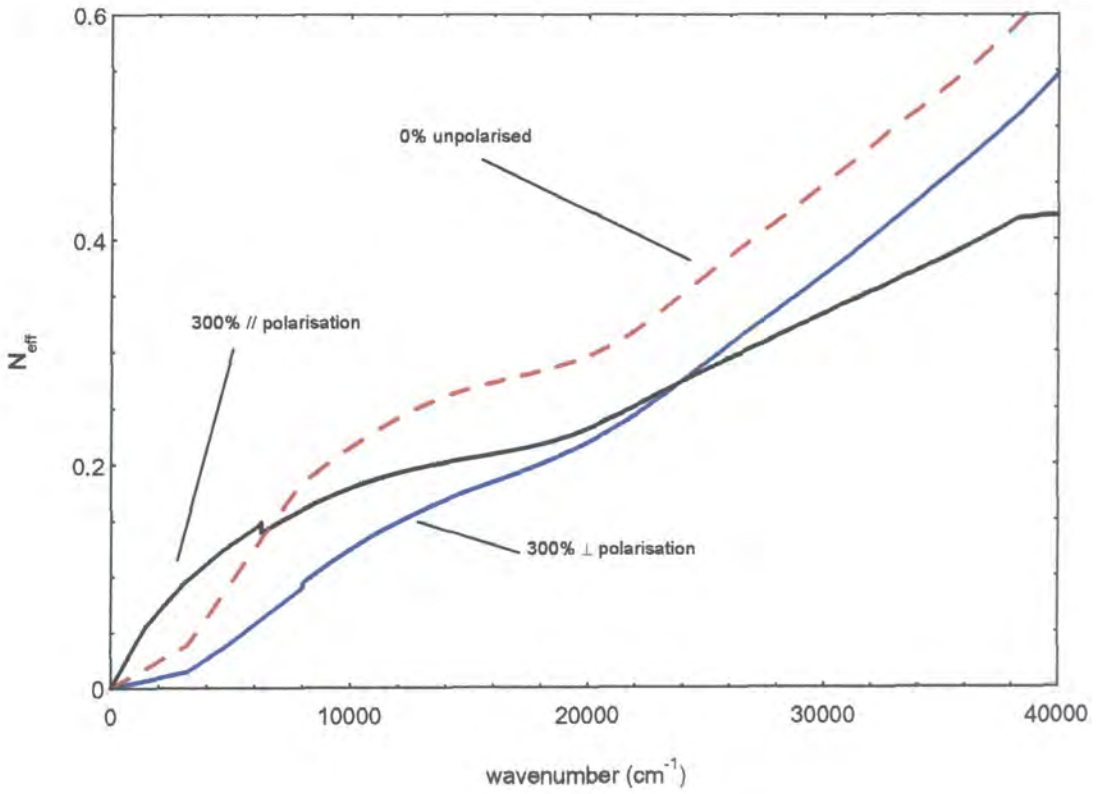

Figure 5.45: Number of effective carriers for 600% elongated ES

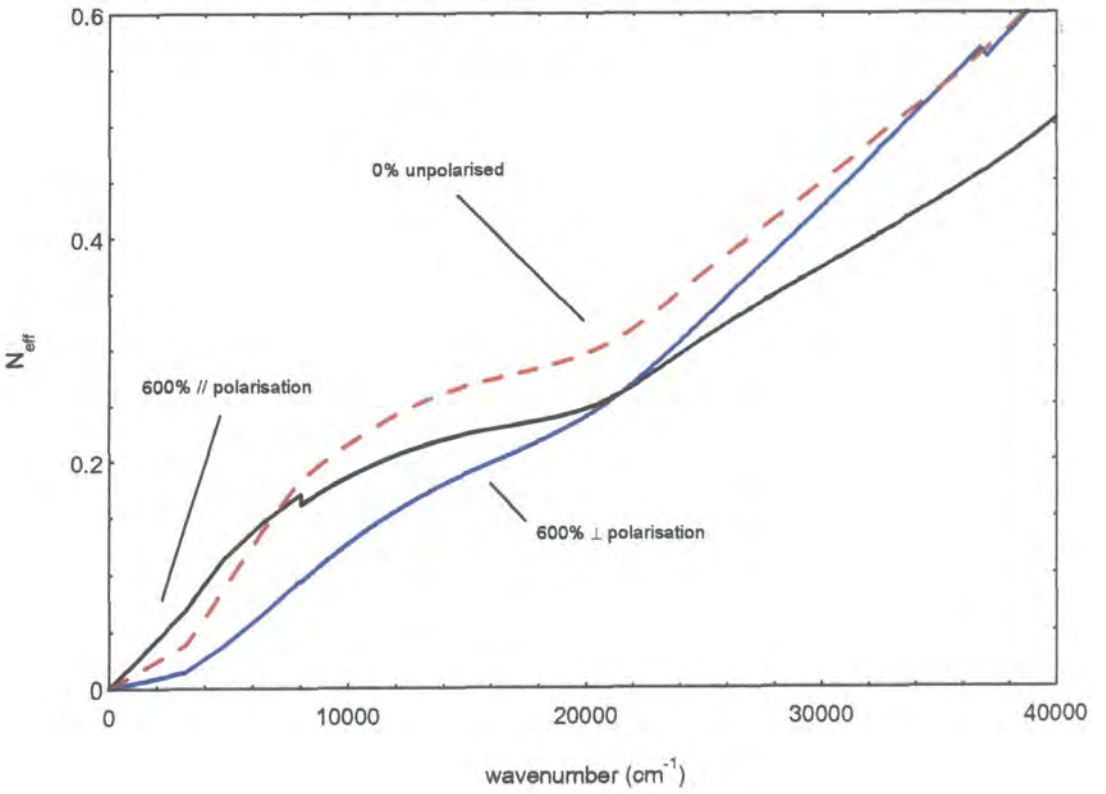

It can be seen from the diagrams that N_{eff} for light polarised parallel to the direction of orientation is higher in the low energy region than for perpendicularly polarised light. This is the region of intra-band absorption, signifying metallic behaviour parallel to the direction of elongation. For light polarised perpendicular to the elongation direction the number of effective carriers increases less rapidly with wavenumber, suggesting increased localisation of charge carriers. The onset of inter-band absorption is evident from the sudden increase in the slope of N_{eff} at ca. 22000 cm^{-1}.

Comparison of figures 5.44 and 5.45 reveal little change in N_{eff} for 300% elongated films compared with 600%. However, the relatively low values of N_{eff} for the elongated samples suggest that maximum theoretical doping is not achieved. This is evident from the fact that N_{eff} for the unoriented sample is higher in much of the spectrum than those values for the elongated samples.

A simple comparison can be made with the number of effective carriers for PANi-CSA (camphor sulphonic acid) calculated by Lee, Heeger and Cao[22]. This is shown in figure 5.46.

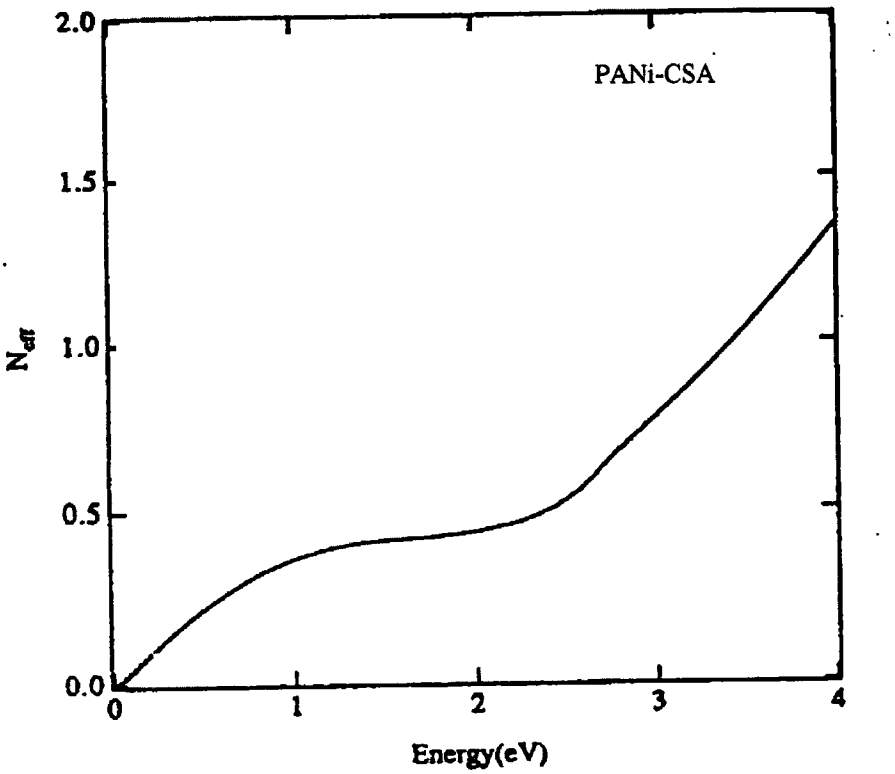

Figure 5.46: Effective number of carriers per unit cell for PANi-CSA.

The number of effective carriers per unit cell approaches 0.5 at the saturation point of the intra-band absorption (ca. 1.2eV), compared with 0.2 for elongated emeraldine salt with incident light polarised parallel to the direction of elongation. This highlights one of the main advantages of polyaniline processed with CSA. Whereas protonation of PANi-NMP takes place in the solid state (i.e. the films are immersed in HCl), the CSA route involves protonation in solution. This leads to a more homogeneous dispersion of the dopant and therefore the electrical properties can be more easily controlled. The CSA route is currently being thoroughly investigated here at Durham[24,25] as it is thought that the intrinsic electrical behaviour of polyaniline can be more clearly understood using this processing technique.

5.8 Summary

This chapter has reported the results from polarised reflectance analysis of oriented emeraldine base and emeraldine salt films. It has been shown that significant anisotropy in the optical properties is observed for light polarised parallel to the direction of elongation compared to that polarised perpendicular. In emeraldine base the anisotropy due to the exciton transition is larger than that due to the π-π^* transition because of the differences in the spatial extent of the two transitions. Furthermore the anisotropy in optical quantities increases with increased elongation, whereas for emeraldine salt there is no marked change in optical properties for 600% elongated samples compared with 300%. One possible explanation for this is the inhomogeneous doping of samples.

For emeraldine salt the optical properties are indicative of metallic behaviour along the direction of elongation - the real part of the dielectric function is negative and there is a well defined peak in the loss function. The optical conductivity has a low energy value of the order of 10^3 Scm^{-1}, which is comparable with the highest measured d.c. conductivity reported earlier. Perpendicular to the direction of elongation the metallic features in the optical quantities are not observed - the real part of the dielectric function remains positive at all frequencies and the loss function peak is less well defined. The number of effective charge carriers per unit cell has been calculated to be lower than that

for polyaniline synthesised under the CSA route, suggesting that the maximum theoretical doping of elongated samples may not have been achieved.

References

1. A H Taylor. *Sci. Papers Bur. Std.* **16**, 421 (1920).

2. *Reflectance Spectroscopy.* W W Wendlandt and H G Hecht. Publ. John Wiley and Sons. (1966)

3. *Optical Properties of Solids.* F Wooten. Publ. Academic Press Inc. (1972)

4. H A Kramers. *Z. Physics* **30**, 522 (1929)

5. R de L Kronig. *Proc. R. Soc.* **133**, 255, (1931)

6. D M Roessler. *Brit. J. Appl. Physics.* **16**, (1965)

7. T G Arkatova, N M Gophstein, E G Makarova and B A Mikhailov. *Sov. J. Opt. Tech.* **48(9)**, 552 (1981)

8. A Kaito, K Nakayama and H Kanetsuna. *J. Polymer Sci. B.* **26**, 1439 (1988)

9. D M Roessler. *Brit. J. Appl. Physics.* **17**, 1313 (1966)

10. A P Monkman and P N Adams. *Synthetic Metals.* **40**, 87-96 (1991)

11. A P Monkman and P N Adams. *Solid State Comm.* **78**, 29 (1991)

12. W S Huang and A G MacDiarmid. *Polymer.* **34(9)**, 1833 (1993)

13. S Stafstrom, J L Bredas, A J Epstein, H S Woo, D B Tanner, W S Huang and A G MacDiarmid. *Phys. Rev. Lett.*, **59**, 1464 (1987)

14. R P McCall, E M Scherr, A G MacDiarmid and A J Epstein. *Phys. Rev. B*, **50** no. 8, 5094 (1994)

15. G Leising. *Synth. Met.* **28**, D215 (1989)

16. Lambda 19 UV/VIS/NIR Spectrometers. User Documentation. (1991)

17. J Eggleston, University of Durham. Personal Communication.

18. D S Boudreaux, R R Chance, J F Wolf, L W Shacklette, J L Bredas, B Themas, J M Andre and R Silbey. *J. Chem. Physics.* **85**, 4584 (1986)

19. S Stafstrom, B Sjogren and J L Bredas, *Synth. Met.* **29**, E219 (1989)

20. *The Optical Constants of Bulk Materials and Films.* L Ward. IOP Publishing Ltd. (1988).

21. *Polyacetylene* by J C W Chien. Publ. Academic Press Inc. (1987).

22. K Lee, A J Heeger and Y Cao. *Synthetic Metals*, **5**, 30 (1994)

23. K Lee and A J Heeger, Y Cao. *Phys. Rev. B*, **48**, no. 20, 14884 (1993)

24. E R Holland, PhD Thesis, University of Durham. (1996)

25. L Abell, P N Adams and A P Monkman. 'Electrical Conductivity Enhancement of stretch-oriented PANi-CSA'. *Polymer Comm.* (In publication)

26. C B Duke, E M Conwell and A Paton. *Chem. Phys. Lett.* **131**, 82 (1986)

27. S J Pomfret. PhD Thesis. Durham University (1995)

28. R D B Fraser, *J. Chem. Phys.* **28**, 1113 (1958)

29. S Hasegawa, M Oku, M Shimizu and J Tanaka. *Syn. Met.* **38**, 37 (1990)

30. *Introduction to Solid State Physics* by C Kittel. Publ. Wiley, New York, 1976.

31. L Abell. University of Durham. Personal Communication.

CHAPTER SIX: SUMMARY AND CONCLUSIONS

6.1 Summary

This thesis has reported the results from a number of experiments performed on the conducting polymer polyaniline, in an attempt to improve our understanding of a complex and challenging material. In particular, the effects of uniaxial elongation of polyaniline films upon the structural and electronic properties have been investigated. Furthermore, some of the main problems encountered concerning characterisation of the polymer have been discussed. The main findings from the research undertaken are summarised below.

A method for preparing high molecular weight polyaniline has been described. It has been shown that the molecular weight depends on a number of parameters including reaction temperature , solution pH at the start of the reaction, ratio of oxidant to aniline, oxidant addition time and total reaction time. Molecular weights in the region of 150000 Daltons were attainable using a reaction temperature of ca. -26° C, compared with values of approximately 20 000 Daltons at room temperature. The molecular weights have been measured using gel permeation chromatography and ^{15}N NMR techniques.

The preparation of thin films of the emeraldine base (EB) form of polyaniline has been described. It is found that EB is moderately soluble in N-methyl-2-pyrollidone (NMP) and therefore an EB/NMP solution can be obtained and free-standing films prepared. The effects of a number of preparation parameters upon the quality of these films have been examined, and a method for obtaining high quality films described. The amount of residual NMP in the as-cast films has been shown by thermogravimetric analysis to vary in different regions of the samples. This is due to the drying process, whereby the samples dry from the edges inwards. Methods to remove the excess solvent as uniformly as possible have been investigated because of the importance of NMP acting as a plasticiser when subsequently elongating the films.

Techniques to obtain highly elongated EB films were a major part of the early experimental work undertaken during this research. It was originally found that reproducibly elongating films to consistent elongation ratios was impossible even under identical conditions. The reason for this was found to be edge imperfections which caused the films to tear rather than fracture. A method for reinforcing the edges of the samples has been described which allows for fairly reproducible elongations of up to 700%. Parameters such as the temperature of the samples during elongation and the speed of elongation were varied to assess their effect on the elongation of samples. It was found that stretching the samples at a temperature of 110 °C and at a speed of 20 mm/minute maximised the reproducibility of elongation.

EB can be converted to conducting emeraldine salt (ES) by immersion in aqueous HCl. This produces an increase in electrical conductivity of up to 12 orders of magnitude. Furthermore, the conductivity of elongated samples is found to be higher in the direction parallel to orientation compared with perpendicular. This is due to increased alignment of polymer chains. The conductivity of ES samples has been measured as a function of elongation for samples elongated up to 700%. The maximum value of conductivity parallel to the orientation direction has been measured to be almost 700 Scm^{-1}, compared with perpendicular conductivity of 190 Scm^{-1}. Thus the maximum electrical anisotropy ($\sigma_{//}/\sigma_{\perp}$) is almost 4. However, the conductivity values have been found to vary at different points within a sample. This has been attributed to inhomogeneous doping of the samples which is dependent upon the variations in molecular morphology and impossible to control.

The mechanical properties of EB films have been studied as a function of initial elongation. The samples were subjected to a constant strain rate and the forces required to maintain this rate were measured. From this it was possible to measure the breaking stress, breaking strain and Young modulus and to attempt to interpret these results in terms of the elongation of the samples. The mechanical testing was performed on six samples at each elongation in order to gauge the reproducibility of results from sample to sample. The main finding from these experiments was the apparent lack of reproducibility in the results. Different mechanical responses were observed from

sample to sample as well as for different elongations, which made quantitative interpretation of the results very difficult. However, certain trends were evident. The breaking stress was observed to increase with initial elongation by almost one order of magnitude, with a maximum breaking stress of 340 MPa for a 500% elongated sample. This behaviour is consistent with increased alignment of polymer chains parallel to the stretch direction. The breaking strain was observed to decrease with increasing elongation for samples stretched up to approximately 300%. Above this value, however, the average breaking strain remained almost constant. This behaviour has been interpreted in terms of the changes in crystallinity of samples when they are elongated at elevated temperatures.

X-ray diffraction experiments have enabled the crystalline fraction of EB and ES to be investigated, and the effect of elongation upon this quantity assessed. It was found that for EB samples elongated to 300% the crystallinity increased by a factor of approximately 1.6 - the crystalline fraction of oriented samples was measured to be 14% compared to 22% crystallinity for 300% elongated samples. However, no further increase was evident for samples with 600% elongations. The crystallinity of emeraldine salt samples was found to be higher than that of the base samples (~29% for unoriented samples). However, a slight decrease in crystallinity was measured for higher elongated samples. It was also found from the X-ray analysis that protonation of EB results in a dramatic structural change, as indicated by the change in the Bragg peaks from the diffractometer scans.

The optical properties of EB and ES have been investigated using reflectance spectroscopy. Furthermore, the use of polarisers has allowed for the variation in optical properties parallel to the direction of elongation to be compared with those perpendicular. A Kramers-Kronig analysis of the reflectance data has allowed for the complex refractive index n-ik to be evaluated as a function of the energy of the incident radiation. This in turn has enabled calculation of the real and imaginary parts of the dielectric function, the absorption coefficient, the optical conductivity, the loss function and the number of effective carriers. The results from the reflectance of emeraldine base have confirmed the existence of the electronic states described previously, and have shown a degree of anisotropy in the optical constants parallel to the direction of

elongation compared with perpendicular. The higher anisotropy of optical constants for higher elongation ratios indicates increased alignment of the polymer chains. The reflectance analysis of emeraldine salt samples has revealed the change in electronic structure upon protonation, namely the formation of the polaron lattice. Again significant optical anisotropy is evident for radiation polarised parallel to the direction of elongation compared with perpendicular. However, there is very little difference in the optical spectra for 600% elongated films compared with 300%. For parallel polarisation the Kramers-Kronig analysis reveals metallic behaviour along the direction of elongation, evident from the negative values of the real part of the dielectric function. The absorption coefficient is slightly higher for 600% elongated samples compared with 300%, but only by a factor of about 0.1. Optical conductivity measurements reveal values approaching 1000 Scm^{-1} in the d.c. limit which is comparable with the d.c. measured conductivities. For light polarised perpendicular to the elongation direction the real part of the dielectric function remains positive indicating less delocalisation of the conductive species. Thus the optical conductivity tends to low values in the d.c. limit.

6.2 Conclusions

It is evident from the results published in this thesis that elongation of polyaniline films has dramatic effects upon structure, as revealed from both the macroscopic (eg. electrical conductivity) and microscopic (eg. X-ray diffraction) measurements. However, analysis of the results in relation to the actual degree of elongation has perhaps posed more questions concerning the effect of elongation than it has answered. In particular it has been shown from the experiments undertaken that the structural and electronic properties of samples elongated to 600% are very similar to those elongated to 300%.

One of the main problems highlighted by the experiments is the variations in properties from sample to sample, making quantitative analysis difficult. This is particularly prominent in the mechanical analysis of emeraldine base samples where the mechanical behaviour has been observed to vary considerably for different samples. Although certain trends do appear the work has not satisfactorily characterised the effect of

elongation upon the mechanical properties. It has shown, however, that an elongated sample is likely to have an increased breaking stress compared to an as-cast film, though from the results reported it would be impossible to predict with any accuracy specific values for this increase. Similarly, mechanical testing has shown that an elongated sample is likely to fracture at lower strains than an isotropic sample, but this is a qualitative rather than quantitative statement. A suggestion has been made that the behaviour could be related to the crystallinity of the samples but this correlation is at the least tentative.

The measurements of electrical conductivity have yielded similar problems in attempting to quantify the effect of elongation. The fact that the conductivity of, for example, a 500% elongated sample has a value of 500 Scm^{-1} at one point parallel to the elongation direction and a value of 150 Scm^{-1} at some other point poses many problems concerning characterisation. One of the possible causes of this discrepancy is the likelihood that samples are not doped homogeneously. If this is the case then the large variations in measured conductivity can be accounted for but quantitative assessment is difficult. However, it is also possible that different regions of a particular sample may be elongated by different amounts. This behaviour could be attributed to the variations in molecular morphology at different points within a sample, or perhaps during the elongation process subtle differences in the temperature of the sample will cause some areas to elongate at a higher rate than others. Furthermore, variations in the amount of NMP at different points in the sample will augment this problem. These anomalies would explain the discrepancies in the measured values of conductivity, and it is likely that it is in fact a combination of these factors which contribute to the irregularities mentioned. Characterisation of the material in terms of the bulk elongation is therefore very difficult to achieve.

6.3 Suggestions For Future Study

As well as the results reported in this thesis it has also been shown that in order to obtain a clearer picture of the quantitative effect of elongation upon the structural properties of polyaniline a very precise regime must be adhered to. This is important not only from a theoretical point of view but also in terms of possible industrial applications.

It has been shown that certain trends relating to structural properties are evident as a function of elongation but it has also been highlighted that further work is needed to clarify the picture. One way of approaching the problem would be to use the same sample for each experiment. The experiments in this work utilised hundreds of different samples. If one sample could have been used and the conductivity, crystallinity, mechanical properties and optical properties all assessed independently then perhaps more information could be derived. It was not possible to carry out experiments in this way for practical reasons.

It would also be of interest to carry out a detailed investigation into the doping of EB films, particularly those at high elongation ratios. If homogeneity of doping can be established then this would remove a large area of doubt from the overall characterisation procedure. It is likely that an adequate quantitative explanation into the effect of elongation upon structural properties of polyaniline will remain elusive until this and the other problems discussed are addressed.

List of Publications

1. "Mechanical Properties of Oriented Emeraldine Base Polyaniline"
   P J Laughlin. ICSM Proceedings 1996 (in publication)

2. "A Further Step Towards Stable Organic Metals - Oriented Films of Polyaniline with High Electrical Conductivity and Anisotropy"
   P N Adams, P J Laughlin, A P Monkman and N Bernhoeft.
   Solid State Comm., **91**, no.11, 875 (1994)

3. "Spin Dynamics Study in Polyaniline - Macroscopic and Microscopic Transport Property Relationship"
   J P Travers, P Leguyadec, P N Adams, P J Laughlin, A P Monkman.
   Synthetic Metals, **65**, no. 2-3, 159 (1994)

4. "Microscopic and Macroscopic Transport Properties of Polyaniline - Effect of Chain Orientation and Hydration"
   J P Travers, P Leguyadec, P N Adams, P J Laughlin, A P Monkman.
   Synthetic Metals, **69**, no. 1-3, 229 (1995)

5. "Polyaniline, Air-Stable Organic Metal - Fact, No Longer Fiction"
   A P Monkman, P N Adams, P J Laughlin, E R Holland.
   Synthetic Metals, **69**, no. 1-3, 183 (1995)

6. "Anisotropy of the Conductivity in Polyaniline Films - Effect of Chain Orientation and Hydration"
   J P Travers, P Leguyadec, P N Adams, P J Laughlin, A P Monkman.
   Journal de Chimie Physique et de Physico-Chimie Biologique, **92**, no.4, 1009 (1995)

7. "Synthesis of High Molecular Weight Polyaniline at Low Temperatures"
   P N Adams, P J Laughlin and A P Monkman
   Synthetic Metals, **76**, no. 1-3, 157 (1996)

8. "Low Temperature Synthesis of High Molecular Weight Polyaniline"
   P N Adams, P J Laughlin A P Monkman and A M Kenwright
   Polymer, **37**, no.15, 3411 (1996)